

Università degli Studi di Napoli Federico II



**DOCTORATE IN EARTH, ENVIRONMENTAL AND  
RESOURCES SCIENCE**

**XXXIII Cycle**

*Doctor Europaeus*

Ciro Cerrone

*Surface uplift and sea level change:  
constraints from Late Pleistocene paleoshorelines*

**Advisor**

Prof. Alessandra Ascione

**Head of the Doctorate**

Prof. Maurizio Fedi

**Co-advisor**

Prof. Gaetano Robustelli

Prof. Paola Tuccimei

2020

*πάθει μάθος*

**Eschilo**

*Eigentlich weiß man nur,  
wenn man wenig weiß;  
mit dem Wissen wächst der Zweifel*

**J. W. Goethe**

*Two voices are there;  
One is of the sea,  
One of the mountains:  
Each a mighty Voice*

**W. Wordsworth**

## Ringraziamenti

Ed eccoci giunti alla fine di questi tre anni di dottorato.

Un lungo percorso scientifico espressione innanzitutto dell'esperienza umana maturata dal contributo vitale derivante dall'incontro di diverse persone che, in un modo o nell'altro, hanno portato alla mia crescita culturale e non solo.

Desidero esprimere prima di tutto la mia affettuosa gratitudine verso Sandra, tutor che mi ha costantemente guidato sin dai miei primi passi nel mondo della ricerca, lasciandomi al tempo stesso totale autonomia e libertà di scelte. Grazie mille per la disponibilità, le giornate sul campo, i saggi consigli, per aver condiviso insieme infiniti ragionamenti, per le critiche costruttive e per il sempre presente supporto in questi anni.

Un sentito grazie va al co-tutor Nino, Prof. Gaetano Robustelli di UniCal, per la sua immensa disponibilità, per le numerose campagne sul campo in Calabria e per le proficue discussioni che ne sono derivate.

Un ringraziamento sincero va al Dott. Michele Soligo e alla co-tutor Prof.ssa Paola Tuccimei, dell'Università RomaTre, per avermi aperto le porte del loro laboratorio e avermi introdotto al mondo delle datazioni geocronologiche.

Un ringraziamento particolare va ai due referee Dr. Paolo Stocchi e Prof.ssa Niki Evelpidou per la loro attenta lettura critica al manoscritto e per gli interessanti spunti di approfondimento che hanno migliorato l'elaborato finale.

Ringrazio poi il Prof. Valentino Di Donato per le analisi biostratigrafiche e per aver allietato le mattinate con provocanti ma sempre stimolanti conversazioni di carattere politico, il Prof. Stefano Mazzoli per gli aspetti tettonici della Piana Campana e la Prof.ssa Giuseppina Balassone per le analisi mineralogiche dei campioni di coralli. Grazie inoltre al Dr. Ettore Valente per i suoi consigli ed il supporto durante le elaborazioni in ambiente GIS e alla disponibilità del Dr. Marco

Meschis con cui ho affrontato le problematiche riguardante il metodo di correlazione sincrona per l'area di Polvica.

Non posso poi non ricordare e ringraziare vivamente chi mi ha accolto durante i miei soggiorni all'estero contribuendo a migliorare il progetto di ricerca tesi: Prof. Ioannis Papanikolau, dell'Agricultura University of Athens e Prof. Alessio Rovere, MARUM-University of Bremen, a cui sono riconoscente per avermi dato l'opportunità di approfondire lo studio di terrazzi marini deposizionali durante la campagna a Curaçao, Antille Olandesi e per la possibilità di contribuire alla realizzazione di WALIS, assieme a Dr. Matteo Vacchi e Prof. Alessandro Fontana che ringrazio.

Infine, non certo per importanza, un ringraziamento particolare agli amici di sempre, ai compagni di scalate (non solo metaforiche), alle nuove amicizie nate durante il dottorato e ai colleghi/amici del gruppo giovani AiGEO per i traguardi raggiunti insieme e per i tanti progetti futuri ancora da realizzare.

*Last but not least*, un grazie di cuore va alla mia famiglia che mi ha sempre sostenuto durante questa avventura e un pensiero particolare va alla piccola Greta per avermi strappato un sorriso anche nei momenti di maggior sconforto.

## Contents

Abstract .....	10
1. Introduction .....	13
2. Sea Level indicators .....	18
2.1 Marine terraces and wave-cut platforms.....	21
2.1.1 Cliff erosion and shore platform formation mechanisms and modelling .....	25
2.1.2 Nomenclature of the geomorphological elements of marine platforms	33
2.1.3 Other erosional sea level indicators .....	34
2.2 Depositional indicators .....	37
2.3 Sedimentological indicators.....	39
2.4 Biological indicators .....	40
2.5 Archaeological indicators .....	41
3. Pleistocene sea level curves .....	43
3.1 Eustatic and Relative Sea level change .....	51
3.1.1 Eustatic sea level change.....	51
3.1.2 Relative Sea level changes .....	53
4. Methods and materials .....	57
4.1 Synchronous correlation of multiple paleoshorelines method .....	58
4.2 Mineralogical characterization .....	59
4.3 Dating methods .....	60
4.3.1 Sample preparation.....	63
4.4 Stable isotope analysis .....	65
5. Geological framework.....	66
5.1 Geological setting .....	66
5.2 Quaternary shorelines along the Tyrrhenian margin of the southern Apennines .....	68

6. New data on late Quaternary paleoshorelines in the Southern Apennines, Italy .....	71
6.1 <i>Evolution of the Campania Plain Quaternary coastal graben (southern Apennines): constraints from raised paleoshorelines</i> .....	71
6.1.1 Introduction .....	71
6.1.2 Materials and methods.....	74
6.1.3 Geological background.....	76
6.1.4 Geomorphological features of the northern boundary of the southern Campania Plain.....	79
6.1.5 The paleoshorelines in the northern margin of the southern Campania Plain.....	83
6.1.6 The buried paleoshoreline remnants in the southern mountain front of Mt. Fellino ridge.....	85
6.1.6.1 The continental deposits burying the paleoshoreline remnants:.....	85
6.1.6.2 Geomorphological, stratigraphical and structural features of the buried paleoshoreline remnants .....	89
6.1.7 The marine terraces outcropping in the piedmont of Mt. Fellino ridge .....	100
6.1.8 Discussion .....	102
6.1.8.1 Paleoshoreline correlation.....	106
6.1.8.2 Implications on the evolution of the Campania Plain coastal graben .....	108
6.2 <i>Tectonic implications of raised Quaternary paleoshorelines in the NE sector of the Campania plain, southern Italy</i> .....	111
6.2.1 Introduction .....	111
6.2.2 Synchronous correlation of multiple paleoshorelines with multiple highstands method applied at the Polvica case study.....	118
6.2.3 Tectonic quantification.....	128
6.2.4 Concluding remarks on the Campania Plain case study .....	132

6.3 <i>Sea level fluctuations along the raised Tyrrhenian margin of northern Calabria-Basilicata (southern Italy): New U-series dating of late Quaternary paleoshorelines</i> .....	134
6.3.1 Introduction .....	134
6.3.2 Geological framework .....	138
6.3.3 Materials and methods.....	141
6.3.3.1 Geomorphological-stratigraphical approach to the study of the marine terraces .....	141
6.3.3.2 U-series dating .....	143
6.3.3.3 Mineralogical characterization of corals.....	144
6.3.4 Geomorphological and stratigraphical features of the marine terraces .....	146
6.3.4.1 The lowest paleoshorelines - T1 .....	149
6.3.4.2 The T2 marine terrace in the Basilicata coastal stretch .....	152
6.3.4.3 The T2 paleoshoreline in the Scalea site .....	157
6.3.4.4 Marine terraces and sea level markers at around 20 m a.s.l.: the T3 paleoshoreline .....	160
6.3.4.5 The T4 paleoshoreline.....	164
6.3.4.6 The T5 paleoshoreline.....	165
6.3.5 Mineralogical analyses, U-series dating and stable isotope results ...	168
6.3.6 Discussion .....	171
6.3.6.1 Age model.....	173
6.3.6.2 Constraints to the late Quaternary uplift and inferences on the sea level history .....	180
6.3.7 Concluding remarks .....	186
7. <i>Last Interglacial sea-level proxies in the Western Mediterranean</i> .....	188
7.1 Introduction.....	188
7.2 Literature overview.....	191
7.3 Sea-level indicators.....	192

7.4 Positioning techniques and vertical datums.....	194
7.5 Age attribution .....	195
7.6 Quality of sea level and age determinations .....	200
7.7 Relative sea level data .....	203
7.7.1 Spain (Mediterranean Coasts and Gibraltar Strait) .....	204
7.7.1.1 Andalucía .....	204
7.7.1.2 Murcia .....	206
7.7.1.3 Comunitat Valenciana (Alicante province) .....	206
7.7.1.4 Islas Baleares (Mallorca) .....	207
7.7.2 Mainland France.....	211
7.7.2.1 Languedoc-Roussillon .....	211
7.7.2.2 Provence- Cote d'Azur .....	213
7.7.3 Mainlan Italy .....	215
7.7.3.1 Liguria.....	215
7.7.3.2 Toscana .....	218
7.7.3.3 Lazio.....	222
7.7.3.4 Campania .....	225
7.7.3.5 Basilicata and Calabria, Tyrrhenian side .....	230
7.7.3.6 The Ionian coast of Basilicata and Calabria .....	232
7.7.3.7 Puglia .....	234
7.7.3.8 Molise, Abruzzo and Marche.....	238
7.7.3.9 Emilia Romagna.....	239
7.7.3.10 Veneto .....	243
7.7.3.11 Friuli Venezia Giulia.....	246
7.7.3.12 Istria, Kvarner Gulf and Dalmatia .....	249
7.7.4 Corsica, Sardinia and Sicily .....	251
7.7.4.1 Corsica .....	251
7.7.4.2 Sardinia .....	254

7.7.4.3 Sicily .....	259
7.7.5 Algeria .....	265
7.7.5.1 Tipasa .....	265
7.7.5.2 Oran and Ain Techmouchent .....	266
7.7.6 Morocco.....	267
7.7.6.1 The Dhâda terrace .....	267
7.7.6.2 Cape Leona .....	268
7.7.6.3 Al Hoceima .....	268
7.8 Final remarks .....	270
7.9 Data availability.....	272
7.10 Author contributions .....	272
8. Discussion on the new data in the regional framework and concluding remarks .....	273
References .....	281
Appendixes.....	327

## Abstract

The aims of this PhD research project are both a reconstruction of the surface uplift of the Tyrrhenian coastal side of the southern Apennines in the Middle-Late Pleistocene time span and a field data acquisition on Relative Sea Level (RSL) indicators in order to better constrain the sea level change for the western sector of the Mediterranean. The field study has been based on detail scale morphotectonic and stratigraphic analyses, which have been carried out by geomorphological analyses on topographic maps and Digital Elevation Models (DEM), on two key areas of the Tyrrhenian coast: the Campania Plain margin and the Basilicata-northern Calabria area. The morphostratigraphical analyses have been integrated by new U-series dating of calcite deposits (speleothems and a calcite vein) and coral *C. caespitosa* samples. The main topics and results can be summarised as follows:

- A study of formerly known and new outcrops of marine terraces has been carried out in the NE margin of the Campania Plain (Fellino Mt.), a Quaternary coastal graben located in the Tyrrhenian side of the southern Apennines;
- Raised paleoshorelines assigned to two raised paleoshorelines (labelled T1 and T2) were detected along Fellino Mt. at variable elevation;
- The synchronous correlation method, based on U-series dating on a calcite vein post-dating the age of T2 terrace, allow relating the T2 and T1 identified paleoshoreline to MIS 9 and MIS 7 respectively;
- Structural data collection allow defining the geometry and kinematics of the main Quaternary structures filling, hence, the existing gap along the borders of the Campania plain. The study reports the first field evidence of Quaternary extensional tectonics affecting the

Campania Plain borders. The identified paleoshorelines are displaced by a major extensional fault zone c. E-W oriented (namely Polvica Fault), and several faults c. N-S and NW-SE oriented with less displacements;

- The uplift fault-related rate of the Polvica Fault, the throw rate and the Earthquake Recurrence Interval (ERI) have been estimated in c. 02-06 mm/y range, 0.4 mm/y and c. 1100 y respectively. The uplift rate is characterised by a spatially variation along the strike of the Polvica Fault;
- A flight of paleoshorelines up to c. 60 m a.s.l. located along the Tyrrhenian sector of the Basilicata - northern Calabria has been investigated by detailed geomorphological-stratigraphical analyses. The flight of paleoshorelines has been constrained in the early 1990s with AAR and U-series dating but the new U-series dating provided in this study has allowed the reconstruction of a chronological framework for the analysed sea level markers. The U-series dating have been performed on *C. caespitosa* corals and calcite concretions, either predating or postdating the paleoshorelines. In particular, the U-series dating allow correlating the T1 terrace at 5 m a.s.l. to the MIS 6e, the T2 at c. 16 m to MIS 5c, the T3 terrace at c 22 m a.s.l. to MIS 5a, the T4 terrace at 35 m .s.l. to the MIS 5e and the higher T5 terrace to MIS 7. The new findings shed light on the Quaternary evolution of the Basilicata area – northern Calabria;
- A Relative sea level (RSL) curve during the Middle-Late Pleistocene time span for the northern Calabria-Basilicata Tyrrhenian sector has been constructed;

- A mean uplift rate of  $0.235 \pm 0.01$  mm/y since the Last Interglacial has been evaluated. The uplift rate is one order of magnitude larger than estimation based on former dating;
- The new data provide new constraints to both the long term evolution of the Tyrrhenian margin of the southern Apennines and the late Quaternary sea level fluctuations in the western Mediterranean. The elevation of MIS 5a, 5c and 6e peaks and the time span of 5a have been evaluated. Such elevations may better constrain ice sheets volume variation during the late Quaternary.
- The geomorphological reconstruction has demonstrated that a mere sequential correlation may be misleading in the interpretation of flights of marine terraces, and indicates that multiple age controls are crucial to unravelling the complex interaction between uplift and sea level fluctuations in uplifted coastal areas;
- A review of MIS 5 paleoshorelines along the western Mediterranean (Spain, France, Italy, Istria, Kvarner and Dalmatia, Algeria and Morocco) has been compiled in the framework of the Word Atlas of Last Interglacial Shorelines (WALIS).

*Si no escalas la montaña,  
jamás podrás disfrutar el paisaje*

**P. Neruda**

## **1. Introduction**

The tricky interaction among the sea level fluctuations, tectonic uplift and the sedimentary inputs controls the occurrence of a flight of marine terraces and the worldwide formation of coastal plains (Lajoie, 1986). The elevation of raised paleoshorelines, and more properly of the wave-cut platform's inner-edge have been broadly used to reconstruct both large-scale and differential vertical motions during the Quaternary. The surface uplift is the "*displacement of the Earth's surface with respect to the geoid*" (England and Molnar, 1990) or using a very good approximation such displacement could be referred with respect to the mean sea level, whenever former sea level has been recorded in some proxies labelled Relative Sea Level (RSL) indicators (e.g., tidal notches, wave-cut platforms or marine terraces).

For surface uplift studies, the elevation of marine terraces or any sea level indicator, represents a first order absolute marker to record vertical crustal motions. However, any change in the rates of the vertical movements can be inferred only if the age of the RSL indicator (e.g., marine deposits associated with the marine terraces) has been well constrained. A study on Quaternary marine terraces, which have been tectonically deformed, can provide several tectonic information such as (I) normal fault-related uplift rates; (II) how slip rate varies along the strike of a fault; and/or (III) Earthquake Recurrence Interval (ERI) and (IV) possible change of uplift through time (Meschis et al., 2018). These kinds of information are of great interest for their tectonic implications on long-term seismic hazard assessment. Indeed, paleoshorelines take shape in line with high sea level peaks

(Anderson et al., 1999) reflecting ongoing coastal uplift. In the last decades, an increasing number of coastal geomorphology studies focused on evidences of highstands during the Quaternary has been carried out due to the growing interest in global warming and climate changes. In fact, remnants of RSL indicators related to highstands higher than modern mean sea level may provide useful insights to the past sea level behaviour, which is crucial to better understand possible future scenarios. However, besides the vertical motions of land, relative sea-level changes stem from the contribution of mean sea surface variations that are relative to the solid Earth. Mean sea surface variations are primarily driven by ice-sheets fluctuations (changes in mass) and, under the eustatic approximation (rigid, non-gravitating Earth) are globally uniform. However, because of Earth deformation and gravity, they are regionally-varying and decay in time. Then, vertical motions due to tectonics/geodynamics/sediment compaction etc. also come into play (Rovere et al., 2016b; Stocchi et al., 2018).

A consequence of such dynamics is that any sea-level indicator on the surface of the Earth is a Relative Sea level indicator. Thus, any reconstruction of the tectonic component is affected by an unavoidable circularity problem, that is the elevation of paleoshorelines in stable areas are used to reconstruct past sea level, but sea level curves are used to calculate uplift rates. However, in some instances the imprint to the RSL by glacio-hydro-isostatic adjustments due to Earth's deformation in response to changing ocean volumes is not the main component. This occurs when elevation of paleoshorelines is at least some  $10^1$ - $10^2$  m higher than that of correlative paleoshorelines from stable areas in the same geographical region. In those instances flights of marine terraces are commonly observed, which are the main expression of crustal uplift and, particularly in regions far away from the ice sheets, any sea level marker can measure a RSL change that is not too different from the eustatic (ocean averaged signal).

The neotectonics reconstructions of an area can be well assessed by morphotectonic studies on coastal features formed during the Quaternary time span. The sea level change is observed by satellite measurements, tide gauges, archaeological proxies and geological respectively, from the shorter to the long-time scale. However, any technique is not able to provide direct measurements of former sea level change, which, instead, is calculated and corrected from *noise* as better explain in **Section 3.1** Eustatic and Relative Sea level change). In Section 3.1 an in-depth description on the main processes and meaning of the relative and eustatic sea level change will be illustrated and in addition particular attention will be pointed out on the dating techniques used to constrain past sea level indicators (**Section 4.3** Dating methods).

This study focuses on sea level markers from the Tyrrhenian side of Southern Apennines mountain belt. The southern Apennines are a fold-and-thrust belt formed from the interaction between the African (Adriatic microplate) and European plates starting from the early Miocene and continuing until the early part of the Middle Pleistocene (Patacca et al., 1990; Sartori, 1990). Starting from late Tortonian times, the shortening in the mountain chain has been coeval with the extension that led to the opening of the Tyrrhenian back-arc basin (Elter et al., 1975; Scandone, 1979). Such extension led to the formation of oceanic basins such as the Vavilov and Marsili basins, and the drowning of the innermost portion of the chain. After the thrusting or shortening phase, the Southern Apennines have been involved in a NE-SW extension, that is still active. In this study, the surface uplift, in terms of uplift rate, has been estimated for two key areas of the Tyrrhenian Sea coastal margin of the southern Apennines mountain belt by means of detail-scale geomorphological and morphotectonic investigations, integrated with geochronological constrains on paleo RSL indicators outcropping in horst blocks of the Tyrrhenian back-arc basin, specifically the NE edge of Campania Plain

Quaternary coastal graben and the coastal sector of Basilicata – northern Calabria. The two study areas have been chosen for their strategic role. In fact, while a large number of indirect data (geophysical investigations or deep boreholes) are available for the Campania Plain (e.g., Barra et al., 1999, Romano et al., 1994; Florio et al., 1999; Cella et al., 2007) there is still a lack of field Quaternary data useful to the reconstruction of the vertical motions recorded by horst blocks at the graben boundaries, more in general, the Quaternary tectonic evolution of the graben.

The second study area, Tyrrhenian sector of Basilicata – northern Calabria, is placed between the Campania coastal belt, in the north, which is considered stable since the Last Interglacial (Ascione and Romano, 1999), and southern Calabria, in the south, which suffered strong uplift in the late Quaternary (e.g., Westaway, 1993; Dumas et al., 1987). However, the boundary between the them is poorly defined (Ferranti et al., 2006). The new data allow a reconstruction of the Quaternary evolution of such coastal sector, which may contribute to implement geodynamic models. Overall new findings have been included in the compilation of a database of the Last Interglacial sea level proxies in the Western Mediterranean in the framework of a Word Atlas of Last Interglacial Shorelines (WALIS).

The study that has been developed with this research has been synthesised in four papers, which collectively compose Chapters 6 and 7 of this dissertation. Of the four papers, three of them have been submitted to peer reviewed journals and are at present under revision, and one is in preparation. In particular, in Chapter 6 the results of the studies carried out in the Campania Plain and Basilicata-northern Calabria coastal stretch are reported, and in Chapter 7 is reported the review on the MIS 5 paleoshorelines in the western Mediterranean.

Specifically:

Manuscript 1 (Section 6.1), *Evolution of the Campania Plain Quaternary coastal graben (southern Apennines): constraints from raised paleoshorelines*, by Cerrone, C., Di Donato, V., Mazzoli, S., Robustelli, G., Soligo, M., Tuccimei, P., Ascione, A. Submitted to *Geomorphology*.

Manuscript 2 (Section 6.2), *Tectonic implication of raised Quaternary paleoshorelines in the NE edge of the Campania Plain, southern Italy*, by Cerrone, C., Roberts, G.P., Ascione, A., Meschis, M., Mazzoli, S., Robertson, J. In preparation.

Manuscript 3 (Section 6.3), *Sea level fluctuations along along the raised Tyrrhenian margin of northern Calabria - Basilicata (southern Italy): New U-series dating of Late Quaternary paleoshorelines*, by Cerrone, C., Ascione A., Robustelli, G., Soligo, M., Tuccimei, P., Balassone, G., Mormone A. Submitted to *Quaternary Science Reviews*.

Manuscript 4 (Chapter 7), *Last Interglacial sea-level proxies in the Western Mediterranean*, by Cerrone, C., Vacchi, M., Fontana, A., Rovere, A. Submitted to *Earth System Science Data*.

## 2. Sea Level indicators

Since the first scientific descriptions of raised Quaternary paleoshorelines (Darwing, 1846; Hutton, 1885; Lyell, 1837), an increasing attention has been devoted to the study of past interglacial periods due to the growing sea level interest related to the global warming issue. The focus of this paragraph is to illustrate the morpho-bio-stratigraphical evidences of the past sea level with a brief mention to the archaeological indicators.

A Relative Sea Level (hereafter as RSL) change occur whenever the elevation of marine forms (e.g. shore platform) or deposits (e.g. cobble beaches) is not in line with the elevation which is supposed to occupy in a modern analog (Rovere et al., 2016a). Many different reasons could justify that elevation gap such as ice volume changes, isostatic crustal adjustments, tectonics force or stratigraphic reasons as compaction-related subsidence. Furthermore, a Relative Sea Level indicator or marker is any evidence of past sea level equivalent to the “*sea level index point*” used in Holocene studies (Rovere et al., 2016 and references herein). Three properties characterize the validity of an RSL indicator. Firstly, the elevation respect to the modern mean sea level (MSL) and position of an RSL indicator need to be referred to a vertical datum and geographic system respectively; in addition, the vertical displacement, which could be relative or absolute, from a previous sea level must be known (see section 3. Pleistocene sea level curves) and finally, an age constrain, relative or absolute, must be provide for the RSL indicator (see section 4.3 Dating methods). To reconstruct paleo-RSL, within its uncertainties, the first two properties described needed to be known and then, from the age of some RSL indicators, some correction, e.g. post-depositional land movement (PD) and glacial isostatic adjustment effects (GIA), could be applied (Rovere et al., 2016a). Rovere et al., 2016 proposed some equations, reported in **Figure 1**, in order to have a standardized procedure to calculate an RSL, its uncertainties and to

correct it from PD and GIA effects. It is defined elevation of an RSL indicator the vertical distance between the indicator itself and MSL, while the elevation error represents the intrinsic precision of the tool used for the measure which must be related to a vertical datum as reference: usually the zero corresponds to the modern MSL.

**Table 1**  
Relevant equations in MIS 5e paleo sea level studies, with definitions. For a calculator containing the equations in this table, see the spreadsheet in the supplementary material.

	Equation	Definitions
Eq. 1	$RWL = \frac{(U_1 + L_1)}{2}$	RWL = Reference Water Level
Eq. 2	$IR = (U_1 - L_1)$	IR = Indicative Range
Eq. 3	$RSL = (E - RWL)$	$U_1$ = Upper limit of landform in the modern analog
Eq. 4	$\delta_{RSL} = \sqrt{E_e^2 + \left(\frac{IR}{2}\right)^2}$	$L_1$ = Lower limit of landform in the modern analog
Eq. 5a	$PD = [RSL - (GIA + ESL)]$	RSL = paleo Relative Sea Level
Eq. 5b	$ESL = [RSL - (GIA + PD)]$	E = elevation of sea-level indicator (measured in the field)
Eq. 6	$PDr = \left[ \frac{ESL - (GIA + ESL)}{T} \right]$	$E_e$ = Error in elevation measurement (standard deviation)
Eq. 7a	$\delta_{PD} = \sqrt{(\delta_{RSL}^2 + \delta_{GIA}^2 + \delta_{ESL}^2)}$	$\delta_{RSL}$ = uncertainty of RSL (standard deviation)
Eq. 7b	$\delta_{ESL} = \sqrt{(\delta_{RSL}^2 + \delta_{GIA}^2 + \delta_{PD}^2)}$	PD = Post-depositional displacement uplift/subsidence
Eq. 8	$\delta_{PDr} = \sqrt{\left(\frac{\delta_{PD}}{T}\right)^2 + \left[\left(\frac{PD}{T}\right)^2 \times \delta T^2\right]}$	PDr = Post-depositional displacement uplift/subsidence rate
		$\delta_{PDr}$ = uncertainty of PDr (standard deviation)
		GIA = Glacio-hydro-isostatic Adjustment contribution
		ESL = Paleo Eustatic Sea Level
		T = age of the paleo RSL indicator
		$\delta_{GIA}$ = uncertainty of GIA (standard deviation)
		$\delta_{ESL}$ = uncertainty of ESL (standard deviation)
		$\delta_T$ = uncertainty of T (standard deviation)

**Figure 1.** Equations to calculate the paleo-RSL

The accuracy of the survey instruments used to measure the elevation of RSL indicators varies, in the best condition, between 0.02/0.08 mm for a different GPS up to  $\pm 20\%$  of the elevation measured in the case of a barometric altimeter (Rovere et al., 2016a). Regarding the accuracy provided by topographic maps and digital elevation models, it depends of the scale or resolution of the map and of the DEM respectively, but in any case, up to some metres.

Both erosional and depositional processes shape a coastal landscape. Erosional sea level indicators could be imprint only in hard rock, on the contrary, soft rocks hardly record evidences of sea level change. Among the erosional indicators are included tidal notches (**Figure 2**), potholes, wave-cut platforms, whereas marine terraces are considered as depositional indicators.



**Figure 2.** Raised Holocene tidal notch at Roseto Capo Spulico (Ionian Calabria)

## 2.1 Marine terraces and wave-cut platforms

It is define marine terrace “*any relatively flat surface of marine origin*” (Pirazzoli, 2005), and/or slightly inclined seaward, which is limited by two steeper cliffs on its both sides (Pirazzoli, 2007) (**Figure 3**).

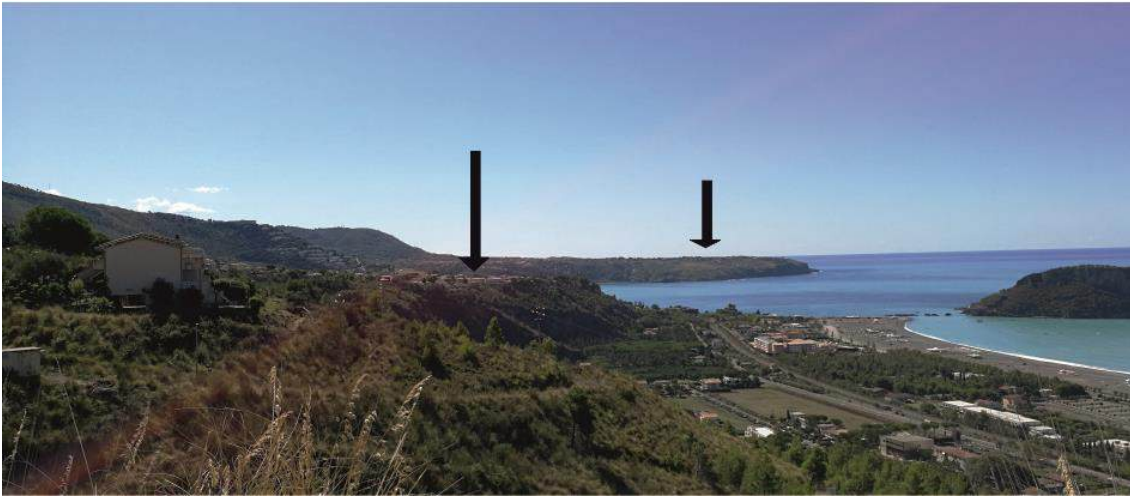


**Figure 3.** Marine terraces in northern Calabria

Along high rocky coast, two different kind of shore platforms develop, both sharing a common slightly seaward slopes, nearly a horizontal surface, but differing for the presence or absence of a significant topographic break, e.g. scarp, on the sea edge (Bird, 1976). Beyond the Bird, (1976) description referred at modern analog, marine terraces are classified as **wave-cut terraces**, in the case the marine erosional processes prevail on their formation, **depositional terraces**, when the depositional component prevail with accumulation of shallow-water and nearshore deposits, and **wave-built terraces**. The wave-built terrace term has been proposed by Gilbert, (1890) to indicate the sandy deposits found on the terraces as result of high storm waves; Gilbert’s acceptance is quite outdated and could be applied more properly to the backshore terrace definition of Johnson, (1919) (Kowalewsky, 1984). Wave-

built terrace, or continental terrace according to Johnson, (1919), is defined as a “*gently sloping coastal surface entirely constructed at the seaward or lakeward edge of a Platform, Abrasion platform wave-cut platform by sediment brought by rivers or derived from the wave cutting and drifted along the shore or across the platform and deposited in the deeper water beyond*” (Gary et al., 1972). The width of a marine terrace spans between some metres up to few km, generally 1-2 km, with a spatial extension along the coast of many kilometres.

In addition, Fairbridge, (1961) introduce the term **wave-cut platform** in order to refer the upper part of a wave-cut terrace depleted of sediments (**Figure 4**).

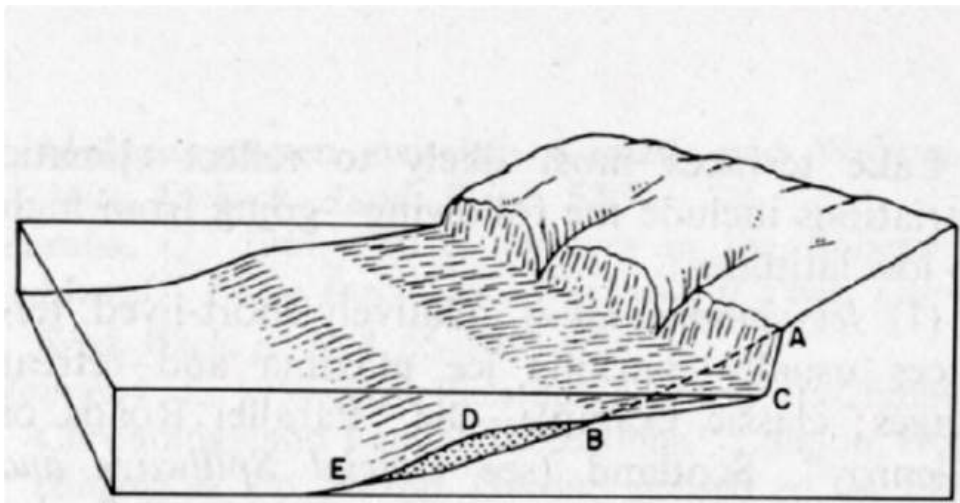


**Figure 4.** A coastal profile (from Filocamo, 2006 after Fairbridge, 1968). AC: paleo-cliff; BC: wave-cut platform and BDE a wave-built terrace

The use of the term terrace or platform is still debated and not so clear between different Authors, however, usually the marine terrace and platform coincide whenever the sediments are not present (Filocamo, 2006). To make more difficult, misunderstanding on the correct term have been arisen also regarding the time formation of the terrace. According to Fairbridge, (1961) the use of platform and terrace is suitable for fossil and modern erosional morphology in a

coastal context, on the other hands, others Authors refer to terrace for the emerged or submerged fossil morphology, while platform is related only to the modern ones (Filocamo, 2006). Often, **shore platform** is used inappropriately as synonym of marine terrace (Rovere et al., 2016a). However, shore-platform indicates a slightly uncovered flat rocky surface up to few tens of metres with an abrupt knickpoint seaward (Kennedy, 2015), while marine terraces have a higher width up to few kilometres covered by marine deposits (Rovere et al., 2016a). According to Sunamura, (1992) and Trenhaile, (1987), shore platforms are classified, based on their slope angle, between totally flat surface and those with gently inclination of  $1^{\circ}$ - $5^{\circ}$ . The actual position of marine terrace, emerged or submerged, is the product not only of the sea level stand but also of vertical tectonic movements, e.g. uplift, subsidence, faults, tilting). To evaluate the coastal uplift of an area (Ascione and Romano, 1999; Gaki-Papanastassiou et al., 2009; Zazo et al., 2007), the inner edge, the intersection between the sub-horizontal terrace surface and the high inclined cliff, of marine terraces is considered a good RSL indicator in the case it is not hidden by scree deposits. However, in the case the inner edge is covered by continental deposits, its position could be inferred assuming the inclination of both the surface and the cliff or calculating the thickness of the colluvium deposit. Carobene, (1980) outlines the complexity of a marine terrace formation as a polyphasic processes. The origin of a marine terrace is articulated in different phases and the physical aspects of wave-cut platform formation will be face on in Section 2.1.1 Cliff erosion and shore platform formation mechanisms and modelling. According to Carobene, (1980) the abrasion strength of a marine transgression firstly shapes the coastline landscape, while during a stillstand, relative stability between the sea level and the coastline, the terrace extends its width by cliff-retreat and then the marine “sedimentary body”, made up of organic and detrital materials, will be formed. Finally, during a regressive phase, when there is a lowering of the sea level, both erosive and

depositional processes, depending of sea retreat speed, reshape the “sedimentary body” (Carobene, 1980). As better explain in the next paragraph, the erosional processes are the result of the direct action of the waves energy, chemical and bioerosion processes. Only hard and solid rocks could record erosional RSL indicator, whereas on soft rocks RSL indicators are not preserved for long time.

### 2.1.1 Cliff erosion and shore platform formation mechanisms and modelling

Even though since the end of XIX century many studies addressed to platform formation and their evolution, Sunamura is considered a pioneer to have correlated, for the first time, cliff erosion with the erosive force of waves.

According to Sunamura, (1977), shore platforms and wave-cut terraces are the product of wave erosion of a receding coastal cliff. Two main forces play an essential role in a cliff erosion process: (I) the “assailing force of the waves” ( $f_w$ ) and (II) the resisting force ( $f_r$ ) of the cliff lithology. (1) Hydraulic, i.e. compression, tension, cavitation and wear, (2) abrasive and (3) wedge actions are part of the assailing forces (I), whereas mechanical properties, i.e. compressive and tensile strength and wear resistance, and structural aspects, i.e. joints, faults and stratification, form the resisting forces (II) of the rocks (Sunamura, 1977 and reference therein).

The abrasive action is due to the moving of pebbles and boulders against the cliff due to the energy waves, which pushes also compressed air into fissures generating the so-called wedge action. The physical and, depending on the lithology, chemical weathering in addition to the continuous stress produced by the action of the waves reduce the resisting force (II). In the case, the assailing forces are greater than the resisting ones a cliff erosion occurs.

Sunamura (1977), using a wave tank and an ideal cliff inclined of  $60^\circ$ , simulated natural conditions in order to connect and quantify the erosive force produced by waves with the sea cliff erosion.

He concluded that the erosive rate, the ratio between the horizontal distance from the pre-eroded face and the time, is directly proportional to the erosive force of the waves. To summarize up that relation:

$$\delta X / \delta t \propto F \quad (1)$$

where  $F$  depends of  $f_w$  and  $f_r$  according to the following law with  $K$  as constant:

$$F = K \ln (f_w / f_r) \quad (2)$$

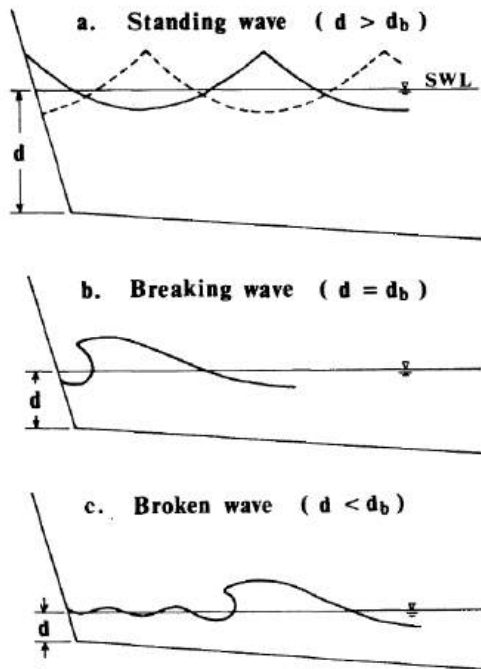


FIG. 8.—Wave types in front of cliff

Figure 5. Different kind of waves against a rocky coast (Sunamura, 1978a)

As a result, erosion occurs whenever the erosive force ( $F$ ) is greater than 0, so when the assailing force ( $f_w$ ) > than the resisting force ( $f_r$ ). Starting by that assumption, Sunamura (Sunamura, 1978a, 1978b) examines in depth the mechanism of shore platform formation, which has been studied firstly by Dana in the middle nineteenth century (1849) (Bartrum, 1926) and many others researchers lately (Sunamura, 1978 and reference therein), but they focused mainly on weathering processes and rocks properties instead of taking into account also the waves dynamics. Sunamura, 1978a used as a case

history the SE platforms of Japan, Pacific Ocean, on a volcanic bedrock along the 20 km Izu Peninsula coast concluding the result of cliff retreat due to the nearshore wave action is the development of shore platforms/wave-cut terrace. Sunamura pointed out the attention on the breaking waves on the shore platform formation in front of a cliff, instead of the standing and broken waves (**Figure 5**)

The latter occurs when the water depth at the cliff base ( $d$ ) is minor than the relative magnitude of the breaking depth of incoming waves ( $d_b$ ). The bottom friction and the turbulence, among other processes, cause a loss of energy proportionally to the distance from the surf zone area, where the waves break (breaking point), whereas the standing waves ( $d > d_b$ ), forming by reflection from

the cliff, have not enough force against the cliff itself. Hence, the breaking waves, which occur when  $d$  is equal to  $d_b$ , are the main agent during the formation of shore platforms along high rocky coast (Sunamura, 1978a) and, in particular, the elevation of the platform depends on the height of this kind of waves in the first phase of platform cutting. However, the initial platform height depends on time and space, as its variables  $d$  and  $d_b$  do. (I) The topography of sea bottom in the nearshore, (II) the gravitational effects of planets and satellites on the tides (astronomical tides), and (III) the effects of storms on the sea level influence the variable  $d$ , while  $d_b$  is function of the height and period of the incoming waves and of the submarine slope gradient (Sunamura, 1978a). Consequently, platform elevation could vary in a same region because of the initial height. For better understating how the shore platform width increases after the initial formation due to the height of the breaking waves in front of a cliff is needed to quantify the assailing and resisting forces of waves and coastal bedrock respectively in addition to considering how the platform formation responds on the effects of time and finally, “*the relative movements of land and se-level*” (Sunamura, 1978a). Taking into account this consideration, Sunamura, 1978b tried to answer at that problem.

Previously to Flemming, 1965, few attempts to model mathematically the shore platform formation using stable sea level have been conducted but lacking in important considerations. For example, Flemming (1965)’s model has not considered the principle of equilibrium; it means that the rate of cliff recession never falls to zero. On the contrary, the model proposed by Sunamura (**Figure 6**) is based on the following conditions: (I) stable sea level; (II) homogeneous and unaltered bedrock and (III) the constant removal of sediments from the cliff retreat with a submarine platform with constant inclination.

For the model has been taken into account previously information of cliff erosion and coastal hydraulics, e.g., erosion rate (Sunamura, 1977); wave height attenuation (Ijima et al., 1956); shallow water wave length and water depth

relationship (Eagleson and Dean, 1966); abrasive action of sand sediments (Sunamura, 1972), which allow Sunamura to formulating the following distance-time equation:

$$x_e = \lim_{t \rightarrow \infty} x = K/\beta \quad (3)$$

where  $K$  and  $\beta$  represent a constant with no and  $L^{-1}$  units respectively, whereas  $x$  is the “recession distance of the cliff during the period  $t$ ” (Sunamura et

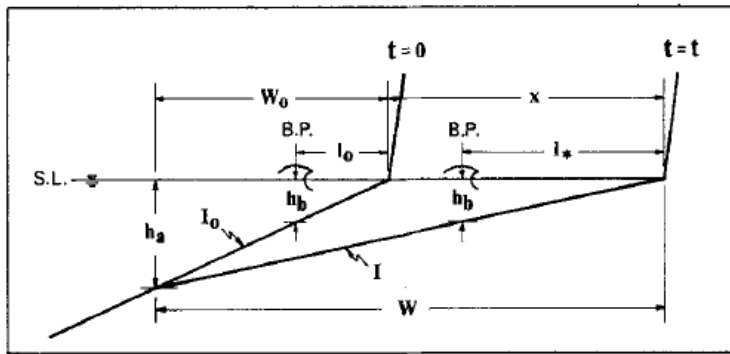


Figure 1. Platform development model.

Figure 6. Schematic cartoon of the platform mathematic development model of Sunamura, 1978b

platform development and its width increase by cliff erosion, but at the same time a wider platform attenuates the wave energy to equal the resisting force ( $f_r$ ) (Figure 7). Hence,  $t$  is a measure of speed to reach the equilibrium, in fact with a small  $t$ , in a short time the platform is in equilibrium, on the contrary with a large  $t$ . Moreover, it is worth to note (I) the former topography due not influence the final one and (II) the lithology, in the case other factors does not change, influence the size and shape of the platform, i.e. weak rocks tend to produce wider and flatter platforms (Sunamura, 1978b). It is worth to note, the elevation of shore platforms with a scarp on the seaward edge presents differences from a place to other along coast e.g., Bird and Dent, 1966; Phillips, 1970; Sunamura, 1978a; Takahashi, 1974, as a results of many factors such as the wave intensity (Johnson, 1931; Kirk, 1977), lithological resistance and structures, e.g. joints and faults (Bird and Dent,

al., 1978b). That means at a growing of the submarine platform corresponds a lowering of the wave action against a cliff, or in other words the assailing force ( $f_w$ ) generates a

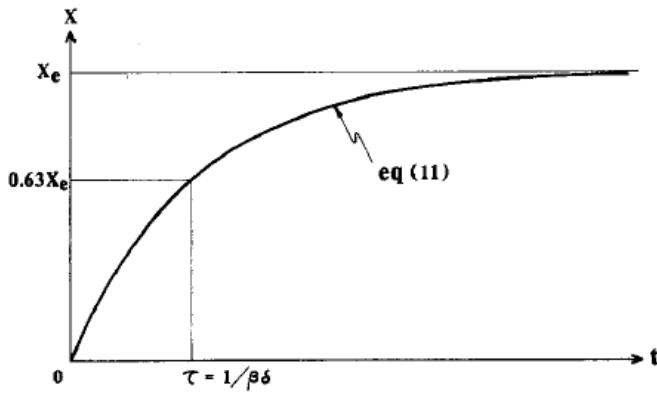


Figure 2. Characteristics of eq (11).

Figure 7. Graphic representation of the eroded distance-time equation (eq. 3) (Sunamura, 1978b)

1966; Kirk, 1977; Phillips, 1970), tidal gauge and finally weathering of the rocks (Bartrum, 1916; Bird and Dent, 1966; Hills, 1972; Johnson, 1931; Trenhaile, 1978; Wentworth, 1938). It is not easy to separate every component and evaluate the role of each one during the platform

elevation processes. However, some attempts have been made by Kirk, (1977), among others Authors, between the platform elevation and the exposure to the wave action, concluding that there is a strictly positive correlation between rock strength and mean elevation of platform, e.g. soft rocks are at a lower elevation (Trenhaile, 1987).

Sunamura, 1991 has quantitatively correlated the role of wave intensity and rock strength (Sunamura, 1983) with the platform elevation by a simplified laboratory experiment.

Based on previously field and laboratory studies (Sunamura, 1978a, 1975 respectively), Sunamura, 1991 point out the importance of waves breaking in front of a rock cliff in shore platform formation processes combined with a trend of pressure attenuation which has a maximum value at  $\sim$  the still water level (SWL) to decrease, according an exponential function (eq. 4), below sea level:

$$p = p_0 e^{a\left(\frac{z}{h}\right)} \quad (4)$$

where  $p_0$  is the pressure at SWL,  $p$  is the pressure below sea level at the negative  $z$  elevation,  $h$  "is the water depth at the wall" and finally  $a$  is a reduction coefficient between 1 and 2 correlated with experimental conditions. The assailing

force ( $f_w$ ), due to the linear relationship between the  $f_w$  of the waves and the intensity of dynamic pressure, has a vertical distribution (**Figure 8**) according to an exponential law (eq. 5):

$$F_w(z) = F_w e^{\beta(z/h)} \quad (5)$$

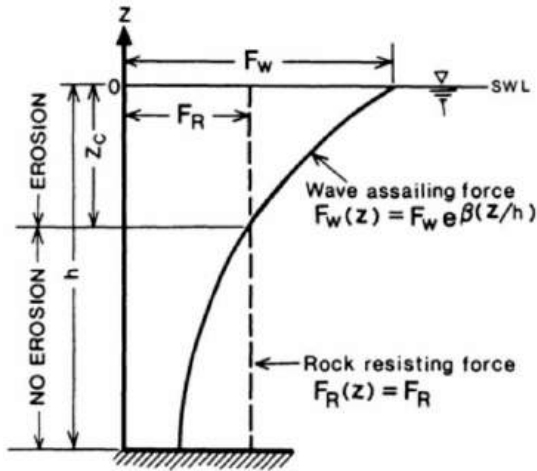


FIG. 1.—Schematic diagram showing vertical distribution of the assailing force of waves and the resisting force of rocks.

**Figure 8.** Assailing ( $F_w$ ) and resisting ( $F_r$ ) forces behavior along a sea-cliff (Sunamura, 1991)

with  $F_w$  as assailing force at SWL and  $\beta$  represents a reduction coefficient of it. Assuming a constant valued of the resisting force of the rocks  $F_r$  along the sea-cliff, so erosion occurs only in the case  $F_w > F_r$ . Starting from these principles, the Sunamura, 1991, experiment using a wave flume on different (soft and hard) lithological rocks, with a constant  $T$  period of waves.

The results of the experiment have been reproduced in in **Figure 9**, where is perfectly visible the changes in the profile of a sea-cliff and the development of a wave-cut notch, which in field condition, evolves into a wave-cut platform due to the progressively notch collapse.

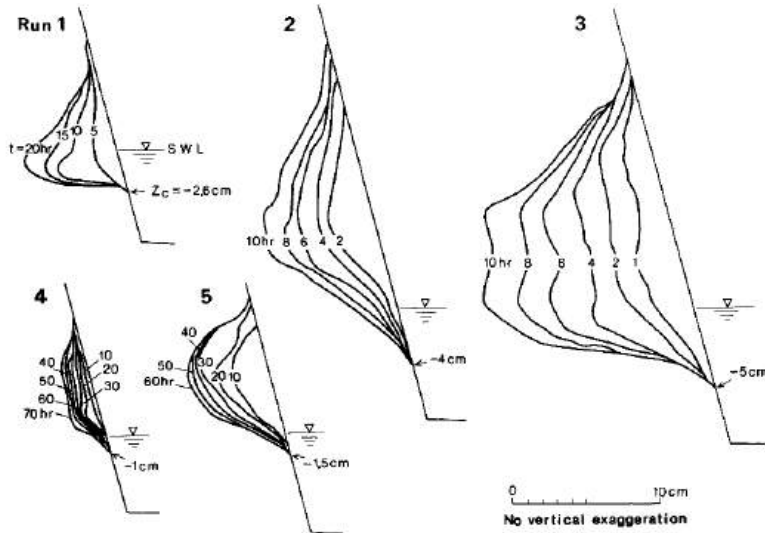


FIG. 2.—Temporal variation of cliff profile.

**Figure 9.** A cliff profile change at different time  $T$  and formation of wave-cut notch (Sunamura, 1991)

It is worth to note that the erosion occurs to a determined point ( $Z_c$ ) below the sea-cliff for the effects of the water buffer action (Sunamura, 1975).

$Z_c$ , the value below which no erosion occurs, represent the

elevation of the wave-cut platform. That elevation, expressed by eq. 6 from the wave-flume experiment of Sunamura, 1991, as argued also by Gill, 1972 and Trenhaile, 1987, is related to the rock strength:

$$\frac{Z_c}{h} = -0.17 [5.8 + \ln \left( \frac{pgH_b}{S_c} \right)] \quad (6)$$

where  $\left( \frac{pgH_b}{S_c} \right)$  is the wave-rock parameters. It means, considering the other parameter constant, the wave-cut platforms in soft rocks are lower than the ones cut in hard rock. Moreover, the difference in platform elevation in two different sites, expressed by  $\Delta Z_c$ , is linearly related with the strength ratio  $\frac{S_{c1}}{S_{c2}}$  with  $S_{c1} > S_{c2}$

(**Figure 10.**) according the eq. 7:

$$\Delta Z_c = -0.17h \ln \left( \frac{S_{c2}}{S_{c1}} \right) \quad (7)$$

so,  $\Delta Z_c$  depends on the wave by the factor  $h$  and by the rock strength.

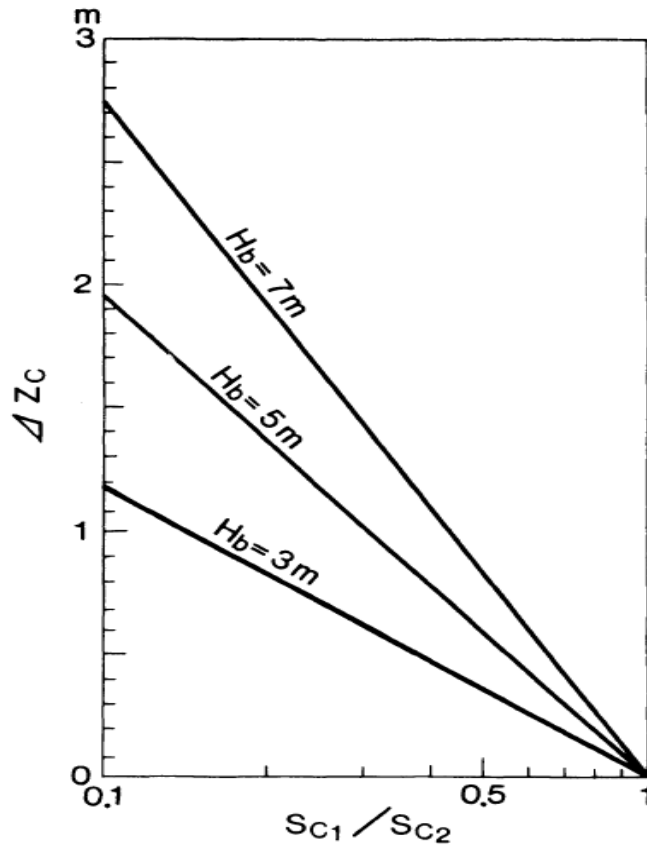


FIG. 4.—Relationship between differences in platform elevation,  $\Delta z_c$ , and strength ratio,  $S_{c2}/S_{c1}$ , at two sites, for three breaker heights:  $H_b = 3, 5,$  and  $7$  m.

**Figure 10.** Biplot between differences in platform elevation and strength ratio (Sunamura, 1991)

### 2.1.2 Nomenclature of the geomorphological elements of marine platforms

Hereafter, the principal morphological elements which constitute a wave-cut platform will be briefly described (**Figure 11**).

The position of a paleoshoreline is indicated as **inner edge** or paleoshoreline angle. The inner edge is considered an excellent paleo sea level indicator because it represents the maximum shoreline elevation reached during a transgression phase. Morphologically, the inner edge is the point between the wave-cut platform surface and the associated former cliff, identified as a knickpoint in the topography. It appears mostly in hard rocks, whereas in presence of soft rock the inner edge usually is covered by colluvial materials making very hard its identification in the field. The **outer edge** or outer rim is intersection between the seaward border of a terrace and the internal cliff. The **terrace surface** is the flat or slightly inclined ( $1^{\circ}$ - $3^{\circ}$ ) geomorphic surface toward the sea bounded by a cliff (or scarp). The angle of inclination  $\alpha$ , measured between the outer and inner edge, is expressed in degrees and, in case of tectonic displacement, could be emphasized and/or against the sea. The **width** of a terrace is the distance between the outer and inner edge.

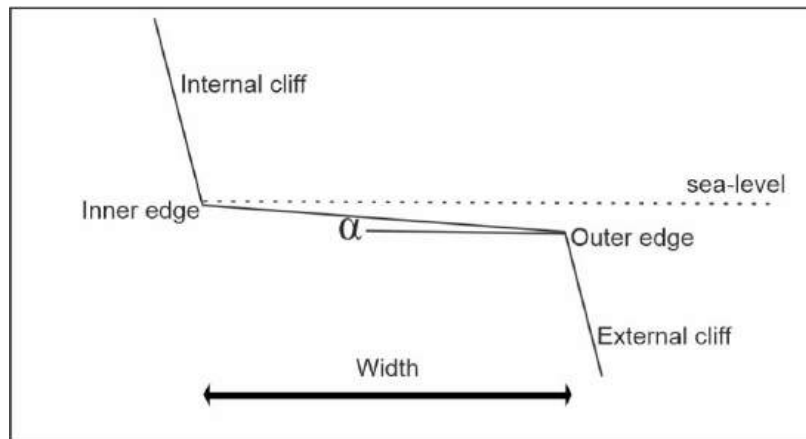


**Figure 11.** Geomorphological elements of a marine terrace, with  $\alpha$  the angle of inclination (modify after Carobene, 1980)

### 2.1.3 Other erosional sea level indicators

Among the most important erosional RSL indicators, notches, potholes, *Lithophaga lithophaga* holes and abrasion or wave-cut platforms are included. Regarding the wave-cut platforms, they have been deeply described in Section 2.1 Marine terraces and wave-cut platforms

- Layers with *Lithophaga lithophaga* holes

Due to the wide elevation range living of bivalves, they are not considered accurate indicators of former sea level. However, in the case the upper limit of *Lithophaga lithophaga* boreholes is organized in a clear and spatially continued horizontal layer, they can be correlated with others geomorphological indicators or used with a good degree of approximation as sea level indicator (Laborel et al., 1994; Pirazzoli, 1996). The vertical elevation of *Lithophaga lithophaga* spans between – 30 m b.s.l to the infralittoral zone, hence the scattered presence of *Lithophaga lithophaga* holes indicates just submersion (Filocamo, 2006).

- Potholes

It is still not clear the relationship between potholes and the former sea level. They have been found both in the intertidal and spray zone (Filocamo, 2006). According to Pirazzoli, (1996) just in sheltered areas, raised potholes indicate past sea level. Morphologically, potholes, typically of in shore platforms are smooth circular or sub-circular depression up to a diameter of few metres (Fairbridge, 1968), made up in rocky bedrock as result of abrasion action of coarse clasts moved by wave energy or chemical dissolution on limestone bedrock,. In Literature, potholes are indicated with many different terms, such as solution pans (Fairbridge, 1968), solution pools (Sunamura, 1992), and coastal pools (Pirazzoli, 1996).

- Notch

“A marine notch or nip is an undercutting several centimetres to several metres deep, left by sea erosion in coastal zones” (Evelpidou et al., 2012a), or more properly in high rocky coasts (Carobene, 1972; Kelletat, 2005; Pirazzoli, 1986), shaped roughly at the Mean Sea Level (MSL) (**Figure 12**). Tidal notches, term coined by Pirazzoli, (1986) are excellent indicators of past sea level, showing a wide lateral continuity in horizontal layers as indentations or undercuts on hard bedrock (Evelpidou et al., 2012a; Rovere et al., 2016a). The tidal notch, according to Pirazzoli, (1986), definition is referred to the midlittoral erosion form especially on limestone bedrock caused by combination of bioerosion, tide excursion, chemical dissolution on limestones, salt weathering and wave strength (Antonioli et al., 2015; Carobene, 2015; Pirazzoli, 1996). For midlittoral zone is indicated the area occupied by tidal range in addition to the average wave high (Evelpidou et al., 2012a). In Literature, as reported by Filocamo, (2006), the term tidal notch has been reported as *interdital notch* (Sunamura, 1992), *midlittoral tidal notch* (Laborel et al., 1994; Laborel and Laborel-Deguen, 1996) or as *encoches de corrosion* (Ozer, 1986). At present, notches have been reported also below the low tide level along the Bermuda coast (Neumann, 1968) or at the elevation corresponding to the high tide (Kelletat, 1988), however, tide notches take form nearby the MSL with the highest point is influenced by local tide, whereas, bioerosion, wave energy along the coast and local chemical processes determine the lowest point (Antonioli et al., 2015; Rovere et al., 2016a). Morphologically, at a longitudinal view, the tidal notches shows a recumbent-V or U shape, with the main concavity point, known as vertex, apex or retreat point, at the MSL (Fairbridge, 1952; Hodgkin, 1964). The time range of highstands influences the morphology of the notch and its preservation. A notch needs few hundreds of years to form but due to cliff retreat processes the notch could disappear in the case the action of the wave/sea is acted

for a long time. In areas with low tide range, e.g, Mediterranean sea, tide notch are very accurate sea level indicators with an error of few decimetres (Rovere et al., 2016a). According to Laborel and Laborel-Deguen, (1996) and Rovere et al., (2015) a better definition of the sea level can be obtained by biological indicators having a narrow elevation distribution. Such a finding, easy to date with radiocarbon method, are particularly useful for Holocene studies, on the contrary the challenge to use tidal notch for former sea level studies is due to the difficult to date directly them. Usually, the age constrain of a tidal notch is chronostratigraphically related to others nearby dated RSL indicators. Hardly biological indicators are preserved in tidal notches formed before the Holocene.

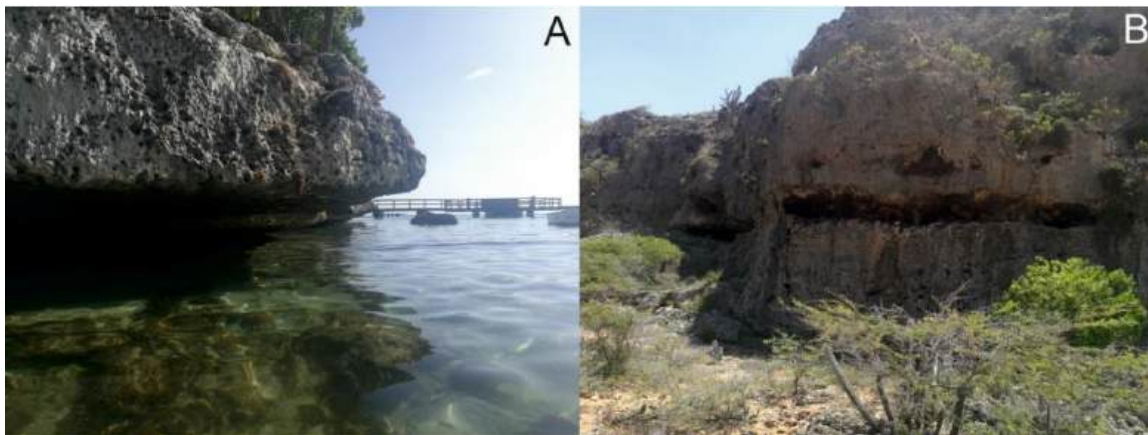


**Figure 12.** A: Present-day tidal notch and B: paleo raised tidal notch at Curaçao island (Southern Caribbean)

It is worthy to not confuse tidal notch with structural and abrasion notches. The formation of structural notches is due differential erosion in heterogeneous rocks, but they can be reshaped by the sea and waves. For these reason Pirazzoli, (1996) include the structural notch into the *wave-cut notches*, where are included also the abrasion notches. Abrasion notches are shaped by the abrasive action of sediments, e.g., sand, gravel or pebbles, against a rocky cliff regardless of the lithologies. Wave-cut notches are not considered good RSL indicator because their origin is not strictly related to former sea level and their elevation range is quite wide.

## 2.2 Depositional indicators

Coral reef terraces are the most representative example of depositional indicators in tectonically stable areas of continental passive margins (Filocamo, 2006 and references therein) (**Figure 13 a**). Coral reef terraces are a kind of marine terrace, extended up to some km in width, but contrary to the marine terraces, which formation is due to both wave erosion and sedimentary deposition, the coral reef terraces are the product of wave abrasion/bioerosion, among the erosive processes, and the growth of coral reef (Anthony, 2008) as bioconstructional processes (Rovere et al., 2016a). The biological component of the coral reef is represented mainly by algae corallines and corals, e.g. *Diploria* and *Acropora palmata* (**Figure 13 b and c** respectively), which lives between the narrow depth ranges up to few metres below sea level (b.s.l.) in tropical or sub-tropical areas. The upper part of a reef presents a slightly flat surface, known as *reef flat*. Since the reef flat develops at almost the sea level during a low tide, coral reef terraces are considered excellent sea level indicators. Moreover, coral reef terraces present the wide advantage to be easily dated with the U-series method (Muhs et al., 1994; Stirling et al., 1998), which has been particularly used for the tectonically active areas of, for examples, Barbados and Papua New Guinea. As for the marine terraces, the paleo sea level corresponds to the point of intersection between the reef flat surface and the paleo cliff, or approximately is deduced from the average terrace elevation or taking into account the highest elevation of corals in growth position (Rovere et al., 2016a). Notwithstanding, awareness to the correct position of paleo sea level must be taken because the water-depth range of each coral species varies significantly up to tens of metres (Hibbert et al., 2016), but by integration of morpho-stratigraphic information with geological one a possible misinterpreting could be avoided (Rovere et al., 2016a). However, microatolls among other benthic species (Woodroffe et al., 2012), are considered excellent sea level indicators because they live in a very

limited range elevation. According to Blancon et al., (2009), the modern reef flats are extended up to 3 m b.l.s., depending of hydrodynamic parameters (Rovere et al., 2016a)



**Figure 13.** a) Example of coral reef terrace in Curacao Island, southern Caribbean sea with a close-up view of fossil examples of *Diploria* (b) and *Acropora palmata* (c) corals

As indicated also in Section 2.4 Biological), *Lithophyllum lichenoides*, a red algae, and *Dendropoma petraeum*, a marine gastropod mollusk (Vermetidae family), are the most precise depositional organism as sea level indicators in the Mediterranean area (Filocamo, 2006).

### 2.3 Sedimentological indicators

Coastal marshes and wetlands environments are particularly sensitive to sea level changes, which is reflected in changes of the microfossils-bearing deposits, lithologies and vegetation succession. Usually, a vibrating sampler is used to extract a sequence of samples, in order to recognize transition between sub-environments by a lithostratigraphical and biostratigraphical analyses. Sea level changes are recorded in the sedimentary sequence successions (**Figure 14**) and then quantitatively related to past sea level. Radiocarbon dating method, up to ~ 50 ka, is applied to date the organic materials of the abovementioned peaty deposits. Compaction processes and possible samples disturbance could affect the accuracy of sea level reconstruction derived by this kind of sedimentological indicators

This kind of study is particularly efficient for Holocene study, which is out of the aim of the present work.



**Figure 14.** Core sequence from Mistras lagoon using a hand coring, Sardinia

## 2.4 Biological indicators

Fossilized biological remains are preserved in rocky coast, where they are located in parallel horizontal layers corresponding to the supralittoral, mid-littoral and infralittoral zones. According to Laborel and Laborel-Deguen, (2005), species living close to the MSL are particularly useful in sea level changes studies, whenever the altimetric elevation between the fossilized remains and the modern analog is accurately measured.

Among that species, as reported in Evelpidou and Pirazzoli, (2015), there are *Lithophyllum lynoides* and *Lithophyllum onkodes* (corallines), *Dendropoma* and *Spiroglyphus* (genus of vermetid gastropods, **Figure 15**, Laborel, 1986), and finally *Idanthyrus* and *Galeolaria* (anellids) (Baker and Haworth, 1999).

In addition to the abovementioned fossilized biological remains, Kázmér and Taboroši, (2012) and Taboroši and Kázmér, (2013) point out the attention on bioerosional marker in rocky limestone lithologies such as the sea urchins traces, which have been used to evaluate the evolution, both subsidence and uplift, of a raised tidal notch in Cephalonia island (Evelpidou and Pirazzoli, 2015). Finally, indirect information, as compaction history of undisturbed samples, of past sea level is provided by biological indicators in core samples.



**Figure 15.** Encrusting vermetids on a carbonate boulder few tens of cm a.s.l. in Punta Caino site (Basilicata)

## 2.5 Archaeological indicators

Whenever an accurate relationship between archeological artefacts with past sea-level has been fixed with precision, then they are considered good sea level indicators (Flemming, 1979). Many different kind of archeological remains could be used in sea level change studies but each one must be interpreted properly because they could assume a different meaning. For example, shell middens or traces of human shelter typically of prehistoric ages and antrophic buildings such as walls, canalized waterways and the floor are all emerged man-made constructions, which provide just rough information about the position of the sea level in the past. On the contrary, remains for which is clear the relation with the sea level, e.g. harbour wharfs, slipways and fish tanks, are meaningfull and precise sea level indicators (Pirazzoli, 1987). In particular, Roman fish tanks, dated 100 BC to AD 100, are considered excellent indicators due to their extreme sea level precision (Pirazzoli, 1979). Greek and especially Roman coastal archeological remains are abundant along the Mediterrenean coasts. Usually, they are slight submerged by the sea, but local behaviour could increase apreciablely the degree of submersion (Flemming, 1969; Flemming and Pirazzoli, 1981; Pirazzoli, 1976). Similarly, in tectonically active areas that ramains are emerged up few metres above sea level. Hence, archeological remains could provide important information about sea level changes in historical times in terms of direction and amplitude (Morhange and Marriner, 2015). Sometimes, the archeological and biological component is combined to provide information about the past sea level (**Figure 16**).

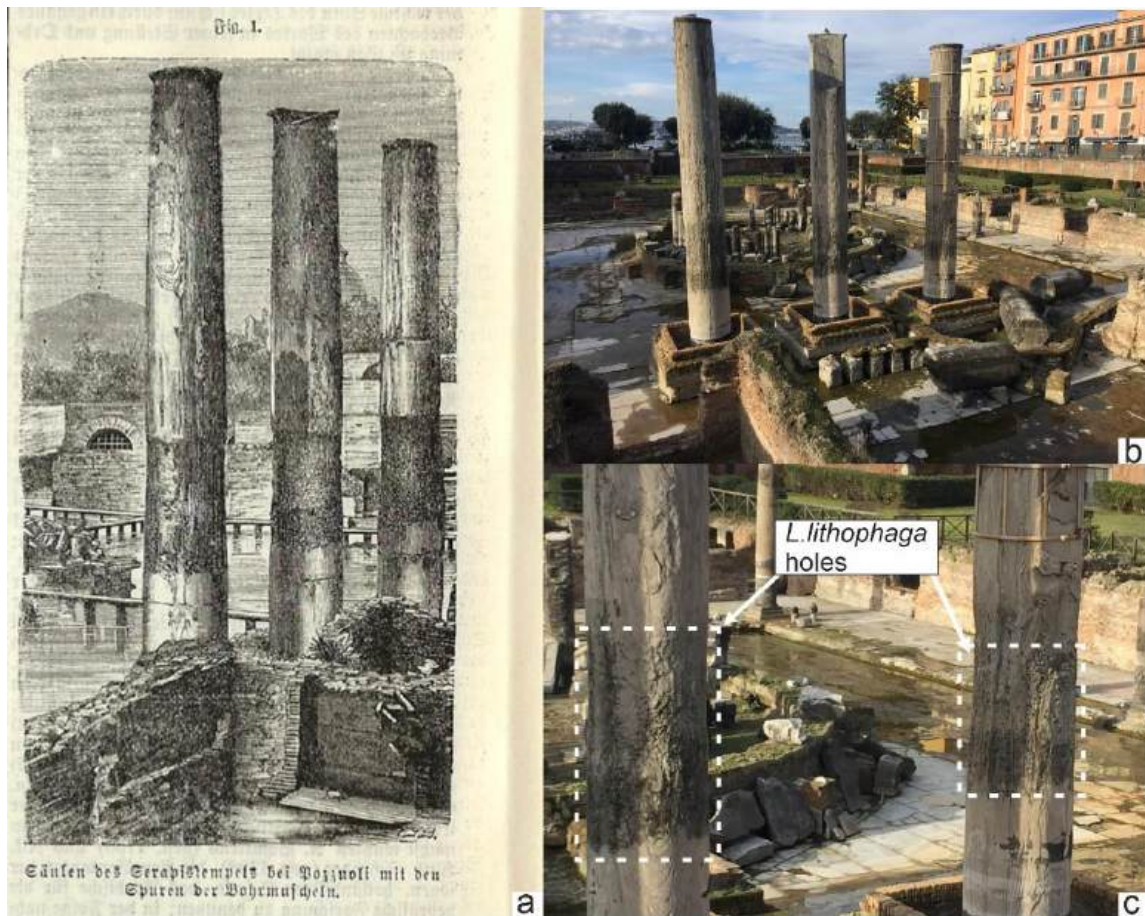


**Figure 16.** a) Macellum or Serapide Temple in Pozzuoli, 1890 (Meyers Konversations-Lexicon stamp). The roman columns present evidence to be have been shaped by the sea for the presence on them of *L. L. lithophaga* holes. b) Modern view of the Serapide Temple, c) close-up view on the Lithophaga holes.  
 Photo b and c by E.P. Prinzi

The present work does not use archeological indicators, neither it is focus on the Antiquity period, so for who is interested to have an insight on the issues may see the following work: Antonioli and Leoni, 1998; Evelpidou et al., 2012b; Evelpidou and Pirazzoli, 2015; Lambeck et al., 2018, 2004b, Auriemma and Solinas, 2009 have proposed a review regarding the different archeological sea level indicators with an insight on their accuracy.

### 3. Pleistocene sea level curves

A wide range of sea level curves have been made available in the last decades (Rohling et al., 2014; Shackleton, 2000; Siddall et al., 2003; Waelbroeck et al., 2002). The sea level curves are of vital importance in morphotectonic studies, where after both a more possible accurate recognition of the inner edges of marine terraces and its chronological constrain, it is possible to calculate the real uplift only if the height of the high-stand sea level corresponding to the formation of the terrace is known.

The worldwide sea level curves are constructed mainly from oxygen-isotope ratio recorded in deep-sea sediments extracted from boreholes. The so obtained proxy data allow calculating continental ice-volume and so infer the sea level history (Shackleton, 2000, 1987; Shackleton and Opdyke, 1973). Astronomical secular variation and geological processes, e.g. plate motion, which affected wide areas are mainly correlated with global sea level change (Caputo, 2007). Before to have a deep look at the sea level curve, it is necessary to explain firstly some basically aspects of the astronomical theory of paleoclimates (Berger, 1981), which influence the global sea level changes.

The astronomical theory is based on the first intuition of Adhemar, (1842) and mainly of Croll, (1875) but only with Milankovitch, (1941) work, a mathematic method took place which validation is especially well apply for the Quaternary period (ca. 2.6 MA) (Head et al., 2008). According to the theory, the alternation of ice (glacial) and warm (interglacial) stages is due to three major cyclic processes which affect earth's orbital parameters in long-term time span influencing the rate of solar insolation and so the solar forcing (**Figure 17**). The cyclic processes are: (I) changes in the eccentricity of the Earth's orbit, every ca. 100 ka, with consequence changes in the distance between Earth and Sun during the aphelion and perihelion; (II) the obliquity of the ecliptic, every ca. 41 ka, is a modification

in the tilt of the Earth's rotational axis; (III) precession of the equinoxes, every ca. 22 ka, which impact on the period of occurrence of seasons during the aphelion and perihelion.

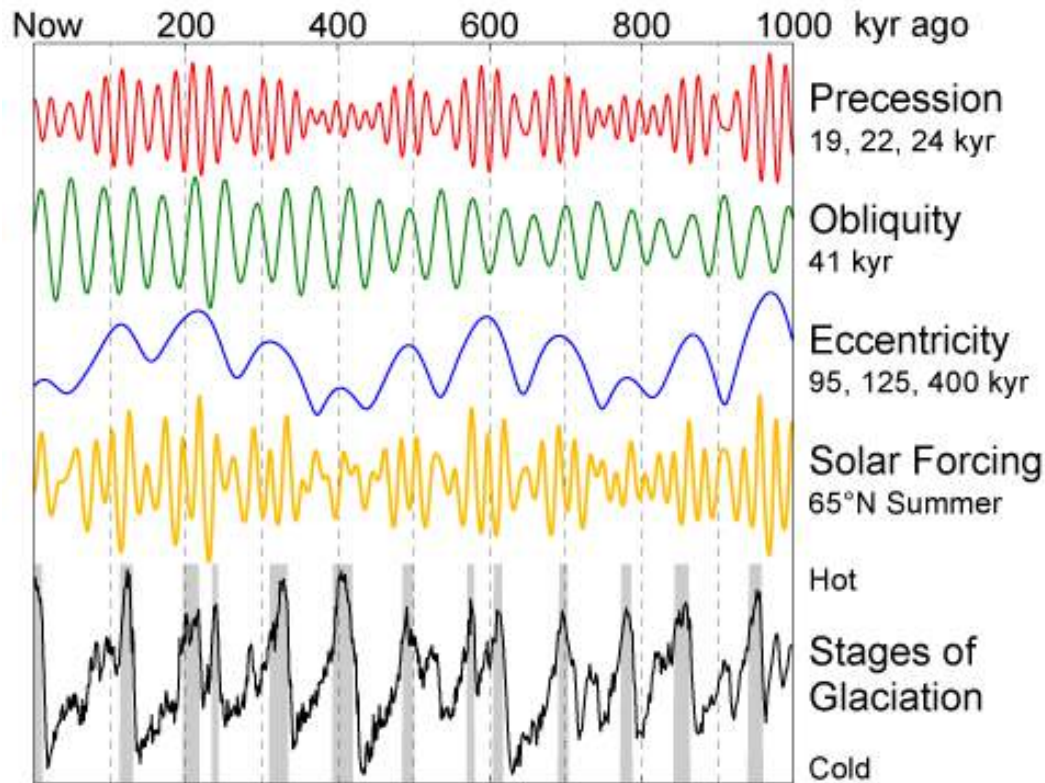


**Figure 17.** The figure illustrates the astronomical cyclic processes, the solar forcing at 65° N and the alternation of glaciation (from Wikipedia, Robert A. Rohde, Global Warming Art project).

The ca. 100 ka cyclic process, from a spectral analysis, results the principal one, while the others two are considered secondary (Imbrie et al., 1993; Piasias et al., 1990; Ruddiman et al., 1989).

The astronomical theory explains the alternation in the advance and retreat of the polar ice caps due to the change in the volume of the ice sheets because of Sun's energy distribution on the Earth surface. This turnover reflects the variation in the global sea level, also known as glacio-eustatic oscillation. During a glacial period (low-stand), more water is stored in the ice caps and less water is available

on the oceans generating a lowering in the sea level, while during a warm period (high-stand) the opposite occurs. The change in the volume of the ocean water is reflected also in changes in water isotopic composition. In fact, the  $\delta^{18}\text{O}/^{16}\text{O}$  ratio between the two isotopes of the Oxygen, currently ca. 1/500 in the oceans, depends on the amount of water available in the oceans. In nature, the Oxygen has three stable isotopes with a different concentration in the atmosphere:  $^{16}\text{O}$  (99.762%),  $^{17}\text{O}$  (0.038%) and  $^{18}\text{O}$  (0.2%). Past sea level, and consequently ice volume changes, is inferred mainly by the analysis of the  $\delta^{18}\text{O}/^{16}\text{O}$  ratio within foraminifera shells made up of  $\text{CaCO}_3$ , to derive paleo-temperatures of the oceans since the foraminifera grow in chemical equilibrium with the sea water. Usually, benthic foraminifera are used for this kind of analysis due to the quite uniform physical-chemical properties, salinity, temperatures and isotopes composition) at the bottom of the oceans (Caputo, 2007). The  $\delta^{18}\text{O}$  is expressed in ‰ referred to the Pee Dee Belemnite (PDB), the Chicago calcite standard, or to the Standard Sea Ocean Water (SMOW). It is worth to mention the key concept of the Oxygen isotope fraction to understand the isotopic changes in the Ocean due to glaciation (**Figure 18**). During a glaciation, more amount of water, depleted of the heavier oxygen isotope ( $^{18}\text{O}$ ) due to the preferably precipitation of the lighter isotope ( $^{16}\text{O}$ ), is stored in the ice cap. Hence, more water is stored on the ice cap, higher the  $^{18}\text{O}/^{16}\text{O}$  ratio of the oceans becomes. On the contrary, during an interglacial period the  $^{18}\text{O}/^{16}\text{O}$  ratio of the oceans decrease for the melting of the ice enriched in  $^{16}\text{O}$ . The strictly relationship between isotopic composition of the ocean, recorded in fossil shells, and ice-volume changes has been reported from the early works of Emiliani (1966, 1955) and Shackleton and Opdyke (1973).

The Oxygen Isotope Timescale (hereafter OIT) (John Chappell and Shackleton, 1986; Imbrie et al., 1984; Shackleton and Opdyke, 1973) are reconstructed statistically by the following assumptions:

- The Standard  $\delta^{18}\text{O}$  is constant at least during the Quaternary time span;
- $\delta^{18}\text{O} \propto$  astronomical cycles;

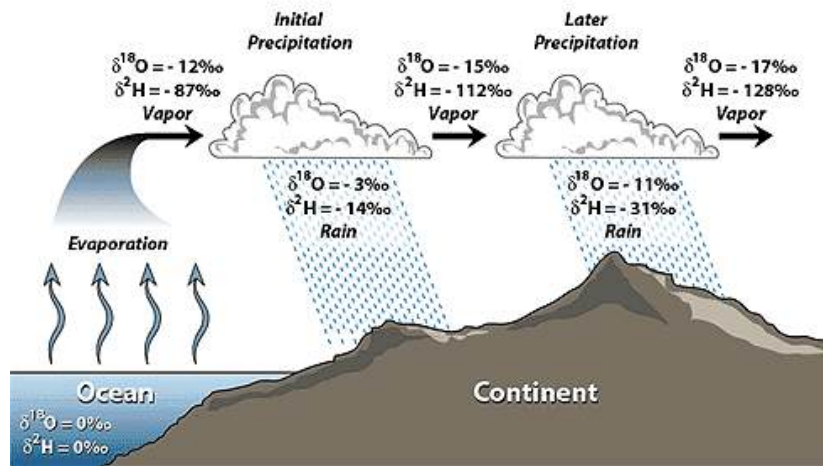


**Figure 18.** The Oxygen stable isotope fractionation cycle

Due to their spatially local and temporal-limited contribution, some natural processes, e.g. (I) steric component subject to changes in temperature (Bryan, 1996) or (I) *dynamic sea surface* (Mörner, 1996), of sea level changes are not considered.

The OIT curves can be converted into sea level curves considering that 10 m sea level (s.l.) are reflected in a  $\delta^{18}\text{O}$  variation of 0.1‰ (John Chappell and Shackleton, 1986; Hodell et al., 2003; Jouzel et al., 2002; Labeyrie et al., 1987; Shackleton, 2000, 1987; Shackleton and Opdyke, 1973), among the most acceptable value, but, other Authors (Fairbanks and Matthews, 1978; Labeyrie et al., 1987; Schrag et al., 1996; Waelbroeck et al., 2002) suggest different conversion values, however, Bintanja et al., (2002) argue a linear relationship between OIT and sea level curves never exists. Secondary factors, such as water temperatures,

salinity, isotopic composition and local hydrological behaviour among others, influence, sometimes only with local effects, the  $\delta^{18}\text{O}$ .

In order to evaluate the tectonic evolution of a coastal sector, to evaluate correctly the vertical movements suffered in an area and to quantify the uplift rate it is necessary to know:

1. the inner edge elevation in case of marine terraces or the former sea level point based on the kind of indicator used;
2. the absolute age of the corresponding RSL;
3. the paleo sea level at the time of the RSL indicator.

While the first two data could be obtained by fieldwork and laboratories activities, on the contrary the last point need to be extracted by former eustatic sea level curves. From the oxygen isotope data are extracted the Marine isotope stage (MIS) which represent the fluctuations of warm and cool periods reflected in sea level changes. The positive peaks are known as highstands while negative peaks are called lowstand. A stillstand occurs whenever the sea level stays at the same elevation for an extended time. According to a nomenclature globally accepted, the highstands are indicated with odd numbers and the substage are followed or by a second odd numbers or with a, c and e letters, while the lowstands are indicate with even numbers followed by a second even number for the substage or with a b, c and f letters. For example, the Last Interglacial, MIS 5 is formed by three positive peaks, e.g. 5a, 5c and 5e or in the same way as 5.1, 5.3 and 5.5. In this study, both the nomenclature including letters and numbers for the substages will be use, e.g. 5e or 5.5 indiscriminately.

A relative sea level (RSL) curve, a plot between sea level elevation and time, is the result of eustatic effects and crustal changes. On the contrary, absolute or eustatic sea level curve, reconstructed on supposed stable sectors, takes into account the total volume of the oceans, which depends of the global

glacial volume and is not affected by crustal displacements (Mörner, 1982). A RSL curve, could be reconstructed assuming a constant and known uplift rate in the studied sector (John Chappell and Shackleton, 1986; Pirazzoli, 1996; Pirazzoli et al., 1993), or, alternatively, it could be reconstructed by interpolation of huge amounts of data such as the present-day elevation, altitude or depth, of RSL indicators constrained with absolute age, especially of fossil corals (e.g., Bard et al., 1990; Bender et al., 1979; Bloom et al., 1974; Chappell et al., 1996; Dumas et al., 2005; Zazo et al., 2002; Caputo, 2007). Erosional processes, natural slope evolution, dating methods limits make difficult and less accurate to reconstruct appropriately the curves for the highstands former to the Last Interglacial and so to derive the surface uplift history of an area (John Chappell and Shackleton, 1986; Pirazzoli et al., 1993)

Studies on RSL indicators of the MIS 5e, taking into account GIA and local tectonics effects, have allowed to estimating globally the eustatic sea level (ESL) between +5.5 and 9 m (Dutton and Lambeck, 2012; Kopp et al., 2009), while along the tectonically “stable” areas of the Mediterranean, RSL indicators elevation regarding the MIS 5e spans from 2 to 8 m (Benjamin et al., 2017) and in particular, 2-3 m elevation range in Mallorca, Balearic Islands (Vesica et al., 2000; Bardají et al., 2009 and reference therein), between 7 to 8 m in western Italy (e.g. Antonioli et al., 2006a) and finally up to 7 m for the eastern Mediterranean (Sivan et al., 2016). Ferranti et al., (2006) and Pedoja et al., (2014, 2011) have compiled a database of the RSL indicators regarding the MIS 5e for Italy and the World respectively. More recently, an update and standardized Last Interglacial (MIS 5e) sea level database is in compilation to the World Atlas of Last Interglacial Shorelines (WALIS). Regarding the Western Mediterranean see Section 7. Last Interglacial sea-level proxies in the Western Mediterranean. Since sea level curves are fundamental to quantify morphotectonic analysis, it is worthy to highlight that many differences, in elevation and duration of each stage

exist between the different curves proposed. Moreover, it is worth noting each curve proposed in Literature presents important uncertainties regarding both the age spans and the sea level elevation of the highstand up to few tens of metres but, according to Caputo, (2007) with underestimate values. For example, reporting the examples from (Caputo, 2007), the Rohling et al., (1998) curve has an elevation range error of  $\leq \pm 11$  m from 500 ka; Waelbroeck et al., (2002) calculates  $\geq \pm 13$  ka for the last 450 ka, while Siddall et al., (2003)  $\pm 12$  for the last 125 ka. The major elevation error, reported by Lea et al., (2002), is quantify in +21/-27 m for the 360 ka time span. An important contribution, about 10-15 % of the sea level signal, is provided by visco-elastic rebound that depends on the elastic deformation response of the Lithosphere and on the viscous flow of the Mantle material (GIA, see Section 3.1 Eustatic and Relative Sea level change). However, in the far field where GIA contribution is of few metres and/or in geological context with high or moderate uplift, its contribution may be neglected because included in the elevation uncertainties of the paleoshorelines. In the following work, the GIA contribution has not been directly calculated.

Caputo, 2007 has reported, sometimes redrawing them in the case no numerical data available, at a uniform scale twelve RSL curves (**Figure 19**). The curves considered have both a millennial scale detail and a time spanning from present time to at least 3-4 major glaciations (ca. MIS 9-11). Some Oxygen-derived isotope curves, converted into sea-curve (dashed lines in **Figure 19**) according the abovementioned standard conversion or according to the suggestion of the Authors in their respectively work, have been included in the Caputo, 2007 compilation.

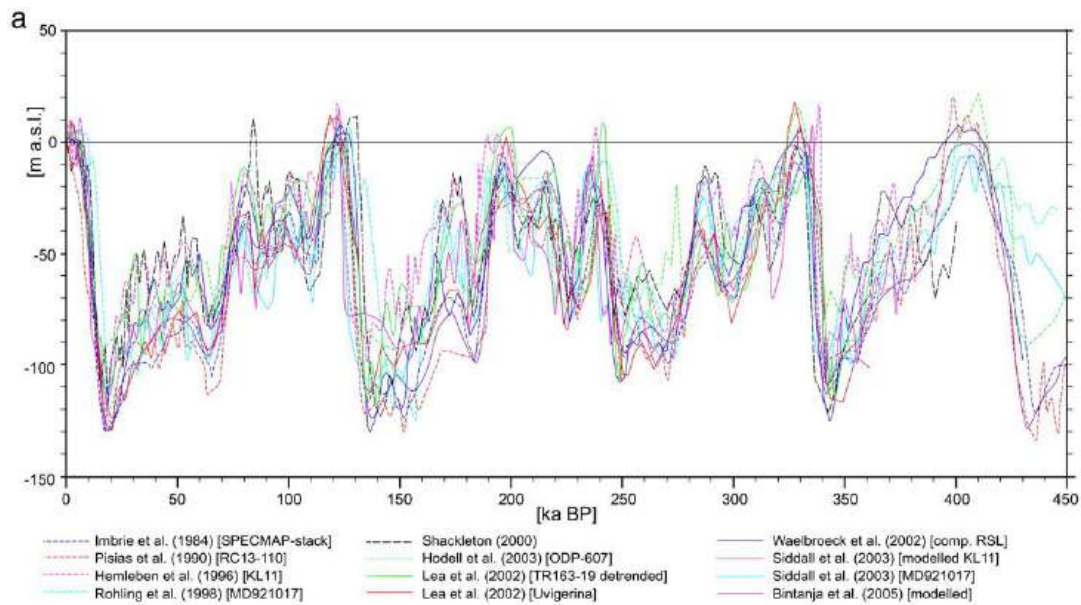


**Figure 19.** a) Reproduction of twelve sea level curves from Literature, in dashed lines the sea level curves derived by OIT (Caputo, 2007)

Besides the type of sea-curve, e.g., OIT-derived, the twelve curves considered are roughly coherent each other, however, an in-depth analysis allow to considering significantly differences both on the elevation of the high/lowstands peaks up to tens of metres and on their duration. Such differences have important implication on morphotectonic and Quaternary evolution studies in terms of vertical uplift rates. In order to have a more accurate reconstruction of the evolution history of the proper area, it is suggested the use of local relative sea level if available in Literature.

### 3.1 Eustatic and Relative Sea level change

From the ancient Greek words *eu* and *statikos* which mean “well” and “static fixed” respectively, derive the modern term eustasy introduced in 1888 by Edward Suess, an Australian geologist, but only in 1906 it has been translated in English (Suess, 1906) to originally define the alternation of transgression and regression phases of the sea due to glaciations (Rovere et al., 2016b). The simple static view of Suess as a response of the ocean mass variation due to the ice sheet fluctuations, with uniform effects at a global scale, is lacking to consider the visco-elastic response of the Earth surface to the weight of the ice-cap. In fact, the ice and water load produce elastic deformation on the Earth surface with locally effects. Hence, sea level changes is define “relative” when referred to the vertical movements between mean sea level (MSL) and Earth surface respect each other (Rovere et al., 2016b). Even if relative sea level changes are more appropriate for local/regional tectonic reconstructions, and eustatic sea level study are used for global investigation on the ice-cap behaviour over time, both are strictly related.

#### 3.1.1 Eustatic sea level change

Eustatic sea level (ESL) change are characterized by uniform and global distribution due to variation in the volume and mass of the ocean (Rovere et al., 2016b). Local processes, e.g. tectonism or compaction of sediments, have no influence on ESL changes, contrary to relative sea level change as better explain lately. Among the mass change causes (I) glacio-eustasy and (II) hydro-eustacy are included (**Figure 20 a-b**). Glacio-eustacy is related with the amount of continental ice sheets accumulated in the time, also as a consequence of astronomical cycles as already mentioned in the former paragraph, whereas hydro-eustasy indicates the distribution of the water in the different hydrological reservoir but not including

the glaciers (Rovere et al., 2016b). Thermal expansion and thermo/halo-steric changes (**Figure 20 c**), by physic-chemical alteration of water properties are the principal geological reasons of volume ocean change in addition to the sedimento-eustasy and tecno-eustasy (**Figure 20 d**) among the geological processes ones, which are influenced by the shape, and possible variations, of the ocean basins. Each process described have effects on different time scale (**Figure 20 d**), for examples the geological processes causing volume ocean changes contributes to ESL change for hundreds of metres in a time of 10 up to 100 million years, on the contrary the mass changes have similar elevation influences but with a shorter, up to 1 million, time response on the ESL.

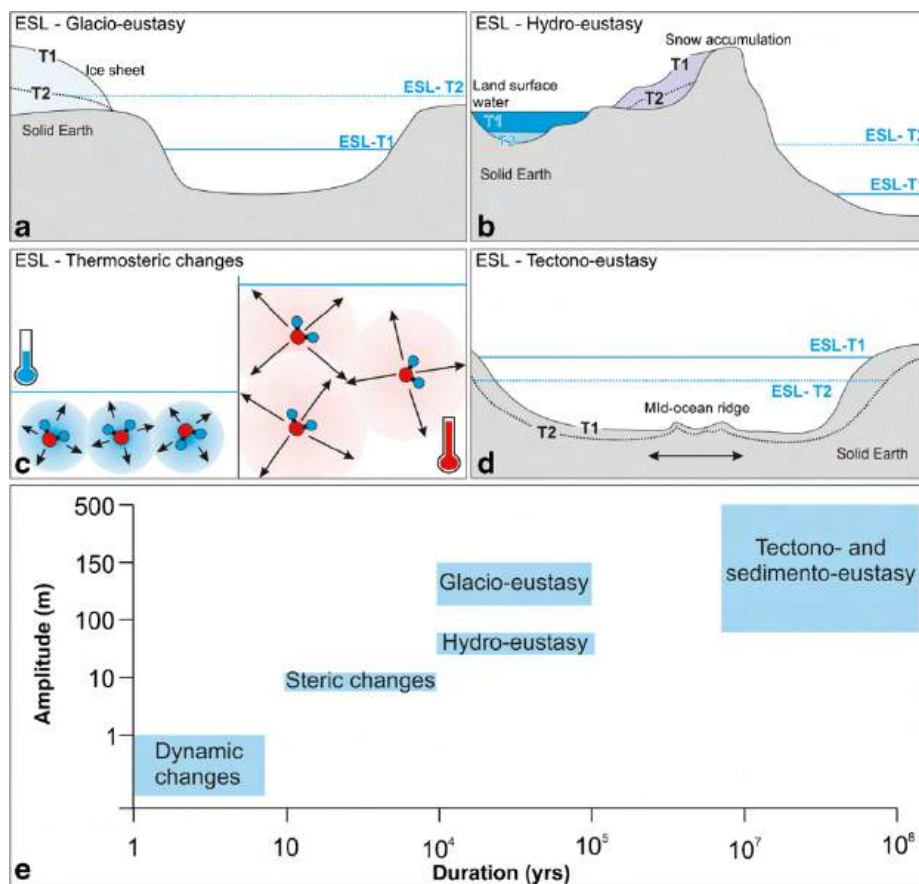


**Figure 20.** Eustatic sea level change are caused by a) glacio-eustasy, b) hydro-eustatic, c) thermosteric and d) tecno-eustasy processes, described in the text, e) whit their effects in terms of duration and amplitude (from Rovere et al., 2016b from Gornitz, 2005 data).

### 3.1.2 Relative Sea level changes

A sea level change is defined as relative whenever its occurrence is related to the vertical, uplift of subsidence, movements of the Earth surface (Kemp, 2015).

Since for definition the sea level is related with the geoid (Mörner, 1982), a model of global sea level representing the equipotential surface of the earth's gravity field, any displacement of the land respect to the sea level can be defined as **surface uplift**. In fact, according to England and Molnar, (1990) definition, the surface uplift is the “*displacement of the Earth's surface respect to the geoid*”. Surface uplift, in its broaden acceptation of positive and negative movements, is reflect in a sea level change taking fixed invariable the eustatic, mass and volume of ocean, component. Among the processes responsible of relative sea level changes, as reported by Rovere et al., (2016b), the (I) Glacio isostatic adjustment (hereafter GIA) and (II) gravitational attraction, (III) tectonic deformation and dynamic topography, (IV) sediment, karst and volcanic isostasy and finally (V) human activities are included (**Figure 21**).

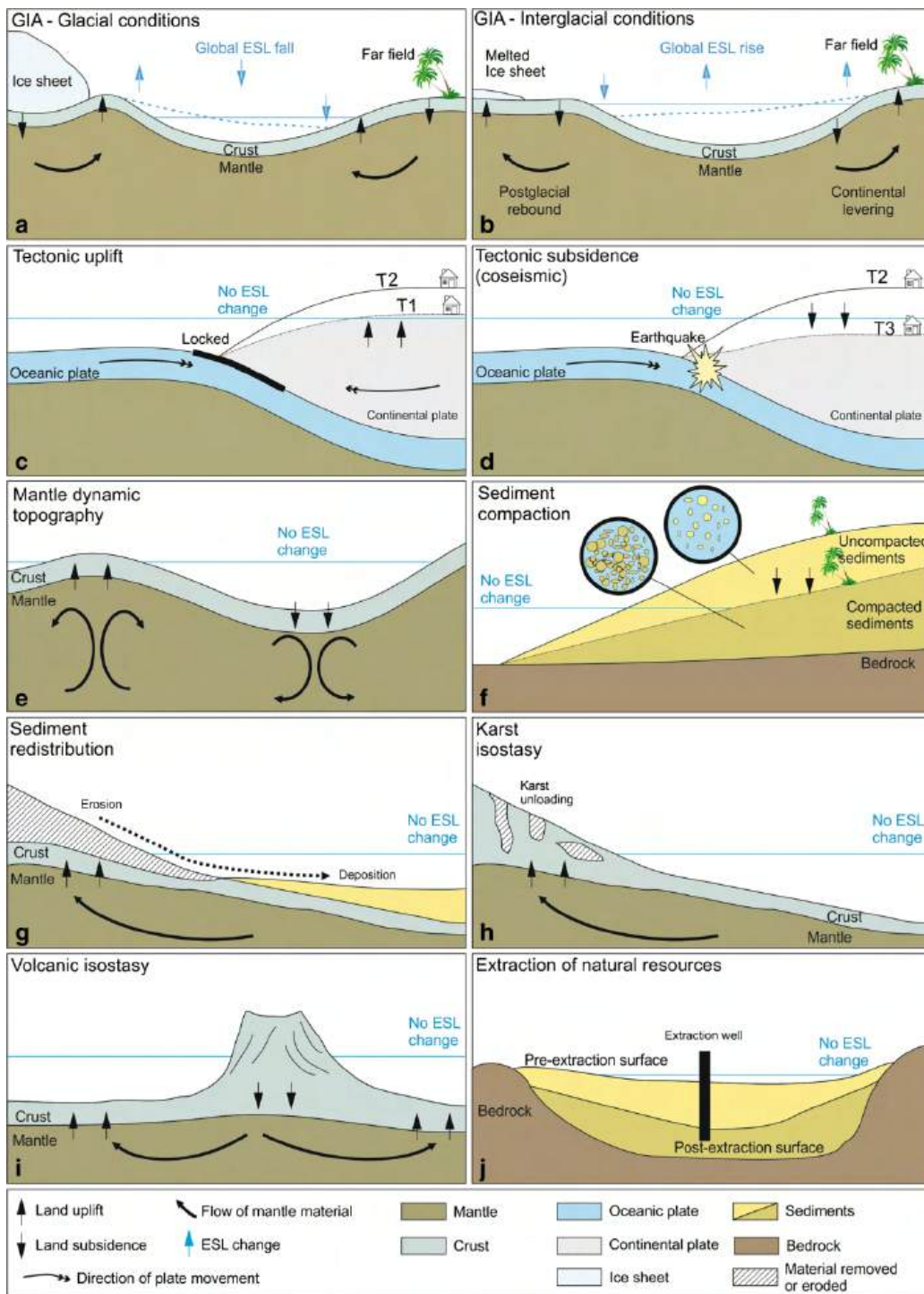


**Figure 21.** Relative sea level processes (from Rovere et al., 2016b): a-b: Glacio isostatic adjustment (GIA); c-d: sea level changes due to earthquake effects in a subduction setting; e: effects on the topography, and hence on the RSL, due to mantle dynamic; f: isostatic adjustment due to sediment compaction on RSL; g: sediment redistribution along coast and its effects on RSL; h: isostatic adjustment due to chemical weathering on limestone bedrock; i: isostasy due to volcanic activity; j: anthropic effects on RSL due to the use of natural resources.

- Glacio isostatic adjustment

The viscoelastic effects on the Earth surface due to the load of the ice and ocean define the Glacio isostatic adjustment (GIA) (Kopp et al., 2015; Milne and Mitrovica, 1998); in particular, the ice load produces a subsidence on the Earth surface, which is compensated by a flexure in its proximities and a subsidence in the far-field according to Hooke's law for elastic body. From the areas in subsidence, a viscous flow is transferred to the peripheral forebulge where a land uplift is recorded. During an interglacial period, the vertical movements abovementioned described are inverted. In addition to the glacio isostasy, it is worthy to underline the gravitational attraction (or “self-gravitational”) between ice mass and the ocean for their implications on RSL change. The GIA contribution is evaluated by numerical modelling according to the sea level equation (SLE, e.g., Mitrovica et al., 1994; Stocchi and Spada, 2007).

- Tectonic deformations and dynamic topography

Fault-related movements cause relative sea level changes due to the shifting of the shoreline along coast (**Figure 21 c-d**) on active margins, while on passive margins, mantle dynamic processes are the mainly responsible of RSL change (**Figure 21 e**). The time scale of fault related tectonic uplift is expressed in a time span between few centuries up to all the Quaternary, while the mantle flow movements generates vertical movements especially in few millions of years, however some effects at the Quaternary time scale could be appreciate (Rovere et al., 2016b and references therein)

- Sediment Compaction

The ejection of water for the load of superimposed sedimentary layers produce a loss of volume for a decrease of porosity, and consequently a land subsidence simultaneously to an increase in the sea level (**Figure 21 f**). The process described is known as compaction/consolidation of sediments, influenced also by biological and anthropic processes (Brain, 2016). The sediment compaction has effects up to some metres and it depends of the bedrock depth.

- Sediment, karst and volcano isostasy

The same isostatic effects of the load/unload of the ice, described in the above paragraphs, is caused also by sediment load or when the it is removed due to sediment redeposition along the coast (**Figure 21 g**). The quantities of sediments generate a flexure of the Earth surface which is compensated when there is a loss of sediments (Rovere et al., 2016b). Similarly, chemical weathering, particularly strong in wet environments with bedrock formed by limestones, can be very incisive to produce isostatic effects called karst isostasy (**Figure 21 h**). Both sediment and karst isostasy can have implication for very long-time span (Dalca et al., 2013). Also the load of a volcano produce a flexure for its weight and a depression around as isostatic response (**Figure 21 i**)

- Human activities

A sea level rise occurs for land subsidence because of anthropogenic use of the soil. In particular, the depletion of natural sources, e.g. as water, oil and gas, produce a lowering of the land level along coast in a magnitude up to some metres in a short time span (decades) (Ericson et al., 2006).

#### **4. Methods and materials**

In Section 6, for the Campania margin and the Calabria-Basilicata boundary, a multidisciplinary approach has been carried out by integration of morphotectonic, Quaternary stratigraphy, structural and biostratigraphical analysis. Moreover, samples collected in the field have been prepared for mineralogical characterization, then I have been personally dated both calcite concretions and corals using the U-series method at the Geochemistry laboratory of RomaTre University. Particular attention has been devoted to a geomorphological approach based on cut-cross relationships among the shorelines constrained by new U-series dating. The geomorphological study has been carried out using detailed topographic maps (1:5000 scale map) and DEMs with resolution 1x1 and 2x2 m (LiDAR). Along the NE edge of the Campania Plain (see Section 6.1.1 ) the lack of appropriate direct dating materials to constrain the wave-cut platform allow to using the synchronous correlation of multiple paleoshorelines method (Section 4.1 Synchronous correlation of multiple paleoshorelines method) The detailed of the methods and materials used for the different studied area has been better explained in their relative paragraphs.

In Section 7. Last Interglacial sea-level proxies in the Western Mediterranean a collection of the Last Interglacial (MIS 5.5, ca. 125 ka) index and limiting, marine and terrestrial, point of the Western Mediterranean have been reported in the frame of the World Atlas of Last Interglacial Shorelines (WALIS).

#### 4.1 Synchronous correlation of multiple paleoshorelines method

The synchronous correlation of multiple paleoshorelines method, developed starting by Roberts et al., (2009), has been used on the paleoshorelines outcropping on the southern slope of Mt. Fellino Ridge, NE edge of the Campania Plain (see Section 6. New data on late Quaternary paleoshorelines in the Southern Apennines, Italy ). The method rejects the widespread accepted “sequential correlation technique”, which is based on the assignation an older or younger highstand to the contiguous, in elevation, dated terrace deposits (Armijo et al., 1996; Bianca et al., 2011; Giunta et al., 2012). The sequential correlation method results inadequate in low uplift rates contest, where younger and higher sea levels could destroy or overprint paleoshorelines from sea level highstands that were lower than current sea level. On the other hands, to avoid that issue, the synchronous correlation method takes into account the upper Quaternary global sea level level curve (<410 ka, data from Siddall et al., (2003) and >411 ka, data from Rohling et al., (2014) with an assigned uplift rate (mm/y) to have a best fit ( $R^2 \sim 1$ ) between the elevation of the paleoshorelines mapped with the supposed one obtained from the “Terrace Age Calculator” derived by the above-mentioned sea level curves.

## 4.2 Mineralogical characterization

For corals it is important to verify their original aragonitic nature and check for the eventual presence of calcite. The occurrence of relevant calcite indicates that weathering processes have affected the coral after its burial, with consequent opening of the chemical system. Therefore, a mineralogical characterization of coral samples was carried out through the X-ray powder diffraction (XRD) method.

For routine mineralogical characterization of each coral sample a GE-Seifert MZVI automated diffractometer (XRD) was used (DiSTAR, University Federico II, Naples), with  $\text{CuK}\alpha$  radiation, 40 kV and 30 mA, 5s per step and a step scan of  $0.05^\circ 2\theta$  in the  $3\text{--}70^\circ 2\theta$  interval. The software package RayfleX (GE Inspection Technologies, 2004) was used for data processing, and phase identification was made by means of the ICDD-PDF2 database. For quantitative XRD phase analysis, i.e. calculation of percentages of aragonite, calcite and all the other associated minerals, we used both the GE-Seifert MZVI instrument (counting 18s per step, step scan  $0.02^\circ 2\theta$ ) and a PANalytical diffractometer (INGV, Osservatorio Vesuviano, Naples), equipped with a high speed PIXcel detector, Ni-filtered,  $\text{CuK}\alpha$  radiation, pyrolytic graphite crystal monochromator, 40 kV and 40 mA, step size of  $0.02^\circ$  and scanning time 8 s/step. The data were refined using the Rietveld method (Bish and Post, 1993 and references therein); the XRD spectra were elaborated with multiple refinements by the GSAS package (General Structure Analysis System; Larson, A. C. and Von Dreele, 2004) and its graphical interface EXPGUI (Toby, 2001), as well as with HighScore Plus software. The Rietveld structural models were based on the American Mineralogical Crystal Structure Database (AMCSD, Downs and Hall-Wallace, 2003).

### 4.3 Dating methods

For coastal geomorphological study, the accurate dating of deposits associated to marine terraces is essential to correlate them with the correct marine isotope stages (MIS) and so to estimate correctly the uplift rate. Many different dating methods have been improved in the last decades and they are separated between absolute or relative. Among the most used absolute dating methods in Quaternary coastal geomorphological investigation, Uranium-series disequilibrium dating (U-series or U/Th hereafter, Vesica et al., 2000), Acid Amino Racemization (AAR, Hearty et al., 1986b), Electron Spin Resonance (ESR) and Luminescence dating (both optically stimulated luminescence, OSL Mauz, 1999, and thermoluminescence -TL) are among the most used, while chronostratigraphic correlation with other dated materials or biostratigraphy are relative dating methods. Each method presents some limitations of applicability within the material used and the typical time of uncertainty as reported in **Figure 22**.

**Table 4**  
Most common dating methods used in Last Interglacial studies.

Method	Typical uncertainty in ka (1-sigma)	Examples
<b>Absolute dating methods</b>		
U-Series	0.5–4 ka	Stirling and Andersen (2009), Dutton and Lambeck (2012) and Obert et al. (2016)
Optically stimulated luminescence	3–7 ka	Mauz et al. (2015) and Carr et al. (2010)
Electro spin resonance	14–20 ka	Pirazzoli et al. (1991) and Schellmann et al. (2008)
Thermo luminescence	15–20 ka or limiting ages (e.g. deposit older than 60 ka)	Woodroffe et al. (1995) and Mauz and Hassler (2000)
<b>Relative dating methods</b>		
Amino acid racemization		Hearty and Kaufman (2000) and Wehmiller (2013)
Biostratigraphy	Usually relative dating methods help to discern between different interglacials.	Avila et al. (2015)
Chronostratigraphic correlation		Choi et al. (2008)

**Figure 22.** Absolute and relative dating methods for coastal investigations (Rovere et al., 2016a)

Hereafter, the main Quaternary absolute dating will be briefly illustrated. The Acid Amino Racemization technique has been largely used in the 80s in the Mediterranean (Hearty, 1986, see Section 7. Last Interglacial sea-level proxies in the Western Mediterranean) to date molluscs living in the littoral and sublittoral zone, e.g., *Glycymeris* and *Arca* genera among others. The method is based on the

degradation and transformations of proteins in fossil shells after their death (Hearty et al., 1986a and references therein). The racemization, known also as epimerization for the isoleucine protein, works by calculation of the ratio between the amino acid D-alloisoleucine and L-isoleucine (known as D/L ratio). Considering that all the living organisms contain only the L amino acid, the D/L ratio is equal to 0 in living organism, but after the death of organisms some processes, e.g., hydrolysis, racemization and other reactions of decomposition, allow to increase the D/L ratio to reach the equilibrium at 1. The time to reach the equilibrium depends on the climate and temperatures, calculated for the Mediterranean between ca. 15 to 2.0 my (Hearty et al., 1986a).

The luminescence (TL and OSL) dating are suitable for deposits bearing quartz and feldspar grains, e.g., loess, aeolian sands and so on (Mauz, 1999 and references therein). The luminescence method is based on the assumption that the crystals trap energy which could be released by electrons movements as light (luminescence) (Aitken, 1985). In the case the luminescence occurs by adding of heat, it takes the name of thermoluminescence (TL), while it is called optically stimulated luminescence (OSL) when stimulated by addition of light.

Similarly, Electron Spin Resonance (ESR) dating is based on the count of unpaired electrons within crystals due to former exposure at natural radiation. The age is provided by a measure of the radiation released starting from the time of formation of the organic matter considered.

For Late Quaternary/Holocene studies the radiocarbon (or  $^{14}\text{C}$ ) absolute dating method is the more appropriate in the case of available organic materials, e.g. bones, shells, wood, peat and so on. The radiocarbon dating range of applicability, as for all the radioisotopic methods (U/Th, Ar/Ar etc), depends on the decay time of the parental radionuclides.

Both corals and calcite concretions (carbonates) are the most suitable materials for precise and accurate dating by U-series disequilibrium methods. The

U-series method works on the natural radioactive decay processes of the U. The uranium decay occurs by a decay chain to reach stable isotopes of lead (**Figure 23**). In nature two U isotopes are present, the  $^{238}\text{U}$  with an abundance of ca. 99% and  $^{235}\text{U}$ , which has an abundance of only the 0.72%. For dating accuracy, it is very important to have a chemically closed system to avoid uptake or leaching phenomena, the incorporation or loss of Uranium respectively from after the formation of the corals or speleothems. Notwithstanding, for a correct dating no detrital thorium must be added in the system, although in this case some correction can be applied.

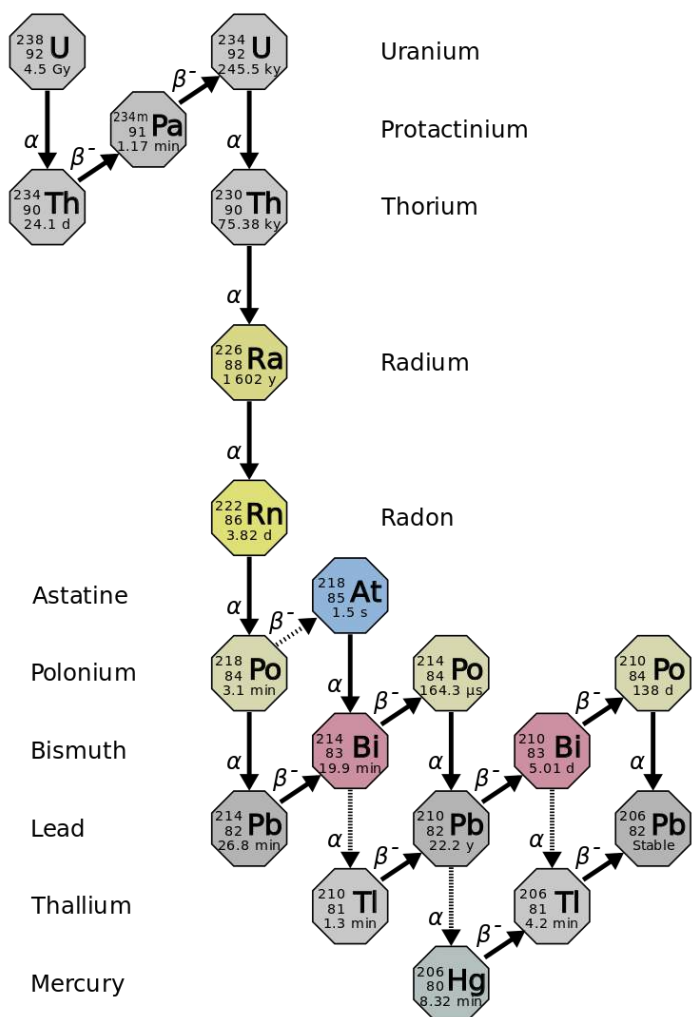


**Figure 23.** Decay chain of isotope  $^{238}\text{U}$  (by Wikipedia).

#### 4.3.1 Sample preparation

I have U-series dated four coral samples and eleven calcite concretion samples, one of which for the Polvica area (see **Section 6**. New data on late Quaternary paleoshorelines in the Southern Apennines, Italy ), while all the other samples come from the Calabria-Basilicata boundary area. Even if only four coral have been dated, fifteen coral samples have been prepared for mineralogical characterization (XRD analysis) but they have showed after-death alteration (calcite contents > 5%) and discarded for further investigations.

The sample preparation have been made at the Chemistry lab of the Department of Earth, Environmental and Resources (DiSTAR, University of Naples Federico II) and it consists in cleaning firstly each sample mechanically using a micro-driller to remove the external parts and to separate the corals from the biocalcarene, then the separated corals (**Figure 24 A**) have been cleaned ultrasonically for few minutes (**Figure 24 B**). For each coral, the internal septa have been separated from the external walls by micro-driller and then the powder have been analyzed at the DiSTAR and INGV (Osservatorio Vesuviano, Naples) for mineralogical characterization. Then, I have dated at RomaTre University the suitable coral and the calcite concretion samples by dissolution of the powder in nitric acid (**Figure 24 C**). The organic matter has been destroyed adding hydrogen peroxides and heating the solution at 100 °C. The solution has been spiked with a solution containing known  $^{228}\text{Th}/^{232}\text{U}$ . The extraction of the U and Th isotopes have been made through ion exchange chemistry columns (**Figure 24 D**). Finally, the extracted U (**Figure 24 E**). and Th have been counted by alpha spectrometer (**Figure 24 F**).

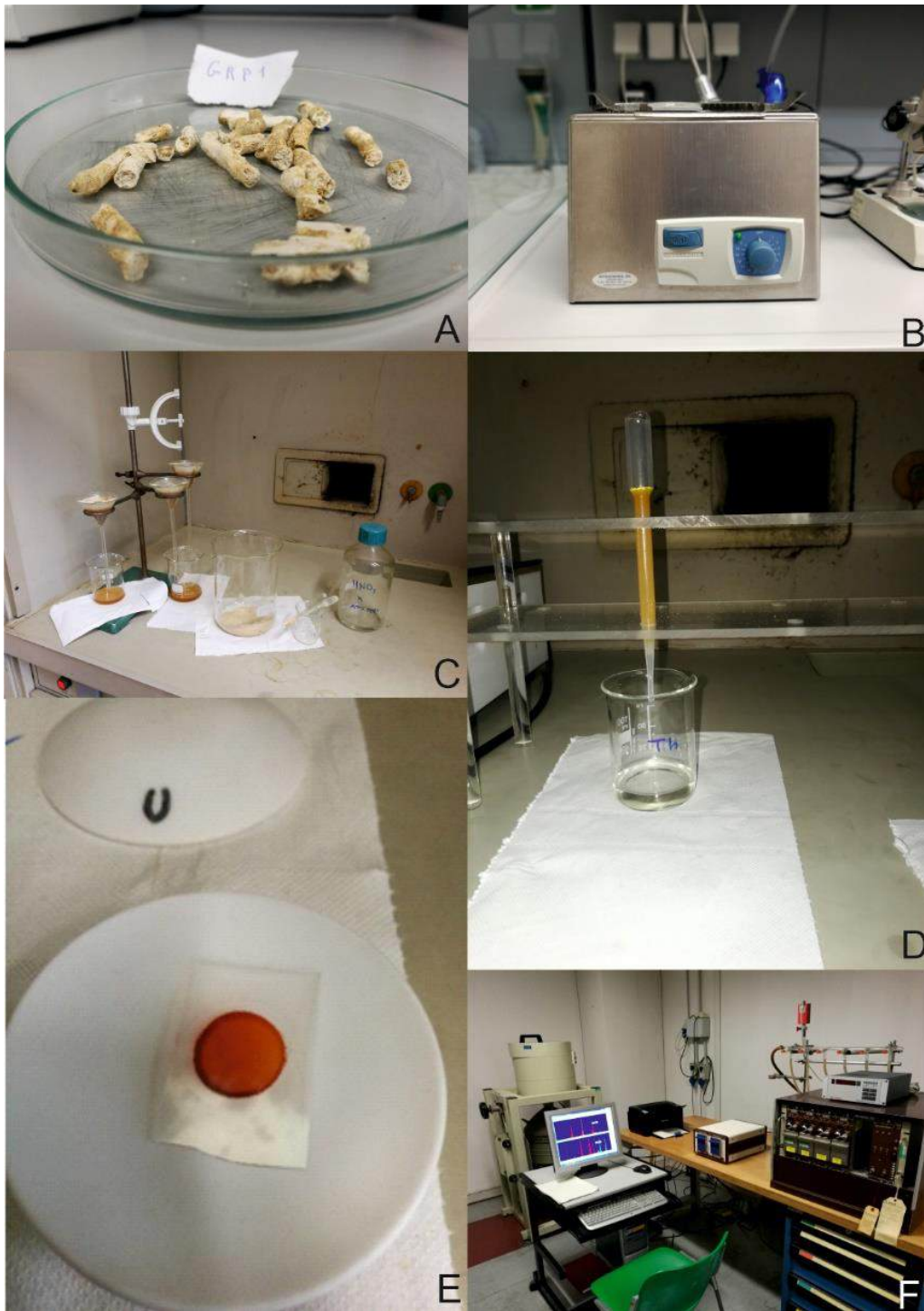


**Figure 24.** A) *C. caespitosa* corals separated mechanically from the biocalcarenes; B) Ultrasonic cleaner used for calcite concretions and corals; C) Dissolution of powder samples into nitric acid and separation from the insoluble fraction; D) Column-extraction of the U and Th isotopes; E) slide within uranium F) Alpha spectrometer

#### 4.4 Stable isotope analysis

Stable isotope analysis have been carried out on three calcite samples from the northern Calabria coast (**Section 6.3**), in order to better define the paleoenvironments of their formation. The calcite standards used at the Institut für Geologie, Mineralogie und Geophysik, Ruhr-Universität Bochum during the measurement of the samples for the stable isotope analysis are reported in the following table (Table 1):

External Std Dev	$\delta^{13}\text{C}$	$\delta^{18}\text{O}$	n
ISO-A	0.06	0.14	41
ACROS	0.07	0.10	19

Table 1: Calcite standards used for stable isotopes analysis

Both calcite standards have been run for the calcite sequence on a ThermoFisher Scientific MAT253 equipped with a GasBench II and a ConFlo IV.

## 5. Geological framework

### 5.1 Geological setting

The Apennines, Alps, Carpathians, Dinarides, Albenides, Hellenides, Betic Cordillera, Rif and Maghrebides constitutes the peri-Mediterranean orogenic belt (**Figure 25**), which evolution is strictly related with the Africa-Eurasia plate convergence starting from Late Cretaceous to Quaternary time span (e.g. Dewey et al., 1989; Mazzoli and Helman, 1994; Schettino and Turco, 2011 and references therein), in addition to the rotation of microplate as the Corsica-Sardinia block, of European affinity, and to the movement of Adria, of African origin (Turco et al., 2012, and references therein). The concave edge of the arcuate portions of the peri-Mediterranean orogenic belt is affected by crustal and lithospheric extension in concomitance with crustal shortening along the chains.

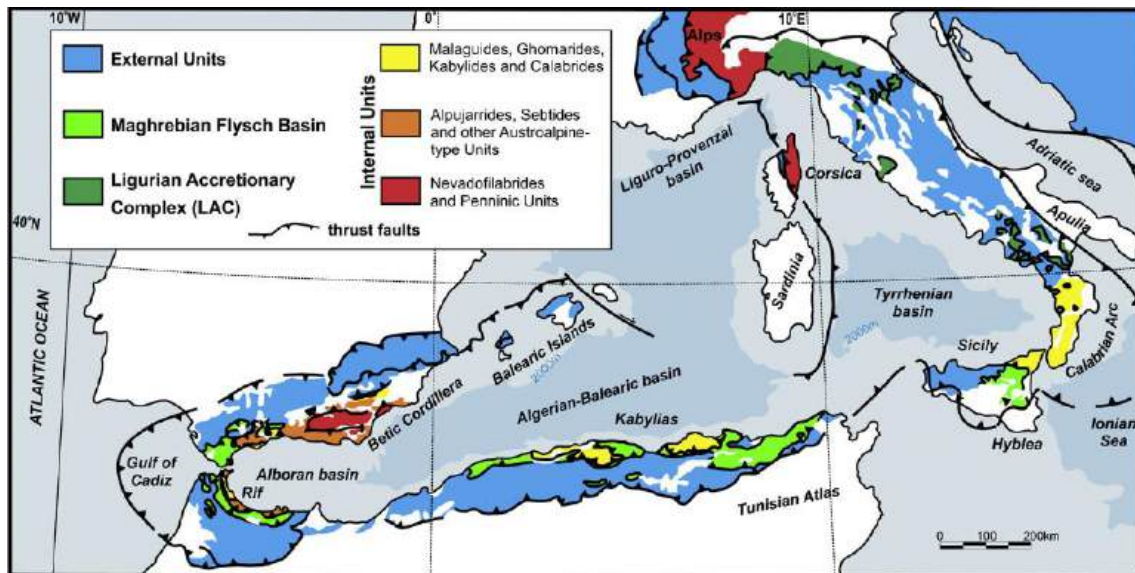


**Figure 25.** Western Mediterranean simplified tectonic sketch (Vitale and Ciarcia, 2013)

The trench roll-back, known also as subduction zone retreat, is the most accredited explanation to justify both the reasons of the shape of the peri-Mediterranean belt and the concomitance of tectonic processes, which have long been debated (e.g., Bouillin, 1984; Channell et al., 1979; Edwards and Grasemann, 2009; Faccenna et al., 2004; Malinverno and Ryan, 1986). The occurrence of the Wadati-Benioff zones strengthens the roll-back theory, according to which the ongoing formation of extensional basins with oceanic lithosphere, e.g., the Liguro-Provençal and Tyrrhenian basins, suffered both on time and space movement of magmatism and volcanic arcs, while on the slab in subduction, a concave shape orogenic belt take form, as occurs in the system formed by the Tyrrhenian Sea, Southern Apennines, Calabrian arc and Maghrebid (Doglioni et al., 1991; Kastens et al., 1988; Malinverno and Ryan, 1986; Royden et al., 1987). The Southern Apennines are the youngest segment (Stanley and & Wezel, 1985) of the peri-Mediterranean orogenic belt with a roughly N-E extension from Campania to northern Calabria. The formation of the southern Apennines may be framed in the Neogene-Quaternary N-S convergence framework between the western margin of the Adria microplate and the European plate (Casero et al., 1988; Dewey et al., 1989; Mazzoli and Helman, 1994; Patacca and Scandone, 2007) and the consecutive south-westward subduction and retreat which led to the opening, starting from late Tortonian (?) of the Tyrrhenian back-arc basin (Dewey et al., 1989; Gutscher et al., 2017; Malinverno and Ryan, 1986; Rehault et al., 1987; Sartori, 1990; Selvaggi and Chiarabba, 1995).

## 5.2 Quaternary shorelines along the Tyrrhenian margin of the southern Apennines

Quaternary uplift rate is generally derived by the elevation of raised paleoshorelines, which represents markers to evaluate surface vertical movements. This paragraph is aimed to illustrate the state of the art regarding the Tyrrhenian coastal side of the Southern Apennines (**Figure 26**), focusing on Campania and Calabria-Basilicata boundary.

- Early Pleistocene

Marine sediments associated to marine terraces up to 350 m a.s.l in Mt. Bulgheria promontory, at Camerota, Licosa and Cava Bianca, have been biostratigraphically correlated to Emilian period for the presence of *Hyalinea baltica* (Pasini, G., Colalongo, 1994), *Hemicytherura truncata* and *Mutulus laticancellatus* (Bonaduce et al., 1987; Borelli et al., 1988; Ciampo, 1976; Sgrosso and Ciampo, 1966). The Emilian marine sediments seal fault scarp dislocate older paleosurface up to 400 m (Romano, 1992). A second order of paleosurface have been recognized up to 1200 m a.s.l., it means the top of Mt. Bulgheria, with indeterminate marine origin, while the formation of the 400 m paleosurface has been related to a marine transgression Plio- Pleistocenic pre-Emilian stage, tentatively related to the Sanernian stage (Early Pelistocene) due to the presence of *Bulimia elegans marginata* and *Calcidiscus macintyreii* (Baggioni et al., 1981; Borelli et al., 1988; D'Elia et al., 1987, Caiazzo et al., 2006 and references therein).

On Capri Island, the oldest marine terraces (Migliara and Mt. Lauro deposits) have been traced up to 300 m a.s.l. (Barattolo et al., 1992) and also in these case it seals faults which dislocates paleosurface between 400 and 500 m a.s.l., which marine origin is still debated. By geomorphological correlation, the marine terraces on Capri Island between 130 and 300 m a.s.l. are related to Lower

or Middle Pleistocene, while on the southern edge of Sorrento Peninsula, at Conca dei Marini Site, the marine terraces up to 200 m a.s.l. is related using geomorphological criterion to Lower Pleistocene (Romano, 1992) in contrast with the interpretation of Brancaccio et al., (1981).

- Middle Pleistocene

Middle Pleistocene evidences of paleoshorelines have been reported for the Cicciano-Polvica area at 150 m a.s.l. (Ietti and Sgrosso, 1963; P Romano et al., 1994b), at 130 m on Capri island (Barattolo et al., 1992) and between 50 and 35 m in Sorrento Peninsula (Cinque and Romano, 1990). In Mt. Bulgheria, the marine terraces between 15 and ca. 150 m have been related to Middle Pleistocene by geomorphological correlation with the Last Interglacial paleoshorelines.

Regarding the Cicciano-Polvica area, new data are presented in this thesis at **Section 6.1** Evolution of the Campania Plain Quaternary coastal graben (southern Apennines): constraints from raised paleoshorelines and **6.2** Tectonic implications of raised Quaternary paleoshorelines in the NE sector of the Campania plain, southern Italy.

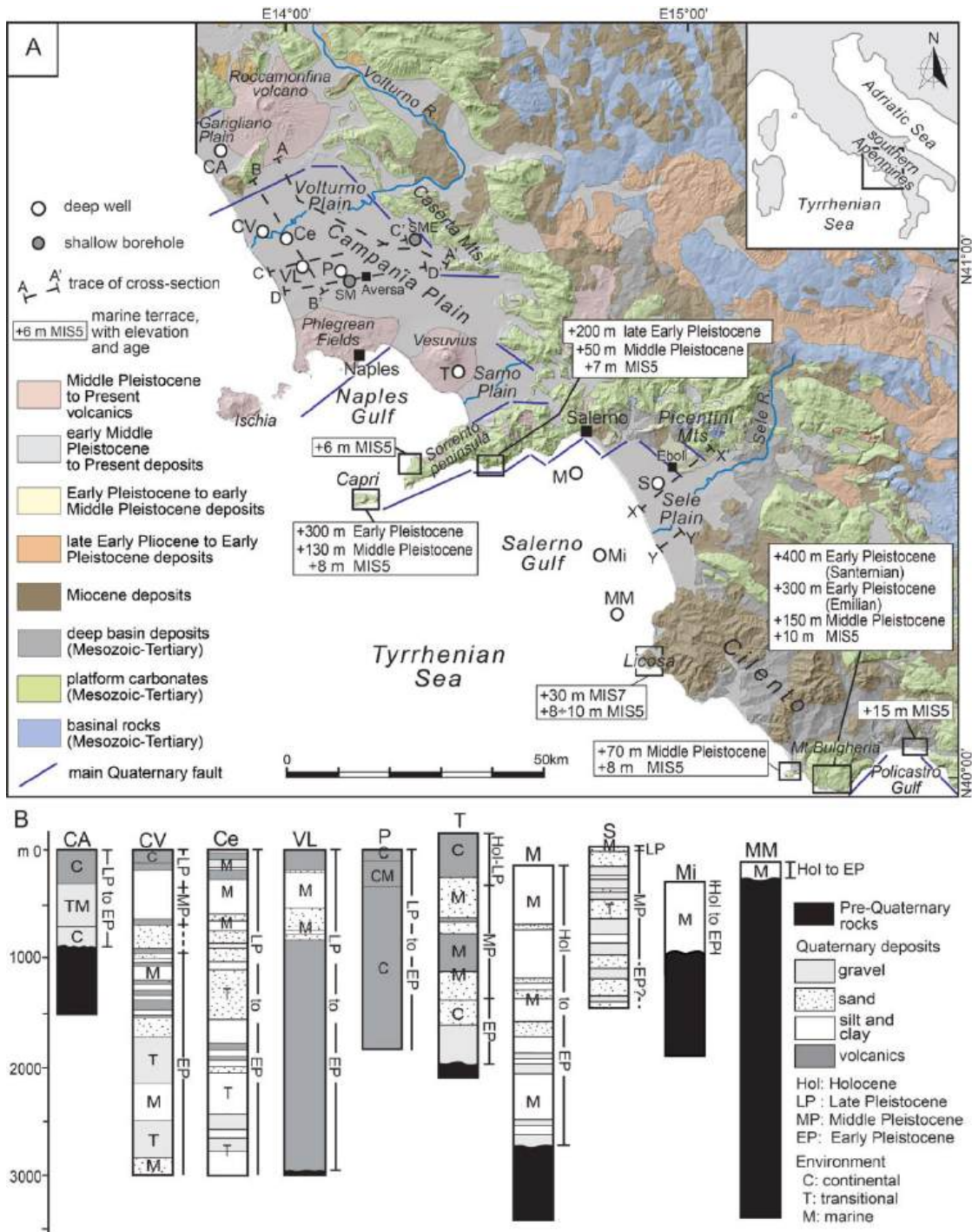


**Figure 26.** A) Quaternary marine terraces ubication with elevation along the Tyrrhenian coast of the Campania-northern Calabria area on a simplified geological map. B) Log of some important boreholes of the area (Santangelo et al., 2017 and reference therein);

## **6. New data on late Quaternary paleoshorelines in the Southern Apennines, Italy**

### *6.1 Evolution of the Campania Plain Quaternary coastal graben (southern Apennines): constraints from raised paleoshorelines*

This section is focused on the NE edge of the Campania Plain, which results are synthesised in the following work:

Manuscript 1- *Evolution of the Campania Plain Quaternary coastal graben (southern Apennines): constraints from raised paleoshorelines* by Cerrone, C., Di Donato, V., Mazzoli, S., Robustelli, G., Soligo, M., Tuccimei, P., Ascione, A., submitted to *Geomorphology*.

#### 6.1.1 Introduction

Raised paleoshorelines, as indicators of past relative sea level positions, are the most reliable markers of uplift along the coasts of both active and passive continental margins. The vertical positions of paleoshorelines result from the complex interaction between crustal motions and sea level fluctuations. Worldwide, flights of marine terraces are used to constrain the amount and timing of vertical motions, once the glacio-hydro-isostatic (GIA) component is removed from the modern vertical position of paleoshorelines. Due to their planar, sub-horizontal geometry, marine terraces are also excellent markers of displacements along faults, thus providing first order constraints to the amount and chronology of fault activity eventually accompanying uplift of coastal areas (Armijo et al., 1996; Meschis et al., 2018; Roberts et al., 2013). Marine terraces have been widely used to reconstruct both large-scale and differential vertical motions of the Tyrrhenian

Sea coastal margin of the southern Apennines mountain belt during the Quaternary (Ascione and Romano, 1999; Dumas et al., 1982; Westaway, 1993). The modern southern Tyrrhenian margin is defined by a series of coastal promontories and deep gulfs, which are the expression of extensional block faulting along major S- to SE-dipping faults occurred since the Early Pleistocene in response to rifting in the Tyrrhenian Sea back-arc basin (e.g. Bruno et al., 2000; Casciello et al., 2006; Florio et al., 1999; Milia et al., 2013; Milia and Torrente, 2015). Raised marine terraces testify to long-term Quaternary uplift in the order of several hundreds of metres of the Sorrento peninsula – Capri island and Cilento promontories and the Calabria coast (e.g. Ascione and Romano, 1999; Barattolo et al., 1992; Carobene and Dai Pra, 1990; Damiani, 1970; Dumas et al., 1982; Filocamo et al., 2009; Miyauchi et al., 1994; Westaway, 1993; **Figure 27**).

In some instances, those terraces have provided constraints to fault activity and chronology crucial to both the reconstruction of the Tyrrhenian margin evolution, and the identification of potentially active structures in the offshore (Ferranti et al., 2008). The coeval evolution of the coastal grabens, which are currently occupied by sea gulfs and coastal plains of variable widths, has been controlled by tricky interaction among subsidence (in the order of thousands of metres), sea level fluctuations and sedimentary inputs (Santangelo et al., 2017). One of the largest coastal grabens along the Tyrrhenian Sea southwestern margin is that occupied by the flat, low-lying and non-incised Campania Plain, which hosts the Campi Flegrei and Vesuvius volcanic areas (**Figure 27**).

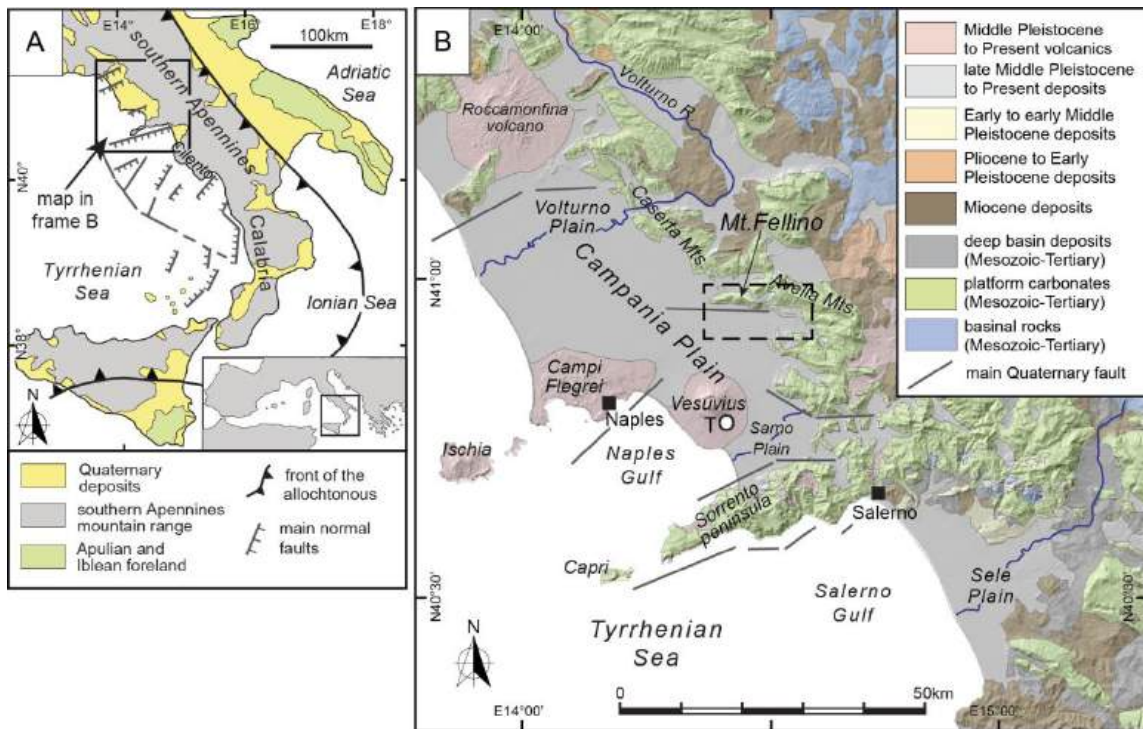


**Figure 27.** A: Tectonic framework of the Tyrrhenian margin of the southern Apennines (redrawn and modified after Moussat et al., 1986). B: Geological framework of the Campania Plain coastal graben (location in diagram A; modified after Ascione et al., 2013); the dashed box indicates location of the study area.

Huge amounts of subsurface data (deep wells, seismic stratigraphy and geophysical data) have allowed outlining the long-term subsidence history of the Campania Plain graben and inferring its large-scale structural setting (Barra et al., 1991; Romano et al., 1994a; Santangelo et al., 2010). Geomorphological information combined with shallow subsurface data have provided evidence for recent (late Quaternary) surface displacements in the northern and southern margins of the Plain and in the areas affected by active volcanism, where exceptionally fast Holocene vertical motions related to volcano-tectonic processes are also recorded (Valente et al., 2019a). Yet, surprisingly, existing information on the Quaternary behaviour of the horst blocks at the Campania Plain margins is limited to the southern coast of the Sorrento peninsula (northwestern boundary of the Salerno Gulf coastal graben; **Figure 27**). No evidence of flights of marine terraces from the overall straight-profile fault escarpments that define the

boundaries of the Campana Plain has been reported to date, with the only exceptions being raised marine deposits recognised by Romano et al. (1994a) from the Mt. Fellino ridge area, in the eastern boundary of the Campania Plain (**Figure 27**). Still nowadays those deposits, which were tentatively correlated with Marine Isotope Stage (MIS) 5 and the late Middle Pleistocene, respectively, represented the only outcrop evidence of Quaternary uplift of the Campania Plain margin. Quarrying activities carried out in the last decades along the southern mountain front of Mt. Fellino ridge provided extensive exposures of those raised marine deposits. Our investigation in this area allowed us to detect a flight of raised paleoshorelines. The reconstructed scenario in which the paleoshorelines were formed, and deformed, provides a comprehensive picture of the syn-tectonic development of shore systems, as well as new insights into the evolution of the Tyrrhenian margin inland of the southern Campania Plain graben.

#### 6.1.2 Materials and methods

A geomorphological study, focused on analysis of evidence of raised marine terraces and deposits, was carried out in the northern boundary of the southern Campania Plain. The topography analysis was carried out using 1:5.000 topographic maps and a 5X5 m DTM released by the Regione Campania, and LIDAR data released by the Italian Ministry of Environment - MATTM. For each of the identified paleoshoreline remnant, the elevation of the conventional paleo-sea level indicator, i.e. the inner-edge of the abrasion platform, and the horizontal extension of the marine terrace have been accurately measured (or well constrained) using both a GPS and 1:5.000 scale topographic data. The study was combined with stratigraphical, micropaleontological and facies analysis of the Quaternary deposits - both marine and continental - associated with the paleoshorelines, and integrated with the analysis of structural data on the faults,

which dissect the Quaternary deposits. Field mapping and sedimentological analyses of continental deposits were primarily performed with the aim of characterizing specific assemblages of genetically associated facies, and then sedimentary processes and depositional architecture. The depositional setting of the massive sands outcropping in the study area was investigated through micropaleontological and granulometric analyses. Granulometric analysis was carried out on 7 samples by wet sieving 100 gr of sediment through a 4000 to 63  $\mu\text{m}$  sieves pile. Grain-size statistics were calculated with GRADISTAT version 8.0 (Blott and Pye, 2001). Micropaleontological analyses were performed on  $> 125 \mu\text{m}$  wash residuals. Dating of Quaternary marine deposits recovered in the study area is difficult. The marine deposits (cobbles/pebbles and sand) are mostly coarse, and their macrofossil content essentially consists of mostly recrystallized shells. In order to get an indirect chronological constraint of the marine deposits, we carried out U-series dating of a sample from a calcite vein that dissects the marine sands in one of the investigated sites (Site 2; **Figure 28**). Continental carbonate deposits are suitable for U-series dating in case the initial content of uranium is sufficient for measurements and if none, or very limited, detrital thorium component is present in the analysed sample. On the contrary, unquantified chemical alteration due to U-absorption from mollusc shells after their death make the U-series method not useful for molluscs dating (Bernart et al., 1985; Kaufman et al., 1996, 1971). The method is based on the isotopic fractionation of  $^{238}\text{U}$  and  $^{234}\text{U}$  (parent isotopes) from  $^{230}\text{Th}$  (daughter isotope), which has a shorter half-life than the parent isotopes. About 30 gr of continental carbonates has been ultrasonically cleaned and powdered. Then, the sample has been dissolved in nitric acid and spiked with  $^{228}\text{Th}$  and  $^{232}\text{U}$  in secular equilibrium. The organic matter has been eliminated adding a few millilitres of hydrogen peroxide and heating at  $100^\circ\text{C}$  for a few tens of minutes. Isotopic activity ratio has been alpha-counted in a high-resolution ion implanted Ortec silicon surface barrier detectors after the extraction of U and Th according to

the guidelines included in Lawrence Edwards et al., (1987). The provided age has been calculated by means of Isoplot/Ex (version 3.0), a plotting and regression program designed by Ludwig, (2003) for radiogenic-isotope data.

### 6.1.3 Geological background

The study area is located in the NE border of Campania Plain coastal graben, along the Tyrrhenian margin of the southern Apennines (**Figure 27**). The formation of coastal basins along the southwestern margin of the southern Apennines occurred as a response to extensional processes active in the southern Tyrrhenian back-arc basin coeval with Neogene to early Middle Pleistocene shortening in the southern Apennines (e.g., Patacca et al., 1990; Sartori, 1990; Savelli and Schreider, 1991). Back-arc extension began in Late Tortonian times in response to the roll back towards the SE of the subducting Apulian-Ionian plate (Elter et al., 1975; Patacca et al., 1990; Scandone, 1979). Through time, the locus of rifting shifted from the central part of the Tyrrhenian basin towards the southeast, and affected the modern southern Apennines margin since the Early Pleistocene with extensional block-faulting along major S- to SE-dipping faults (Bruno et al., 2000; Casciello et al., 2006; Milia et al., 2013; Milia and Torrente, 2015; Sartori, 1990; **Figure 27**). Extensional processes in the Campania Plain graben were accompanied by volcanism, which has originated intense explosive eruptions since ca. 400 ka and is still active in the Campi Flegrei area and Vesuvius (Barberi et al., 1978; Brocchini et al., 2001; Ippolito et al., 1973; Rolandi et al., 2003; Rosi and Sbrana, 1987; Santangelo et al., 2017, and references therein)

Regional scale evidence indicates that formation of the Tyrrhenian coastal grabens started in the Early Pleistocene in response to the activity of extensional faults with main NW-SE and roughly E-W and NE-SW trends, which collectively offset the carbonate rocks that crop out in the grabens' margins by around 3000-

4000 m (e.g., Argnani et al., 1989; Bartole et al., 1984; Bruno et al., 1998; Caiazza et al., 2006; Cinque et al., 2000a; Florio et al., 1999; Moussat et al., 1986). In the Campania Plain graben, master faults dipping towards S and SW have been imaged by seismic profiles and geophysical (magnetic and gravity) data both inland and in the offshore, and define the boundaries of two main sub-basins, the northern one occupied by the Volturno River Plain, and the southern one including the Gulf of Naples and active volcanic areas (e.g., Bruno et al., 2000; Casciello et al., 2006; Florio et al., 1999; Milia et al., 2013; Milia and Torrente, 2015 and references therein; **Figure 27B**). Consistently, stratigraphic data from shallow wells and/or geomorphological evidence indicate that faults with trends around E-W located at the northern boundaries of the Volturno River plain and southern Campania Plain sub-basins were responsible for late Quaternary subsidence (e.g. (Brancaccio et al., 1994; Cinque et al., 2000a; Scandone et al., 1991; **Figure 27**). A more than 3000 m thick succession of shallow marine, transitional and alluvial deposits (Ippolito et al., 1973; ViDEPI, 2009) testifies to fast subsidence of the northern Campania Plain since the beginning of the Calabrian stage (e.g., Brancaccio et al., 1991). Subsidence appears to have started later in the southern Campania Plain, where marine deposits recovered at around 1400 m depth have been framed in the 1.24 to 0.90 Ma time span and a collapse event occurred around 0.4-0.3 Ma followed by fast subsidence is recorded (Brocchini et al., 2001). Besides being mainly controlled by the interaction between subsidence and sea level fluctuations, the geomorphological-stratigraphical evolution of the Campania Plain was influenced by emplacement of abundant pyroclastic products of intense explosive eruptions that occurred since 400 ka (Rolandi et al., 2003) and climaxed at ~39 ky with the eruption of the Campanian Ignimbrite, which blanketed the floors of the alluvial plains of the Campania Plain and surrounding region with a pyroclastic cover ranging in thickness from ~1 to several tens of metres (e.g., Giaccio et al., 2017; Valente et al., 2019a). Afterwards, several explosive eruptions occurred in the

Campi Flegrei volcanic field and in the southern part of the Campania Plain graben, where the Somma-Vesuvius volcano was active since ~33 ka (Giaccio et al., 2008). Nowadays, variable thicknesses of Late Pleistocene-Holocene pyroclastic products cover the top surfaces and slopes of the ridges surrounding the Campania Plain (e.g., ISPRA, 2014a, 2014b, and references therein, **Figure 28**). Shallow marine deposits recovered in boreholes located at short distance from the carbonate elevations at the eastern boundaries of the Campania Plain indicate that, during the late Quaternary, the complex sedimentary dynamics governed by subsidence, sea level fluctuations, alluvial sedimentation and abundant accumulation of both primary and reworked pyroclastic deposits caused repeated coastline migrations exceeding 30 km (e.g., Bellucci, 1994; Cinque and Irollo, 2004; Cinque, 1991; Santangelo et al., 2017, 2010). Following emplacement and subsequent incision of deep valleys in the Campanian Ignimbrite plateau during the Last Glacial Maximum, pyroclastic inputs conveyed by both the Campi Flegrei and Vesuvius favoured filling up of the inner part of the graben and coastal progradation during the late Holocene (Amorosi et al., 2004; Barra et al., 1996; Bellucci, 1998; Cinque, 1991; Romano et al., 1994a; Santangelo et al., 2017; Valente et al., 2019a). Little is known on the vertical motions of the horst blocks at the basin boundaries. Raised marine terraces from the southern coastal belt of the Sorrento peninsula (northern boundary of the Salerno Gulf coastal graben; **Figure 27**) point to uplift of such a horst block of around 200 m since the early part of the Middle Pleistocene (Cinque and Romano, 1990). On the other hand, shorelines from the southern coast of the Sorrento peninsula correlated with MIS 5e and 5a through geomorphological reconstructions and/or geochronological data (Th/U method; Brancaccio et al., 1978; Iannace et al., 2003; Riccio et al., 2001) and located in the elevation ranges of 8 to 6.5 m and 3.5 to 1.5 m, respectively, testify to ceasing of uplift of that horst block since the Late Pleistocene. Evidence of raised Quaternary marine deposits in

the eastern boundary of the Campania Plain is only detected in the southern slope of the Mt. Fellino ridge (location in **Figure 27B**).

The backbone of Mt. Fellino ridge, similar to the other elevations at the boundaries of the Campania Plain, is composed of Mesozoic carbonate rocks. The Mesozoic succession of Mt. Fellino ridge is deformed by a km-scale overturned anticline associated with a thrust that brought Jurassic rocks (outcropping in the eastern part of the ridge) over the Cretaceous terms of the carbonate succession that form the western part of the ridge (Bravi et al., 2006; ISPRA, 2014a). According to Bravi et al. (2006), the contractional structures are dissected by high angle faults that cut across the ridge and strike-slip faults at its southern and northern boundaries, with the latter structure towards the east separating Mt. Fellino ridge from the Avella Mts. ridge (**Figure 27B, Figure 28**). In that area and, particularly, along the southern slope of Mt. Fellino ridge, Romano et al. (1994a) highlighted the occurrence in a quarry located in the Canello village (western termination of the ridge) of sandy deposits located at ~50 m a.s.l. that they correlated with the Last Interglacial and, in a quarry located in the eastern part of the ridge, of marine pebbles at ~ 120 m a.s.l., which were correlated with the late part of the Middle Pleistocene.

#### 6.1.4 Geomorphological features of the northern boundary of the southern Campania Plain

The Campania Plain coastal graben, although featuring an overall NW-SE trend, is characterised in the southern part by an irregular and indented perimeter. The deeper indentations of the Campania Plain are those located at the northern and southern flanks of the roughly E-W oriented, 676 m high Mt. Fellino horst that, together with smaller carbonate hills rising above the Roccarainola village, represent downfaulted blocks of the higher Avella Mts. ridge to the NE (Bravi et

al., 2006; **Figure 27; Figure 28**). The plain to the north of Mt. Fellino ridge is punctuated by small carbonate hills; it stands about 15-20 m higher and is less flat than the plain to the south. The latter, hereinafter labelled Polvica plain, is undissected by the drainage network (it was repeatedly reclaimed in the 17th and 18th centuries; Ruberti and Vigliotti, 2017) and stands around 30-35 m a.s.l. At the eastern termination of Mt. Fellino, the Polvica plain rises gently towards the NE and E to reach about 100 m a.s.l. at the toe of the Roccarainola hills, and even higher elevation further to the east, due to the presence of a gently inclined, poorly incised glacis. The glacis represents the distal part of a depositional slope accreted by alluvial fans fed by streams dissecting the elevated Avella Mts. and ridges to the E (**Figure 28**).

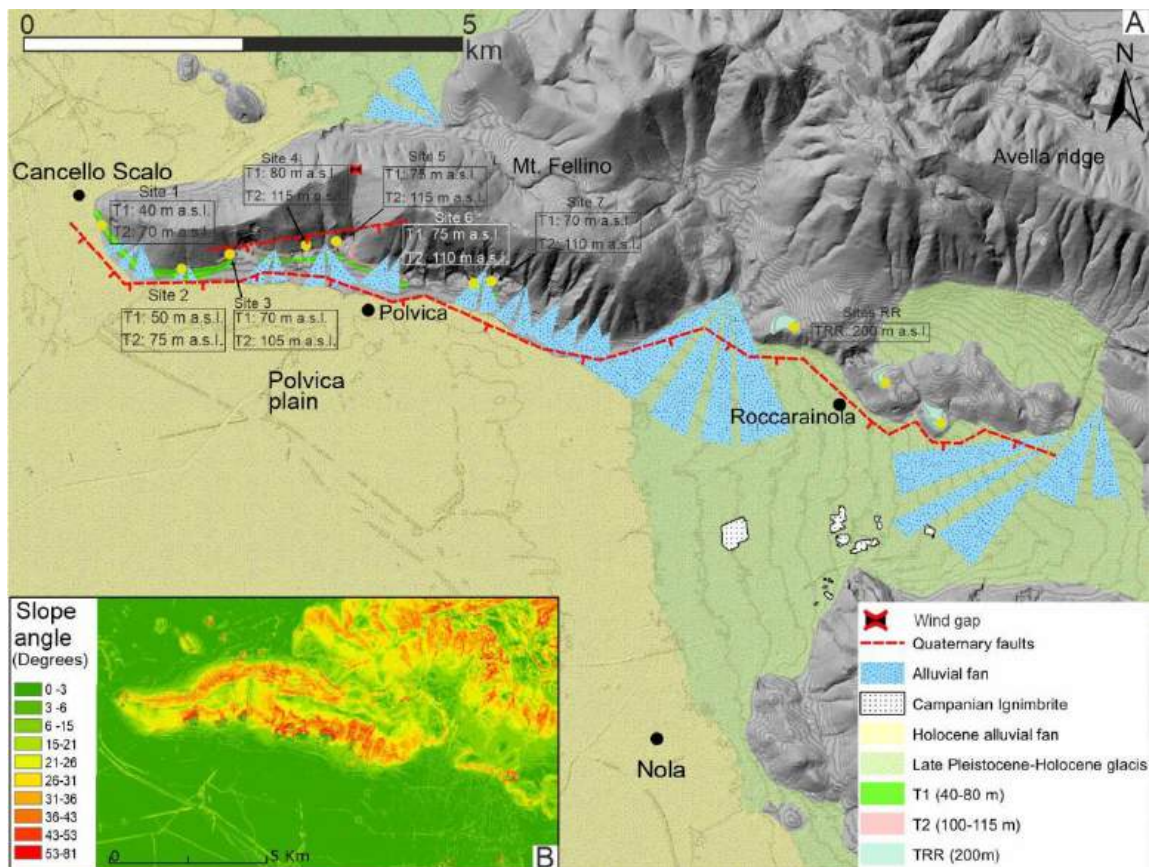


**Figure 28.** A: Geomorphological map of the northeastern edge of Campania Plain with 10 m interval contour lines. Boxes indicate the elevation of T1, T2 and TRR marine terraces in the study area. B: Slope angle map in degrees.

Alluvial deposits pertaining to the glacia, which surround and partly bury the Roccarainola hills, crop out in several quarries dug in the Polvica plain. They consist of several metres thick sediments mainly composed of calcareous gravel strata interbedded with sandy layers and lenses and volcanoclastic beds composed of pumices and cinder. In all outcrops, such deposits overlay the distinct Campanian Ignimbrite layer, which constrains their age to the upper Late Pleistocene-Holocene.

The features of the slopes of the Mt. Fellino horst block is similar in shape to the greatest majority of carbonate fault escarpments widespread in the Apennines. Those escarpments feature straight profiles with slope angles ranging

between about 25° and 35° and their shapes are fundamentally invariant either if the slopes are entirely cut in the limestones, or they are partly/entirely formed of slope breccia accumulated during the recession and replacement of the originally steep carbonate cliffs (Ascione and Cinque, 1997; Brancaccio et al., 1979; Cinque et al., 1993). However, when examined in detail, topography of Mt. Fellino ridge is asymmetrical. The profile of the northern slope is entirely straight and steep (~35°-40° inclined) (**Figure 28B**). The southern mountain front features an overall composite profile that is suggestive of a long-term polycyclic evolution. That slope is characterised by a smooth upper segment, which in the central part of the ridge is characterised by a hanging concavity at 330-340 m a.s.l., and a steep mid segment with mean slope angle increasing from the west to east, which is almost entirely formed in slope breccia deposits (**Figure 28**). In the central-eastern part of the ridge, the slope profile is broken by a hanging concavity that ends around 100 m a.s.l. and occurs rather continuous along the slope, as shown by field evidence and inferred from old topographic maps produced around year 1950, prior to development of extensive and widespread quarrying. In the middle part of Mt. Fellino ridge, a wide and straight, misfit valley forms a deep saddle in the ridge crest thus suggesting valley beheading (**Figure 28**). That valley is aligned along one of the main N-S oriented high-angle faults that dissect the ridge. Fault block motions associated with these structures are also made evident by changes in the ridge width associated with steps in the ridge crest (**Figure 28**).

The lowermost part of Mt. Fellino southern escarpment crops out discontinuously between the upper Late Pleistocene-Holocene (**Figure 28**). Some outcrops (quarry cuts in sites 2 and 3; location in **Figure 28**) show that the alluvial fans at the toe of the Mt. Fellino mountain front consists of abundant, poorly weathered and reworked pyroclastic deposits interlayered with gravel beds and, at some places (outcrops nearby Site 3; location in **Figure 28**) tephra lenses and

layers. In their proximal parts, those alluvial fans are inset in, and partially cover, older alluvial fan deposits made up of mainly coarse-grained deposits (see Section 5.2 Quaternary shorelines along the Tyrrhenian margin of the southern Apennines). An excavation located in the westernmost part of the ridge exposes, below the alluvial fan deposits, a several metre thick outcrop of the Campanian Ignimbrite deposit. Based on such a stratigraphical evidence, an upper Late Pleistocene – Holocene (< 39 ka) age may be assigned to the alluvial fans that form the piedmont of Mt. Fellino ridge.

#### 6.1.5 The paleoshorelines in the northern margin of the southern Campania Plain

The highest marine terrace in the area is found in the Roccarainola hills (hereafter labelled RR site; **Figure 28; Figure 29**).

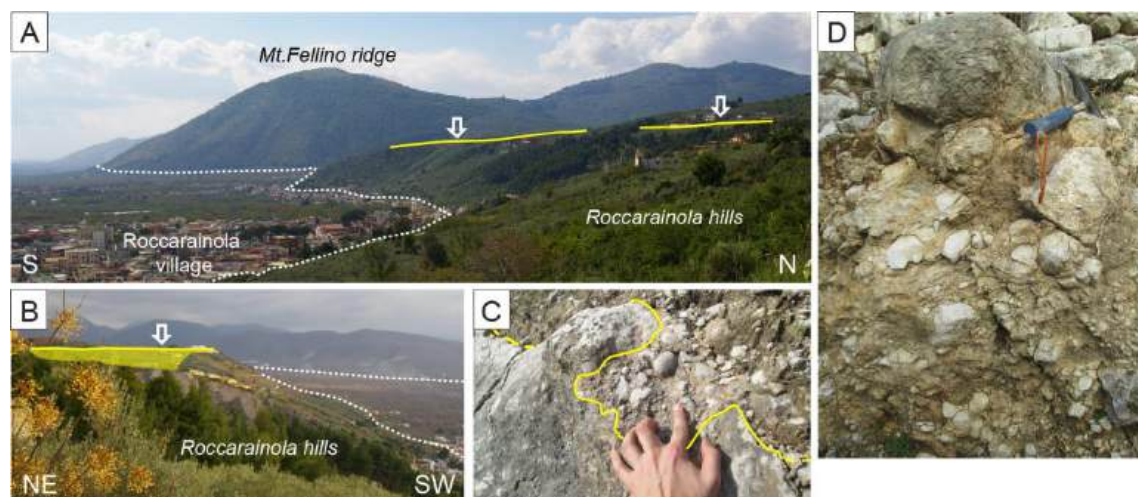


**Figure 29.** A and B: views from the east and northwest, respectively, of the wide, c. 200 m high marine terrace, marked by the yellow lines and arrows (the light-yellow area in the photo in B marks the terrace surface), sculpted in the Roccarainola hills (location in Fig. 2); the white dotted lines mark the limit of the gently sloping depositional surfaces of the alluvial fans, which form the glacis at the eastern termination of the Polvica plain; in the image in A, Mt. Fellino ridge is visible in the foreground. C and D: Close-up views of the Roccarainola marine terrace, showing the abrasion platform, marked by the yellow line, covered by pebbles (photo in C) that pass upwards to coarse pebbles and marine sands, shown in the image in D.

There, geomorphological evidence and, in particular, the presence of wide flat surfaces eroded on N- to NE-dipping carbonate strata of the low hills at the NE boundary of the Polvica plain, suggest coastal modelling. Those surfaces, extended up to c. 200 m in width, are for the most part either bare or covered by colluvial deposits and reddish soils formed on recent - Holocene – pyroclastics (ISPRA, 2014a). Their marine origin is indicated by a matrix-supported basal conglomerate with well rounded carbonate pebbles, a few cm to a few dm in size, which evolves in a thin layer of loose sands (diagrams C and D of **Figure 29**). Benthic foraminifera assemblages, not very abundant, include *Ammonia parkinsoniana* and *Elphidium crispum*, suggesting an infralittoral marine deposition (Sgarella and Moncharmont Zei, 1993). Scattered planktonic *Globigerina* spp. specimens were also found. The marine deposits were recovered in the outer part of the RR abrasion platform, at 195 a.s.l., and an elevation in the 200-220 m range is estimated for the inner edge of this terrace.

Besides the Roccarainola area, several paleoshoreline remnants were identified along the southern fault escarpment of Mt. Fellino ridge. The straight profile of the Mt. Fellino southern fault escarpment masks the remnants of marine landforms and deposits that crop out at variable elevations in a series of quarries (Sites 1 to 7; location in **Figure 28**), hidden below coarse-grained continental deposits. Those buried paleoshoreline remnants and the overlying deposits are described in detail in the following **Section 6.1.6**, starting from the upper continental sediments. The detailed surveys carried out in the investigated area also allowed identification, in the lowermost part of Mt. Fellino southern escarpment, of planar surfaces representing coastal morphologies, which are described in **Section 6.1.7**.

## 6.1.6 The buried paleoshoreline remnants in the southern mountain front of Mt. Fellino ridge

### 6.1.6.1 The continental deposits burying the paleoshoreline remnants:

The raised marine deposits that crop out in sites 2 to 7 are partly eroded and covered by coarse grained continental deposits (**Figure 30** to **Figure 35**). Facies analysis has aimed at pointing out specific assemblages of genetically associated facies (facies association) to interpret depositional systems.

The clastic bodies occur grouped into distinct stacking stratal units separated by bounding surfaces usually marked by reddish paleosols or by erosively concave-up bases giving an overall low-angle cross-stratification from a distance (sites 3, 4). The stacking pattern of the stratal units also suggests a vertical growth and a basinward progradation or down-stepping of clastic bodies (**Figure 30D**, **Figure 30E**); the magnitude of their depositional slopes have average values varying up to 22°. Clastic deposits were studied along sharp, vertical to steeply sloping artificial scarps; they usually alternate at the base of the succession with marine conglomerates and sandstones. The surveyed cuts provide a reasonable representation of depositional processes building an alluvial fan system (sensu Blair and McPherson, 1994) consisting of 4 facies (a to d).

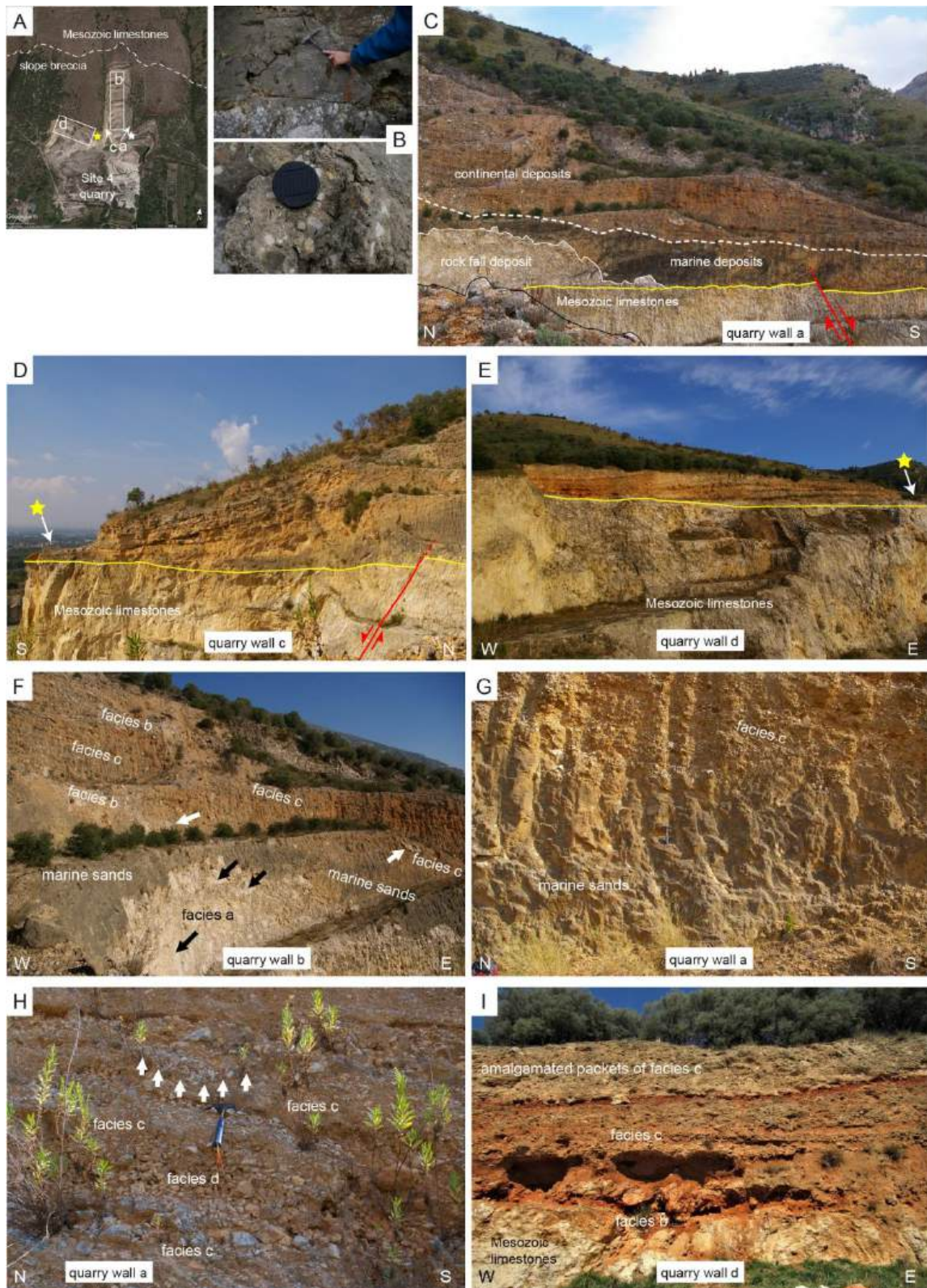


**Figure 30.** A: Google Earth image of the quarry labelled Site 4, showing locations of outcrops described in the text and shown in photos B to I. B: Close-up views of the conglomerates and arenites (upper image) and fossiliferous arenites with pebbles (lower image) that lay onto the abrasion platform in the outcrops marked in diagram A by the white and yellow stars, respectively. C, D and E show views of the outcrops in the quarry walls indicated by ‘a’, ‘c’ and ‘d’ in diagram A, showing the abrasion platform (marked by the yellow lines) and boundaries between the marine deposits and the continental deposits; the traces of the faults that displace the abrasion platform are shown in images in C and D; the yellow stars in diagrams D and E indicate location of the outcrop marked by the yellow star in diagram A. Diagrams D and E are also indicative of the stacked vertical and basinward stepping architecture of clastic bodies; diagrams F, G, H and I show detailed views of outcrops in Site 4, with indication of the sedimentary facies d.

Facies a: massive, pebble to boulder clast-supported conglomerate (fragmented rock slide deposit)

This facies consists of clast-rich, unsorted, pebbly to boulder gravel. The clasts are typically subangular to angular and equant in shape. Individual beds cannot be traced laterally in radial and transverse cuts, even though a large scale of bedding is locally present. Poor sorting is also highlighted by the presence of blocks and bedrock slabs (black arrows in **Figure 30F**; **Figure 32A**), and a certain amount of whitish, fine-grained calcareous matrix. This facies is typically sharply bounded and, despite its irregular geometry, exhibits an arcuate, wedge-shaped morphology (**Figure 30F**).

Altogether, the massive, ungraded nature and poor sorting of this facies are suggestive of sediment gravity processes resulting from bedrock failures (Blair and McPherson, 1994), likely due to the massive, flow-like motion of fragmented rock from rock slides (Brideau, M. and Roberts, 2015; Hungr et al., 2014). The downward movement is accompanied by partial bedrock disintegration, producing an unsorted granular mass composed of very large clasts and variable proportions of a cataclastic matrix.

Facies b: pebble to boulder gravel (rockfall deposit)

This consists of lens-shaped beds of subangular to angular, clast-rich, unsorted, granule to cobble gravel with yellowish matrix fines. Beds can be traced in transverse cuts for metres with faint planar parallel stratification (sites 3, 4). Pieces of evidence of single, up to boulder-size clast are occasionally noticed within the clastic successions. Indeed, the sedimentary wedges of the Sites 3 and 4 are punctuated by whitish, individual rock fragments embedded in reddish-yellowish clastic beds (white arrows in **Figure 30F**). It is reasonable to assume that bedrock slopes suffered rock fragmentation by rock slide processes. Once slope stability thresholds are exceeded, the fragmented bedrock falls downslope to develop wedge-shaped beds. Similarly, disjointed blocks, slabs or wedges were also prone to failure.

Facies c: massive to crudely stratified, locally amalgamated, pebble-to-cobble conglomerate (debris-flow deposits).

This facies, the bulk of the clastic successions, consists of clast-rich and matrix-rich, pebbly coarse to fine cobble gravel. Gravel content is variable and, in most cases, is dispersed in a brownish-reddish matrix-supported fabric (sites 2 to 7; **Figure 30G**; **Figure 31**; **Figure 32**; **Figure 33**; **Figure 34**; **Figure 35**). However, beds with higher gravel concentrations approach clast supported fabrics. Clasts are typically subangular to angular and mainly equant in shape. Most beds appear to be ungraded, but both normal and inverse grading are occasionally observed (**Figure 30H**); they frequently pinch out against the underlying beds and locally have a trough-shaped base and a lenticular geometry, with rare planar-cross-sets. The bed boundaries are typically sharp, with tabular to irregular geometry, but undulatory, scoured bases also occur. The beds of this facies tend to be stacked upon one another and amalgamated into bedsets, locally characterized by lenticular, scour-confined bedsets (sites 3 e 4; **Figure 30I**), up to a few metres thick, and metres to tens of metres in longitudinal extent.

The matrix to clast supported, unsorted, cobble to pebble gravel texture of this facies is diagnostic of debris flows (Johnson, 1984; Pierson, 1980; Rasmussen, 2000; Shultz, 1984), even though grading may account for coarse-grained hyperconcentrated flows (Benvenuti and Martini, 2002; Smith and Lowe, 1991). However, failure of colluvial slopes and the resulting transformation of a colluvial slide into a debris flow is considered the primary sediment-transport mechanism (e.g. Blair and McPherson, 1994). In this regard, the presence of matrix fine and embedded paleosol layer greatly support the development of a mantle of colluvium generated through high bedrock weathering. Further, the presence of downfan-dipping, lenticular wedge-trough units are the result of switching of the position of the active depositional lobe across the fan through time.

#### Facies d. Pebble to fine cobble lenses (surface lag deposits)

This facies consists of clast-supported, moderately to poorly sorted, granular pebble to cobble gravel in beds up to 40 cm thick. The thickest beds tend to have a lenticular to wedge geometry (**Figure 30H**) and extend laterally for some metres. These gravel beds are also present in isolated erosive-based pockets (white arrows in **Figure 30H**) interstratified with debris-flow deposits (Facies c). This facies has a better sorting and a clast supported texture due to lack of matrix fines.

The matrix-free, clast-supported, pebble to cobble gravel deposits of this facies developed by erosion and fine-fraction winnowing of the underlying debris-flow deposits by clear-water flows. Clear-water flows are typically documented to represent the dilute tail of debris flow events (Blair and McPherson, 1998; Sohn et al., 1999), or ordinary low energy overland flows responsible for the washing of debris-flow deposits (Blair, 1999; Blair and McPherson, 1994).

#### 6.1.6.2 Geomorphological, stratigraphical and structural features of the buried paleoshoreline remnants

Impressive outcrops of the buried paleoshoreline remnants sculpted in the southern escarpment of Mt. Fellino ridge occur in sites 2 to 7 (**Figure 28**), where the Jurassic or Cretaceous carbonates are cut by sub-horizontal abrasion platforms located at variable elevations. In the outcrops in sites 3 to 7 (**Figure 28**) the horizontal abrasion platforms are located at elevations in the range of 105-115 m and are characterised by minimum horizontal extension of 200-250 m. The types and thicknesses of the marine deposits, which cover the abrasion platforms, vary laterally along the inferred paleo-coast trace (**Figure 28**).

An excellent 3D exposure of the stratigraphic succession associated with the raised paleoshoreline remnants and the contact between the marine deposits and the rock fall deposits fed by the paleo-sea cliff is provided by the quarry cuts in Site 4 (**Figure 30A**). The innermost part of the platform at the western side of Site 4 is located 100 m a.s.l., whereas in the eastern side it reaches 115 m a.s.l. In the outcrops located close to the platform rim (stars in **Figure 30A-D-E**), the abrasion platform is covered by a few-metre thick succession that, from the base, is made up of well-rounded carbonate pebbles passing upward to fossiliferous calcarenites locally rich of bivalves, among which *Cardiidae*, containing lenses of pebbles and angular carbonate clasts at the top (**Figure 30B**). These features are indicative of marine deposition with inputs from a nearby retreating paleo-sea cliff. The conglomerate-calcarenite deposits pass upwards and towards the inner part of the platform into yellowish marine fossiliferous medium sands (Samples 4a-4b, Supplementary materials) and high quartz content, which show gently south-dipping laminations. The fossil content consists of valves and fragments of mollusks. The sands locally have a brownish color and alternate with layers of coarse sand and conglomerate up to about 10 m thick. In the innermost part of the outcrop, the sands onlap massive rock fall deposits that rest on the abrasion platform (quarry wall b in **Figure 30A**; diagrams C and F of **Figure 30**). Overall,

the entire exposed succession is indicative of the development and lateral growth of the abrasion platform (testified by the laterally changing composition of the marine deposits and presence of inputs from the paleo-sea cliff from the rim to the platform innermost part), and the evolution of a littoral sedimentary system. This was initially fed by erosion of the carbonate rocks of the platform-paleo sea cliff system, and then by allogenic inputs, which are testified by the low degree of textural and compositional maturity of the yellowish sands.

The mutually facing N-S trending quarry cuts of Site 4 (quarry walls a and b in **Figure 30A**) expose high angle, S-dipping faults, which clearly dissect with a c. 1 m offset, the abrasion platform (**Figure 30C** and **D**). The fault trace is less evident in the soft marine sands that overlie the abrasion platform and disappears in the overlying coarse grained sediments.

Slightly different stratigraphic successions are associated with the outcropping abrasion platforms in the nearby sites 5 and 3 (**Figure 28**). The paleoshoreline remnant outcropping in Site 5 (**Figure 31**), well exposed in a N-S oriented quarry wall, consists of a horizontal wave-cut platform located at 115 m a.s.l. covered by about 3 m thick cross-bedded, moderately sorted, fine arenites (Sample 5a, supplementary materials) that, in the inner part of the abrasion platform, pass laterally into a coarse-grained massive deposit (**Figure 31**).

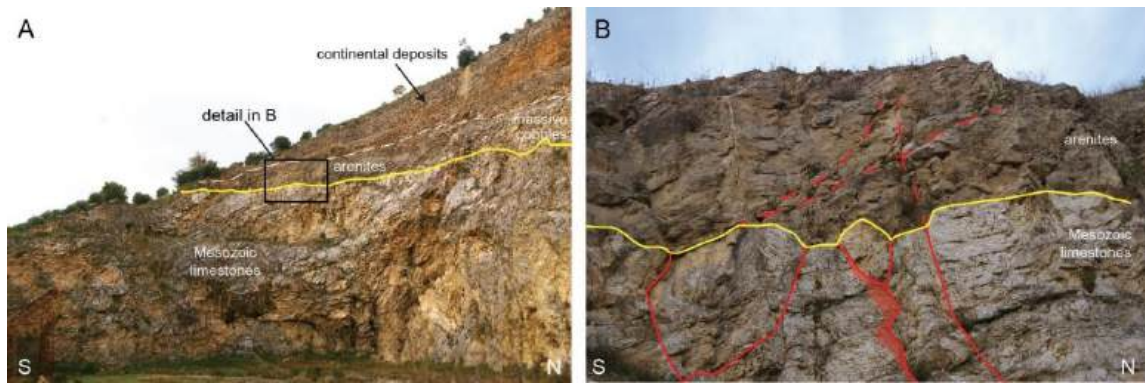


**Figure 31.** A: View of the buried marine terrace exposed in the quarry of Site 5, with indication of the marine (arenites, passing laterally into a massive cobbly deposit) and continental sediments that overlie the abrasion platform, which is marked by the yellow line. B: Detailed view of part of the outcrop at Site 5 (location in A); yellow line as in A. The red lines mark the traces of NNW striking steep faults offsetting the abrasion platform and locally passing into the overlying arenites. The latter are also cut by S dipping, moderate- to low-angle surfaces that may be interpreted as normal faults.

An infralittoral deposition of the arenites is indicated by the occurrence of *Ammonia parkinsoniana*, a benthic foraminifera which in the Mediterranean Sea area, mostly occurs in infra-littoral sandy bottoms (Sgarrella and Zei-Montcharmont, 1993), together with scattered planktonic Globigerinidae. The marine sands are erosively overlain by coarse-grained, clinostratified continental deposits. The marine-continental succession is dissected by faults. In particular, the abrasion platform is dissected by NNW striking steep faults that locally pass into the overlying sands, which are also cut by S dipping, moderate- to low-angle surfaces that may be interpreted as normal faults (**Figure 31B**).

On the eastern side of the quarry of Site 3, Quaternary clastic deposits cover a thin yellowish sandy layer, which rests on the wave-cut platform on the bedrock at an elevation of 110 m a.s.l. (**Figure 32**).

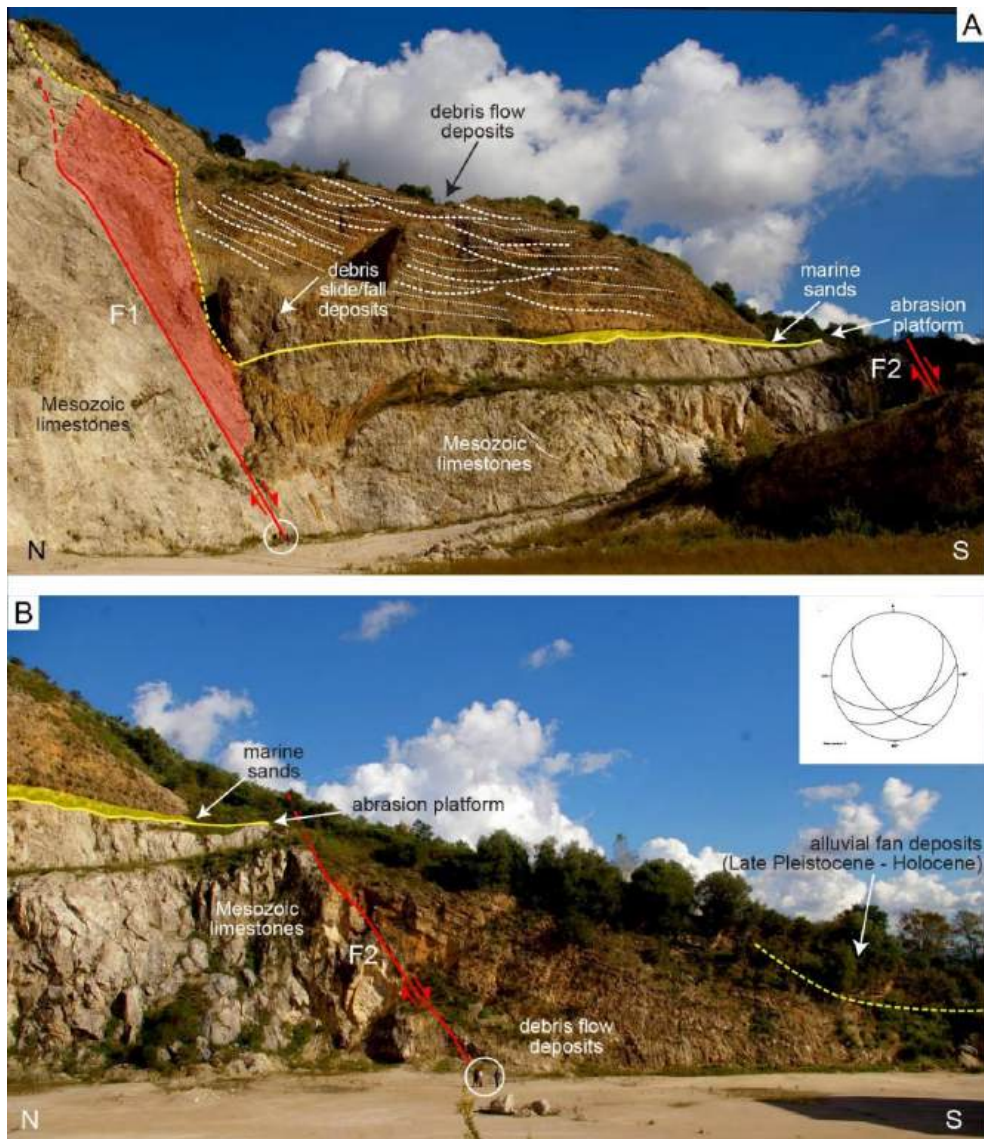


**Figure 32.** Views of the northern (A) and southern (B) parts of the outcrop in Site 3 (note locations of the same fault F2 in the two images); dashed yellow lines indicate superimposed erosive-based units of debris-flow facies; red lines follow traces of the S-dipping faults F1 and F2; note, in the white circles, persons for scale. A: Abrasion platform located 110 m a.s.l. (marked by the yellow line) covered by sandy deposits (marked by the yellowish band) that, towards the inner part of the abrasion platform, pass laterally into a wedge-shaped debris slide/fall deposit and are covered by debris flow deposits (thick dashed lines mark erosive contacts between debris flow units and thin dashed lines mark debris strata). The light-red area marks the fault F1 plane, partly exhumed by quarrying. Note, in the hanging wall block of fault F1, the rollover structure that involves both the limestones and abrasion platform and truncation of debris strata against fault F1 plane. B: View of the blocks in the footwall and hanging wall of fault F2; in the latter block, note the drag fold involving the downthrown debris flow deposits, which are unconformably covered by alluvial fan deposits related to the upper Late Pleistocene - Holocene alluvial fans in the piedmont of Mt. Fellino ridge. In the upper right corner, lower-hemisphere, equal-area projection shows data of faults exposed at Site 3.

The occurrence of the benthic foraminifera *Ammonia parkinsoniana* into the sandy layer suggests an infralittoral marine deposition (Sample 3b, Supplementary materials). A major normal fault dipping 49° towards the S (168° dip-direction; fault F1 in **Figure 32A**) bounds towards the N the abrasion platform and overlying marine and continental facies deposits. A rollover anticline affects the limestones in the hanging wall of fault F1 (**Figure 32A**). Worthy to note, the abrasion platform, which dips a few degrees towards the N, is also involved by the rollover anticline in the fault F1 hanging wall and the clastic wedge manifest growth of the south facing scarp of the fault F1 as well, with the exception of the uppermost strata of the breccia, which seal fault F1 (**Figure 32A**). Southwards, a synthetic normal fault dipping 52° to the SW (230° dip-direction; fault F2 in **Figure 32**) dissects both the abrasion platform and the overlying deposits. In fact, in the hanging wall of fault F2 the abrasion platform is lowered below the quarry floor and the outcropping deposits consist of a horizontal reddish fine sand (Sample 3a, Supplementary materials) paleosoil at the bottom, passing upward into clinostratified sandy matrix-to clast-supported conglomerates forming a southerly aggrading and prograding depositional slope consisting of debris flow bedsets (**Section 6.1.6**). The downthrown debris flow deposits are involved by a drag fold (**Figure 32B**) and are separated by an angular unconformity from fan sediments rich in reworked and *in situ* pyroclastic deposits, which are part of the upper Late Pleistocene-Holocene bayada at the piedmont of Mt. Fellino ridge.

Intense quarrying activity has been carried out in the eastern part of Mt. Fellino ridge (sites 6 and 7; **Figure 28**), where only few outcrops of the raised paleoshorelines are available. Of those quarries, the huge one in Site 6 corresponds to one of the outcrops detected by Romano et al. (1994a). There, an abrasion platform (**Figure 33A-D**), which cuts the limestone strata dipping at high angle towards the S-SE, is covered by a thin veneer of clast-supported, well-rounded

carbonate pebble sand cobble which pass upwards to a decimetre-thick layer of arenites with quartz grains (**Figure 33 B-C**). The elevation of the abrasion platform inner edge is located at 110 m a.s.l. (**Figure 33**).



**Figure 33.** Views of the outcrop in Site 6. A-D: Abrasion platform marked by white line located at 110 m a.s.l. covered by a thin layer made up of well rounded pebbles and sands (B-C)

A thicker marine unit crops out in an elongated monolith in the nearby Site 7 (location in **Figure 28**). There, the abrasion platform, which is located at 110 m

a.s.l. (the platform inner part is not preserved) and cuts intensely fractured and weathered limestones, is covered by a ~ 10 m thick layer of yellowish massive sands (**Figure 34**).

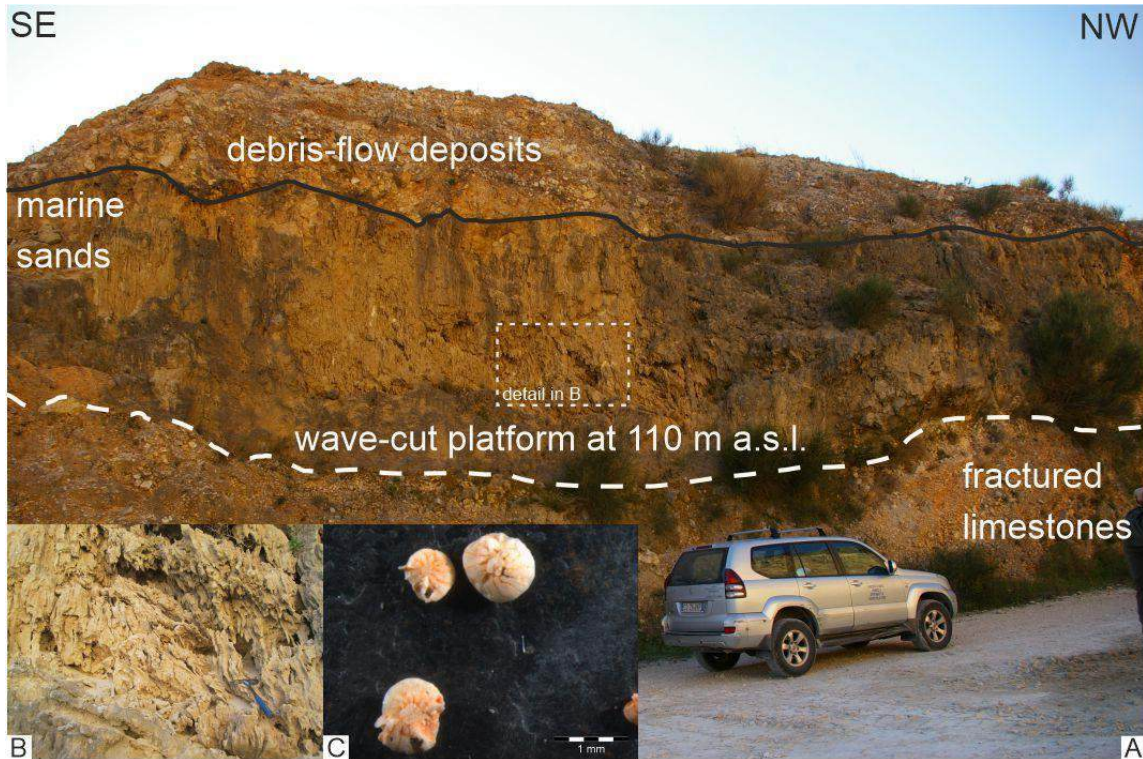


**Figure 34.** A: Wave-cut platform on fractured limestones at 110 m a.s.l in Site 7 with associated (B) marine sands, which contains (C) *Ammonia parkinsoniana*. The succession is closed by debris-flow deposits.

A marine environment of the sands outcropping in Site 7 is testified by micropaleontological analyses, which revealed the occurrence of the *Ammonia parkinsoniana*.

Evidence for buried paleoshoreline remnants in the western part of Mt. Fellino southern escarpment is available in the quarries of sites 1 and 2. Of those outcrops, the one in Site 2 corresponds to the Canello marine terrace of Romano et al. (1994a). There, orthogonal cuts due to recent quarrying allow a perfect 3D view of the horizontal geometry of the abrasion platform and a reappraisal of its

elevation (formerly evaluated + 50 m; Romano et al., 1994a), which is 75 m a.s.l. The abrasion platform, which has a minimum horizontal extension of c. 150 m, cuts fractured limestones dipping towards the SE with an angle of 20°. The abrasion platform is covered with sandy deposits, loose to well-cemented, ~ 4-5 m thick (**Figure 35 A-B**).



**Figure 35.** Marine Terrace at 75 m a.s.l. in Site 2. A-B: Abrasion platform on Mesozoic limestones with associated marine sand deposits; C-D: on marine sands, reddish alluvial fan and Late Pleistocene-Holocene alluvial fan deposits lay. In D is indicated the location of the close-up view of the calcite vein illustrated in **Figure 36 B**

According to the results of the granulometrical analysis (Samples 2a-2b, Supplementary materials), these deposits consist of medium to fine, coarse skewed, gravelly sands (**Figure 35**). A shallow marine deposition is indicated by the occurrence, though not abundant, of *Ammonia parkinsoniana*. The marine, sandy succession is closed by alluvial fan deposits made up of massive, crudely stratified, well-cemented conglomerate with sub-angular and rare rounded gravel-size clasts. Though not always clear, the transition between the marine sand and fan deposits is locally characterized by alternating beds (**Figure 35 C-D**). We correlate the sands of Site 2 with the deposits cropping out at the western termination of Mt. Fellino ridge, in Site 1, where a spatially limited sandy deposit overlying the Mesozoic carbonate bedrock crops out at 70 m a.s.l. The deposit of Site 1 consists of poorly cemented whitish sands, which underlies a colluvial matrix-supported deposit with rare angular carbonate clasts.

At Site 2, the sandy deposits are dissected by a dense network of high angle faults and fractures. A series of faults, roughly N-S striking, are made clearly evident by metre-scale displacements of the abrasion platform (**Figure 36 C**).



**Figure 36.** A: NNW striking transfer faults with details of kinematics indicators (calcite shear fibres showing oblique slip involving a left-lateral strike-slip component). B: Calcite vein (from which samples C.PI2 were gathered) within the sand marine deposits. (C) N-S striking faults affected the abrasion platform at Site 2. Lower-hemisphere, equal-area projection in the upper right corner shows the attitude of normal faults (black great circles) and transfer faults (green great circles) exposed at Site 2. Dots on top of the great circles show plunge of shear fibres (where present). All transfer faults at this site display a sinistral strike-slip component of motion.

The structural assemblage at this site includes roughly E to ENE striking normal faults and hybrid extension-shear fractures, and N to NNW striking transfer faults showing oblique-slip kinematics characterized by dominantly normal dip-slip components of motion and sinistral strike-slip components. The strike-slip component of motion becomes dominant for some of the N to NNW striking transfer faults, which locally also show associated flower structures (**Figure 36A**).

In particular, a positive flower structure is observed at a restraining bend of a NNW striking strike-slip fault. Altogether south-dipping normal faults and oblique-slip faults define a hard-linked fault system consisting of a segmented, E to ENE striking extensional system compartmentalized by N to NNW striking transfer faults. Tension fractures and extension veins also occur subparallel to both the main normal faults and the oblique-slip transfer faults. The veins are filled with calcite, generally occurring as blocky crystals. A sample of calcite (sample C.PI2) was collected from a vein associated with a transfer fault (Fig. 10B) in the marine sands for U-series dating. The  $^{230}\text{Th}/^{232}\text{Th}$  activity value excludes the contribution of detrital fractions, indicating that the obtained age (316 +87/-53 ka, Table 6.1.1) is robust.

Sample ID	Locality	Sample type	$^{238}\text{U}$ [mg/g]	1 $\sigma$	$^{234}\text{U}/^{238}\text{U}$	1 $\sigma$	$^{230}\text{Th}/^{234}\text{U}_{\text{meas}}$	1 $\sigma$	$^{230}\text{Th}/^{232}\text{Th}$	1 $\sigma$	$^{230}\text{Th}/^{234}\text{U}_{\text{calc}}$	1 $\sigma$	Age (ka)	1 $\sigma$	$^{234}\text{U}/^{238}\text{U}_{\text{calc}}$	1 $\sigma$
C.PI2	Polvica	speleothem	0.159	± 0.003	0.995	± 0.016	0.943	± 0.020	158.124	± 8.957	-	-	316.0	87 / - 53	0.988	± 0.039

**Table 6.1.1** Results of U-series dating

### 6.1.7 The marine terraces outcropping in the piedmont of Mt. Fellino ridge

Where exposed between the piedmont upper Late Pleistocene-Holocene alluvial fans, the lowermost part of Mt. Fellino southern escarpment is characterised by a stepped profile, which represents the only morphological appearance of marine terraces along Mt. Fellino ridge. Such an interpretation is supported by evidence from Site 2, where a paleoshoreline is well exposed in a quarry cut. The paleoshoreline consists of an abrasion platform eroded in the Cretaceous limestones with inner-edge at 50 m a.s.l. (i.e., about 25 m below the paleoshoreline described in **Section 6.1.7**). The abrasion platform is covered by a few metres thick shallow marine succession composed of carbonate pebbles that pass upwards into calcarenites with bivalve shells and shell casts (**Figure 37**).

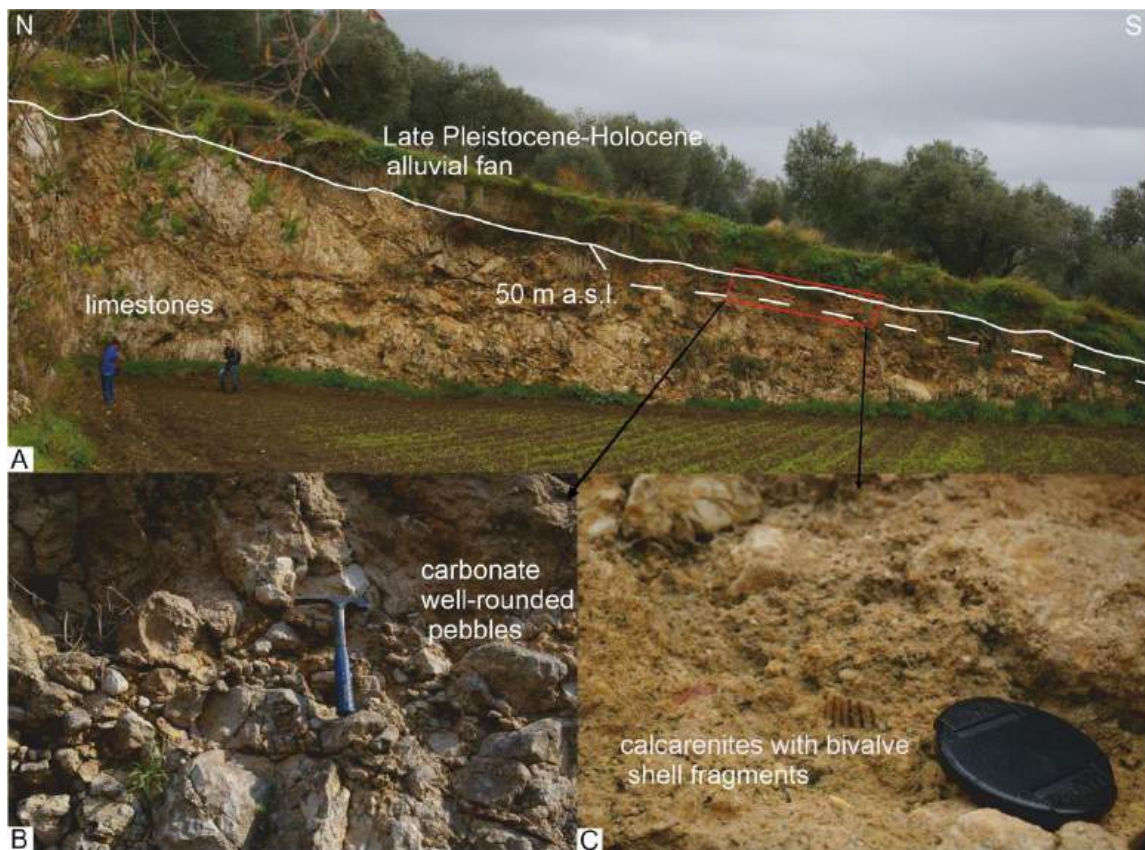


**Figure 37.** A: The lower marine terrace (T1) exposed in Site 2 at 50 m a.s.l. B and C: close-up views of the well-rounded pebbles at the bottom of the marine succession (B) and marine sands with fragments of bivalves (C).

The marine succession is eroded on top and covered by few metre-thick alluvial fan deposits mainly composed of fine grained, reworked recent volcanic deposits, which are part of the Late Pleistocene-Holocene coalescing alluvial fans at the piedmont of Mt. Fellino ridge. Based on such evidence, we interpreted as marine terraces the several flat surfaces carved on the carbonates passing internally to steep slopes/paleo-sea cliffs. These terraces have been detected from the western termination to the central part of Mt. Fellino ridge (**Figure 28**). In particular, they occur in Site 1 at 40 m a.s.l., in the western side of Site 3 at 75 m a.s.l. and at c. 80 m a.s.l. in the area around Site 4 and Site 5. To the east of Site 5, remnants of such terraces occur at 75 m and 70 m a.s.l. in the areas around Site 6 and Site 7, respectively.

### 6.1.8 Discussion

The Mt. Fellino ridge and the adjacent Roccarainola area allow the first comprehensive appraisal of raised marine terraces in the horst blocks within the broader Campania Plain coastal graben. The various quarries cut in the southern mountain front of Mt. Fellino ridge and outcrops in the Roccarainola area provide evidence for shoreline development and evolution of coastal systems in response to erosional/depositional processes governed by relative sea level change in the framework of crustal mobility.

The raised paleoshorelines detected in the investigated area testify to the deep indentation of the Campania Plain occupied by the modern Polvica plain as a gulf during the evolution of the coastal graben. Along the southern mountain front of Mt. Fellino ridge, a flight of two paleoshoreline remnants occurs, although elevations of each remnant (both upper and lower) vary along the inferred paleo-coast, while a single paleoshoreline was identified in the Roccarainola area. The outcropping horizontal abrasion platforms are covered by pebbles and/or sands or arenites, which in most cases are characterised by a macrofossils and/or a microfossil content (Site RR; terraces around 100 m a.s.l. in sites 3 to 5 and 7 and at + 75 m in Site 2), which is indicative of an infralittoral marine deposition.

The good preservation of the marine to continental successions associated with the buried marine terraces outcropping along the southern mountain front of Mt. Fellino ridge may be related to two concomitant conditions, one being the large widths (> 100 m) of the shore systems and the other the presumably fast burial of the marine deposits by tens of metres thick continental deposits. Collectively, the outcrops of sites 3 to 7 provide a proper picture of the paleoshoreline, hereinafter labelled T2 (**Figure 28**), sculpted at 100-115 m of elevation in the southern fault escarpment of Mt. Fellino. Particularly in sites 3 to 5, a well-preserved transgressive-regressive sequence is associated with the T2 abrasion platforms,

which are covered by marine sands that are overlain by – and partially pass laterally to – erosive-based alluvial fan deposits. The alluvial fan deposits are commonly stacked in metres-thick units separated by erosive surfaces that, at various sites, cut paleosoils possibly formed on pyroclastic products. Overall, the maximum thickness of the shallow marine succession (c. 10 m or more in sites 4, 5 and 7) overlying the abrasion platform is indicative of a relative sea level rise accompanying marine sedimentation. The well-developed, southerly prograding alluvial fan system overlying the marine sediments is indicative of coastal progradation during the sea-level highstand and, possibly, the following sea level fall. The variable thickness of the marine deposits along the T2 shoreline (from c. 1 m in Site 6 to c. 10 m in other sites) is possibly due to erosion, or paleoenvironmental conditions variable from sheltered environments to environments prone to coastal erosion.

Evidence from sites 3, 4 and 5 indicates that marine terrace T2 and overlying continental deposits were displaced by high angle, roughly S-dipping faults, with fault offsets made particularly evident by displacements of the abrasion platforms (e.g., **Figure 30**, **Figure 31**; **Figure 32**; **Figure 36**; **Figure 38**). At Site 3, the crosscutting relationships between fault F1 and both the basal rock fall/slide deposits (coeval with the marine sands) and overlying debris-flow strata (**Figure 32 A**) are indicative of fault growth accompanied by recession of the bedrock scarp (**Figure 38**).

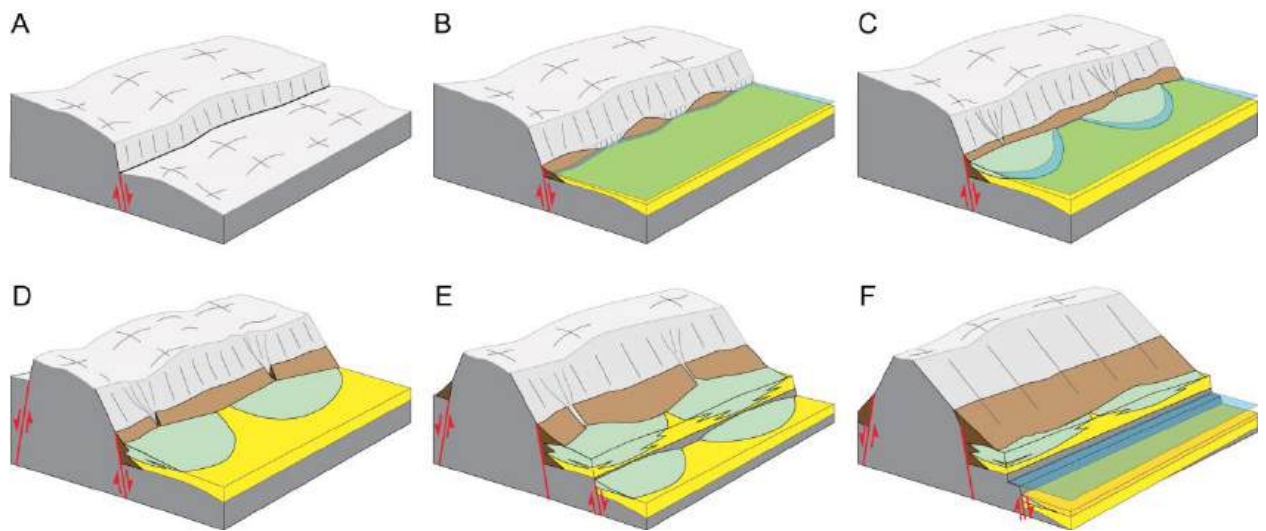


**Figure 38.** Cartoon of the reconstructed late Quaternary evolution of Mt. Fellino ridge area, in response to block faulting and relative sea level fluctuations; block diagrams in A to F (not in scale) are successive stages. Following block-faulting in stage A, a coastal environment is established in the hanging wall block of fault F1 with the sea level rise and highstand of stage B, when formation of the T2 marine terrace occurred. Stage C shows coastal progradation during sea level highstand, and Stage D represents growth of the continental facies system during the following sea level fall. Following activation of fault F2 during stage E, a new marine terrace (T1) is formed during the following sea level rise, during Stage F.

Fault F1 is not observed in the nearby outcrops of sites 4 and 5 (which share a common geomorphological and stratigraphical setting with outcrops of Site 3), as its trace continues N of the quarry wall at Site 4 (**Figure 30 A**) and the lateral contact between the continental deposits overlying terrace T2 and the Mesozoic bedrock is not well exposed at Site 5. Synsedimentary activity of fault F1 most probably favoured abundant scree production along the rising cliff. Rock fragmentation and related scree deposition along the carbonate escarpments in the Apennines are generally interpreted as mainly resulting from climatic control, particularly frost action during cold stages (e.g., Giraudi and Frezzotti, 1997; Scarciglia et al., 2003; Tucker et al., 2011). However, the abundance of both reddish paleosoils (both *in situ* and re-deposited; **Figure 30**) indicative of warm conditions and debris-flow deposits resulting from colluvial slide processes suggest that factors other than climate – likely repeated fault slip events – favoured rock

fragmentation and cliff collapsing (inferred by rock slide and rock fall deposition recorded at times at the base of fan wedges) in our case example. Sealing of fault F1 by the uppermost debris-flow strata (**Figure 32 A**) indicates, in agreement with theoretical models (e.g., Ascione and Cinque, 1997), ultimate erosion and replacement of the fault escarpment in the footwall of fault F1 postdating fault activity. The overall basinward-stepping of the depositional system, the progressive onlap of the clastic wedge onto fault F1 (**Figure 32 A**) and the dragging of the clastic wedge along fault F2 point to fault F2 activity postdating deposition of the lower continental succession. These evidences account for a basinward migration of fault activity (hence fault F2 activated after fault F1). Based on outcrop data, a minimum vertical separation of the order of 70-80 m after formation of marine terrace T2 can be estimated for fault F1, and a minimum vertical separation of c. 30 m can be estimated for the younger fault F2. Fault F1 was most probably active also prior to/coeval with the formation of marine terrace T2, as suggested by both the large rock slide/fall deposits in the innermost part of the abrasion platform, and the large size (minimum width of 200-250 m) of the abrasion itself at sites 3 to 5. Theoretically the formation during a sea level highstand of a wide horizontal platform across carbonate rocks would require a long time in presence of an elevated and steep coastal morphology (comparable in shape to the several hundreds of metres high and steep modern Mt. Fellino escarpment), and a shorter time in presence of a less elevated/smooth rocky coast (e.g., Cinque et al., 1995). The latter condition, in the scenario of our study area, would have arisen from the formation of the abrasion platform in a previously lowered block in the hanging wall of fault F1. Based on the negligible change of elevation of marine terrace T2 towards the E along the Mt. Fellino escarpment, we may hypothesise that, after T2 formation, either displacements comparable to that observed along fault F1 affected the entire length of the ridge (i.e., fault F1 is part

of a fault system that produced comparable offsets along its whole length), or the F1 hanging wall block was relatively stable in terms of absolute vertical motions.

#### 6.1.8.1 Paleoshoreline correlation

Based on the similarity of minimum widths of the abrasion platforms reconstructed for Site 2 (c. 150 m) and sites 3 to 5 (c. 200-250 m), and on the comparable evolution of the paleo-shore system as inferred from facies of the marine and overlying continental deposits, we correlate to T2 the paleoshoreline remnants cropping out at 70-75 m a.s.l. in sites 1 and 2 in the western part of Mt. Fellino ridge. As for sites 3 to 5, the fossiliferous marine sands cropping out at Site 2 pass upwards into alluvial fan deposits composed of coarse-grained gravel wedges, locally resting erosively on re-deposited reddish paleosoils. The correlation between paleoshoreline remnants grouped in terrace T2 is also supported by both the absence of any evidence of marine terrace around 100 m a.s.l. in the western part of the Mt. Fellino southern escarpment, and morphostratigraphical evidence pointing to those remnants as clearly distinguishable from the surfaces that form the lower steps of the marine terrace flights identified at sites 1 to 5. In fact, where not bare, the latter surfaces are covered only by deposits of the Late Pleistocene-Holocene alluvial fans, which are inset, and partly cover, the fan deposits that overlie the marine deposits of paleoshoreline T2 (e.g., **Figure 32 A; Figure 35 C-D**). Such a stratigraphical setting both indicates an age of surfaces that form the lower steps of the terrace flights younger than T2 age, and does not pose any constraint on relative age among those surfaces, which we mutually correlate and label marine terrace T1 (**Figure 28**).

Our reconstruction indicates that the elevation of paleoshoreline T2 is laterally variable, showing a roughly symmetrical decrease from 115 m a.s.l. in the central part of Mt. Fellino ridge towards the two sides of the mountain front.

Consistently, no evidence of T2 has been found in the quarry located to the east of Site 7 (**Figure 28**), where the quarry floor lays 130 m a.s.l. Similarly, the elevation of T1 increases from c. 40 m a.s.l. at the western termination of Mt. Fellino ridge toward the east, to reach 80 m of elevation in Site 4 and then decreases to 70 m a.s.l. in Site 7. Less clear is the morphostratigraphical position of the wide marine terrace standing at c. 200 m a.s.l. in the Roccarainola hills relative to paleoshoreline T2 in the southern mountain front of Mt. Fellino ridge. Based on its elevation, the Roccarainola marine terrace could be considered older than the T2 terrace. However, such a chronological relationship is not proven due to both absence in the Roccarainola area of net evidence of marine terraces lower than the 200 m high terrace, and lack of evidence of raised paleoshoreline at elevation around 200 m along Mt. Fellino southern escarpment even in the N-S oriented cross-sections of that escarpment, which are exposed in the high quarry walls (reaching an elevation > 300 m a.s.l.) of both sites 6 and 7. We cannot exclude that, along Mt. Fellino ridge, coastal landforms higher than the T2 have been obliterated by subsequent slope/sea-cliff retreat, or even fault displacements. Indeed, the occurrence of relic coastal morphologies is suggested by the hanging concavity located at 330-340 m a.s.l. in the mid part of Mt. Fellino ridge, which may reliably testify to a marine terrace older than T2 in that area.

The  $^{230}\text{Th}/^{234}\text{U}$  isotopic dating of the calcite vein (Sample C.PL2, **Table 6.1.1**) that dissects the T2 marine infralittoral sands outcropping in Site 2 provides an important *ante quem* constraint to the formation of terrace T2. The calcite formation needs freshwater circulation, which occurs when the terrace resides in subaerial condition, i.e. during a relative sea level fall. The 316 +87/-53 ka age provided by U-series dating presents a large and asymmetric range of uncertainty due to the proximity to the upper limit of the method. It means that the sample is certainly older than 263 ka, with a maximum peak of probability ~316 ka. Such a dating, which represents the only age control to the flight of marine terraces in the

northern boundary of the southern Campania Plain, suggests a late Middle Pleistocene age for marine terrace T2. Our correlation, based on evidence from new multiple outcrops, of the T2 paleoshoreline remnants outcropping in sites 2 and 6, respectively, implies reinterpretation of their former distinction in two terraces by Romano et al. (1994a). In addition, our dating indicates that the correlation proposed by Romano et al. (1994a) of marine terrace T2 in the Canello area with MIS 5e must be amended. In fact, based on our dating and available chronological framework for the late Quaternary Marine Isotope Stages (e.g., Rohling et al., 2014; Siddall et al., 2003; Waelbroeck et al., 2002), an age > MIS7 is assessed for marine terrace T2. Although the time lag between T2 development and formation of the dated calcite vein cannot be defined, evidence for synsedimentary fault activity from the outcrops of Site 3 suggests that faulting and related fracturing (with calcite vein formation) of the T2 sands/arenites at Site 2 might approximate the age of those deposits, which can be correlated with MIS 9. Based on such a correlation, marine terrace T1 can be confidently ascribed to MIS 7, while for the Roccarainola terrace a correlation with the older MIS 11 may be hypothesised.

#### 6.1.8.2 Implications on the evolution of the Campania Plain coastal graben

Our data indicate that fault motions along roughly E-W trending structures controlled the formation of a deep gulf in the modern Polvica plain, bounded towards the north by a headland represented by the Mt. Fellino ridge. Evidence from Site RR, where coarse-grained continental facies deposits do not cover the shallow marine deposits, indicates that the Roccarainola carbonate blocks had been downthrown relative to, and separated from, the nearby Avella Mts. ridge prior to formation of the marine terrace at 200 m a.s.l. Morphostructural evidence and, particularly, the different slope angles of the northern and southern escarpments of Mt. Fellino ridge, and the beheaded valley in the mid part of ridge (which suggests the former occurrence of a S-flowing drainage), are both suggestive of an overall

younger age of the northern fault escarpment relative to the southern one (**Figure 38**). Evidence from Site 3 (particularly, the chronological relationships between faults F1 and F2) points to migration of activity of the roughly S-dipping faults towards the south. Fault F2 that crops out in that site is probably part of a fault system, which for the most part is buried along the Mt. Fellino southern mountain front. In the field, no net evidence of sealing of fault F2 by any of the outcropping units has been identified. Fault F2 and the fault system at the toe of Mt. Fellino ridge is expected to have contributed to uplift of marine terraces T2 and T1 developed along the ridge.

Based on evidence from Site 2, the faults offsetting the T2 marine deposits define a hard-linked extensional fault system in which relay zones between adjacent E-W striking normal fault segments are mostly offset by NNW striking, oblique-slip transfer faults. Therefore, the two main fault sets are interpreted as part of a single, roughly E-W striking, segmented extensional fault system. The stratigraphic evidence for fault activity suggests that the roughly NNW striking faults in this area represent inherited structures (as indicated by tens to hundreds of metres vertical separations observed in pre-Quaternary carbonate substratum) that were reactivated during the Quaternary as oblique-slip faults with variable strike-slip components of motion. If that was actually the case, the hard-linked extensional fault system documented in this study would be mostly controlled by the pre-existing compartmentalization of the system by N-S striking faults, rather than by 'broken' relay ramps (i.e., relay ramps offset by newly formed transfer faults). On the other hand, the main normal fault segments pointed out in this study are consistent with major extensional structures that controlled the Quaternary tectonic evolution of the Campania Plain and adjacent offshore (Naples Bay; e.g. Milia and Torrente, 1999, 2013). Earthquake focal mechanisms and fault slip data indicate that active deformation within this area occurs as a result of a N-S trending horizontal extension, which is at variance with that (SW-NE oriented) dominating

in the surrounding area and over most of the Apennine chain (Milano et al., 2004). Discussing the tectonic origin and geodynamic implications of this discrepancy is beyond the scope of this study (the interested reader may refer to Milano et al., 2004, 2002;Valente et al., 2019b; in any case, it is worth noting that roughly N-S to NNW-SSE extension largely controlled the tectonic evolution of the Tyrrhenian margin in the study area, as the normal faults with the largest cumulative dip separation (in excess of 3000 m) are E- to ENE striking (Bruno et al., 2000; Mariani and Prato, 1988; Milia et al., 2013; Milia and Torrente, 2015, 1999).

Concluding remarks, including considerations expressed in the next section, will be reported in **Section 6.2.4** Concluding remarks on the Campania Plain case study

## *6.2 Tectonic implications of raised Quaternary paleoshorelines in the NE sector of the Campania plain, southern Italy*

Manuscript 2- *Tectonic implication of raised Quaternary paleoshorelines in the NE edge of the Campania Plain, southern Italy* by Cerrone, C., Roberts, G.P., Ascione, A., Meschis, M., Mazzoli, S., Robertson, J., in preparation.

### 6.2.1 Introduction

The “sequential correlation method” has been widely used to correlate the paleoshorelines with sea level highstands (Armijo et al., 1996; Gallen et al., 2014), assigning the consecutive, successive or previous, highstand to a dated one. However, the sequential correlation method is misleading for the “removal” or overprinting problem (Ascione and Romano, 1999; Meschis et al., 2018; Roberts et al., 2013; Robertson et al., 2019). It means that paleo-sea-level highstands, which are higher than the previous ones, could erode older paleoshorelines that may thus not be preserved (Roberts et al., 2013; Westaway, 1993) leading misunderstanding in the interpretation of flights of paleoshorelines not directly dated. Hence, recently to avoid this problem a synchronous correlation method (**Section 4.1** Synchronous correlation of multiple paleoshorelines method) has been developed for the Mediterranean area (Houghton et al., 2003; Meschis et al., 2018; Roberts et al., 2013, 2009; Robertson et al., 2019). This method has been applied to the flight of paleoshorelines sculpted in the southern mountain front of Mt. Fellino ridge, i.e. in the footwall block of the Polvica Fault.

The hereafter called Polvica Fault is an ~ E-W trending extensional fault zone with a length of about 15 km, which corresponds to one of the main structures at the NE boundary of the Campania Plain. The Polvica fault bounds the southern slope of Mt. Fellino ridge and continues eastwards to the Avella Mt. for a total length of around 15 km (**Figure 39**). The Polvica Fault bounds to the north the

Acerra sub-basin of the major Campania Plain graben, evidenced by geophysical surveys (Cella et al., 2007). Geophysical surveys (Ortolani and Aprile, 1978), indicate that the carbonate bedrock reaches a maximum depth of 3 km in the Acerra sub-basin depocenter. By subsurface information other E-W trending extensional faults to the S of the Polvica Fault are inferred to have downthrown the bedrock. To the N of the Polvica Fault, E-W trending normal faults parallel to the master fault have been recognized on the field producing displacements in the order of some metres of the wave-cut platforms (**Figure 32**). The wave-cut platforms and the associated marine-continental deposits are dissected by oblique-slip NW-SE and ~ N-S trending transfer and extensional faults. These are interpreted as release faults (Destro, 1995), formed in response to throw variation along the strike of the master faults.

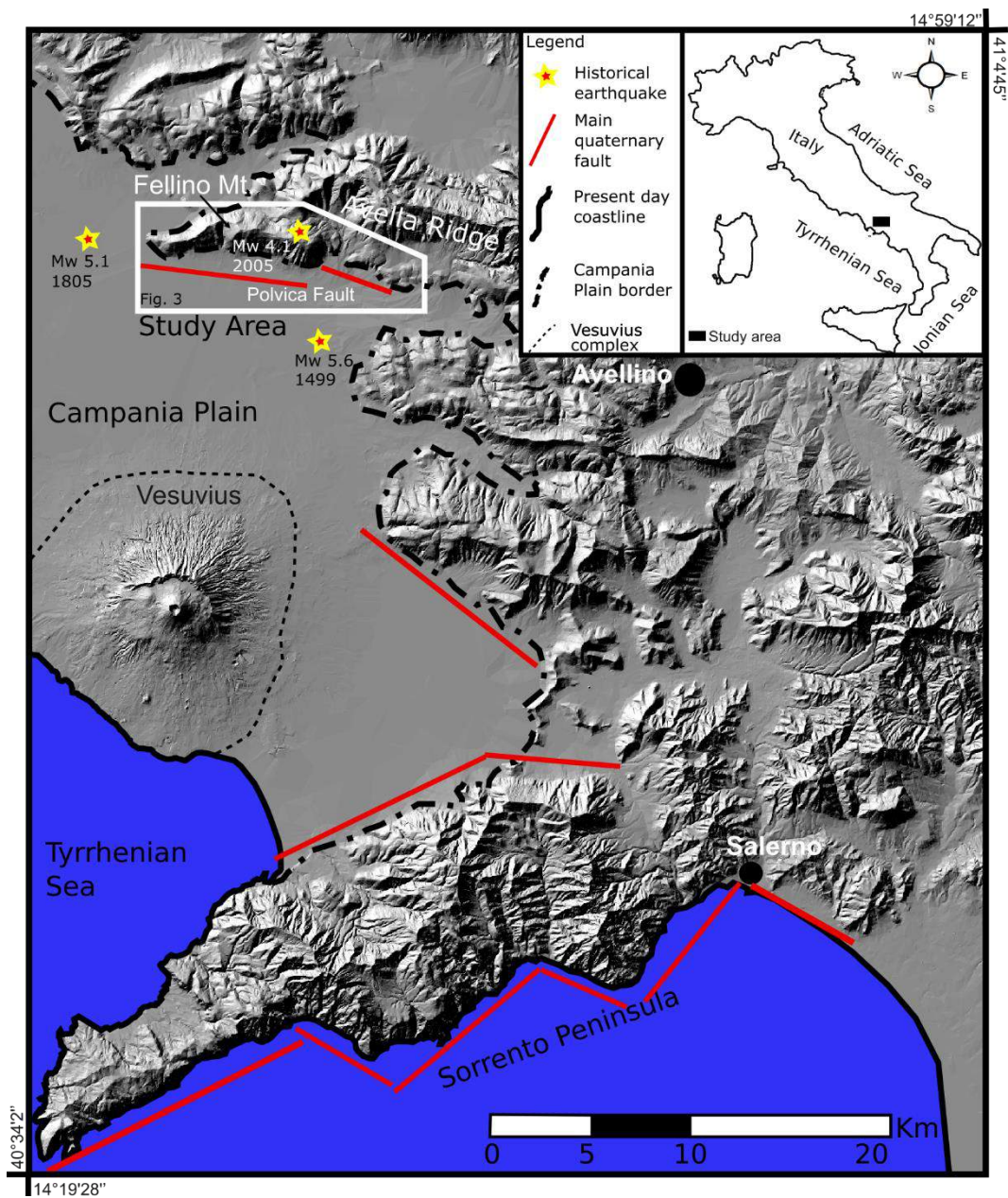


**Figure 39.** Study area map on a 10-m resolution DEMs (Tarquini et al., 2012, 2007) with location of historical earthquake from the *Catalogo parametrico dei terremoti italiani 2015 (CPTI15)* (Rovida et al., 2020, 2019) and main Quaternary fault. In the white polygon is located the study area, which is detailed in figure 41.

In the Campania Plain only low to moderate seismicity in historical times has been recorded and no evidence of surface ruptures has been reported for this area, leading the Database of Individual Seismogenic Sources (DISS3.2.1, DISS

Working group, 2018, **Figure 40**) to indicate no active source both inside and at the borders of the Campania Plain. Among the faults at the boundaries of the Campania Plain, the Polvica Fault, which based on evidence discussed so far has shown to have controlled the Quaternary tectonic evolution of the Campania plain, even if is not considered as a potential seismogenic source in the DISS database. However, widespread field evidence and, in particular, the presence of raised Middle Pleistocene paleoshorelines, are obvious indicators of late Quaternary vertical motions. In such a framework, an in-depth analysis aimed at constraining both the rate of Quaternary slip and age of the most recent activations of the Polvica Fault appears of fundamental importance in the correct assessment of seismic hazard possibly associated to that fault (**Figure 40a**). Such an assessment is even more important considering that both the Campania Plain area is densely populated and several settlements are located along Polvica Fault trace. Indeed, according to the CTPI15 catalogue (Rovida et al., 2016), a low to moderate seismicity has occurred in historical time in the area around Polvica Fault (**Figure 39**).

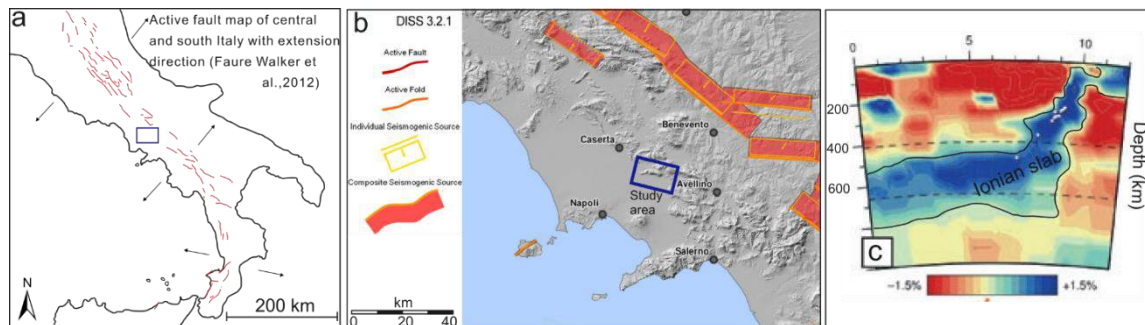


**Figure 40.** Active fault map of central and south Italy with extension direction (modified from Faure Walker et al., 2012); in the blue rectangle is located the study area; **b**) Active faults around the study area (blue rectangle) from the Database of Individual Seismogenic Sources (DISS 3.2.1, DISS Working group, 2018). Note the Polvica Fault is not considered as active fault; **c**) Transect from Balearic island to the off-shore of Puglia, passing from Campania Region (see Ascione et al., 2012) showing a tomographic image of P-wave velocity anomalies. The Ionian slab beneath southern Apennines is evidenced, while white dots indicate the earthquake epicentre.

Although the Campania Plain has been largely studied in the last few decades, the geological evolution of the Plain has been mainly reconstructed by subsurface data, e.g. seismic stratigraphy, geophysical surveys, deep and shallow wells data (Barra et al., 1996; Florio et al., 1999; Milia and Torrente, 2015; Santangelo et al., 2010; Amorosi et al., 2012; Brancaccio et al., 1995; Milia et al., 2013; Santangelo et al., 2017). However, poor surface information is available useful to the reconstruction of the displacement history of the faults at the boundaries of the Plain. Mostly due to the poor evidence of markers, such as paleoshorelines, in the elevations at the boundaries of the Campania Plain, also the vertical motions of those elevations have not been evaluated. However, a former assessment of the Polvica Fault slip had been performed by Cinque et al. (2000), based on data published in Romano et al. (1994a). Romano et al. (1994a) reported evidence of a marine terrace in the Canello area (eastern sector of the Mt. Fellino ridge), which was tentatively correlated with the uppermost first marine unit found in a borehole in San Marcellino (about 22 km eastward) dated  $126 \pm 11$  ka (U-series dating on *C. caespitosa*) and of a marine conglomerate at 130 m a.s.l. outcropping along the southern slope of Mt. Fellino ridge (Cicciano area) related to Middle Pleistocene. Based on such findings, and geomorphological-stratigraphical evidence, Cinque et al., (2000a) estimated for the ~ S-dipping fault at the southern boundary of Mt. Fellino ridge a mean slip rate of ~ 1 mm/y since the Late Pleistocene, higher than the mean long term throw rate in the range of 0.4-0.6 mm/y since the Early Pleistocene (1.5 Ma - Present) inferred from considerations on the geomorphological-stratigraphical setting.

An investigation aimed at providing new data on the displacements recorded along of the Campania Plain, namely the Polvica Fault, was carried out. In particular, the study aimed at shading light on the geometry, kinematic and chronology of the Polvica Fault zone through an in-depth analysis of the raised paleoshorelines that crop out along the Mt. Fellino ridge. The study integrates the

results of the field study carried out on the outcropping paleoshorelines (**Figure 39**) evidence deriving from both a detail-scale geomorphological analysis of Mt. Fellino ridge area and the inspection of few available data from the shallow subsurface of the adjoining alluvial plain (hereinafter, Polvica plain).

The activity of the Polvica Fault has been investigated through a spatio-temporal reconstruction of uplift recorded by Mt. Fellino ridge. Such a reconstruction has been based on the spatial distribution and inferred ages of the marine terraces sculpted in the southern mountain front of Mt. Fellino ridge. For the uplift history reconstruction, the synchronous correlation of multiple paleoshorelines with multiple sea-level highstands method, described in **Section 4.1**, has been applied to the Polvica Fault. Based on such a reconstruction, the throw rate of the Polvica Fault has been assessed. Based on geometry of the Polvica Fault and the evaluated slip rate, seismic hazard of the study area may be assessed by magnitude and earthquake recurrence interval for the Polvica Fault inferred, according to the Wells and Coppersmith, 1994 relationship.

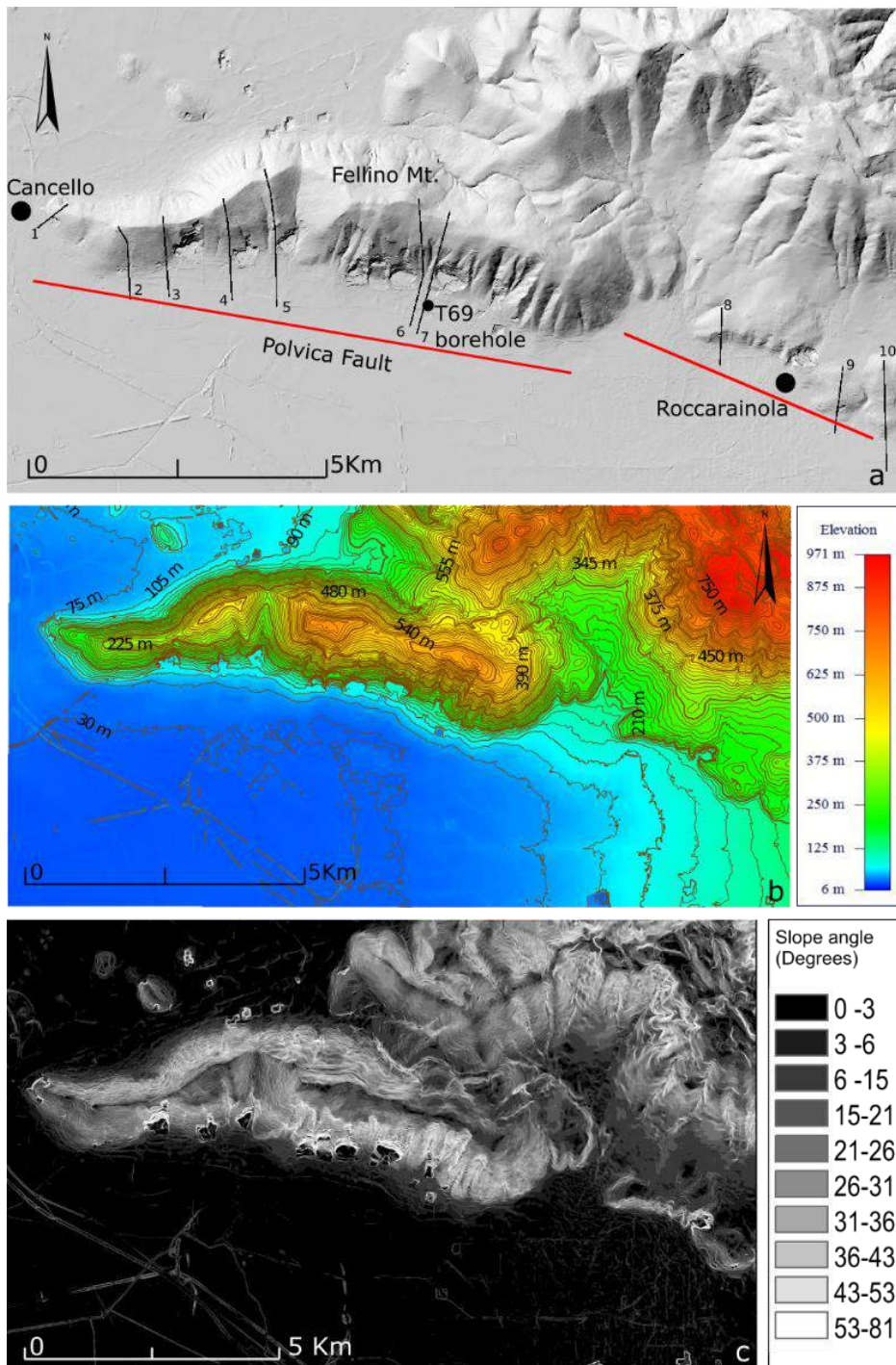


**Figure 41.** A 5-m resolution DEMs of the study with a) an hillshade as basemap, where the 10 topographic profiles and T69 borehole location are shown; b) elevation map with 15m contour lines; c) slope angle map in degrees.

### 6.2.2 Synchronous correlation of multiple paleoshorelines with multiple highstands method applied at the Polvica case study

The synchronous correlation of multiple paleoshorelines method (Houghton et al., 2003; Roberts et al., 2013, 2009) was applied to the flight of marine terraces identified either in the field and/or by the geomorphological analysis of topographic data. The topographic data used for the geomorphological analysis are the Regione Campania 1:5.000 scale maps and a 5X5 m resolution Digital Terrain Model (DTM, **Figure 41**) released by the Regione Campania. In the field the elevation of the inner edge (where visible) of the wave-cut platform has been measured/estimated using 1:5.000 scale topographic maps and a handheld GPS receiver. For each wave-cut platform outcrop recognized in the field, a topographic profile has been reconstructed for a total of 10 profiles (with numbering increasing from the west to the east; **Figure 41a**) striking perpendicular to the southern slope of Mt. Fellino. ArcMap 10.4 software was used for the construction of the topographic profiles. As independent age constraint to synchronous correlation of multiple paleo-shorelines method, the U-series age of a calcite vein (sampled in a site located along profile 2; **Figure 41**), associated with a fault, which dissects the shallow-water deposits of marine terrace T2 was used. The Quaternary stratigraphy field data were integrated by subsurface data from published and unpublished boreholes located in the Polvica plain. At the Polvica plain – Mt. Fellino ridge junction, Late Pleistocene-Holocene volcanic and alluvial fan deposits form a rather continuous piedmont gently graded to the quasi-flat alluvial plain surface (**Figure 28**). In front of the mid part of Mt. Fellino ridge, the toe of the piedmont is paralleled by an elongated, depressed area, lying a couple of metres below the surface of the adjacent part of the Polvica plain and where, according to local witnesses, a marshy environment establishes during the wet season (**Figure 28**). Accordingly, data from shallow boreholes point to the occurrence, in the shallow

subsurface, of few m thick, fine grained deposits rich in organic matter, consistent with the persistence of a marshy environment in that area. Overall, the features of that area could represent the effect of recent northward tilting/subsidence of that part of the Polvica plain along the Polvica Fault.

The boreholes include the T69 borehole (**Figure 42**) located few tens of metres to the south of the southern fault scarp of Mt. Fellino ridge (location in **Figure 41a**). T69 borehole reaches the top of the Mesozoic limestone at 116 m below the sea level. A geological cross-section along profile 7 (**Figure 41a**) and intercepting T69 borehole has been constructed (**Figure 42**).

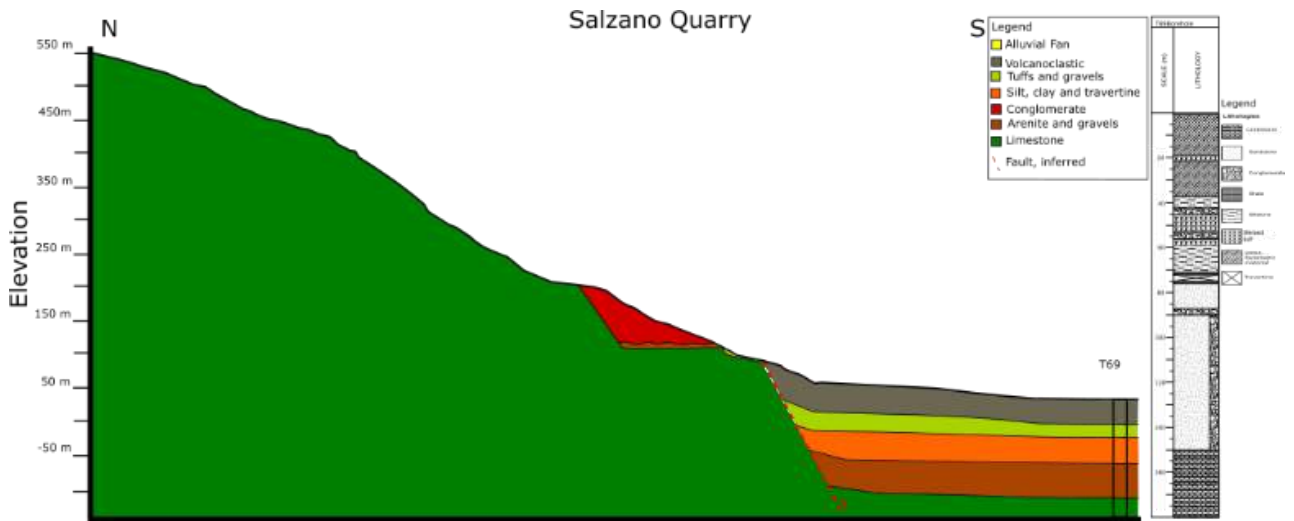


**Figure 42.** Geological cross-section along the Salzano Quarry, where T69 borehole is located. On the right, a sedimentological detail of T69. See fig.3a for location.

The synchronous correlation method has been adequate to match all the measured paleoshoreline terrace elevations with the predicted ones. The paleoshoreline elevations have been correlated along the strike of the Polvica Fault. By the  $316 \pm 87/- 53$  ka age of the dated calcite vein (**Table 6.1.1**), the uplift rates have been calculated and connected with the displacement of the active normal Polvica Fault.

Along profile 2 (**Figure 41**) two distinct wave-cut platforms have been recognised in the field. The lower and younger one crops out at 50 m (T1), whereas the second one at 75 m a.s.l. (T2) has been to > 263 ka, the minimum age provide by the calcite vein dating. The wave-cut platforms related to the terrace T2 are located at different elevations along the Mt. Fellino Ridge, between ca. 70 to ca. 200 m, but they have been correlated to the same terrace because they share common stratigraphic features as better explained in **Section 6.1.8.1**. The marine terrace in the Roccarainola area outcropping at ~ 200 m a.s.l. and labelled TRR in **Section 6.1.8.1**, has been correlated with the T2 by the synchronous correlation method. The lowest marine terrace (T1), which has been identified along the profiles 1-6 in the fields, spatially between 40 up to ca. 75 m.

It is worth noting that the elevation of the identified marine terraces decreases laterally relative to the centre of the ridge in accordance with the tips of the Polvica Fault. However, eastwards the elevation of the T2 first decreases and then abruptly increases. The latter anomaly may be interpreted as a result of a fault bend, which could intensify the slip (Iezzi et al., 2018) of the Polvica Fault.

In **Figure 43** the best fit, obtained by iteration of the uplift rate for each profile illustrated in **Figure 41**, between mapped and predicted paleoshorelines elevations by synchronous correlation method has been illustrated.

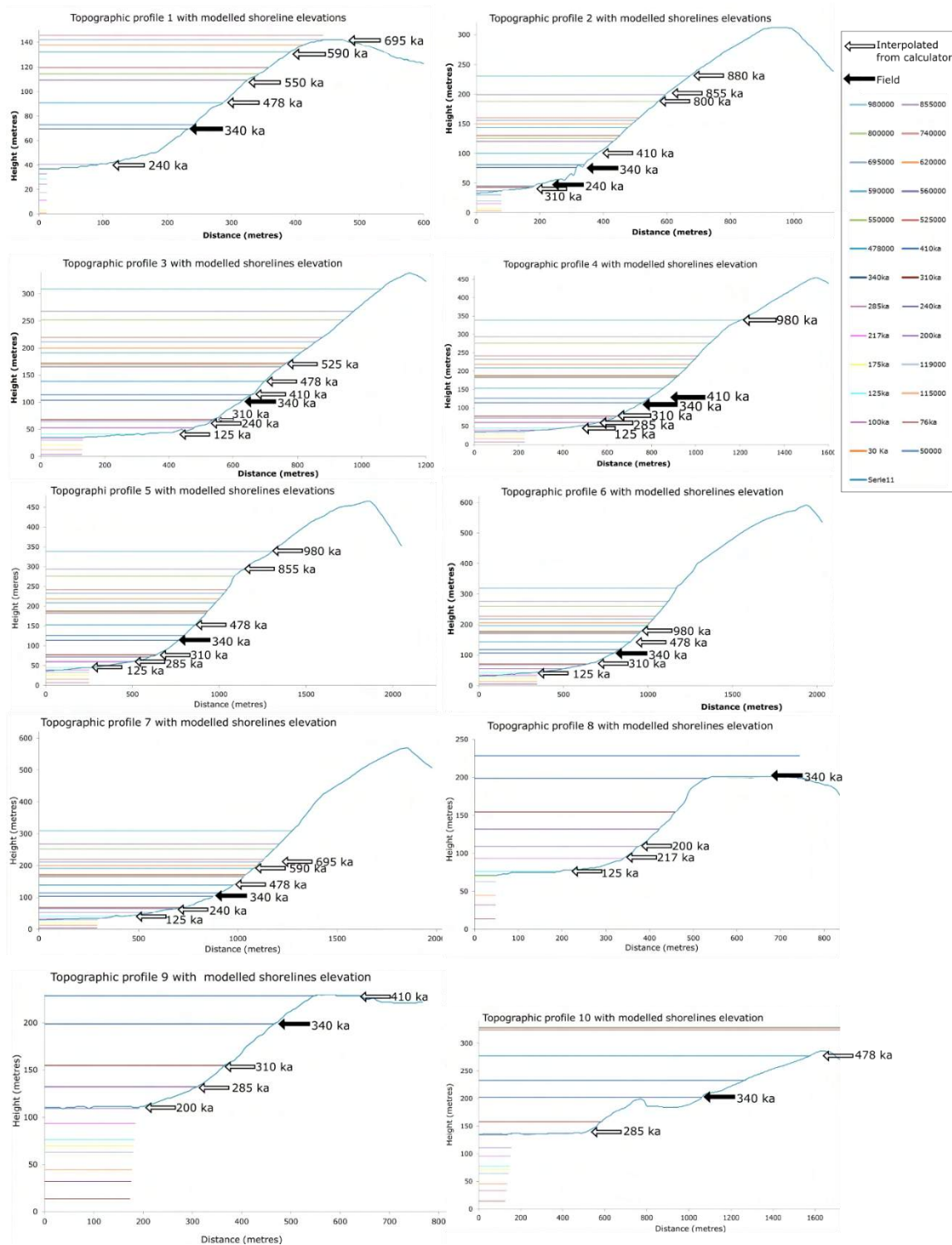


**Figure 43.** Topographic profiles from 5-m resolution DEMs (Regione Campania) where modelled and mapped paleoshorelines elevations are reported. On Table 6.1.2 are indicated the detail of each profile while the location of them is visible in Figure 4.

In addition to the paleoshorelines mapped in the field, small-size flat surfaces, south-dipping (i.e., dipping towards the paleo-coastline), have been taken into account for the modelling. Although marine deposits are not associated with those surfaces, their perfect coherence with the modelling may be considered as an indirect evidence of their marine origin. In fact, the coefficient of determination  $R^2$  between the field-based and predicted paleoshorelines elevations from the DEM, including the flat surfaces, is very close to 1 (**Figure 44b**). Moreover, a very good match is between the elevations measured on the DEM and the ones predicted by the synchronous method is found (**Figure 44a**). These findings are suggestive of a good correlation and reliable uplift rate values (**Figure 44b**). The elevations of the mapped shoreline angles with the related ages, which have been assigned through the synchronous correlation method, have been reported in the Table 6.1.2, while **Figure 43** shows the 10 topographic profiles with mapped and modelled paleoshorelines elevations.

Paleoshoreline (profile number)	DEMs elevations (m)	Expected elevations (m)	Field elevations (m)	Our proposed age (Ka)	Lat (decimal degrees)	Long (decimal degrees)
4 (1)	41	41	-	240	40.994505°	14.421577°
7 (1)	70	70	70	340	40.994588°	14.422711°
9 (1)	90	91	-	478	40.994725°	14.424018°
11 (1)	115	115	-	550	40.994836°	14.424799°
12 (1)	134	132	-	590	40.994926°	14.425576°
13 (1)	142	142	-	695	40.995128°	14.426087°
4 (2)	49	45	50	240	40.985881°	14.438716°
6 (2)	43	43	-	310	40.985174°	14.438389°
7 (2)	66	76	75	340	40.986846°	14.438104°
8 (2)	91	81	-	410	40.986923°	14.438089°
9 (2)	105	100	-	478	40.987401°	14.438022°
14 (2)	177	188	-	800	40.988950°	14.437684°
15 (2)	199	200	-	855	40.989254°	14.437773°
16 (2)	242	231	-	980	40.989943°	14.437517°
1 (3)	42	41	-	125	40.985103°	14.447414°
4 (3)	62	65	-	240	40.987656°	14.446634°
6 (3)	72	68	-	310	40.987760°	14.446579°
7 (3)	-	104	105	340	40.988545°	14.446315°
8 (3)	116	114	-	410	40.988731°	14.446244°
9 (3)	140	139	-	478	40.989075°	14.446145°
10 (3)	174	172	-	525	40.989656°	14.445933°
1 (4)	46	45	-	125	40.985353°	14.458279°
5 (4)	61	61	-	285	40.987222°	14.458097°
6 (4)	78	77	-	310	40.988070°	14.458063°
7 (4)	-	114	115	340	40.989245°	14.457991°
8 (4)	-	126	120	410	40.989312°	14.457927°
16 (4)	339	339	-	980	40.993023°	14.457600°
1 (5)	45	45	-	125	40.984530°	14.465858°
5 (5)	65	61	-	285	40.987351°	14.465894°
6 (5)	74	77	-	310	40.988667°	14.465961°
7 (5)	-	114	115	340	40.989886°	14.466097°
9 (5)	149	153	-	478	40.990763°	14.466074°
15 (5)	294	294	-	855	40.993736°	14.465477°
16 (5)	320	339	-	980	40.994595°	14.465391°
1 (6)	41	43	-	125	40.981434°	14.492081°
6 (6)	75	71	-	310	40.984582°	14.492035°
7 (6)	104	107	110	340	40.985860°	14.492818°
9 (6)	142	143	-	478	40.986572°	14.492730°
10 (6)	179	178	-	525	40.987137°	14.492160°
16 (6)	330	319	-	980	40.989041°	14.492181°
1 (7)	42	41	-	125	40.980706°	14.494852°
4 (7)	64	65	-	240	40.983981°	14.495553°
7 (7)	-	104	110	340	40.985601°	14.495902°
9 (7)	143	139	-	478	40.986504°	14.495949°
12 (7)	192	191	-	590	40.987231°	14.495860°
13 (7)	213	212	-	695	40.987496°	14.495958°
1 (8)	75	76	-	125	40.973823°	14.549839°
2 (8)	110	109	-	200	40.976875°	14.550368°
3 (8)	90	94	-	217	40.976357°	14.550449°
7 (8)	201	199	200	340	40.978866°	14.550763°
2 (9)	111	109	-	200	40.965861°	14.570192°
5 (9)	135	132	-	285	40.966841°	14.570700°
6 (9)	157	155	-	310	40.967386°	14.571026°
7 (9)	201	199	200	340	40.968201°	14.571423°
8 (9)	230	229	-	410	40.968689°	14.571796°
5 (10)	136	135	-	285	40.964517°	14.577831°
7 (10)	198	202	200	340	40.965434°	14.579023°
9 (10)	286	277	-	478	40.973599°	14.579266°

**Table 6.1.2.** Marine terrace elevation from DEM and fieldwork with age assigned via synchronous correlation

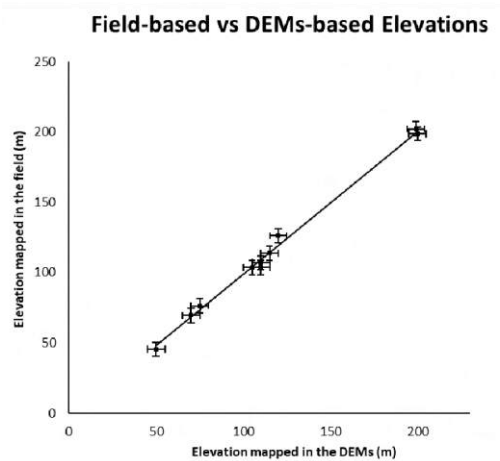
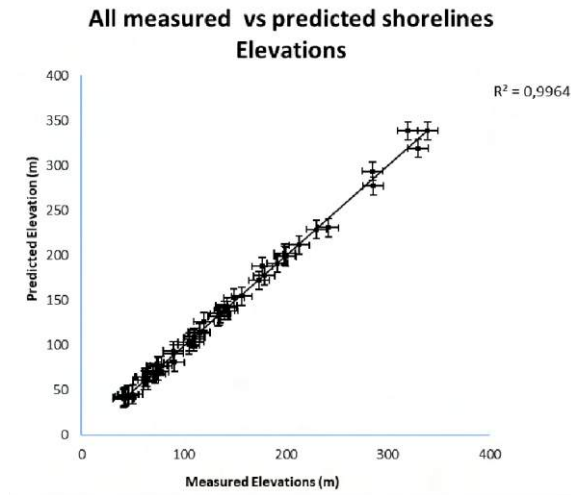


**Figure 44.** a) It shows the relationships between all the measured and predicted shorelines elevation, while in b) it is reported the relationship between field-based and DEM-based

As an age constraint for the modelling has been used the 316  $+87/-53$  ka of the calcite vein including in the sands of T2 (profile 2). The dating gives an important *ante quem* marker about the time formation of the T2 wave-cut platforms of the study area. Indeed, the continental calcite formation needs freshwater circulation namely when the terraces resides in subarial condition. The U-series age dating presents a huge and asymmetric range of uncertainties due to the

proximity to the upper limit of the method, however, the sample certainly is older than 260 ka with a maximum peak of probability ~316 ka.

The synchronous correlation method allows correlation of undated paleoshorelines with highstands of the Middle Pleistocene.

Assuming that the paleoshorelines at +75 m a.s.l. in profile 2 is > 260 ka, through the iteration, the T2 was assigned to the highstand of 340 ka. It has been obtained by iteration of uplift rate along Polvica Fault. Consequently, the wave-cut platform at + 50 m a.s.l. (T1) corresponds to the 240 ka one. Besides T1 and T2, the sub-horizontal surfaces identified by geomorphological analysis of the DEM may be associated by the synchronous correlation method with positive sea level peaks of the Middle and Late Pleistocene, and particularly to peaks dated: 125, 200, 217, 285, 310, 478, 525, 550, 590, 695, 800, 855, 980 ka. The above-mentioned surfaces are neither present in all profiles, not altogether in a single profile (**Table 6.1.2**). Most of the Middle Pleistocene synchronously derived age of paleoshorelines have been identified in the Mediterranean Sea (e.g., Roberts et al., 2013, 2009).

A good match between the measured paleoshoreline elevations with the predicted elevations has been obtained using the synchronous correlation method along the strike of Polvica Fault (**Figure 43-Figure 44**). The paleoshoreline elevations have been correlated along the strike of the Polvica Fault. In profile 2, for instance, is clearly visible how the 310 ka paleoshoreline is located lower than the 240 ka one due to possible overprinting phenomena (Meschis et al., 2018).

It is worth noting that the uplift rate varies along the strike of Polvica fault. In particular, the uplift rate in the central part of the fault (HW) is 0.32 mm/y and it decreases to 0.19 mm/y towards the western tip. Conversely, from the centre towards the east the uplift rate firstly decreases and then it increase abruptly up to 0.58 mm/y as a consequence of fault bend (Iezzi et al., 2018) (**Figure 45a**). It is also worth noting these uplift values may result from a combination of a “regional”

uplift component and a fault-related one. However, it is clear that the fault-related component has controlled the uplift rate variation along the strike of Polvica Fault (**Figure 45a**) and the associated along-strike tilting of the paleoshorelines (**Figure 45c**).

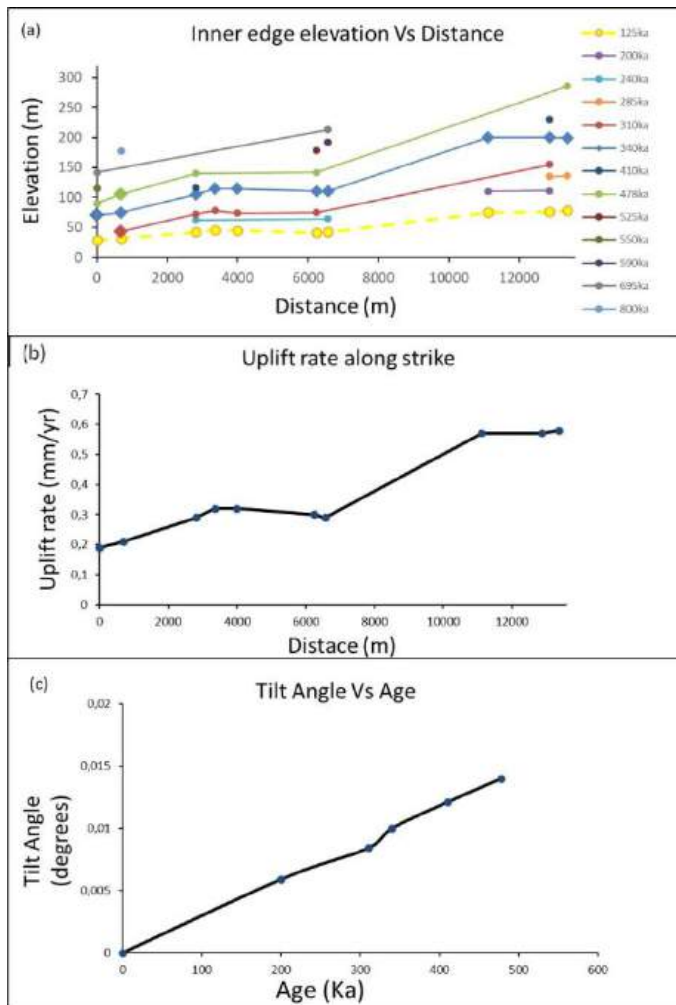


**Figure 45.** The diagrams show evidence of Quaternary activity for Polvica Fault. In (a) is shown the spatial distribution along the Polvica Fault strike of the paleoshorelines elevations. Circles indicate the elevations of paleoshorelines mapped by DEM, whereas the rhombus are the mapped in the field ones. The yellow dashed line represents the expected elevation of the MIS 5e from the model (see text). In (b) the uplift rate vs distance along the strike of Polvica Fault is shown. The uplift rate varies spatially and it is lower at the western tip point and higher in the fault bend zone. Finally, in (c) is illustrated the marine terraces tilting due to the Quaternary activity of Polvica Fault. The older terraces present higher tilt than the younger ones which had a shorter history of faulting activity

In particular, lower tilt angles characterise the lower paleoshorelines, whereas the older and higher paleoshorelines show higher tilt angles due to a longer tectonic history. The tilt angle values, calculated according to Meschis et al., 2018, vary between  $0.005^\circ$  and  $0.014^\circ$  (**Figure 45c**). By integration of the results of the synchronous correlation with subsurface stratigraphy data from the T69 borehole (T69 borehole, **Figure 42**), cumulative offset produced by the Polvica Fault zone may be inferred using information from profile 7. In particular, by: (i) correlation of the buried marine deposits with the oldest one in the marine terraces identified along Mt. Fellino ridge by the geomorphological analysis of the digital topography data, (ii) the depth of the carbonate bedrock below the marine sands in the T69 borehole (which, with some approximation associated with possible local morphological irregularities, is indicative of the depth of the lowered abrasion platform underlying the marine sands), (iii) the assumed elevation of the 980 ka old marine terrace along profile 7, as inferred from the marine terrace synchronous correlation, (iii) the 980 ka age assigned by the synchronous correlation method to that marine terrace. Based on the above listed constraints, the inferred maximum long term rate of the vertical slip component for the Polvica Fault, considering a displacement of 425 m in a 980 ka time span, is in the order of 0.4 mm/y. It is worth noting that the estimated vertical slip rate has been evaluated along a cross section located, along Mt. Fellino range, to the east of the segment where maximum uplift is recorded.

As visible in **Figure 45** the paleoshorelines related to MIS 5e (~125 ka) would be located at an elevation spatially (from W to the E) ranging from 29 to 78 m a.s.l., and thus at elevations systematically lower than those of the adjoining Holocene Campania Plain and the piedmont, which also rise gradually eastwards (**Figure 41**).

### 6.2.3 Tectonic quantification

A study on the relationship between multiple Middle Pleistocene paleoshorelines, sea level curve (**Figure 46**) and active normal faulting have been carried out.

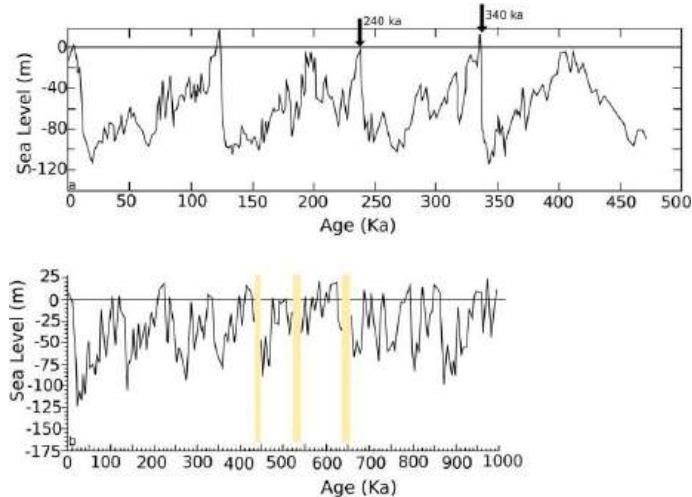


**Figure 46.** a) sea level curve from Siddal et al., 2003 and b) Rohling et al., 2014 used in the modelling with the recognized paleoshorelines (black arrow)

Overall evidence, i.e. the presence of drainage anomalies, uplifted and displaced Middle Pleistocene wave-cut platforms, and overall morphotectonic evidences point to the late Quaternary activity of the Polvica Fault zone, which may be considered an active fault, according to the definition of Chapman et al., (2014) and Yeats, (2012).

The synchronous correlation method on the paleoshorelines along Mt. Fellino ridge has allowed evaluating the uplift rate, which varies along the strike of Polvica Fault. In particular, the estimated uplift ranges from a minimum value of 0.19 mm/y at the Polvica Fault western tip to 0.58 mm/y in the eastern part, due to the geometry of Polvica Fault (**Figure 45**). Such a variable uplift is consistent with along-strike variation of the slip rate of the Polvica Fault zone. However, those values do not account for a “regional” uplift component. Computing the “regional”

uplift component is not easy for several reasons: (i) available information from the Tyrrhenian side of the southern Apennines is indicative of uneven long-term uplift, with the regional-scale marine terrace record being indicative of overall long-term uplift increasing southwards to reach high values in southern Calabria (e.g., Dumas et al., 1987; Westaway, 1993; Ferranti et al., 2006 and reference therein); (ii) in the Tyrrhenian coastal stretch that includes the area investigated with this study (namely, the Campania coastal stretch), flights of marine terraces occur only in the horst blocks of the peri-Tyrrhenian graben, which, similar to the study area, may have recorded fault-related plus regional uplift components; (iii) most of the marine terraces in the Campania coastal stretch and, particularly, the Middle Pleistocene marine terraces are undated, and chronologically framed by geomorphological reconstructions. However, based on chronological framework of marine terraces from the raised headlands in the Campania coastal stretch, uplift rates of around 0.2 mm/y (Sorrento peninsula; Cinque and Romano, 1990; Caiazzo et al., 2006) and 0.12 mm/y (southern Cilento; Ascione and Romano, 1999) are inferred for the Middle Pleistocene to present time span. If these values are considered, the fault-related uplift component for Mt. Fellino ridge (the maximum uplift of which exceeds c. 0.2 mm/y) is evident. However, it is worth noting that evidence from both the raised headlands and coastal grabens to the north and south of the Campania Plain points to uplift and subsidence, respectively, substantially ceased since the Last Interglacial (see **Section 7.7.3.4** Campania). In contrast, subsurface data from the Campania Plain point to subsidence continuing after the Last Interglacial (Romano et al., 1994a; Santangelo et al., 2010; Santangelo et al., 2017 and reference therein). Consistent with continuing vertical displacements in the Campania Plain, our reconstruction on the Mt. Fellino area suggests ridge uplift continuing after the Late Pleistocene. Although deposits buried in the Polvica plain are undated, the hypothesis of post-Last Interglacial displacements along the Polvica Fault zone is consistent with the overall framework. By such a hypothesis,

we may assume that the hanging wall block of the Polvica Fault has not been involved in the regional uplift and, thus, the 0.4 mm/y vertical differential displacement associated to that extensional fault zone effectively corresponds to the fault slip.

Recent crustal deformation along the Polvica Fault zone evaluated so far using sea level indicators may be used to infer the earthquake recurrence interval by the throw rate. Perhaps minor faults are contributing to the extension, but the main deformation is produced by Polvica Fault, which is responsible for the shaping of the Pleistocene to Holocene alluvial-coastal plain and the NE border of the Polvica plain.

Using common empirical correlation (Galli et al., 2008; Wells and Coppersmith, 1994), the earthquake recurrence interval ( $T_{mean}$ ) for Polvica Fault, has been estimated. We have used a length of the fault of 15 km, as a consequence using the Galli et al., 2008 formula:

$$M_w = 4.7248L \text{ (km)}^{0.1046} = 6.27$$

a maximum earthquake magnitude  $M_w$  6.27 is estimated, with an earthquake recurrence interval of 1162 years. These values have been calculated assuming a rupture along the entire length of the Polvica Fault, and  $T_{mean}$  value may decrease if only part of the structure would rupture. In addition, the obtained  $M_w$  and  $T_{mean}$  values have been obtained assuming a coincidence of the western

Polvica Fault tip with the termination of Mt. Fellino ridge. However, if the fault continues without any segmentation below the Campania Plain surface, larger  $M_w$  and slip events would be estimated.

Overall results of this study point to the late Quaternary activity of the Polvica Fault zone. However, based on the historical record no major earthquake has been recognised to have affected the study area. Such an apparent inconsistency could be explained with the Coulomb stress transfer theory (Mildon et al., 2017), based on which the Polvica Fault could have been “deactivated” in very recent

times as a consequence of the recent activation of other extensional faults in the mountain belt interiors. Conversely, if no “deactivation” has occurred, the current activity of the Polvica Fault might generate earthquakes of Mw and slip events in the order of those we roughly evaluated. Although some assumptions and uncertainties affect our estimates of possible earthquake ruptures, based on our results on late Quaternary activity of the Polvica Fault zone further, more in-depth analyses addressing reassessment of the seismic hazard for the densely populated Campania Plain are strongly recommended.

#### 6.2.4 Concluding remarks on the Campania Plain case study

The integrated study of paleoshorelines carried out in this study provided constraints to their formation, deformation and age. Such constraints represent the first field evidence of the extensional tectonics that has been affecting the Campania Plain coastal graben. Our work fills a significant gap of knowledge for an area that attracted a plethora of geophysical studies, but surprisingly lacked direct geological observations on outcropping Quaternary units and associated structures. Therefore, our results provide to date unique constraints to the geological evolution of the Campania Plain, which developed within the wider framework of the Tyrrhenian back-arc basin. Overall evidence indicates that Middle Pleistocene displacements along major, roughly S-dipping faults, which interacted with late Quaternary sea level fluctuations, controlled the evolution of the Campania Plain margin in the study area.

Our findings show that marine terraces, even reaching several hundreds of metres in width, may be obscured or deleted not only by erosion (e.g., paleo-sea cliff retreat, as commonly hypothesized when terraces are rare and sparse along steep rocky coasts) but also by burial by continental facies deposits accumulated during cliff recession and slope evolution. In our case example, such a condition was determined by the presence of high rocky cliffs prone to rock fragmentation and collapsing possibly controlled, besides frost action during cold stages, by fault-related cliff growth continuing after marine terrace formation. Hence, our case study indicates that, in geomorphic scenarios comparable to the one we have analysed, topography analysis alone may fail in the effective identification of marine terraces. Moreover, in this work constant uplift rate on the Polvica extensional fault from the Middle Pleistocene onward has been presented. In particular, the attention has been devoted to the Middle Pleistocene paleoshorelines, which have been deformed by the Polvica Fault. The

paleoshorelines have been also analysed by modelling with the synchronous correlation method. Evidencing how Polvica Fault zone has moved and raised the wave-cut platforms on the Mt. Fellino ridge at least from the Middle Pleistocene allows us to consider it is as an active fault (Chapman et al., 2014). That fault might have been recently deactivated. If, conversely, the fault is effectively still active, the magnitude and slip rate estimated so far rise the crucial question of a careful assessment of seismic hazard for the Campania Plain, where several densely populated towns are settled.

### *6.3 Sea level fluctuations along the raised Tyrrhenian margin of northern Calabria-Basilicata (southern Italy): New U-series dating of late Quaternary paleoshorelines*

Manuscript 3- *Sea level fluctuations along the raised Tyrrhenian margin of northern Calabria-Basilicata (southern Italy): New U-series dating of late Quaternary paleoshorelines* by Cerrone, C., Ascione A., Robustelli, G., Balassone, G., Soligo, M., Tuccimei, P., submitted to *Quaternary Science Reviews*.

#### 6.3.1 Introduction

In the last decades, growing attention has been devoted to the reconstruction of sea level fluctuations recorded during interglacial periods, when warmer temperatures and depletion of ice sheets as a response of long-term orbital control triggered rises of the sea level. Such attention rests on the acknowledgement of the crucial importance of paleoclimatic indicators in understanding the mechanisms governing temperature change and its effects, as such issues may spread light on the present warm period and the future (e.g., IPCC, 2013; Kattsov et al., 2005; Turney and Jones, 2010; Lunt et al., 2013; Dutton et al., 2009a). For instance, the Last Interglacial period, or Marine Isotope Stage - MIS 5e, is acknowledged as an analogous for better understanding the consequences of modern global warming (e.g., IPCC, 2013). In this regard, paleoshorelines represent first order indicators of sea level fluctuations. In coastal sectors not affected by crustal displacements, these markers allow the reconstruction of sea level curves. These provide measures of total volume of the oceans, which depends on the global glacial volume (Mörner, 1982). In fact, once the glacio-hydro-isostatic contributions, which cause the spatial variability to the field-estimated sea level worldwide, are evaluated, eustatic, or ice-volume equivalent sea level change may be determined (Lambeck and

Chappell, 2001; Lambeck and Purcell, 2005; Creveling et al., 2015). Where tectonically-induced crustal displacements occur, relative sea level (RSL) change can be reconstructed assuming a constant and known uplift rate in the studied sector (Chappell and Shackleton, 1986; Pirazzoli, 1993, 1996). Crucial to any of such reconstructions is the availability of reliable constraints to both elevation and age, such as those obtained from fossil corals, of sea level markers (e.g. Bloom et al., 1974; Bender et al., 1979; Bard et al., 1990; Chappell et al., 1996; Zazo et al., 2002; Dumas et al., 2005; Caputo, 2007; Rovere et al., 2016a).

To date a well-constrained field-based sea level change determination, essentially supported by coral dating, is available for the last interglacial-glacial cycle (e.g., Bender et al., 1979; Bard et al., 1990; Pirazzoli, 1996; Chappell et al., 1996; Stirling et al., 1998; Yokoyama et al., 2000), and database of the RSL indicators of MIS 5e in the World's coasts and the coasts of Italy have been compiled (Ferranti et al., 2006; Pedoja et al., 2011, 2014), recently implemented by an updated and standardized MIS 5e sea-level database for the western Mediterranean Sea compiled in the framework of the World Atlas of Last Interglacial Shorelines (WALIS; see **Section 7. Last Interglacial sea-level proxies in the Western Mediterranean**). Data on the Last Interglacial sea level markers supported by the computation of Glacio-hydro-Isostatic Adjustment (GIA, Lambeck and Chappell, 2001; Lambeck and Purcell, 2005; Creveling et al., 2015) and taking into consideration local tectonics effects, have allowed estimating globally the MIS 5e eustatic sea level, which is framed between 5.5 m and 9 m a.s.l. (Dutton and Lambeck, 2012; Kopp et al., 2009). However, less constrained are sea level fluctuations that occurred prior to the Last Interglacial period as erosion of marine terraces increases with age, and assumptions of long-term constancy of uplift may be unsuitable (e.g., Pirazzoli et al., 1993; Caputo, 2007).

A region suited to the study of sea level markers and the reconstruction of sea level fluctuations is the Basilicata - northern Calabria sector of the southern

Apennines mountain belt (**Figure 47**), where coral-bearing paleoshorelines occur. In this region, impressive flights of marine terraces testify to long-term Quaternary uplift of the margin of the southern Tyrrhenian back-arc basin in the order of several hundreds of metres (e.g., Dumas et al., 1982; Carobene and Dai Pra, 1990; Westaway, 1993; Ascione and Romano, 1999; Filocamo et al., 2009). The amount of Quaternary uplift of the southeastern margin of the Tyrrhenian sea basin has been variable, with the southernmost segment (southern Calabria) affected by larger uplift compared with the northern segment (e.g., Damiani, 1970; Dumas et al., 1982; Westaway, 1993; Ascione and Romano, 1999). The differential uplift is better expressed by the variable elevations of the markers of the Last Interglacial sea-level peak. In southern Campania they are located a few metres higher than coeval indicators from stable areas in the Tyrrhenian sea margin, pointing to slow uplift of that region (Esposito et al., 2003). Conversely, in southern Calabria, uplift rates of  $\sim 1$  mm/y since the Last Interglacial have been estimated by several authors and related to the sum of a regional plus a local component, which is associated with the activity of large normal faults (Cosentino and Gliozzi, 1988; Westaway, 1993; Miyauchi et al., 1994; Bordoni and Valensise, 1999; Tortorici et al., 2003; Dumas et al., 1982, 1987; Dumas and Raffy, 2004; Ferranti et al., 2006). The northward transition, or boundary, of the fast uplifting sector of the Apennines is undefined due to the lack of data in a  $\sim 100$  km long coastal strip (Ferranti et al., 2006). Further north, the northern Calabria to Basilicata appears as a key area for the reconstruction of a comprehensive framework of recent uplift of the southern Apennines Tyrrhenian margin, although contrasting interpretations have been provided to date on the late Quaternary behaviour of that area (e.g., Damiani, 1970; Westaway, 1993; Ferranti et al., 2006; Filocamo et al., 2009).

Using a combined geomorphological and morphostratigraphical approach, we studied the relative sea-level markers that occur in a  $\sim 25$  km-long coastal belt extended from Basilicata to northern Calabria. Several of the identified

paleoshorelines are characterised by shallow marine deposits bearing coral *Cladocora caespitosa*, encrusting algae and mollusks, formerly dated by Carobene et al. (1986) and Carobene and Dai Pra (1990, 1991). Field evidence, constrained by new U-series dating of coral samples and calcite concretions either predating, or postdating, the identified paleoshorelines, allowed the reconstruction of a chronological framework for the analysed sea level markers and constraining the late Quaternary uplift of the investigated sector of the Tyrrhenian coastal margin. By overall data, constraints to the late Quaternary sea level history of the Tyrrhenian Sea can be inferred.

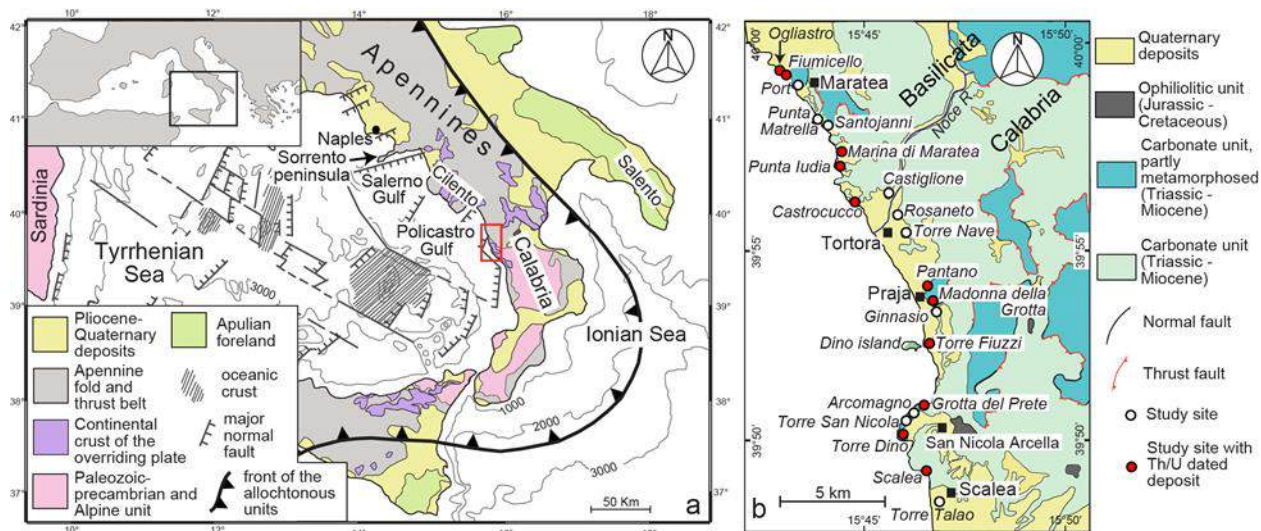


**Figure 47.** a: Simplified tectonic sketch of the Tyrrhenian Sea basin and southern Apennines mountain belt (redrawn and modified after Moussat et al., 1986), with indication of the study area (red box), shown in detail in diagram b. b: Geological sketch of the Basilicata - northern Calabria margin of the Tyrrhenian basin (redrawn and modified after Iannace et al., 2007), with indication of the study sites.

### 6.3.2 Geological framework

An indented coastal perimeter featuring narrow headlands and bays characterise the steep rocky coast of the investigated area, which extends for about 25 km along the eastern margin of the Tyrrhenian Sea basin (**Figure 47 a**), between the Campania coastal belt, in the north, which is almost stable since the last interglacial, and southern Calabria, in the south, where the late Quaternary shorelines are strongly uplifted. In particular, the study area stretches from Maratea (Basilicata region), in the north, to Scalea (northern Calabria), in the south (**Figure 47 b**).

The rocky backbone of the study area is formed of Triassic to Miocene carbonates that are tectonically overlain by ocean-derived ophiolitic nappes (Iannace et al., 2007, 2005), with both units being part of the southern Apennines fold and thrust belt (**Figure 47 b**). Neogene to Early Pleistocene NE-verging thrusting in the southern Apennines was coeval, since the late Miocene, with back-arc extension and opening of the Tyrrhenian Sea basin, both related to the eastward retreat of the west-dipping subducting Apulian-Ionian slab (e.g., (Butler et al., 2004; Faccenna et al., 2001; Gueguen et al., 1998; Malinverno and Ryan, 1986; Patacca et al., 1990; Royden, 1993; **Figure 47 a**). Crustal stretching and sea-floor spreading was earlier localised in the present-day central part of the Tyrrhenian basin (Vavilov basin) and later, since  $\sim 2$  Ma, it migrated to the southeast, in the Marsili basin (e.g., Gueguen et al., 1997; Kastens et al., 1988; Sartori, 1990; Savelli and Schreider, 1991; **Figure 47 a**). Quaternary, roughly NW-SE oriented extension active in the southeastern Tyrrhenian basin affected the southern Apennines margin with formation of a series of coastal grabens (e.g., Caiazza et al., 2006; Moussat et al., 1986; Rehault et al., 1987). In the horst blocks, the occurrence of raised Quaternary marine terraces testifies to the attainment, since the Early Pleistocene, of a coastal perimeter that approximates the modern one (Ascione and Romano,

1999; Filocamo et al., 2009). Ceasing of shortening in the southern Apennines at ~ 0.7 Ma was followed by regional-scale uplift of the mountain range and foothills to the east of it occurred in response to detachment and rebound of the Ionian slab (Ascione et al., 2012; Cinque et al., 1993; Patacca and Scandone, 2001). Fast uplift, with rates exceeding 1 mm/y, is inferred from Middle and Late Pleistocene raised marine terraces spanning along the Ionian coastal belt of Basilicata and Calabria and Tyrrhenian coast of southern Calabria (e.g., Amato, 2000; Bordoni and Valensise, 1999; Cosentino and Gliozzi, 1988; Dumas et al., 1982; Dumas and Raffy, 2004; Ferranti et al., 2006; Miyauchi et al., 1994; Santoro et al., 2013; Tortorici et al., 2003). Consistently, geomorphic evidence from the Aspromonte massif, in southern Calabria, points to relatively slow uplift during the early Pleistocene followed by pulses of rapid uplift during the Middle-Late Pleistocene (Robustelli, 2019). Raised Holocene shorelines from southern Calabria point to fast uplift continuing nowadays in southern Calabria (Ferranti et al., 2008) resulting from the summation of a regional plus a local component associated with activity of large normal faults, which would account for values ranging between 0.1 and 0.7 mm/y of vertical fault slip (e.g., Bordoni and Valensise, 1999; Ferranti et al., 2007; Ghisetti, 1992; Miyauchi et al., 1994; Monaco and Tortorici, 2000; Tortorici et al., 2003; Westaway, 1993). The rapidly uplifting region is well correlated with sectors of fast surface horizontal motion documented by geodetic velocities and high seismic release (Ferranti et al., 2007, 2006), with devastating historical earthquakes occurred in 1783, 1908 and 1925 (e.g., Rovida et al., 2019). A much more subdued seismicity characterises the sector of the Basilicata-Calabria coastal belt, where both inland and offshore historical seismicity is sparse and of moderate ( $M \leq 5$ ) energy release (<https://emidius.mi.ingv.it/CPTI15-DBMI15/>).

A flight of marine terraces reaching elevations ranging from ~130 m, in the north, to ~170 m a.s.l., in the south (Filocamo, 2007; Filocamo et al., 2009 and

reference therein), characterises the landscape of our study area. As most marine terraces are undated, there is a long debate on the chronological framework of relative sea level markers and the Quaternary uplift rate of the study region. For instance, the highest marine terrace (located from 130 to 170 m a.s.l.) has been associated with MIS 5e by Westaway (1993), who estimated an uplift rate around 1 mm/y since the Last Interglacial. The same terrace has been related to the late part of the Early Pleistocene by Filocamo (2007) and Filocamo et al.(2009) who correlated a lower marine terrace (located at 100 m of elevation in the coastal sector spanning from San Nicola Arcella to the Scale cape; **Figure 47 b**) with MIS 19. Filocamo et al. (2009) also highlighted that the flight of Early Pleistocene marine terraces (which south of Scalea reach 240 m a.s.l.) testifies to uplift accompanied by block-faulting, which substantially ceased since the Middle Pleistocene.

The chronological framework by Filocamo et al. (2009) rests on literature dating of terraces and deposits located within ~ 20 m a.s.l. in the Maratea to Cetaro coastal stretch (Calabria). Based on  $^{230}\text{Th}/^{234}\text{U}$  measurements on coral *Cladocora caespitosa* and D/L measurements on bivalves by Carobene et al. (1986) and Carobene & Dai Pra (1991), the authors distinguished the *Cladocora* bearing deposits located in our study area in the ~12-17 m elevation range, related to the late MISs of the Middle Pleistocene, from those located in the ~5-9 m elevation range, related to MIS 5e. Shorelines located in the ~5 - 2 m elevation range were correlated to either MIS 5c or MIS 5a. The resulting uplift rate in the range of 0.05 - 0.03 mm/y since the Last Interglacial was estimated by Ferranti et al. (2006) for the coastal area investigated with this study.

### 6.3.3 Materials and methods

The study was carried out through the combination of geomorphological and stratigraphical analyses with U-series disequilibria dating of coral samples and of calcite concretions either predating, or postdating, the identified paleoshorelines. Coral samples were pre-treated through mineralogical analyses aimed at testing their original aragonitic nature. Stable isotope analyses were performed at Bochum University (Institut für Geologie, Mineralogie und Geophysik, Ruhr-Universität) to better constrain the water formational environment of three of the sampled calcite concretions.

#### 6.3.3.1 Geomorphological-stratigraphical approach to the study of the marine terraces

In order to outline the large-scale coastal geomorphology framework of the area, we first mapped the flights of terraced surfaces in the entire investigated coastal belt, with a particular focus on the younger terraces located in the first tens of metres (c.60) a.s.l., which former studies had related to the Middle and Late Pleistocene (Carobene et al., 1990, 1991). For the analysis of topography, we used 1:5.000 scale maps edited by Regione Calabria and Regione Basilicata, and LiDAR data with resolutions of 1x1 and 2x2 m. The identified marine terrace remnants are small-size (ranging from few metres to few tens of metres) and spatially discontinuous. In the study area, as commonly along rocky coasts, information on relative paleo-sea level obtained from mapping of terraces using topographic data alone may be misleading unless it is integrated by detail-scale field data. In fact, slope breccia and alluvial fan sediments commonly bury the marine terrace surfaces (e.g. Carobene and Dai Pra, 1990, 1991; Esposito et al., 2003; Filocamo et al., 2009), thus hampering the estimation of paleo-sea level elevation.

Detail-scale field surveys were carried out at several sites (locations of the investigated sites are shown in Fig. 1b) aiming at: (i) the identification and mapping

of sea level markers, (ii) the reconstruction of the relative chronology among multiple sea level markers identified at each site, and (iii) the spatial correlation among markers outcropping in different sites based on relative chronology of sea-level markers of a single sites. Thus, at each study site detailed morpho-stratigraphical reconstructions were carried out through the detection of erosional/depositional markers of paleo-sea levels and investigation of the cross-cut relationships between those features and continental deposits and landforms. The identified depositional indicators of past sea level consist of clastic (sands, pebbles and boulders) shore deposits, biocalcarenites and coral and algal bioconstructions, while the erosional indicators are abrasion platforms, tidal notches, coastal caves and *L. lithophaga* hole bands. As a sea-level marker, we considered the abrasion platform-sea cliff edge, or shoreline angle, which corresponds to the highest elevation reached by the sea during an interglacial period (Lajoie, 1986). The platform inner edge is an essential geodetic marker to take into account in sea level and tectonic studies (Jara-Muñoz et al., 2019, and reference therein), especially in the western Mediterranean area where the tide range is in the order of a few cm ( $\pm 0.25$  m; Antonioli et al., 2015). The elevations of the abrasion platform inner edges were constrained by crossing the topographic and GPS data, and/or using a laser distance meter. The position of the inner edge, where buried by a continental cover, was geometrically reconstructed using the intersection point between the profiles of the paleo-sea cliff and marine platform surface. The error in the elevation of the sea level markers ranges from a few cm up to 1 m depending on whether the inner edge is apparent or buried, respectively. For the key paleoshorelines, the sea level markers elevations were used to accurately estimate the relative sea level (RSL) through the IMCalc tool (Lorscheid and Rovere, 2019). The IMCalc tool allows to compute the ‘indicative meaning’ by modern analog based on the closest data from the Coastal Point Database (CPD), where waves and hydrodynamic characteristics of the area are included. The indicative meaning

(Shennan, 2015; Van De Plassche, 1986) assesses at what elevation a sea level marker was formed relative to the water sea-sheets using the indicative range (IR) and reference water level (RWL) by mathematical relationship described in Rovere et al. (2016a).

#### 6.3.3.2 U-series dating

Coral (*Cladocora caespitosa*) specimens from bioconstructions overlying the abrasion platforms, or blanketing paleo-sea cliffs, were sampled for geochronological analyses. Calcite concretions either predating or postdating marine deposits were also sampled and geochronologically analysed in order to constrain the age of marine deposits not bearing corals, or bearing undated corals due to weathering/recrystallization (see Section **6.3.3.3 Mineralogical characterization of corals**), or to cross-check the geochronological data from corals. Calcite concretions and corals are considered excellent samples to be dated with U-series disequilibria methods because in most cases they consist of pure calcium carbonate, free from a detrital component that makes problematic the dating of dirty carbonates. The  $^{230}\text{Th}/^{234}\text{U}$  method is the most widely used dating technique applied to continental carbonate deposits and corals and is based on the extreme fractionation of the parent isotopes  $^{238}\text{U}$  and  $^{234}\text{U}$  from their long-lived daughter  $^{230}\text{Th}$  in the hydrosphere. On the contrary, molluscs are not suitable for U-series dating due to an open-system postmortem history, in fact the discrepancy between the U-series dating on corals and molluscs could be from ten to hundred of thousand years because of postmortem processes of U-uptake not quantitatively quantify (Kaufman et al., 1971, 1996; Ivanovich et al., 1983; Carobene et al., 1986). Uranium, markedly more soluble than Th in the surface and near-surface environments, is readily mobilised as the highly soluble uranyl ion ( $\text{UO}_2^{2+}$ ) and its complexes, whereas Th is easily hydrolyzed and precipitated or adsorbed on detrital particles. Uranium is co-precipitated with  $\text{CaCO}_3$  on

exsolution of CO<sub>2</sub>, while Th is generally negligible. In the absence of detrital Th, <sup>230</sup>Th only forms in situ by radioactive decay of co-precipitated U. In a closed system the extent to which the <sup>230</sup>Th/<sup>234</sup>U activity ratio has returned towards unity is a function of time, taking into account also the state of disequilibrium between <sup>234</sup>U and <sup>238</sup>U (Kaufman and Broecker, 1965).

For U-series dating only corals with >95% aragonite have been used. In fact, no-altered corals are originally made up of aragonite. Each sample of *Cladocora caespitosa* coral and calcite concretion has been cleaned mechanically by washing it with de-ionized water and ultrasonically cleaned for a few minutes. Then, the preparation of *Cladocora caespitosa* samples consists in dividing the corals between the internal septas from their external walls with the help of a microdriller because the different thickness may react differently to the alteration processes (Roberts et al., 2009). Such a procedure implied splitting of most of the samples in two sub-samples, distinguished by labels w (wall) and s (septas).

For U-series dating about 3 g of corals and 40 g of calcite were selected and dissolved in nitric acid. Few millilitres of hydrogen peroxide were added and heated at 100 °C in order to destroy organic matter. Isotopic complexes of uranium and thorium were extracted according to the procedure described in Lawrence Edwards et al. (1987) and alpha-counted using high resolution ion implanted Ortec silicon surface barrier detectors. The ages were calculated by means of Isoplot/Ex (version 3.0), a plotting and regression program designed by Ludwig (2003) for radiogenic-isotope data.

### 6.3.3.3 Mineralogical characterization of corals

For corals it is important to verify their original aragonitic nature and check for the eventual presence of calcite. The occurrence of relevant calcite indicates that weathering processes have affected the coral after its burial, with consequent

opening of the chemical system. Therefore, a mineralogical characterization of coral samples was carried out through the X-ray powder diffraction (XRD) method.

For routine mineralogical characterization of each coral sample a GE-Seifert MZVI automated diffractometer (XRD) was used (DiSTAR, University Federico II, Naples), with  $\text{CuK}\alpha$  radiation, 40 kV and 30 mA, 5s per step and a step scan of  $0.05^\circ 2\theta$  in the  $3\text{--}70^\circ 2\theta$  interval. The software package RayfleX (GE Inspection Technologies, 2004) was used for data processing, and phase identification was made by means of the ICDD-PDF2 database. For quantitative XRD phase analysis, i.e. calculation of percentages of aragonite, calcite and all the other associated minerals, we used both the GE-Seifert MZVI instrument (counting 18s per step, step scan  $0.02^\circ 2\theta$ ) and a PANalytical diffractometer (INGV, Osservatorio Vesuviano, Naples), equipped with a high speed PIXcel detector, Ni-filtered,  $\text{CuK}\alpha$  radiation, pyrolytic graphite crystal monochromator, 40 kV and 40 mA, step size of  $0.02^\circ$  and scanning time 8 s/step. The data were refined using the Rietveld method (Bish and Post, 1993, and references therein); the XRD spectra were elaborated with multiple refinements by the GSAS package (General Structure Analysis System; Larson and Von Dreele, 2004) and its graphical interface EXPGUI (Toby, 2001), as well as with HighScore Plus software. The Rietveld structural models were based on the American Mineralogical Crystal Structure Database (AMCSD, Downs et al., 2003).

#### 6.3.4 Geomorphological and stratigraphical features of the marine terraces

The c. 25 km long, rocky Tyrrhenian coast extending from Basilicata to northern Calabria is characterised by the occurrence of narrow coastal plains and indented promontories (**Figure 47 b**). The largest coastal plain develops between the Castrocucco headland and the Dino island, while much narrower coastal plains occur to the south, between the Torre Fiuzzi and Grotta del Prete headlands, and in the Fiumicello di Maratea bay (**Figure 47 b, Figure 48**). The rocky slopes of headlands and the inner boundaries of coastal plains are mainly composed of densely fractured dolostones, or dolomitic limestones (Iannace et al., 2007; **Figure 47 b**), onto which marine terraces are sculpted (**Figure 48**). The highly weathered bedrock is responsible for developing large and thick alluvial fan bodies, and slope breccia (**Figure 48**) which almost systematically hide the terrace inner edges. At some sites (i.e., the Fiumicello, Punta Iudia and Torre Dino), the abrasion surfaces are shaped on well-rounded beach conglomerates resting on carbonate bedrock (see below).

The highest and widest marine terraces occur south of the Castrocucco headland; northwards, just small size terraces occur below c. 40 m a.s.l. The remnants of the highest terrace form a rather continuous belt of wide, poorly inclined surfaces that progressively rise southwards, from c. 130 m a.s.l. in the left side of the Noce River to 160 m a.s.l. in the Scalea area, while the lower marine terraces are generally much smaller and fragmented (**Figure 48**). The abrasion terraces are frequently marked by *L. lithophaga* holes and typically mantled by patches of conglomerates and arenites, sometimes rich in bivalves, e.g. *Spondylus*, *Ostrea* and *Cerastoderma*. In addition, algal and coral (*Cladocora caespitosa*) bioconstructions are widespread in the marine terraces located up to c. 40 m a.s.l. These marine terraces, and those located up to c. 60 m a.s.l., are the main focus of our study. In the investigated coastal belt, several pieces of evidence indicative of

the reshaping of both subaerial landscape by coastal processes, and marine landforms by subaerial erosion/deposition, testify to a multistage geomorphic evolution governed by repeated relative sea-level fluctuations. Based on overall data, we distinguished five paleoshorelines labeled T1 to T5 (**Figure 48**). In the following subsections, a detailed morpho-stratigraphical characterisation of some key outcrops of the various paleoshorelines is provided, along with reconstructions of the relative chronology of the coastal and subaerial sculpturing events. The outcrops described below are the most explanatory for the reconstruction of a relative sea-level history for the study area, due to the presence of multiple geomorphological/stratigraphical evidences and/or U-series dating.

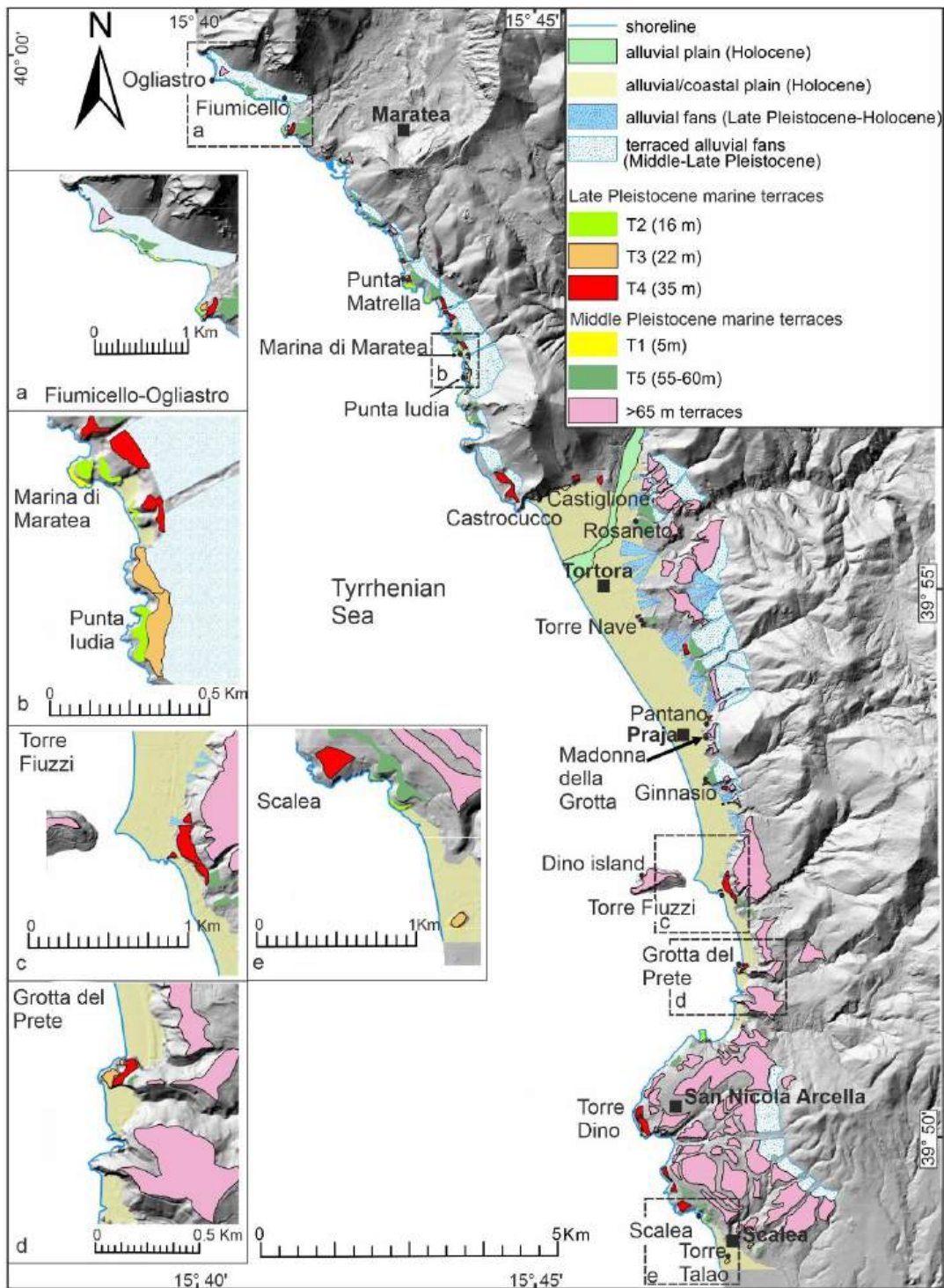


**Figure 48.** Geomorphological map for the northern Calabria - Basilicata coastal sector. In the small boxes (a to e) detail of the key outcrops from north to south indicated in the map by dotted black lines: a: Fiumicello - Ogliastro area; b: Marina di Maratea; c: Torre Fiuzzi; d:Grotta del Prete and e: Scalea.

#### 6.3.4.1 The lowest paleoshorelines - T1

The lowest marine terrace, hereinafter labelled T1, crops out extensively in the northern part (Basilicata region) of the investigated coastal belt (e.g., Fiumicello, Ogliastro Cape, Marina di Maratea, Maratea port sites, **Figure 48**, **Figure 48a** and **Figure 48b**) and in the Torre Talao sea stack, which rises above the modern beach of Scalea (location in **Figure 47b**). The best exposures of marine terrace T1 occur in the northern flank of the Fiumicello bay and adjacent Ogliastro Cape (**Figure 49** and location in **Figure 47b**). Because of a continental cover, locally tens of metres thick, the terrace inner edge is not exposed in those sites, and its outcropping innermost part is noticeable up to 5 m a.s.l. (**Figure 49a**).

The Fiumicello terrace is marked by marine deposits, hereinafter labelled T1 deposit (**Figure 49**). The T1 deposit is mostly composed of biocalcarenites bearing bivalves and both fragments and globular colonies of *C. caespitosa* corals (samples FMC01, FMCO8 and OGL3; **Figure 49b**). At the northern border of the Fiumicello bay (**Figure 49a**) conglomerate lenses made up of well-rounded pebble to cobble-sized carbonate clasts are interspersed within the biocalcarenite. The T1 deposit rests erosively on calcareous bedrock and is covered by tens of metres of alluvial fan deposits (hereinafter, UU; diagrams a, d and e of **Figure 49**) consisting chiefly of bedsets of massive to crudely stratified, locally amalgamated, pebble-to-cobble conglomerates; basal bedding contacts are sharp and irregular, with relief of up to 0.7 m.

The Ogliastro Cape terrace (**Figure 48a** and **Figure 49e**) is composed of beachface deposits (hereafter labelled OG deposit) resting erosively on calcareous bedrock. The OG deposit consists of well-stratified sand and gravel beds that are typically well-sorted and well segregated into horizontal to gently inclined seaward beds with inclination of up to 5° (**Figure 49f**). Beds show distinct vertical

variations in clast sorting size, ranging from sand to fine pebble, and are occasionally composed of bimodally sorted, rounded pebbles. Seaward the beds tend to wedge out forming low-angle cross-stratified bundles. The OG deposit is dissected by sub-vertical, roughly N-S trending fractures and crevices filled with the foregoing T1 biocalcarene (Figure 49f). The marine succession is capped by UU deposits consisting of alternating massive to crudely stratified, locally amalgamated, pebble-to-cobble sized gravel beds and clast-supported sheet conglomerates occurring in laterally continuous beds that extend up to 20 m. Both the outcrops of the Fiumicello bay and Ogliastro Cape show that the base of the alluvial UU deposit is marked by reddish paleosoils some decimetres thick (Figure 49d and e). The UU alluvial conglomerates and the T1 deposit are mantled and/or filled by calcite concretions. Two laminated calcite concretions, one c. 3 cm thick inset in the T1 biocalcarene and outcropping in the Fiumicello site (sample FMC07; Figure 49c) and the other covering the T1 deposit of the Ogliastro Cape site (sample OGL2), have been sampled for U-series dating and stable isotope analyses.

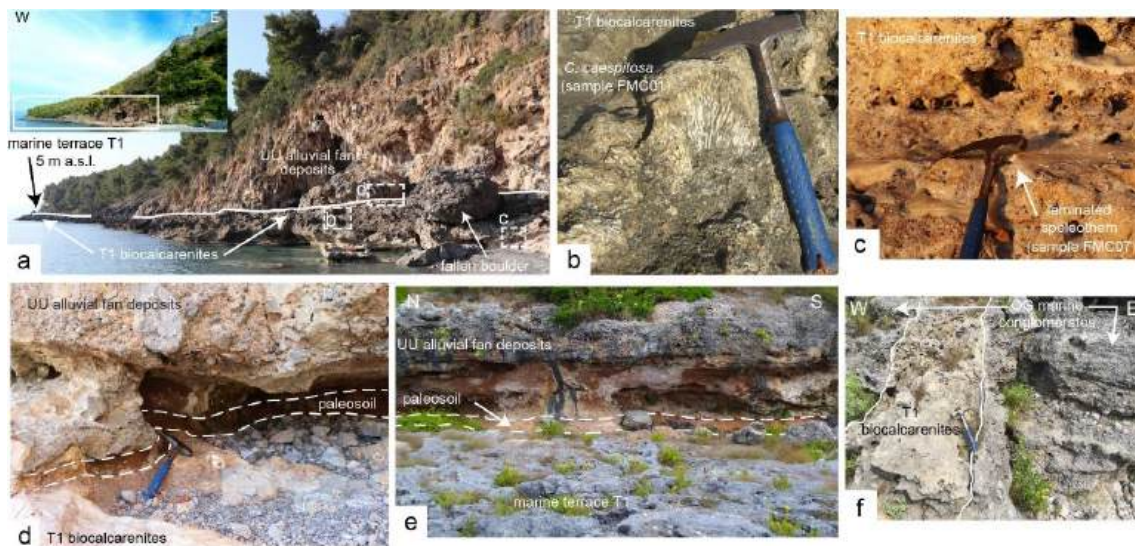


**Figure 49.** The T1 marine terrace in the sites of Fiumicello (diagrams a to d) and Ogliastro (diagrams e and f). a: Close and panoramic (inset) views of marine terrace T1, covered by the c. 100 m thick UU alluvial fan deposit, in the northern flank of the Fiumicello bay. b: Close-up view of one of the *Cladocora caespitosa* globular colonies (sample FMC01; location in diagram a) that are widespread in the T1 biocalcarenite. c: Close-up view of a laminated speleothem (sample FMC07; location in diagram a) inset in the T1 biocalcarenites. d and e: Contact surface, marked by a reddish paleosol, between the T1 biocalcarenites and the UU alluvial fan deposit in the sites of Fiumicello (diagram d; location in a) and Ogliastro cape (diagram e). f: Detailed view of the T1 biocalcarenites filling a N-S oriented crevice formed in the OG marine conglomerates.

#### 6.3.4.2 The T2 marine terrace in the Basilicata coastal stretch

In the Marina di Maratea - Punta Iudia area (location in **Figure 47b**, **Figure 48b**), crosscutting relationships among erosional and depositional marine landforms indicate a composite morphostratigraphic framework (**Figure 50**). In that area, there is evidence of three marine terraces, namely T1, T2 and T4 (**Figure 48**, **Figure 48b**, **Figure 50a** and **Figure 51a**). The T2 deposit corresponds to a few metres thick marine succession (**Figure 50b**), well exposed in the Marina di Maratea bay and adjacent coastal stretch; it consists of a basal, decimetre-thick conglomerate made up of pebble- to cobble-sized clasts with coarse sand matrix, passing upward into about 4 metre-thick bioconstruction made up of encrusting algae, gastropods, bivalves and a large amount of colonial corals and fragments of *C. caespitosa*. Several pieces of evidence indicate that the T2 deposit buries a pre-existing coastal morphology sculpted in the carbonate bedrock, cropping out extensively in the Marina di Maratea area. The buried coastal morphology consists of a planar, sub-horizontal abrasion platform and relative paleo-sea cliffs, with inner edge elevation at + 5 m (**Figure 50c**), which we correlate to the T1 paleoshoreline outcropping in the Fiumicello site. Evidences indicating that the T1 paleoshoreline predates the T2 deposits are (i) densely distributed lithophaga holes, locally filled by biocalcarenites, which are widespread along the carbonate paleo-sea cliffs associated with the T1 (northern side of the Marina di Maratea bay; **Figure 50d-f**), and (ii) the basal conglomerate of the T2 marine succession regularly covers the T1 abrasion platform but is missing on the on top of the coastal promontories around the Marina di Maratea bay, where the T2 marine deposit consists only of a thin biocalcarenite cover (e.g., southern side of the Marina di Maratea bay; **Figure 51**).

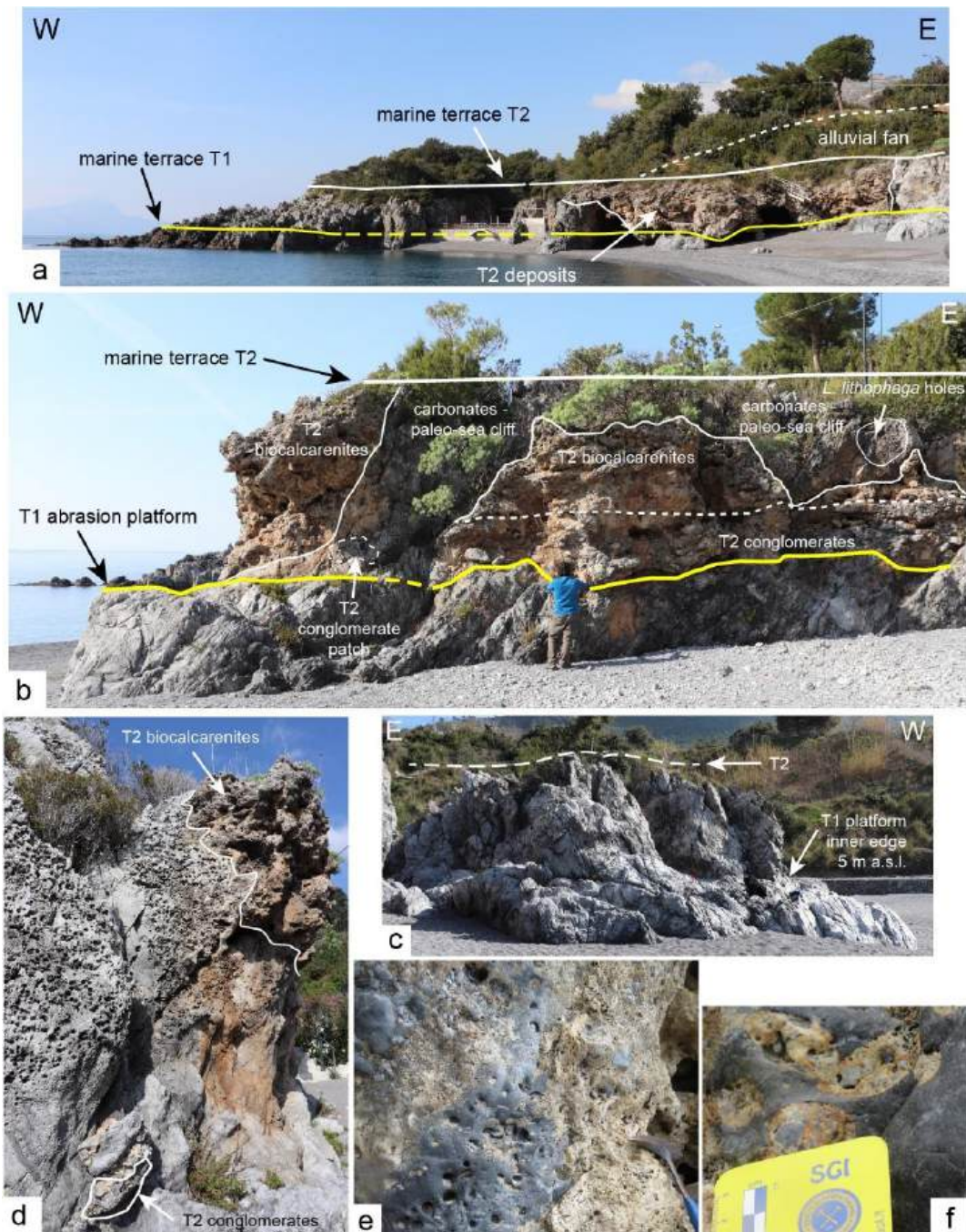


**Figure 50.** a: Panoramic view of the T1 and T2 marine terraces in the Marina di Maratea bay (northern side). b: The T2 marine succession (conglomerate, passing upwards into biocalcarenites) laying onto the T1 abrasion platform and patched onto the correlative paleo-sea cliff; note the flat top surface of the T2 deposits. c: The T1 abrasion platform rising above the modern beach, with the inner edge well exposed. d: view of part of the T1 paleo-sea cliff, potholed by densely distributed *L. lithophaga* holes and patched by the T2 conglomerate (base of the cliff) and biocalcarenites bearing *C. caespitosa* bioconstructions (upper part of the cliff). e and f: Close-up views of the *L. lithophaga* holes that affect the T1 paleo-sea cliff (patched by the T2 deposit), filled with T2 biocalcarenites.

The reconstruction of the T2 marine terrace was performed using, as indicator, the eroded top surface of the carbonate bedrock suspended above the paleo-sea cliffs of the T1 terrace. Such a surface ranges in elevation from c. 6 ÷ 8 m (outer rim) to c. 15 m, where its inner edge is well exposed in the headland to the south of the Marina di Maratea bay (**Figure 50a**); it is interpreted as an abrasion surface, is overall planar, slightly seaward dipping and largely patched by biocalcarenes (**Figure 51b**). Landwards, in the Marina di Maratea bay southern side, the T2 surface is covered by coarse grained slope breccia (**Figure 51e**), while in the northern side the T2 deposit is covered by alluvial fan deposits (**Figure 51d**) composed of stratified, fine- to coarse-pebble conglomerates, with angular gravel clasts set in reddish silty to sandy matrix. Beds are ungraded and extend laterally for metres, even though low angle erosive bases occasionally occur.

South of Marina di Maratea, at the Punta Iudia site (**Figure 51a**), the T2 conglomerates and biocalcarenes form neptunian dikes filling several metres deep, subvertical crevices in the carbonate bedrock. Here an apparent reddish paleosoil is interposed between the T2 deposit and the slope deposit cover, which consists of massive to crudely stratified conglomerates made up of angular to subangular, pebble- to boulder-sized clasts; basal bedding contacts are very irregular and locally sharp; the matrix is locally abundant and consists of a mixture of greyish and brownish poorly-sorted sand and silt.

*C. caespitosa* bioconstructions have been sampled both in the site of Marina di Maratea bay (samples MMR10 and MMR11) and Punta Iudia (sample PDR).

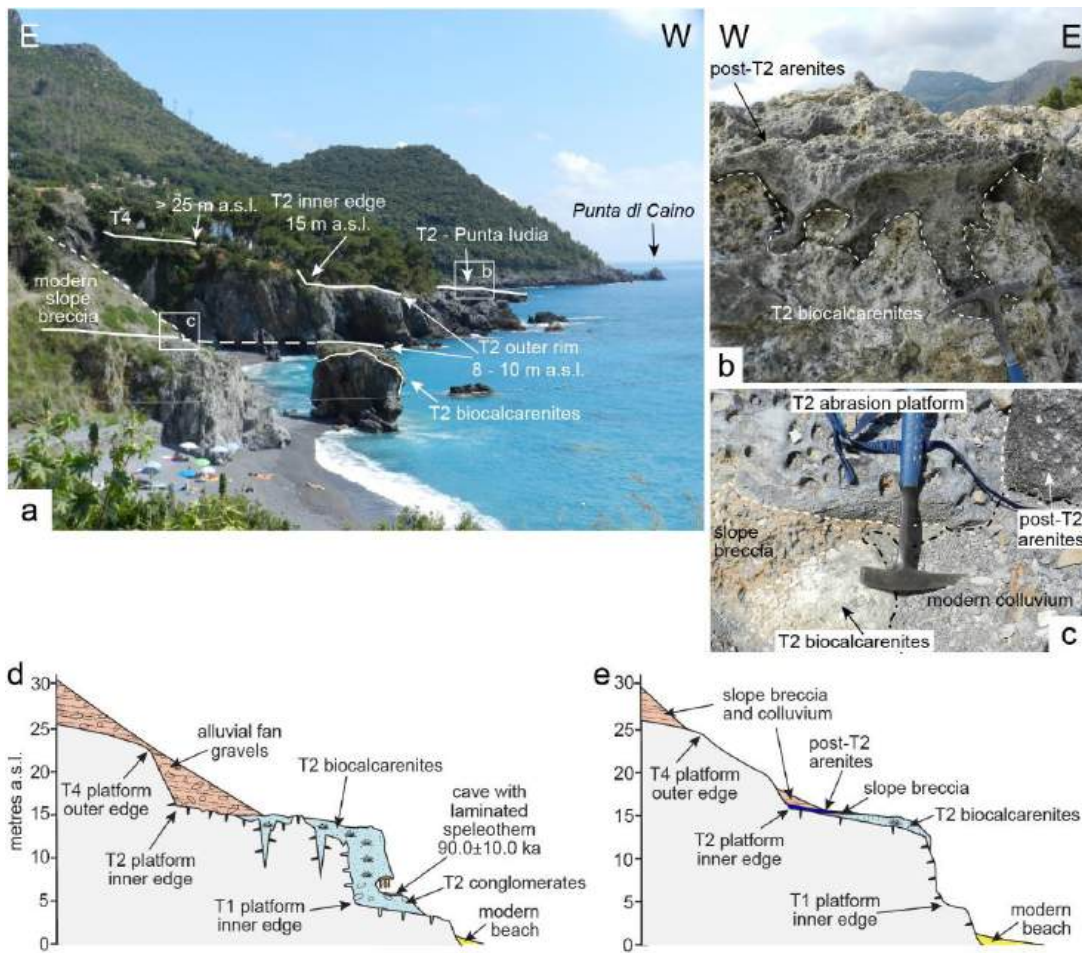


**Figure 51.** a: Panoramic view of paleoshoreline T2 in the southern side of the Marina di Maratea bay and Punta Iudia (in the background), with indication of locations of photos in diagrams b and c. Note, in the photo centre-left, the outer rim of an abrasion platform, the inner part of which is buried below a continental cover. b: The T2 coral-bearing biocalcarenes erosively covered by marine arenites, outcropping in the Punta Iudia site. c: Outcrop of the inner part of marine terrace T2 in the southern part of the Marina di Maratea bay, showing the abrasion platform boreholed by *L. lithophaga* holes and partly covered by the T2 biocalcarenes, bearing fragments of *C. caespitosa*, which are mantled by slope breccia; both the biocalcarenite and breccia deposits are erosively covered by coarse-grained arenites, which mark a post-T2 relative sea level fluctuation. d and e: Morphostratigraphic sketches of the marine and continental landforms/deposits outcropping in the northern (diagram d) and southern (diagram e) sides of the Marina di Maratea bay, with indication of location of one of the dated speleothems (sample MMR2).

Similar to Marina di Maratea area, in the northern Punta Matrella Cape - Santojanni bay area well developed marine terraces are suspended above the modern sea cliffs at c. 8 ÷ 9 m a.s.l. (outer rim of the abrasion surfaces) from which they gently rise landward. In the northern border of the Santojanni bay, behind the modern beach, the abrasion platform is marked by patches of biocalcarenes and a

coarse-grained conglomerate, including clasts potholed by lithophaga. In the Punta Matrella headland, the abrasion surface cut in the carbonate bedrock is potholed by *L. lithophaga* and patched by conglomerates and biocalcarenites rich in bivalve shells and balanides. The abrasion platform rises up to 15 m a.s.l., where the inner edge is locally apparent. Where not exposed, the innermost parts of marine terrace T2 are covered by subaerial deposits generally composed of alluvial fan sediments and, in some instances, slope breccia deposits. As for Marina di Maratea site, both alluvial fan and slope breccia deposits are composed of crudely stratified unconsolidated beds made up of pebble- to cobble-sized clasts set in a reddish matrix. Outcrops of this coastal stretch reveal that the T2 marine terrace has been reworked by further coastal processes after its formation. This reworking is inferred from the presence of arenites and fine-grained conglomerates which rest erosively on the T2 deposit. Specifically, they patch an irregular morphology and fill crevices and potholes sculpted on the T2 deposit (**Figure 51b**). Locally (on the c. 15 m a.s.l. abrasion platform in the inner boundary of the Marina di Maratea bay; **Figure 51c**), thin remnants of continental conglomerates with reddish matrix are interposed between the arenites and the underlying, eroded T2 bioconstructions (**Figure 51e**).

In the Marina di Maratea - Punta Iudia coast, the T2 deposits and carbonate bedrock are affected by metre-size horizontal caves and conduits (**Figure 51d**). Such caves, occasionally filled with continental breccia, are floored by laminated speleothems and coated by flowstones. Some of these calcite concretions have been sampled for U-series dating. Particularly, we sampled the laminated speleothems that floor two caves located in the Marina di Maratea bay (samples MMR2 and MMR12, respectively; Supplementary Figure S1) and a cave formed in the T2 calcarenite in the Punta Iudia site (sample PDA2).

#### 6.3.4.3 The T2 paleoshoreline in the Scalea site

The T2 marine terrace is the lowest in a flight of three terraces that shape the headlands of the Scalea coast (location in **Figure 47 b**, **Figure 48b**). The two upper marine terraces are located at ~ 40 m and 60 m a.s.l., respectively (**Figure 52 a**). They consist of wide erosion surfaces cut in the carbonate bedrock and locally covered by patches of marine sands and pebbles and buried by alluvial/colluvial deposits.

A remnant of the T2 marine terrace is located in the sea cliffs just to the north of the Scalea village (**Figure 52 a**). This marine terrace consists of an abrasion platform, slightly sea-dipping, marked by *L. lithophaga* holes and covered by patches of coarse-grained sandstones to fine-pebble-grade gravels and bioconstructions, which consist of encrusting algae, bryozoans, gastropods and colonies and fragments of *C. caespitosa* occasionally developing decimeter-size globular growth forms (**Figure 52b**). The biocalcarenes are potholed by *L. lithophaga* holes filled by yellowish and reddish fine-grained sediments, which represent the distal and basal part of several metre-thick slope deposits, which extensively crop out in the sea cliff at the inner border of the bay. The slope deposits consist of stratified, up to 20° inclined, clast-supported conglomerates made up of angular to subangular, pebble- to boulder-sized clasts. The matrix is composed of reddish and yellowish fine-grained sediments, and is locally abundant to form occasionally matrix-supported beds (**Figure 52e**). The biocalcarenes are also affected by potholes (**Figure 52c**) and crevices coated by calcite concretions and covered by slope and colluvial deposits (**Figure 52c**). The biocalcarenes are also affected by potholes (**Figure 52c**) and crevices coated by calcite concretions and covered by slope and colluvial deposits (**Figure 52e**), which collectively indicate subaerial conditions postdating the formation of T2. Both a *C. caespitosa* colony

and a calcite concretion overlying one of the coral bioconstructions have been sampled for U-series dating (samples SLC and SLC05, respectively).

The T2 abrasion platform in the Scalea site cuts the limestone bedrock at elevations  $> 12$  m (outer edge). The T2 inner edge is hidden by the above mentioned slope deposits. However, by GPS measurements integrated with detail-scale topographic data, for the T2 platform inner edge we estimated an elevation in the range of  $+ 16 \pm 1$  m. Overall, The high similarity of paleoshorelines T2 in the Scalea and Marina di Maratea - Punta Iudia sites, suggests that the *L. lithophaga* boreholes affecting the T2 biocalcarenes in the Scalea site (**Figure 52d**) represent an indication of a further marine reshaping of the Scalea marine terrace.



**Figure 52.** View of Scalea Site, with the flight of three distinct marine terraces located at + 60 m (T5), + 35 ÷ 40 m (T4) and + 16 m (T2), respectively. Photos in b to e show close-up views of marine terrace T2. b: Biocalcarenite bearing *C. caespitosa* growth form, sampled for U-series dating (sample SLC). c: Pit holes coated by calcite concretions, indicative of subaerial erosion affecting the biocalcarenites; the pit holes are covered by colluvial deposits. d: The eroded abrasion surface of the T2, with remnants of patches of biocalcarenites (light grey), potholed by *L. lithophaga* holes. e: Biocalcarenites patched onto the carbonate bedrock, affected by post-depositional subaerial erosion, which is testified by metre-size crevices coated by calcite concretions (sample SLC05) and filled by slope breccia with reddish matrix.

#### 6.3.4.4 Marine terraces and sea level markers at around 20 m a.s.l.: the T3 paleoshoreline

At several sites along the coastal stretch between the Castrocucco and Scalea headlands, there is evidence for raised sea level markers at c. 20 m of elevation, which we collectively label T3 paleoshoreline. The best exposures of those markers crop out in the Grotta del Prete site (location in **Figure 47 b**; **Figure 48**; **Figure 48d**) where an apparent abrasion platform cuts the limestone bedrock **Figure 53**).



**Figure 53.** a: Panoramic view of the T3 marine terrace in the Grotta del Prete site (location in **Figure 47**), with indication of the abrasion platform located in the 15 ÷ 22 m elevation range, covered by marine and colluvial deposits; in the background, the wide flat surface of marine terrace T4 in the Torre Fiuzzi site is visible. b: Close up view of the sampled *C. caespitosa* colony (sample GRP2), included in the biocalcarenites of the Grotta del Prete marine succession. c: The marine deposits of the Grotta del Prete marine terrace, made up of conglomerates passing upwards to biocalcarenites bearing *C. caespitosa*; this succession is overlain by an arenite body, marked on top by a reddish paleosoil, which is covered by colluvium.

The inferred elevation of the platform inner edge is c. 22 m a.s.l., with an uncertainty of  $\pm 1$ , because of a colluvial cover. The abrasion platform is mantled by an up to 20 cm thick conglomerate composed of pebble- to boulder-size clasts. The matrix is locally abundant and consists of coarse- to very coarse-grained sandstone. An overlying bioconstruction consists of encrusting algae, bryozoans, gastropod and bivalve shells, and colonial corals (*Cladocora caespitosa*). A *C. caespitosa* specimen has been sampled for Th/U analyses (samples GRP1 and GRP2; **Figure 53b**). The bioconstructed body is blanketed by coarse-grained sandstones to granule-grade deposits showing horizontally to low-angle lamination; at the top beds are bundled into weakly discordant sets (**Figure 53c**). It is noteworthy that sandstones are common as infill of bioconstruction crevices and potholes as well as mantle the basal gravel lag. Evidence of pedogenesis at the top of these sediments indicates a subaerial exposure (Scarciglia et al., 2006).

Evidence of the T3 paleoshoreline is widespread in the sea cliffs behind the Praia coastal plain and to the south of the Grotta del Prete site. At Ginnasio Site (location in **Figure 47b**; **Figure 48**), the T3 paleoshoreline consists of an evident abrasion platform cut on calcareous-dolomitic bedrock with a well-exposed inner edge at 25 m. The abrasion platform is potholed by densely distributed *L. lithophaga* holes well apparent also along some crevices, which preserve decimeter-size globular growth forms of *C. caespitosa* as well as bioconstruction composed of gasterops and encrusting algae. To the north, at the Pantano site (location in **Figure 47 b**) a bioconstruction consisting of encrusting algae, gastropods, bivalves and coral fragments is evident up to 20 m a.s.l. The above quoted crevices with biocalcarene bearing *C. caespitosa* are filled with massive subrounded, pebble- to cobble-sized gravels interpreted as deposited at the base of the paleo sea-cliffs, as also suggested by the presence of occasional clasts of beach conglomerates sourced by the outer edge retreat of the higher terrace. Similarly, massive and ungraded conglomerates made up of subrounded, pebble- to boulder-

sized clasts mantle the cliff behind the modern beach of San Nicola Arcella, along the path to Arcomagno, at about 20 m a.s.l.; clasts are locally potholed by densely distributed *L. lithophaga* holes.

To the south, another evidence of the T3 paleoshoreline is the apparent abrasion platform, lacking in marine deposits, which can be noticed at the top of an isolated rock within the modern beach of San Nicola Arcella (19 m a.s.l.). The foregoing T3 terrace may be correlated southward to Torre San Nicola (inner edge at about 20 m) terrace. Evidence of the T3 paleoshoreline occurs also in the Castrocuco headland, which bounds the Noce River alluvial plain to the north. Both in the inland and coastal parts of the Castrocuco headland, there is evidence of relative sea level stands, with the highest being the c. 130 m a.s.l. marine terrace located at the inner rim of the Noce River plain (Filocamo, 2009). In the southwestern part of the Castrocuco headland, a marine terrace carved on carbonate bedrock in the west and on well-cemented slope deposits in the east, crops out in the elevation range between c. 15 m (outer rim) and 20 m a.s.l. (inner edge). The sedimentary cover consists of a basal conglomerate composed of pebble- to fine cobble-size clasts passing upward to alternating coarse-grained sandstones fine pebble-grade gravels showing horizontally stratification. Regular and parallel stratification along with good clast-size sorting are interpreted as the result of swash and backwash processes in the upper beachface. Beach deposits also patch laterally the paleo-sea cliff and are covered, to the east, by slope breccia deposits. To the south, at c. 20 m close to the Praia - Tortora exit of the SS 18 road, beach deposits rest erosively on calcareous bedrock. The foregoing marine terraces elevation is comparable to that of a dense distribution of *L. lithophaga* holes up to c. + 20 m (**Figure 54a**) along the sea cliff located to the west along the Castrocuco headland, behind the northernmost part of the modern beach. Furthermore, along the active sea cliff at the headland termination, the field surveys have shown the occurrence, at c. 15 ÷ 20 m a.s.l., of neptunian dykes of fossiliferous calcarenites

filling open fissures (**Figure 54b**) coated by 2 - 3 cm thick laminated calcite concretions. One of these concretions (sample CSC8, **Figure 54d**) is potholed by densely distributed *L. lithophaga* boreholes filled with calcarenites (**Figure 54b-d**). In the uppermost part of the Castrocucco sea cliff, remnant of a tidal notch in the 35 ÷ 40 m elevation range is recognised and correlated with T4 terrace.

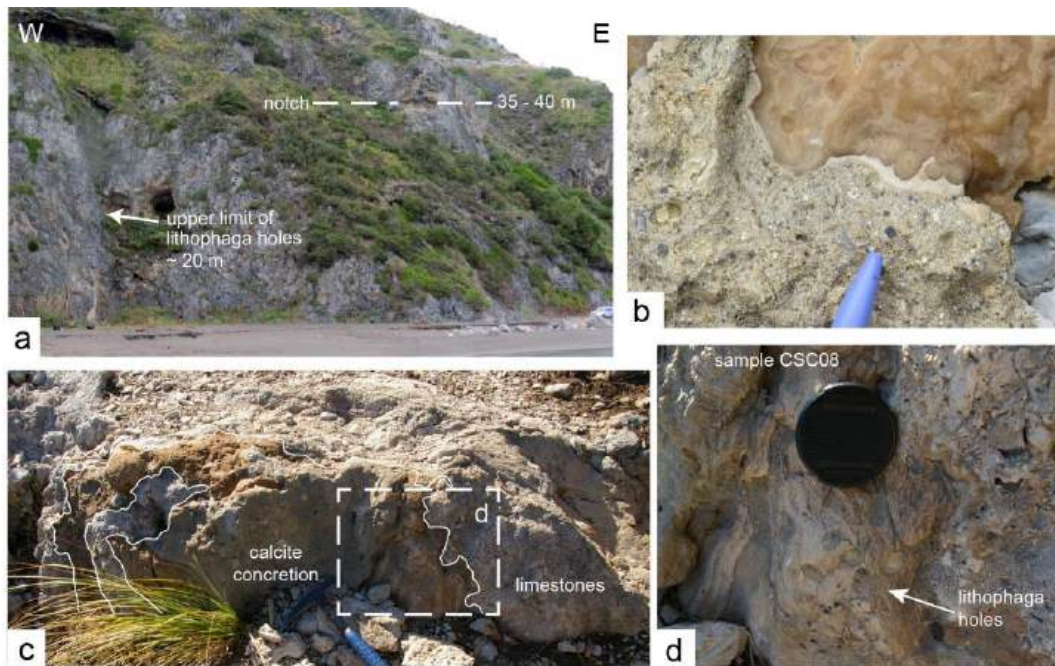


**Figure 54.** a: The sea cliff behind the Castrocucco beach, with the remnants of the tidal notch located at c. 35 ÷ 40 m a.s.l. and indication of the upper limit of *L. lithophaga* holes. Diagrams b to d show outcrops located c. 20 m a.s.l. at the southeastern edge of the Castrocucco headland. b: Detailed view of a neptunian dyke filled with carbonate concretions onto which biocalcarenes are patched. c and d: Outcrop-scale and close-up views of the calcite concretion inset in the carbonate bedrock; both the bedrock and the calcite concretion (sample CSC08) are potholed by densely distributed *L. lithophaga* holes and patched by marine arenites, which fill also the *L. lithophaga* holes.

#### 6.3.4.5 The T4 paleoshoreline

The best exposure of T4 paleoshoreline occurs in the Torre Fiuzzi area, where a wave-cut platform on dolomitic bedrock has its outer edge at ~ 18 m while the inner edge has been detected and measured at 35 m a.s.l. (**Figure 55**; **Figure 48c**). The wave-cut platform, slightly seaward-dipping, is mantled by a few metres thick biocalcarenite bearing *Cladocora caespitosa* colonies, which has been sampled for Th/U analyses (samples TFZ1 and TFZ2).



**Figure 55.** View of Torre Fiuzzi Site with relative T4 marine terrace at 35 m a.s.l.

An abrasion platform at elevation comparable to that of Torre Fiuzzi (i.e., 30 ÷ 35 m) cut on dolomitic bedrock occurs in the Torre Dino site. The platform inner edge is marked by *L. lithophaga* holes and the platform is covered by patches of pebble- to cobble-sized gravels. Interspersed within the pebbles/cobbles, there are patches of calcite concretions, sampled for stable isotope and U-series analysis (sample TRR1).

Raised sea level indicators at ~ 40 m of elevation occur along the Castrocucco headland. They consist of the remnants of a tidal notch (**Figure 54a**) that, to the east, can be correlated to an abrasion platform (35 ÷ 40 m elevation range) covered by dm-thick fine- to coarse-grained, rounded pebbles. To the south, at the inner margin of Tortora coastal plain (**Figure 48**), a related abrasion platform

cut on dolomitic bedrock extends for about 2 km and is locally patched by dm-thick, well-cemented, rounded gravels; its outer edge ranges from + 20 to 30 m, but its inner edge is covered by tens of metres thick alluvial fan deposits forming a planar depositional slope; it is composed of clast supported, sheet conglomerates made up of alternating beds of angular, pebble to fine cobble grade clasts and pebbly sandstone. Stratification is plane parallel but internal truncation surfaces may be observed as well as yellowish and reddish intervening paleosols.

#### 6.3.4.6 The T5 paleoshoreline

Evidence of the T5 paleoshoreline is widespread along the inner margin of the Praia coastal plain. Here, a large karst cave (Madonna della Grotta site; location in **Figure 47b**; **Figure 48**) is located from c. 50 to 65 m a.s.l. in the abandoned sea cliff that bounds the modern coastal plain of Praja village. A marine reshaping of the Madonna della Grotta (MdG) cave during a sea-level stand is testified by the occurrence of poorly sorted, fine pebble- to sandy matrix-supported conglomerate of pebble to boulder grade which mantle the southern edge of the cave (**Figure 56**). The conglomerates are interpreted as the result of progressive accumulation of cliff-collapsed material that outrops from c. 50 to 58 m a.s.l. Gravel sediments and carbonate bedrock are affected by *L. lithophaga* holes. Using the upper limits of the *L. lithophaga* holes and conglomerates as sea level indicators, paleoshoreline T5 is constrained in the 55 ÷ 60 m elevation range. Both the lithophaga holes and conglomerates are mantled by a several cm-thick flowstone (**Figure 56**). The basal part of this flowstone has been sampled for U-series analysis (sample MDN01) in order to constrain the upper age limit of paleoshoreline T5.

The MdG paleoshoreline can be correlated with several abrasion platforms outcropping both to the north of that site, in the sites of Torre Nave and Castiglione headlands and Rosaneto (**Figure 47b** and **Figure 48**) where *L. lithophaga* holes are

locally well apparent. To the south, the best exposure of paleoshoreline T5 may be noted along the Ginnasio headland, higher than paleoshoreline T3 at the Ginnasio site (Section **6.3.4.4** Marine terraces and sea level markers at around 20 m a.s.l.: the T3 paleoshoreline; **Figure 48**); here a marine terrace cutting the dolomitic bedrock crops out at ~ 65 m a.s.l. is blanketed by a 2 m thick gravel beach deposit characterized by thin and regular stratification with gently dipping ( $\sim 3^\circ$ ) seawards. The marine sediments are covered by alluvial fan deposits of which the fan landform is still recognizable. Fan sediments consist of west-inclined, well-stratified, clast-supported conglomerates composed of alternating beds of angular pebble to fine cobble grade and pebbly sandstone. The beds tend to be stacked upon one another, forming bedsets that tend to pinch-out both laterally and downward, occasionally characterised by concave-up erosional surfaces. It is worth noting that the alluvial fan deposits rest unconformably also on paleoshoreline T3 at Ginnasio site.

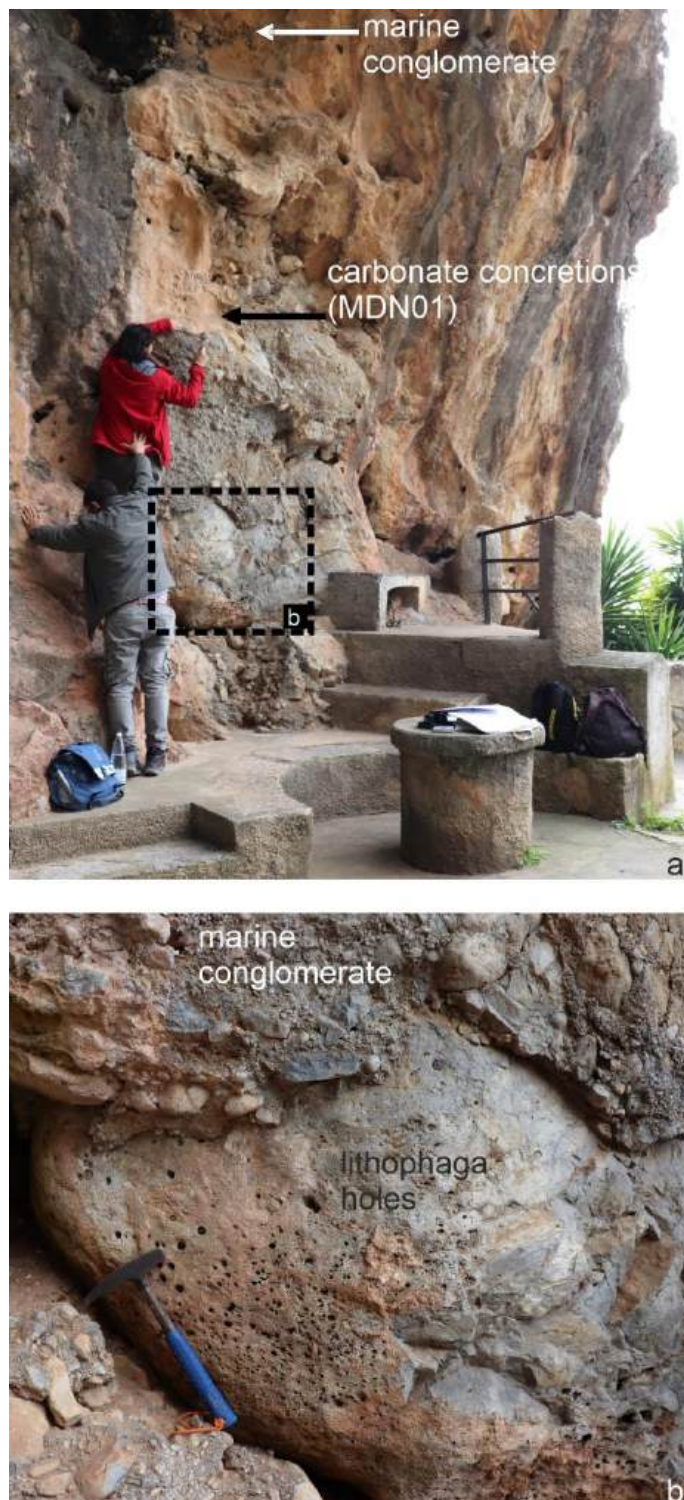


**Figure 56.** a: View of the southern wall of the Madonna della Grotta cave, with evidence of the 55 ÷ 60 m a.s.l. paleoshoreline coated by a flowstone (sample MDN01); arrow indicates the top of the marine conglomerates. b: Close-up view of the marine conglomerates patched onto the carbonate bedrock, which is burrowed by *L. lithophaga* holes.

### 6.3.5 Mineralogical analyses, U-series dating and stable isotope results

X-ray diffractometry analysis has allowed selection of corals sampled for U-series dating. Based on XRD results some of the samples with relatively high calcite content (20-30%) were discarded, while the aragonitic nature of corals sampled in Scalea, Grotta del Prete, Torre Fiuzzi and Fiumicello sites, with moderate calcite amount that is always below 3%, has been assessed (**Table 6.3.1**). The acceptability of the analysis result (**Supplementary Table T1**) was judged by the weighted reliability factor ( $R_{wp}$ ), the profile agreement factor ( $R_p$ ) and a goodness of fit indicator ( $\chi^2$ ). In fact, on fifteen different coral samples, only four of them have been suitable for geochronological analysis, whereas all the others show a significant opening of the chemical system (**Table 6.3.1**).

sample ID	sample type	Aragonite %	Calcite %	Dolomite %	Quartz %	Gypsum %
FMCO1	Coral	97.5	2.4	0.1		
FMCO8w	Coral	77.8	22.2			
FMCO8s	Coral	75.9	24.1			
GRP1	Coral	78.8	17.4	2.8	1.0	
GRP2	Coral	96.9	3.1			
MMR10w	Coral	68.8	29.1			2.1
MMR10s	Coral	62.5	35.7			1.8
MMR11s	Coral	74.1	25.4		0.5	
MMRR11w	Coral	87.3	12.2		0.5	
OLG3	Coral	1.2	98.8			
PDR	Coral	59.0	32.5	8.5		
SLC	Coral	97.6	1.9	0.5		
TFZ1	Coral	59.5	38.0	0.8	1.7	
TFZ2	Coral	92.6	6.7		0.7	
TFZ2W	Coral	98.0	0.8			1.2
TRR1	Speleothem		100.0			

**Table 6.3.1** Results of XRD quantitative analyses of sampled corals (wt. %)

U-series analyses, both on calcite concretions and corals, have shown that  $^{230}\text{Th}/^{232}\text{Th}$  activity ratios are always higher than 80, indicating that samples do not contain a significant detrital fraction. Furthermore, the uranium content of corals, about 2-3 ppm, approaches the average value of uranium abundance in living corals and the initial  $^{234}\text{U}/^{238}\text{U}$  activity ratio ( $^{234}\text{U}/^{238}\text{U}_i$ ) of marine carbonates generally approaches that of the marine water. These data are an evidence of the general good quality of obtained ages. The results of the U-series analyses are summarised in **Table 6.3.2**.

Sample ID	Locality	Lat	Long	Sample type	$^{234}\text{U}$ [mg/g]	1 $\sigma$	$^{234}\text{U}/^{238}\text{U}$	1 $\sigma$	$^{234}\text{Th}/^{238}\text{U}_{\text{meas}}$	1 $\sigma$	$^{230}\text{Th}/^{232}\text{Th}$	1 $\sigma$	$^{230}\text{Th}/^{232}\text{U}_{\text{meas}}$	1 $\sigma$	Age (ka)	1 $\sigma$	$^{234}\text{U}/^{238}\text{U}_{\text{meas}}$	1 $\sigma$
GRP2	Grotta del Prete	39.859910°	15.791797°	coral	2.468	± 0.062	1.150	± 0.025	0.544	± 0.016	131.844	± 12.509	-	-	83.8	± 3.6	1.190	± 0.032
SLC	Scalea	39.819173°	15.783385°	coral	2.066	± 0.041	1.254	± 0.024	0.608	± 0.016	146.208	± 14.051	-	-	98.0	± 4.0	1.335	± 0.032
FMCD1	Fiumicello	39.998549°	15.698754°	coral	1.806	± 0.045	1.095	± 0.021	0.785	± 0.040	124.200	± 13.136	-	-	161	± 18	1.150	± 0.033
TFZZW	Torre Fiuzzi	39.871695°	15.786390°	coral	2.287	± 0.046	1.052	± 0.018	0.673	± 0.021	87.949	± 12.641	-	-	120	± 7	1.073	± 0.025
POA2	Punta Iudia	39.954596°	15.735311°	speleothem	1.038	± 0.034	1.193	± 0.013	0.476	± 0.022	8.096	± 0.301	-	-	64	± 6	1.231	± 0.016
OGL2	Ogliastro	39.999880°	15.690515°	speleothem	0.215	± 0.005	1.009	± 0.019	0.510	± 0.015	109.354	± 14.221	-	-	78	± 3	1.011	± 0.024
MMR12	Marina di Maratea	39.959416°	15.734494°	speleothem	0.485	± 0.016	1.058	± 0.021	0.525	± 0.019	3.324	± 0.059	0.461	± 0.029	67	± 6	1.070	± 0.025
FMCD7	Fiumicello	39.998538°	15.698920°	speleothem	0.598	± 0.012	1.046	± 0.011	0.532	± 0.020	60.019	± 7.583	0.528	± 0.071	81	± 5	1.082	± 0.014
MND01	Grotta della Madonna	39.896664°	15.784890°	speleothem	1.067	± 0.047	0.979	± 0.018	0.814	± 0.031	1.955	± 0.061	0.749	± 0.058	152	33 / -26	0.968	± 0.028
SLC05	Scalea	39.819138°	15.783407°	speleothem	0.539	± 0.017	1.075	± 0.018	0.634	± 0.028	6.283	± 0.245	0.602	± 0.046	99	± 12	1.099	± 0.024
PNT3	Pantano	39.897712°	15.784326°	speleothem	1.333	± 0.037	1.009	± 0.011	0.395	± 0.015	113.780	± 12.502	-	-	54.8	± 2.7	1.011	± 0.013
CSC8	Castrouccio	39.932927°	15.746692°	speleothem	0.345	± 0.006	1.018	± 0.013	0.765	± 0.022	12.745	± 0.507	0.753	± 0.026	151.0	± 11	1.028	± 0.020
MMR2	Marina di Maratea	39.958403°	15.734543°	speleothem	0.385	± 0.012	1.079	± 0.023	0.584	± 0.022	13.800	± 0.609	0.568	± 0.041	90.0	± 10	1.102	± 0.030
TRR1	Torre Dino	39.839211°	15.769875°	speleothem	10.363	± 0.452	0.980	± 0.007	0.513	± 0.034	2.288.467	± 321.587	-	-	78.8	± 7.7	0.975	± 0.008

**Table 6.3.2** Uranium contents (mg/g), activity ratios, and  $^{230}\text{Th}/^{234}\text{U}$  ages of the analysed corals and calcite concretions (1  $\sigma$ ). The analysed corals are *Cladocora caespitosa* specimens with a calcite content <3 %. A better view of this table is reported in the appendix.

Stable isotope analyses of the calcite concretions sampled at the sites of Ogliastro, Fiumicello and Torre Dino were carried out. Both calcite standards used at the Ruhr-Universität Bochum (**Supplementary Table T2**) were run for the calcite sequence on a ThermoFisher Scientific MAT253 equipped with a GasBench II and a ConFlo IV. The results (**Supplementary Table T3** and **Supplementari S2**) show that both  $\delta^{13}\text{C}$  and  $\delta^{18}\text{O}$  are negative values, which indicate that all of the analysed calcite samples have been deposited by freshwater solutions.

### 6.3.6 Discussion

In the flight of marine terraces located from a few metres up to ~160 m a.s.l., which are well exposed all along the Tyrrhenian coast of Basilicata-Nord Calabria, we have focused our study on those outcropping in the 5 to 55 ÷ 60 m elevation range. The analysed marine terraces consist of paleoshorelines characterised by distinct erosional and/or depositional sea-level markers, and paleoshorelines located in the + 5 ÷ 35 m elevation range are characterised by the occurrence of *Cladocora caespitosa* bioconstructions. Based on detail-scale morphostratigraphic reconstructions integrated by dating of corals and calcite concretions either postdating or predating the sea-level markers, we have spatially correlated the paleoshorelines remnants. These have been related to five marine terraces: T1, located 5 +1/-0 m a.s.l.; T2, located at +16 ± 1 m a.s.l.; T3, with inferred inner edge at + 22 ± 1 m; T4, with elevation in the 35 ÷ 40 m range due to the presence of marine/alluvial fan deposits (**Figure 48**), and with a measured inner edge at 35 m a.s.l. (Torre Fiuzzi site); T5, located in the 55 ÷ 60 m elevation range. Locally, as for the Ginnasio staircase, clastic sediment exposures, contact relationships between marine and continental deposits, and their apparent cross-cutting relationships clearly indicate that the investigated coastal stretch suffered alternating morphodynamics, that is the area experienced multiple periods of marine aggradation onto which slope and/or alluvial fan systems prograded. Specifically, there are sites where evidence of drowning of subaerial landforms occurs, e.g. the Madonna della Grotta site (Section **6.3.4.5** The T4 paleoshoreline), as well as reworking by coastal processes of some of the earlier marine terraces during younger relative sea level rises. Examples of such reworking occur in the Marina di Maratea site, where paleoshoreline T2 is covered by continental deposits overlain by marine arenites (Section **6.3.4.2** The T2 marine terrace in the Basilicata coastal stretch), and in the Scalea site, where the T2 biocalcarenite is affected by

*L. lithophaga* holes, which postdate the biocalcarenite cementation (Section **6.3.4.3** The T2 paleoshoreline in the Scalea site). Evidence for reworking in the coastal environment of older marine remnants is found also in the Ogliastro cape site, where the T1 paleoshoreline marked by the T1 biocalcarenite clearly postdates the OG marine conglomerate (Section **6.3.4.1** The lowest paleoshorelines - T1). An old age of the OG relative to the marine terraces T1 to T5 is inferred from the occurrence of N-S trending fractures that dissect the OG, a feature that is not observed in any other of the analysed marine successions. However, the elevation (anyway  $> + 5$  m) of the paleoshoreline correlative to the OG deposit is undetermined. Particularly clear is the reworking of paleoshoreline T1 in the Marina di Maratea site (Section **6.3.4.2** The T2 marine terrace in the Basilicata coastal stretch). It is worth noting that the best exposures of paleoshoreline T1 occur in the sites of Ogliastro - Fiumicello, where the good preservation of the T1 biocalcarenites may be related to the emplacement, during a cold stage/substage occurred soon after the T1 formation, of an UU continental cover, which originally was much more extended seawards than at present. Such interpretation is consistent with evidence that the exposure of the T1 in the Fiumicello and Ogliastro sites results from exhumation of that marine terrace in response to differential sea cliff retreat (possibly even during the Holocene), favoured by the presence of the weak paleosoil interposed between the biocalcarenite and UU deposit (Section **6.3.4.1** The lowest paleoshorelines - T1). Absence of the T1 along most of the investigated coastal stretch may result from reworking and erosion of that marine terrace, where not buried and in general outside the sheltered environments such as Marina di Maratea bay, by sea storms even in present times. In fact, at the terminations of several of the minor headlands, there are small-size, gently inclined and low-lying ( $< 5$  m a.s.l.) capes that could be eroded remnants of the T1.

The new U-series dating allow a reassessment of the marine terrace chronological framework, which both implies a re-evaluation of the late Quaternary

vertical motions of the investigated coastal stretch and allows posing new constraints to the magnitude of recent glacioeustatic sea level fluctuations in the Tyrrhenian Sea, discussed below.

#### 6.3.6.1 Age model

The new U-series dating on *C. caespitosa* corals differ from ages provided in previous works (Carobene et al., 1986, Carobene and Dai Pra 1990, 1991). Corals, dated by U-series method in these old papers, were strongly recrystallised. Calcite contents ranged between 3 and 25 %, showing a significant alteration of samples after their burial. Moreover, uranium contents were inversely correlated with the calcite contents, demonstrating that the process of recrystallization produced a significant loss of uranium, thus opening the chemical system. Since the age is directly correlated with the  $^{230}\text{Th}/^{234}\text{U}$  activity ratio, a loss of uranium made higher the isotope ratios, increasing the age of corals. This inference is strongly supported by the high correlation coefficient ( $r^2 = 0.99$ ) of uranium abundances of five corals versus their correspondent calcite percentage (**Supplementary Figure S3**).

In addition, corals from the shoreline deposits located at higher elevation are characterised by higher calcite contents and lower uranium abundances, indicating that the older the relative age of corals the stronger the alteration and the consequent induced increase of the age (Supplementary Figure S4). This rationale, supported by a correlation coefficient of 0.99 for 4 samples, suggests that the recrystallization process was constant and continuous over time. Finally, the lack of correlation between the  $^{234}\text{U}/^{238}\text{U}$  activity ratios and the elevation of marine deposits suggests that the fluids producing the alteration were characterised by different composition and the weathering processes had different intensity and

duration. Based on that, in our opinion the coral ages are not reliable and the reconstructions based on them are to be considered misleading.

The new U/Th data provide a robust chronological framework for the identified paleoshorelines and relative sea level fluctuations in the Basilicata - northern Calabria coastal stretch. As it is shown in **Table 6.3.3**, ages of dated corals and calcite concretions match those of warm stages/substages and cooler periods of the Middle and Late Pleistocene, respectively. All of the dated deposits are younger than the last warm stage of the Middle Pleistocene, i.e. MIS 7, which is framed in the 190 - 235 ka age range (Waelbroeck et al., 2002).

Sample ID	Dated deposit	MIS 3	MIS 4 and MIS 5a – MIS 4 transition		MIS 5					MIS 6	
			5a	5b	5c	5d	5e	6a = 6d	6c		
PNT3	speleothem	54.7±2.7 ka									
PDA2	speleothem		64.0±6.0 ka								
MMR12	speleothem		67.0±6.0 ka								
OGL2	speleothem		78.0±3.0 ka								
TRR1	speleothem		78.8±7.7 ka	↔	78.8±7.7 ka						
FMC07	speleothem		82.0±5.0 ka	↔	82.0±5.0 ka						
GRP2	coral			83.8±3.6 ka							
MMR2	speleothem				90.0±10.0 ka						
SLC05	speleothem				99.0±12.0 ka						
SLC	coral					98.0±4.0 ka					
TFZ2W	coral							120.0±7.0 ka			
CSC8	speleothem									151.0±11.0 ka	
MDN01	speleothem									152.0±33/-26 ka	
FMC01	coral										161.0±18.0 ka

**Table 6.3.3.** Correlation of dated deposits with late Quaternary Marine Isotope Stages

In the identified paleoshorelines, the T2 terrace remnant from the Scalea site is precisely dated based on ages from both a coral and the overlying speleothem. In other instances, e.g. deposits from the Ogliastro and Marina di Maratea - Punta Iudia sites, the sampled corals (samples OLG3, PDR and both septas and walls of samples MMR10 and 11; **Table 6.3.5**) were unsuitable for U-series dating due to a

low aragonite content, or the time lags between the coral and speleothem/s ages are too large to precisely constrain the marine terrace age (e.g., samples from the Fiumicello and Ogliastro sites). The lack of multiple direct age control on single paleoshorelines is, however, effectively integrated by information obtained through the morphostratigraphic investigations, which allow expanding spatially age constraints of the surveyed sites (**Table 6.3.4**).

Paleoshoreline label	elevation (m)	Coral Th/U age (ky)	Calcite concretion Th/U age (ky)	Marine Isotope Stage
T5	55 ± 5		> 152.0 +33/-26	MIS 7
T1	5 +2/-0	161.0 ± 18.0	> 78.0 ± 3.0; > 82.0 ± 5.0	MIS 6e
T4	35 ± 1	120.0 ± 7.0	< 151.0 ± 11.0; >78.8±7.7 > 64.0 ± 6.0; > 67.0 ± 6.0; > 90.0±10.0; < 99.0 ±	MIS 5e
T2	15 ± 1	98.0 ± 4.0	12.0	MIS 5c
T3	22 ± 1	83.8 ± 3.6	> 54.7±2.7; > 67.0 ± 6.0; < 151.0 ± 11.0	MIS 5a

**Table 6.3.4** Age model for the raised paleoshorelines and correlation with Marine Isotope Stages

Overall, the  $151.0 \pm 11.0$  ka age of the CSC8 sample allows correlation of the speleothem outcropping at the southeastern edge of the Castrocucco headland with MIS 6 (**Table 6.3.3**), and testifies to a relative sea level elevation of at least 20 m during the following MIS 5, proved by the *L. lithophaga* holes, which affect that speleothem. Coral ages from the sites of Torre Fiuzzi, Scalea and Grotta del Prete indicate that the flight of marine terraces in the Maratea - Scalea coastal stretch records each of the MIS 5 sea level peaks. In particular, the  $120.0 \pm 7.0$  ka age of the Torre Fiuzzi paleoshoreline (sample TFZ2W; **Table 6.3.2**) points to correlation of T4 with the Last Interglacial, or MIS 5e (**Table 6.3.4**). The duration of MIS 5e, which according to Stirling et al. (1998) and Shackleton et al. (2002) spans in age from ~128 to 116 ka, has been recently reassessed, based on data from paleoshorelines southern Cilento (location in **Figure 48b**), by Bini et al. (2020) who place the MIS 5e peak at 123 ka, with an upper limit at 120 ka. The coral

(sample SLC, aged  $98.0 \pm 4.0$  ka) and speleothem (sample SLC05,  $99.0 \pm 12.0$  ka; **Table 6.3.2**) from the Scalea site constrain paleoshoreline T2 to MIS 5c, framed between 106 and 93 ka (Lisiecki and Raymo, 2005; Spratt and Lisiecki, 2016) and further indicate a correlation of the speleothem with the cold MIS 5b (**Tables 6.3.3** and **6.3.4**). Our correlation of paleoshoreline T2 with MIS 5c contrasts with its former attribution to MIS 5e based on isoleucine epimerization ratios (aminozone E; Carobene and Dai Pra, 1991) of the T2 biocalcarenes outcropping in the Marina di Maratea site. However, such a discrepancy may be reconciled based on recent findings from the Mediterranean area, which indicate that the high coefficients of variation for epimerization values make the distinction between single substages of the same MIS difficult (Torres et al., 2013). Dating of the coral sample from Grotta del Prete site (GRP2,  $83.8 \pm 3.6$  ka; **Table 6.3.2**) allows a correlation of paleoshoreline T3 with MIS 5a (**Table 6.3.4**), which is framed in the 85 - 80 ka age range by Lisiecki and Raymo (2005) and Spratt and Lisiecki (2016), well fits the 84.2 - 82.3 ka age duration of MIS 5a estimated by Tuccimei et al. (2006) based on data from Mallorca island (Western Mediterranean). Consistent with such a chronological framework are the ages of the speleothems, which postdate paleoshorelines T4, T2 and T3. In fact, the speleothems, which clearly postdate paleoshoreline T2 in the Marina di Maratea - Punta Iudia area, can be correlated with MIS 5b (sample MMR2, aged  $90.0 \pm 10.0$  ka) and the younger MIS 4 (or MIS 5a/MIS 4 transition), based on the  $67.0 \pm 6.0$  ka and  $64.0 \pm 6.0$  ka ages of samples MMR12 and PDA2 (**Tables 6.3.3** and **6.3.4**). Similarly, the attribution of paleoshoreline T3 to MIS 5a is supported by the  $54.7 \pm 2.7$  ka age (sample PNT) of the speleothem, which postdates the *L. lithophaga* holes at c. + 20 m at Pantano site and can be correlated with MIS 3 (**Tables 6.3.3** and **6.3.4**). In addition, the  $78.8 \pm 7.7$  ka age (sample TRR1) of the speleothem that postdates the Torre Dino terrace (and possibly correlated with either MIS 5b or MIS 5a/MIS 4 transition) is consistent with the attribution of paleoshoreline T4 to MIS 5e.

The above age model results in an elevation of MIS 5a paleoshorelines higher than that of the MIS 5c marine terraces. A direct superposition between deposits related to those paleoshorelines is not proven by dating. However, evidence from the Scalea site of *L. lithophaga* holes affecting the T2 biocalcarenes, and from the Marina di Maratea - Punta Iudia sites of subaerial exposure between two superposed marine deposits, are both consistent with a reworking of the MIS 5c marine terrace T2 during a later sea level rise. Worthy to note, the dated MIS 5a bioconstruction of the Grotta del Prete marine terrace is mantled by arenites. Clear evidence of subaerial exposure at the top of the bioconstruction is not found, hence the sand infills of the biocalcarene crevices may result from high frequency eustatic variability over MIS 5a, consistent with depositional evidence of marine terraces from southernmost Calabria (e.g., Dumas et al., 2005).

Age constraints for paleoshoreline T5 are inferred from the Madonna della Grotta site, where the sea-level markers are mantled by a flowstone that can be related to MIS 6 (sample MDN01, aged  $152 \pm 33/-26$  ka; **Tables 6.3.3** and **6.3.4**). Considering the karst environment that hosted the Madonna della Grotta paleoshoreline, it is reasonable that the marine deposits patched on the cave walls were cemented soon after their deposition, fairly correlated with one of the MIS 7 peaks, during the following sea level fall.

The dated *C. caespitosa* (sample FMC01) associated with paleoshoreline T1 outcropping at the Fiumicello site is aged  $161.0 \pm 18.0$  ka, thus framed in the cold MIS 6 time range. The T1 biocalcarene is postdated by two speleothems aged  $78.0 \pm 3.0$  ka (sample OGL2) and  $82.0 \pm 5.0$  ka (sample FMC07), which do not strictly constrain the age of paleoshoreline T1. However, much information on the T1 relative age is available in the Marina di Maratea site, where morphostratigraphic evidence indicates that the + 5 m marine terrace predates deposition of the T2 marine succession. Further information on relative age of

paleoshoreline T1 can be inferred from the chronostratigraphic framework for paleoshorelines T2 to T5 discussed above, which clearly indicates that paleoshorelines correlated with positive paleo-sea level peaks of MIS 5 and 7 are all raised above c. 15 m a.s.l. Hence, correlation of paleoshoreline T1 with MIS 6e, a marked warm period recorded in the 165 - 175 ka time span during the cold stage MIS 6 is reliable (**Table 6.3.4**).

The age model discussed so far allows assessment of relative sea level positions during the late Quaternary for the investigated area. For MIS 5 paleoshorelines, the relative sea level positions have been re-calculated using the methodology in Rovere et al. (2016a; **Table 6.3.5**).

**Table 6.3.5:** Relative Sea Level positions calculated for the MIS 5 paleoshorelines following Rovere et al. (2016a)

MIS Terrace label	Long (°E)	Lat (°N)	Elevation measured (m)	Elevation error (m)	CPD point distance (km)	Indicative meaning				Relative Sea Level	
						Upper Limit	Lower limit	IR	RWL	RSL (m)	RSL error (m)
5e T5	15.789974°	39.871515°	35	1	0,72	1,09	-0,79	1,88	0,15	34,85	1,37
5a T3	15.791856°	39.859922°	22	1	0,58	1,09	-0,79	1,88	0,15	21,85	1,37
5c T2	15.783410°	39.819173°	16	1	0,19	1,09	-0,79	1,88	0,15	15,85	1,37

The relative sea level curve reconstructed for the study area is shown in **Figure 57**. Besides elevations of the dated paleoshorelines, the curve of **Figure 57** relies on ages and vertical positions of dated calcite concretions, which constrain the upper limit to the elevations of coeval relative sea-level. Those constraints are supported by stable isotope results on concretions inset in the marine deposits of paleoshorelines T1 (Fiumicello and Ogliastro sites) and T4 (Torre Dino site; **Supplementary Figure 2**), which rule out a deposition from marine water that could be hypothesised based only on their elevations and ages, with uncertainties on the latter ones partially covering age of MIS 5a (**Table 6.3.3**).

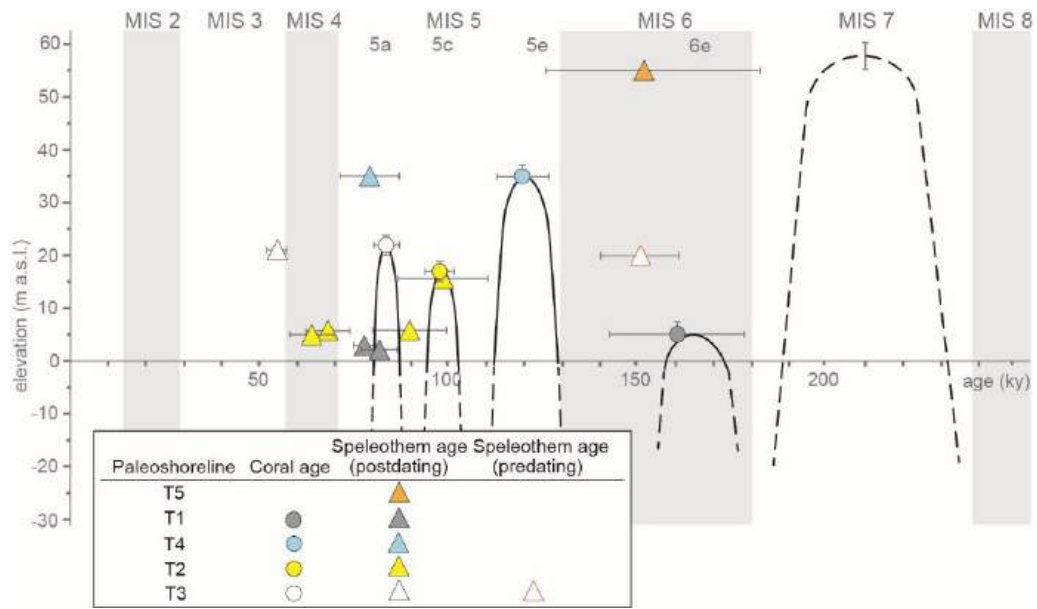


**Figure 57.** Relative sea level curve reconstructed for the investigated Basilicata - northern Calabria sector of the southern Tyrrhenian margin. Dated paleoshorelines are indicated by circles; bars indicate paleoshoreline elevation range and uncertainty, or  $2\sigma$ , of coral age. Triangles indicate dated speleothems, with age error bars; triangle colours are set based on colours of paleoshorelines that are predated, or postdated, by the dated speleothems at the different sites.

### 6.3.6.2 Constraints to the late Quaternary uplift and inferences on the sea level history

The new chronological framework for the analysed flight of raised marine terraces implies a reappraisal of the late Quaternary uplift for the investigated area. Particularly, the reconstructed relative sea level curve represents a robust starting point for the evaluation of recent uplift. Isolating the tectonic component from the curve is not straightforward, if uncertainties on eustatic elevations of late Quaternary sea level peaks are considered. However, among positive sea level peaks that imprinted the investigated coastal stretch, only on MIS 5e there is a general consensus. In fact, although varying worldwide as a result of GIA (e.g., Creveling et al., 2015), it is widely accepted that MIS 5e sea level was higher than the present one (e.g., Siddal et al., 2003; Waelbroeck et al., 2002; Hearty et al., 2007) and set in the 2 ÷ 9 m elevation range (e.g., Hearty et al., 2007; Siddal et al., 2006), with + 6.6 m as the most probable peak (Kopp et al., 2009). Along stable areas of the Mediterranean, RSL indicators of MIS 5e span from 2 m to 8 m a.s.l (Benjamin et al., 2017), being located at + 2 ÷ 3 m in Mallorca, Balearic Islands (Vesica et al., 2000; Bardaji et al., 2009, and reference therein), + 5 ÷ 8 m in the Tyrrhenian coast of peninsular Italy (Antonioli et al., 2006a-c, and references therein; Ferranti and Antonioli, 2007) and up to + 7 m in the eastern Mediterranean (Sivan et al., 2016). Accordingly, a sea level of  $6 \pm 3$  m a.s.l. is considered reliable for the Mediterranean Sea (Lambeck et al., 2004).

Using as a reference MIS 5e, we evaluated a mean uplift rate in the Last Interglacial to Present time span for our study area. The uplift rate was calculated following the classical Lajoie (1986) equation [ $U = (E-e)/A$ ], where the uplift rate (U) is the ratio between the elevation difference between the terrace inner edge (E) and sea level (e), and the age of the sea level peak (A). For the uplift rate calculation, we used the elevation of the MIS 5e relative sea level position as

recalculated based on paleoshoreline T4 (**Table 6.3.5**), which is  $34.85 \pm 1.37$  m a.s.l., and assumed a sea-level elevation of 6 m (Lambeck et al., 2004b; Kopp et al., 2009). Then, considering that in the Mediterranean areas sea level peaks occur at different times according to the varying geographical location (Stocchi et al., 2018), we assumed for the MIS 5e peak the 123 ka age calculated by Bini et al. (2020) for nearby areas. The resulting mean uplift rate since the Last Interglacial is in the range of  $0.235 \pm 0.01$  mm/y.

The uplift rate that we estimated exceeds by one order of magnitude that of c. 0.03 mm/y (e.g., Ferranti et al., 2006, and references therein) previously estimated for the same area based on former geochronological data by Carobene et al. (1986) Carobene and Dai Pra (1990, 1991). Combining our data with those from the Tyrrhenian coastal belt stretching from the fundamentally stable Sorrento peninsula, in the north, to southern Calabria, an overall large-scale increase of uplift since the Last Interglacial may be inferred. In fact, from the north to the south, the uplift varies from null to 0.07 mm/y (Ferranti et al., 2006) to 0.235 mm/y in Basilicata - northern Calabria (this study), to  $0.4 \div 1.35$  mm/y in southern Calabria (Ferranti et al., 2006) where local, faulting-induced contributions are superimposed on the regional-scale vertical motions (e.g., Dumas and Raffy, 2004; Miyauchi et al., 1994; Bordoni and Valensise, 1999; Tortorici et al., 2003; Antonioli et al., 2006b-c; Ferranti et al., 2006). In our instance, no evidence of a fault-related contribution to uplift has been identified. Specifically, the spatial distribution of the identified paleoshorelines does not show any net evidence of displacement both along and across the coast in the entire investigated sector, which extends for about 25 km in length. The rather invariant vertical position of each paleoshoreline (particularly, the MIS5 paleoshorelines, which crop out rather continuously along the coast) is suggestive of a large-scale, deep-seated phenomenon governing uplift, rather than of local, fault-related processes, including faulting in the offshore,

where however some moderate magnitude historical earthquake is recorded (e.g., Rovida et al., 2019).

With the assumption of a constant uplift of  $0.235 \pm 0.01$  mm/y, the fragments of the relative sea level curve of Fig. 11 can be corrected for the tectonic component using paleoshoreline elevations, as it is graphically shown by the correlation scheme of **Figure 58**.

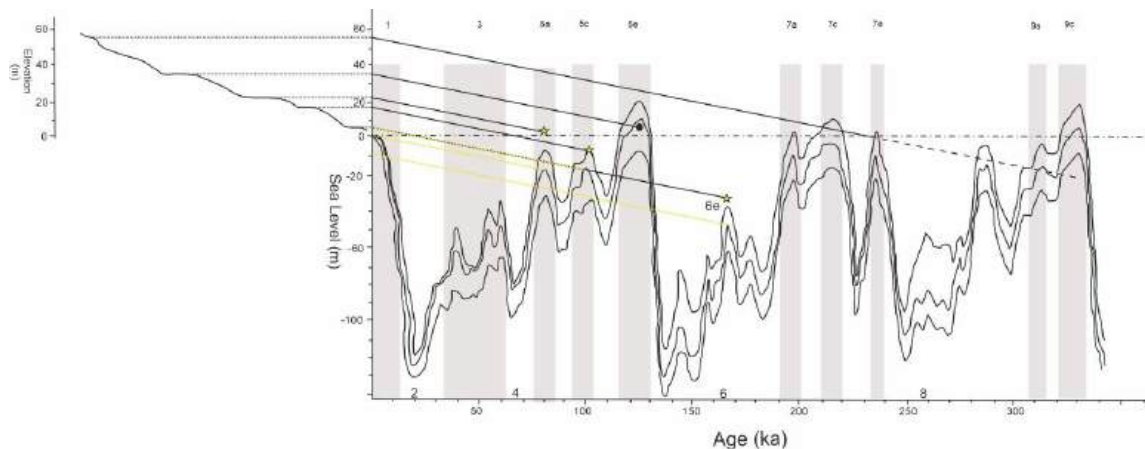


**Figure 58.** Graphical correlation between dated paleoshorelines in the Basilicata - northern Calabria sector of the Tyrrhenian coast and late Quaternary sea-level highstands. The sea level curve used for reference is redrawn after Waelbroeck et al. (2002), with the associated confidence interval. The correlation is based on a constant 0.235 mm/y uplift rate (black lines), assuming a paleo sea level elevation of + 6 m (black dot). The sea level values calculated for MIS 5a, 5c and 6e are marked by the yellow stars. The yellow lines indicate the expected elevations of the MIS 5a, 5c and 6e paleoshorelines, assuming paleo sea level values from the Waelbroeck et al. (2002) global curve.

Based on elevations of the T2 and T3 paleoshorelines, the inferred sea levels for MIS 5a and 5c relative to the present mean sea level (shown for reference in **Figure 58**) are of  $+ 2.26 \pm 1.37$  m and  $-8.6 \pm 1.37$  m, respectively. Global scale estimations of MIS 5a sea level vary between - 30 m a.s.l. in Papua New Guinea (Lambeck and Chappell, 2001) and 3 ÷ 5 m a.s.l. along the eastern coast of the USA (Wehmiller et al., 2004), with a - 20 m a.s.l. mean value based on curves by Lea et al. (2002) and Waelbroeck et al. (2002; **Figure 58**). However, our estimation of sea level of MIS 5a peak agrees with estimates by Neumann and Hearty (1996; Bahamas), Shackleton (2000) and Hearty (2002; Bermuda) and with those of

Bardaji et al. (2009) and Ginés et al. (2012) for the Mallorca island (western Mediterranean). In particular, using data from emergent and submerged Phreatic Overgrowths on Speleothems (POS), Ginés et al. (2012) proposed an eustatic curve for MIS 5 highlighting an elevation between  $\sim +1.5$  m and  $+2.5$  m for MIS 5a peak. Consistently, a MIS 5a level of  $+1.5 \div 2$  m is estimated by geomorphological evidence from stable areas of southern Italy located along both the Tyrrhenian Sea and Ionian Sea coasts, namely the Sorrento peninsula and Salento (locations in Fig. 1a; Riccio et al., 2001; Belluomini et al., 2002; Iannace et al., 2003), where an elevation slightly higher than the modern one is inferred also from MIS 5a beach deposits (Mastronuzzi et al., 2007). In contrast, Bini et al. (2020) have inferred an elevation below the Present sea level for both MIS 5a and MIS 5c by data from southern Cilento. Using information from the Ogliaastro speleothem, a  $\sim 78$  ka (sample OGL2) age limit to MIS 5a peak and an upper limit of c.  $-13 \div 14$  m to the sea level at that age may be inferred. Similarly, by the speleothem from Marina di Maratea aged 90 ka (sample MMR 2) it can be inferred that the sea level during MIS 5b was at least below c.  $-16$  m.

Regarding MIS 5c peak, which based on global scale curves ranges from c.  $-8$  m (Shackleton, 2000) to much below  $-20$  m (e.g., Waelbroeck et al., 2002; Siddall, 2003; Spratt and Lisieki, 2016), less numerous field-based information is available from the Mediterranean area. The low amount of data on MIS 5c somehow supports our evidence on its level less elevated than MIS 5a, and with findings of MIS 5c paleoshorelines essentially in areas affected by fast uplift, e.g. southern Calabria and northern Sicily (Hearty et al., 1986; Balescu et al., 1997; Bianca et al., 2001, Mauz and Hussler, 2000). With reference to the MIS 5c paleoshoreline identified at c.  $5$  m a.s.l. in northern Cilento (Iannace et al., 2001), this attribution was based on dating of a coralline algae sample extracted from a calcilutitic biogenic deposit. Considering the difficulty of separating the biogenic part from the younger cement and the detrital component, it is possible that the

analyzed sample was a mixture between these materials and therefore the age is not reliable.

Assuming the  $0.235 \pm 0.01$  mm/y uplift rate value as constant even earlier than the Last Interglacial, we infer from paleoshoreline T1 a sea level of - 34 m ( $-33.94 \pm 0.165$  m) for MIS 6e (**Figure 57**). As no other field evidence of coeval paleoshorelines in the Mediterranean area is known to date, we cannot cross check our evaluation of MIS 6e peak. However, it is widely acknowledged that the sea level during the relatively warm MIS 6e was located some tens of metres below the Present sea level, and our result appears definitely consistent with some global-scale estimates of MIS 6e peak at c. - 30 m a.s.l. (Siddal et al., 2003, Shackleton, 2000), while contrasts estimations by, e.g., Waelbroeck et al. (2002), Spratt and Lisieki (2016), which collectively pose that peak much below the value that we estimated.

The graphical construction shown in **Figure 58** indicates that the elevation of paleoshoreline T5 matches several peaks of MIS 7 to 9. Our preferred correlation of T5 is with MIS 7 peaks due to both field evidence discussed above and the lack, between the T4 and T5, of other marine terraces, which should occur if the T5 was older than MIS 7. According to most global-scale curves, MIS 7 peaks were located from a few to 10 m below the present mean sea level (e.g., Shackleton, 2000; Waelbroeck et al., 2002; Cutler et al., 2003; Siddal et al., 2003). For T5, a correlation with MIS 7e may be hypothesised by both our graphical construction, which would rule out a correlation with MIS 7a (**Figure 58**), and evidence from submerged speleothems from the Tyrrhenian Sea, which indicates that during MIS 7c the sea level was  $< -18$  m a.s.l. (Dutton et al., 2009a). Thus, assuming constancy in uplift at c. 0.24 mm/y an elevation around the Present sea level may be inferred for MIS 7e. An elevation around the Present one (or below it, if the uplift was faster during the Middle Pleistocene) agrees with findings of MIS 7 paleoshorelines in southern Italy, which are all from tectonically raised areas (e.g., Dumas et al., 1982,

1987; Cinque and Romano, 1990; Cinque et al., 1994; Miyauchi et al., 1994; Tortorici et al., 2003; Amato, 2000; Bianca et al., 2011; Monaco et al., 2017).

The uplift rate that we evaluated, and values inferred for MIS 5a and 5c, MIS 6e and MIS 7 sea level peaks, all rely on an assumed MIS 5e sea level value set based on mean elevation of paleoshorelines of that age from stable areas in the Mediterranean. The assumed value bears an eustatic plus a component due to a water load, which in the central sector of the Mediterranean Sea caused subsidence and related relative sea level rise during the MIS 5e (e.g., Rovere et al., 2016b, Stocchi et al., 2018; Bini et al., 2020). Modeling carried out to date suggests that, along the coast of central Tyrrhenian Sea, the contribution of glacio-hydro-isostatic adjustment is in the range of  $0.75 \div 2$  m for MIS 5e paleoshorelines (Stocchi et al., 2018). Even assuming a 2 m value for GIA, the overestimation of the uplift would be in the order of  $10^{-3}$  mm/y, thus falling in the uncertainty that we associated with our uplift rate estimation and related sea level evaluations.

### 6.3.7 Concluding remarks

The new morphostratigraphical and geochronological data on Basilicata-northern Calabria paleoshorelines indicate that morphology of the investigated coastal stretch has been strongly imprinted by uplift and coeval sea level fluctuations which, in the study area, has driven multiple re-shaping of the coastal belt, by alternating shallow marine and continental processes. Our evaluation of the Basilicata - northern Calabria late Quaternary uplift, of one order greater than previously estimated, points to the need for both a reassessment of the chronostratigraphic framework of the upper part of the marine terrace flight in the study area and, more importantly, in depth investigations of sea level markers located to the south of the study area. Such investigations are meaningful to the definition of the late Quaternary tectonic behaviour of a coastal area struck by several moderate to strong offshore earthquakes in historical times (e.g., Locati et al., 2016; Rovida et al., 2019), although their sources are still undefined.

The detailed morphostratigraphical analysis of the marine terraces, supported by U-series dating, has allowed unravelling the presence, in the study area, of sea level markers related to each of the three eustatic peaks of MIS 5, of MIS 7 and the cooler MIS6. In the Fiumicello and surrounding area, the MIS 6e paleoshorelines have been well preserved from later erosion by burial of slope and/or alluvial fan deposits sourced, during younger MIS 6 substages, by frost action in the steep slopes and river basins hanging above the coast.

Our findings on the vertical distribution of the dated marine terraces in the investigated coastal stretch clearly demonstrates that a mere sequential correlation of paleoshorelines based on assumption that the higher is the older may be strongly misleading in the interpretation of flights of marine terraces. Hence, our results indicate that multiple age controls are crucial to unravelling the complex interaction between uplift and sea level fluctuations in tectonically active coastal areas.

An important implication of the new data provided by this study is represented by the multiple constraints to the history of the sea level fluctuations in the Tyrrhenian Sea. The net evidence of re-shaping of the coast by each of the three peaks of MIS 5 and MIS 6e in a moderately uplifting area, is a clear evidence that the paleo-elevations of the MIS 5a, 5c and 6e sea level peaks were confined in a range, around/below the sea level, less pronounced than that predicted by most of the global-scale sea level curves (e.g., Siddal et al., 2003, Waelbroeck et al., 2002, Spratt and Lisiecki, 2016). Nonetheless, our evaluation of MIS 5a peak is consistent with several findings from the western Mediterranean (e.g., Bardaji et al., 2009; Mastronuzzi et al., 2007; Gines et al., 2012). The reconstructed MIS 5a, 5c and 6e paleoelevations may contribute to a better definition of GIA models for the Mediterranean and constraining ice volume variations during the late Quaternary.

## ***7. Last Interglacial sea-level proxies in the Western Mediterranean***

Manuscript 4- *Last Interglacial sea-level proxies in the Western Mediterranean*, by Cerrone, C. Vacchi, M., Fontana, A., Rovere, A., submitted to *Earth System Science Data*

The data used in this study were compiled in WALIS, a sea-level database interface developed by the ERC Starting Grant “WARMCOASTS” (ERC-StG-802414), in collaboration with PALSEA (PAGES / INQUA) working group. The database structure was designed by A. Rovere, D. Ryan, T. Lorscheid, A. Dutton, P. Chutcharavan, D. Brill, N. Jankowski, D. Mueller, M. Bartz, E. Gowan, and K. Cohen. The data points used in this study were contributed to WALIS by Ciro Cerrone (Southern Italy and Mediterranean), Matteo Vacchi (France, Corsica and Sardinia), Alessandro Fontana (Adriatic Sea), and Alessio Rovere (Spain and Tyrrhenian Northern Italy).

### **7.1 Introduction**

This paper describes the Last Interglacial (here broadly defined as Marine Isotopic Stage 5e, MIS 5e) sea-level database for the Western Mediterranean, that was compiled standardizing data contained in published scientific papers. The database was created using the WALIS interface, available at this link: <https://warmcoasts.eu/world-atlas>. This interface allows standardizing data and metadata on Pleistocene relative sea-level indicators and associated ages. The database described in this study represents the output of a tool embedded within the WALIS interface, that allows exporting all data in spreadsheet format. As a result, the Western Mediterranean database presented in this work is in .xls format, is open access, and available as Cerrone et al, 2021b

(<https://doi.org/10.5281/zenodo.4497365>). Field descriptions are available at the following link: <https://doi.org/10.5281/zenodo.3961544> (Rovere et al., 2020).

The data compiled in this manuscript were extracted from 179 studies (Figure 59a), that were reviewed between March 2020 and January 2021 (Figure 59b). Therefore, data contained in papers that appeared after this timeframe are not included in our database. The majority of the studies we reviewed were published within the last 40 years (Figure 59c).

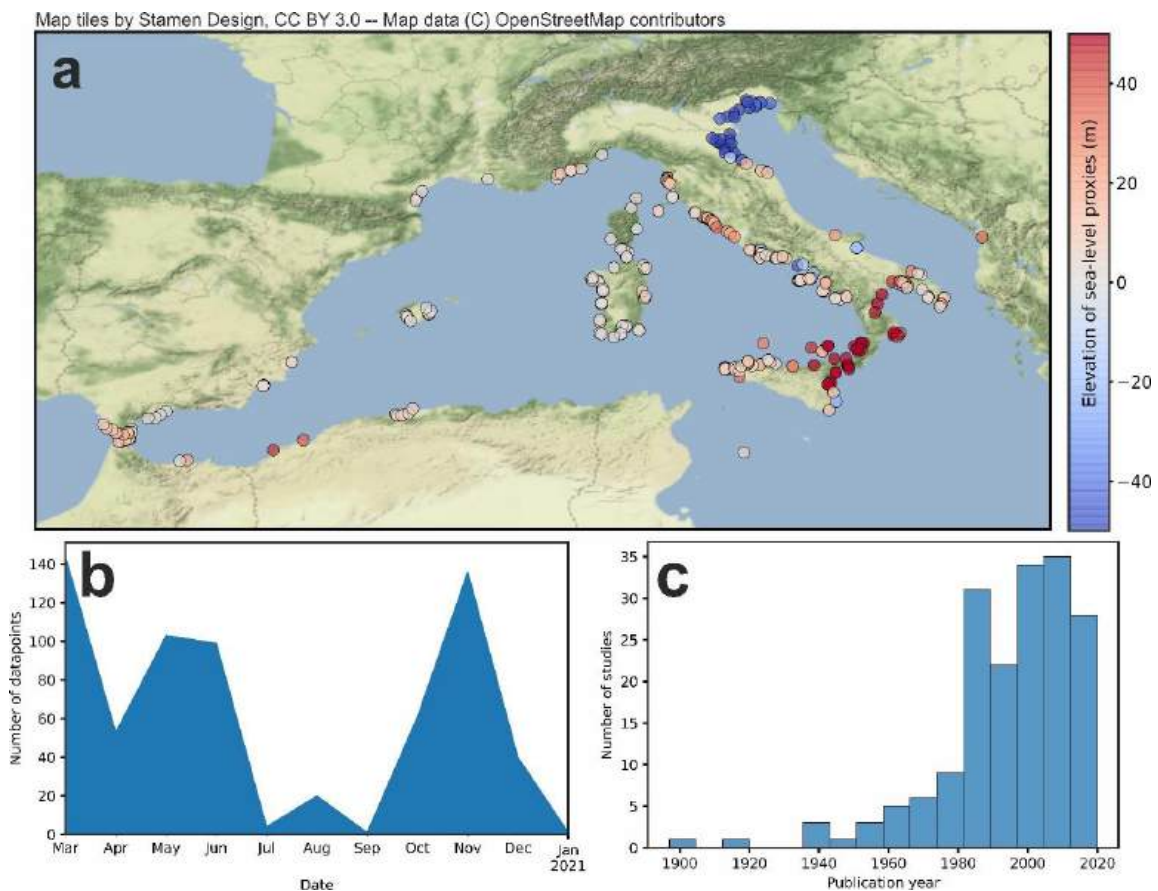


**Figure 59.** Overview of the Western Mediterranean database. a) Elevation of sites within the reviewed geographic area; b) Data ranges of database creation; c) Year of publication of reviewed studies.

In the following sections, we first give an overview of the classic literature describing the Last Interglacial sites in the Western Mediterranean. While many of

these older studies mentioned in this section do not contain all the metadata required by the WALIS interface, they represent the foundations upon which successive studies inserted in our database were developed. Next, we give a brief description of the types of sea-level indicators, elevation measurement techniques, sea level datums, and dating (or age attribution) techniques contained in our database. We then turn to the description of the sea-level datapoints inserted in the database divided by National / Regional / Provincial boundaries. This part of the MS serves as a supplement to the data, where we provide additional descriptions and/or information on choices made during the compilation.

## 7.2 Literature overview

In the Western Mediterranean, the investigation of Quaternary marine and coastal deposits dates back more than one century. At the beginning of the 20<sup>th</sup> century, several geologists worked on both sides of the basin describing outcrops correlated to the “Tyrrhenian” sea-level highstand (Issel, 1908; de Lamothe, 1911; Gignoux, 1913; Blanc, 1936). This “first wave” of authors was followed by a series of geologists who detailed the first stratigraphic descriptions and uncovered new sites (e.g., Butzer and Cuerda, 1962; Ottmann, 1954; Bonifay and Mars, 1959). This “second wave” was helped by the development of dating techniques such as U-Series (Stearns and Thurber, 1965), which helped to strengthen previous chronological correlations, that were heretofore based almost uniquely on (bio)stratigraphy.

These studies laid the foundation upon which, in the 1980s and 1990s, studies on Western Mediterranean Last Interglacial outcrops flourished. Among the many works done in these two decades, it is worth mentioning the work of (Hearty, 1986), who applied Amino Acid Racemization to a vast number of Mediterranean sites. This work appeared on a Special Issue of the journal “Dating Mediterranean shorelines”, edited by Ozer and Vita-Finzi (1986). This volume also contains the first (to our knowledge) Mediterranean-wide synthesis of Last Interglacial data (Flemming and Webb, 1986) and the first application of Electron Spin Resonance dating on Western Mediterranean outcrops (Brückner, 1986).

The renewed interest stirred by the “Dating Mediterranean shorelines” volume reflected in a large number of studies in the late 1990s and 2000s. Our Western Mediterranean database is largely based on these studies (see the detailed regional descriptions below) and on the regional/national data syntheses that were carried out by several authors in the last 20 years (Bordoni and Valensise, 1999; Nisi et al., 2003; Zazo et al., 2003; Ferranti et al., 2006).

### 7.3 Sea-level indicators

Within the Western Mediterranean context, we identified eleven types of sea-level indicators (**Table 7.1**). The most widespread sea-level indicators are marine terraces, beach deposits (or beachrocks), and tidal notches (

**Figure 60**). A large percentage of sites are also characterized by the presence of marine or terrestrial limiting points. Whenever mentioned by the original study, we assigned the upper and lower limits of the indicative meaning using modern analog data. When not possible, we used the IMCalc tool (Lorscheid and Rovere, 2019) to extract ex-situ values for the calculation of reference water level and indicative range (i.e., the relationship between the dated facies and the contemporary mean sea-level, Shennan et al., 2015).

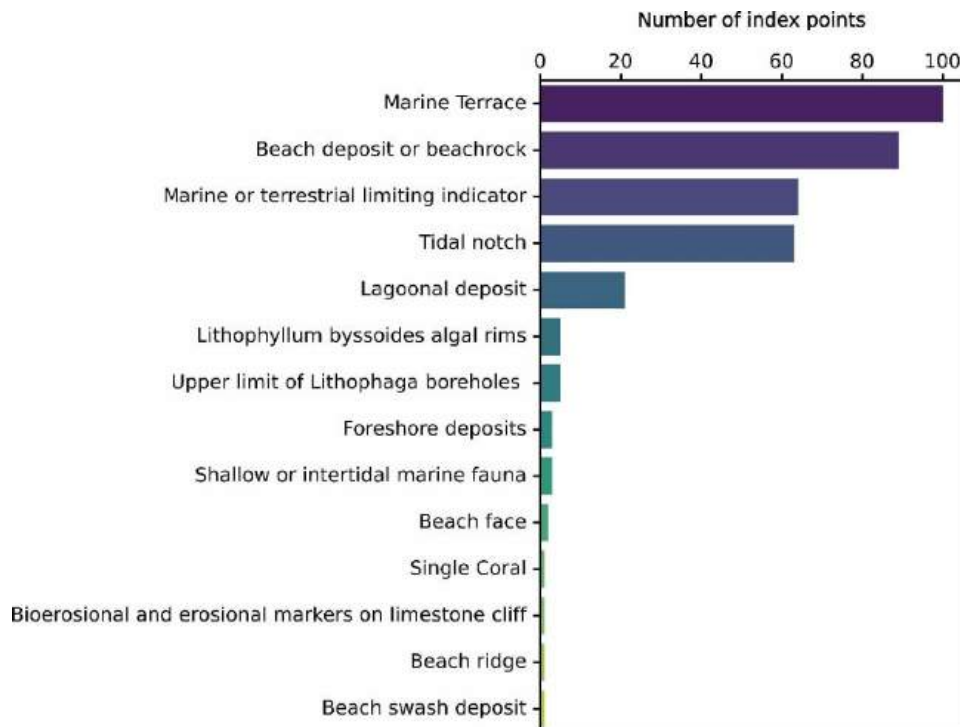


**Figure 60.** Types of sea-level indicators and number of sites where they are present within the Western Mediterranean database

RSL indicator	Description	RWL	IR
<b>Beach deposit or beachrock</b>	From Mauz et al., 2015: “ <i>Fossil beach deposits may be composed of loose sediments, sometimes slightly cemented. Beachrocks are lithified coastal deposits that are organized in sequences of slabs with seaward inclination generally between 5° and 15°</i> ” Definition of indicative meaning from Rovere et al. (2016)	(Ob + db)/2	Ob to db
<b>Beach ridge</b>	Otvos,2000 defines beach ridges as “ <i>stabilized, relict intertidal and supratidal, eolian and wave-built shore ridges that may consist of either siliciclastic or calcareous clastic matter of a wide range of clasts dimensions, from fine sand to cobbles and boulders</i> ”. Definition of indicative meaning from Rovere et al. (2016)	(SWSH + Ob)/2	SWSH to Ob
<b>Beach swash deposit</b>	Beach face between mean sea level and foredune. Upper Limit (UL) = spring tidal range / 2 or, mean higher high water; Lower Limit (LL) = MSL	(UL + LL) / 2	UL to LL
<b>Foreshore deposits</b>	Beach deposits characterized by a horizontal or gentle seaward-dipping lamination	(MHHW to MLLW)/2	MHHW to MLLW
<b>Lagoonal deposit</b>	Lagoonal deposits consist of silty and clayey sediments, frequently characterized by the presence of brackish or marine water fauna (Rovere et al., 2016). Usually, lagoon sediments are horizontally laminated (Zecchin et al., 2004). Definition of indicative meaning from Rovere et al. (2016).	(MLLW + mLd)/2	MLLW to mLd
<b>Bioerosional and erosional markers on a limestone cliff</b>	Relicts of bioerosional (e.g., <i>L. lithophaga</i> boreholes) or erosional indicators on a sparse elevation range on a limestone cliff		Distance between MSL and the difference of upper bound of occurrence minus lower bound
<b>Lithophyllum Byssoides algal rims</b>	Upper intertidal fossil algal rim (Sechi et al., 2020)	(HAT-MSL)/2	HAT-MSL
<b>Shallow or intertidal marine fauna</b>	Marine fauna usually associated with very shallow water or intertidal environments		Based on the upper and lower limits of living modern analog faunas
<b>Upper limit of Lithophaga boreholes</b>	Boreholes created by mollusks of the <i>Lithophaga</i> genus, forming a well-delineated band on a rocky shoreline around the tidal level (Laborel and Laborel-Deguen, 1994)	(MLLW to LAT)/2	MLLW to LAT
<b>Marine Terrace</b>	From Pirazzoli et al., 2005: “ <i>Any relatively flat surface of marine origin</i> ”. Definition of indicative meaning from Rovere et al., 2016	(SWSH+ db) / 2	SWSH to db
<b>Tidal notch</b>	Tidal notches are “ <i>indentations or undercuttings cut into rocky coasts by processes acting in the tidal zone (such as tidal wetting and drying cycles, bioerosion, or mechanical action)</i> ” (Antonioli et al., 2016). Definition of indicative meaning from Rovere et al. (2016)	(MHHW + MLLW)/2	MHHW - MLLW

**Table 7.1.** Sea-level proxies used in the Western Mediterranean database. Abbreviations as follows. RWL=Reference Water Level; IR=Indicative Range; Ob=Ordinary berm; db=breaking depth; SWSH=Storm Wave Swash Height; MHHW= Mean Higher High Water; MLLW=Mean Lower Low Water; mLd = modern Lagoon depth; HAT=Highest Astronomical Tide; LAT=Lowest Astronomical Tide; MSL=Mean Sea Level;

## 7.4 Positioning techniques and vertical datums

The elevation of the large majority of sea-level index points reported in the database was measured with metered tapes or rods and is referred generally to as “mean sea-level”, with no additional information provided (**Figure 61a,b**). Whenever the elevation measurement technique was not reported, we set the elevation error to 20% of the elevation value. If only the sea-level datum was not reported, we added 5% to the reported elevation error. Also, we remark that the majority of studies do not report precise coordinates for the sites investigated. Therefore, we had to reconstruct the geographic location of many sites with the aid of geolocation services (e.g. Google Earth). This means that the location reported in the database is, for many sites, only indicative (**Figure 61c**).

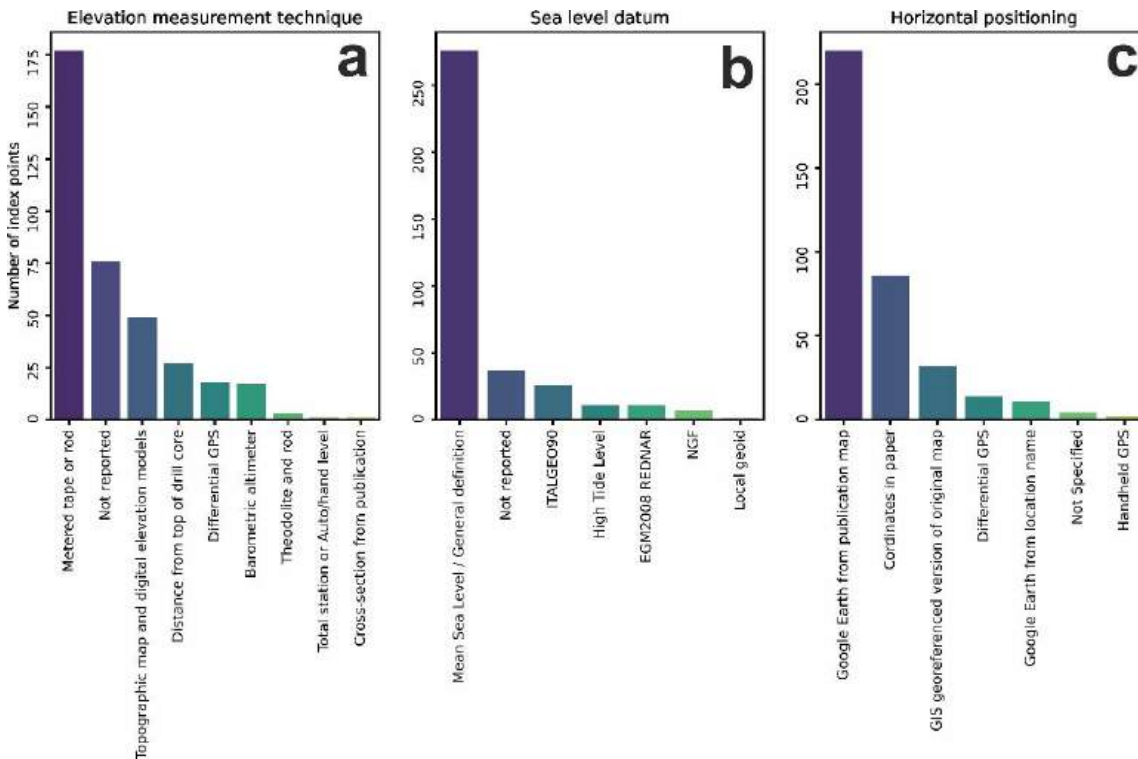


**Figure 61.** Elevation measurement (a), sea level datums (b) and horizontal positioning (c) associated with sea-level indicators in the Western Mediterranean database.

## 7.5 Age attribution

In the Western Mediterranean, Last Interglacial sea-level indicators have been assigned an age through a large array of techniques **Figure 62**. U-Series was used to date corals preserved at several locations (**Figure 62a**). The vast majority of dated corals are specimens or fragments of *Cladocora caespitosa* (Linnaeus, 1767). Nearly two-thirds of the corals were dated with Mass Spectrometry, while one third was dated via the older alpha-counting technique. We also included in the database 33 U-Series ages on mollusks or corallineaceous algae (**Figure 62b**). We remark that, due to issues with the open-system behavior of mollusks and corallineaceous algae, WALIS only allows the attribution of a general Marine Isotopic Stage to each sample, which we based on the reported ages and, if present, correlated discussions in the original manuscripts. While we did not include in our compilations the cave deposits from Mallorca and Croatia (that were, as remarked in the introduction, already compiled in WALIS by Dumitru et al. (2020), we inserted several speleothems that were dated in Southern Italy and Morocco to support the chronological attribution of sea-level indicators in these areas (**Figure 62c**). Optically Stimulated Luminescence (OSL), Thermo Luminescence (TL), Infrared stimulated Luminescence (IRSL) and Electron Spin Resonance (EER) techniques were used to date coastal deposits at several locations, mostly in Italy (**Figure 62d-f**). Much more widespread is the use of Amino Acid Racemization (AAR) on mollusks (**Figure 62e**). This technique was used to strengthen biostratigraphic correlations among sites. In general, mollusks falling into “Aminozone E” were correlated to MIS 5e thanks to *Cladocora* corals dated with U-Series at sites where mollusks and corals were found in the same deposit (Hearty et al., 1986).

Chronostratigraphic and bio-stratigraphic correlations among sites are common in the Western Mediterranean (**Figure 62g**). Among these, one of the

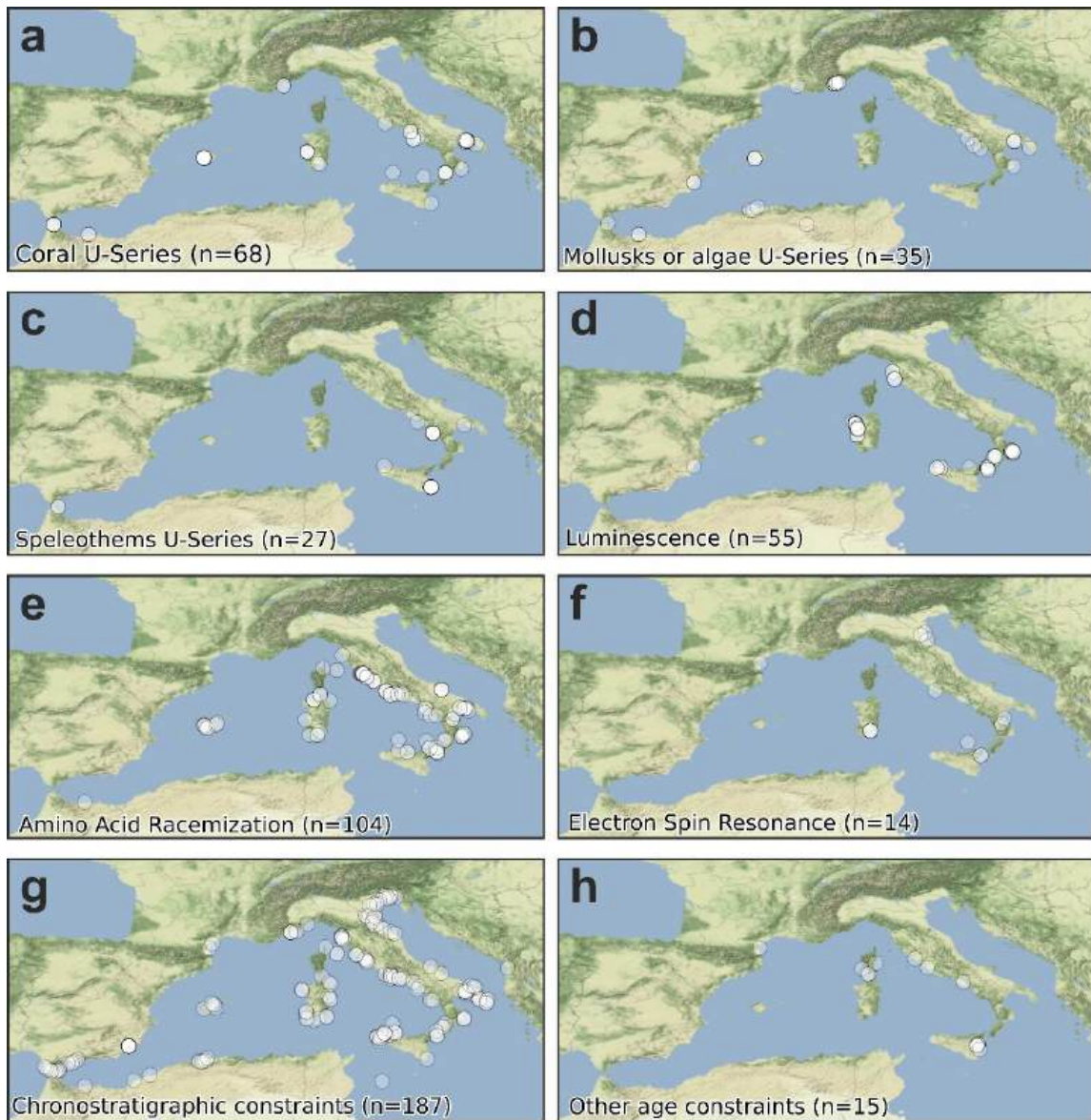
most widespread is related to the presence, embedded within Pleistocene deposits, of Senegalese fauna (for a detailed description, see Benjamin et al., 2017). The “Senegalese fauna” term is used to identify an assemblage composed of the following species: *Persististrombus latus* (Gmelin, 1791), *Conus testudinarius*, *Cantharus viverrata*, *Tritonium ficoides*, *Natica lactea*, *N. turtoni*, *Mytilus senegalensis*, *Arca Geissei*, *Cardita senegalensis*, and some other minor species (Gignoux, 1913). The designation of this kind of fauna derives from the fact that the most representative species of the Senegalese fauna, *P. latus* (**Figure 63**, currently lives along the Atlantic coasts of western Africa at warm low-latitudes, from Angola to Senegal. Deposits with Senegalese fauna are encountered throughout the Western Mediterranean, excluding the coasts of the northern part of the Adriatic Sea.

The presence, within a Western Mediterranean Pleistocene deposit, of Senegalese fauna or *P. latus* is often used to denote an MIS 5e age of the deposit itself. But this chronological attribution has been challenged, at least for the Mediterranean coasts of Spain, by the fact that *P. latus* was found on marine terraces dated to MIS 5, MIS 7, and MIS 9 (Zazo et al., 2003). Details on the arguments for and against the attribution of *P. latus*-bearing deposits to MIS 5e are summarized in a series of comments-replies to Bardají et al., 2009 by Mauz and Antonioli, 2009 and Bardají et al., 2009. In our compilation, we assigned deposits bearing Senegalese fauna a general MIS 5 age, meaning that we deem it possible that this faunal assemblage was present in the Western Mediterranean at least throughout the different warm peaks of this Marine Isotopic Stage. We also remark that, at many sites where Senegalese fauna was described, independent datings (e.g., AAR, Luminescence, U-Series) confirmed the MIS 5e age of the deposit. Moreover, we highlight that, in Western Mediterranean Pleistocene sea-level studies, the species name *Strombus bubonius* (Lamarck, 1822) is widely used to indicate the gasteropods of the Strombidae family, instead of the more appropriate

*Persistrombus latus* (Gmelin, 1791) as recently established by Kronenberg and Lee (2006) and Harzhauser and Kronenberg (2008). Throughout our database, we, therefore, used *P. latus* even when the original authors used *Strombus bubonius*.

A second particular type of chronostratigraphic attribution is the one related to tidal notches (Antonioli et al., 2018). Tidal notches (**Figure 64**) are sea-level indicators that have a very narrow indicative range, but that cannot be dated directly due to their erosive nature. In general, tidal notches have been dated indirectly by association with nearby deposits of known age. In our compilation, we, therefore, assigned to each tidal notch an age corresponding to the nearest deposit for which a chronological constraint is available, similarly to the approach followed by Antonioli et al. (2018).

In the database, we inserted also a small number of “Other” age constraints (**Figure 62h**), e.g., limiting radiocarbon dates or Argon / Argon ages for which there is no standard template within WALIS.



Map tiles by Stamen Design, CC BY 3.0 – Map data (C) OpenStreetMap contributors

**Figure 62.** Geographic location of dated samples (or chronostratigraphic attributions), divided by type of analysis.



**Figure 63.** Bioclastic calcarenite bearing *Persistrombus latus* (reported in many publications with its former name, *Strombus bubonius*) at Il Fronte site, Taranto, Puglia, Italy. Photo C. Cerrone



**Figure 64.** Tidal notch on the Orosei cliffs, Sardinia, Italy. Note the modern notch carved at present sea level. Photo by A. Rovere.

## 7.6 Quality of sea level and age determinations

Within WALIS, it is possible to insert a quality score for age and RSL information associated with each sea-level indicator. The ranking follows a simple score (from 0 to 5), that is codified following the general guidelines given in the WALIS documentation (Rovere et al., 2020) and reported verbatim in **Table 7.2**. In general, if a site was dated only with one among U-Series on mollusks, AAR, or chronostratigraphic constraints, it was given an “Average” score. Sites where several dating techniques were used concurrently, giving coherent results, received a higher score. Tidal notches are a particular case, as they can be dated only indirectly. For these indicators, the age information quality was systematically set to “Poor”. We remark that this is a conservative choice, as the quality of the indirect age attribution for notches might be higher if the dated deposits are close to the notch. In our compilation, we followed whenever possible the WALIS guidelines. In case our quality assessment deviated from the guidelines, the reasons for the scoring choice were detailed in the “Quality notes” field.

Overall, nearly 40% of points in the database have above average quality for both age and RSL information, with only three sites reaching an excellent score in both categories (**Figure 65**).

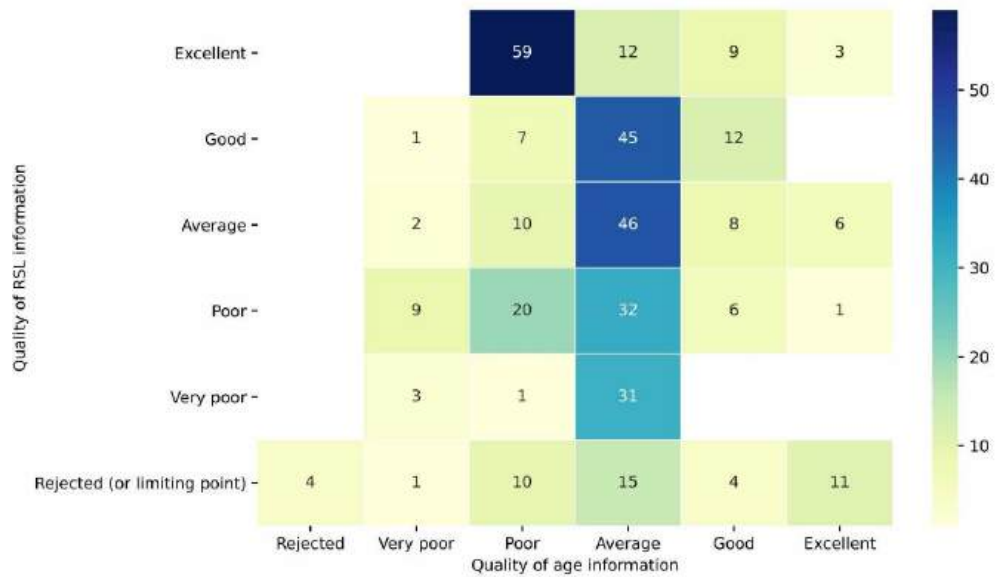


**Figure 65.** Heatmap summarizing the quality of age and RSL information as estimated within the Western Mediterranean database. Numbers in each cell detail the number of sites with the corresponding RSL/age quality ranking.

**Table 7.2.** Quality ranking as suggested by the WALIS guidelines (verbatim from Rovere et al. (2020), originally published under CC-BY 2.0 license)

<b>RSL indicators quality ranking</b>	
<b>5 (excellent)</b>	Elevation precisely measured, referred to a clear datum and RSL indicator with a very narrow indicative range. Final RSL uncertainty is sub-metric.
<b>4 (good)</b>	Elevation precisely measured, referred to a clear datum and RSL indicator with a narrow indicative range. Final RSL uncertainty is between one and two meters.
<b>3 (average)</b>	Uncertainties in elevation, datum, or indicative range sum up to a value between two and three meters.
<b>2 (poor)</b>	Final paleo RSL uncertainty is higher than three meters
<b>1 (very poor)</b>	Elevation and/or indicative range must be regarded as very uncertain due to poor measurement/description / RSL indicator quality
<b>0 (rejected)</b>	There is not enough information to accept the record as a valid RSL indicator (e.g. marine or terrestrial limiting)
<b>Age information quality ranking</b>	
<b>5 (excellent)</b>	Very narrow age range, e.g. few ka, that allows the attribution to a specific timing within a substage of MIS 5 (e.g. 117±2 ka)
<b>4 (good)</b>	Narrow age range, allowing the attribution to a specific substage of MIS 5 (e.g., MIS 5e)
<b>3 (average)</b>	The RSL data point can be attributed only to a generic interglacial (e.g. MIS 5)
<b>2 (poor)</b>	Only partial information or minimum age constraints are available
<b>1 (very poor)</b>	Different age constraints point to different interglacials
<b>0 (rejected)</b>	Not enough information to attribute the RSL data point to any Pleistocene interglacial.

## 7.7 Relative sea level data

In the following sections, we describe the datapoints inserted in the Western Mediterranean database, starting from the coasts of Spain and proceeding clockwise across the basin. In the text, we refer to the elevation of sea-level indicators as “*a.s.l.*” (above present mean sea level) or “*b.s.l.*” (below present mean sea level). These represent the elevations we derived from the original studies. For regions where sea-level indicators span a significant latitudinal or longitudinal gradient, we present maps and paleo RSL elevation/distance graphs. Site names inserted in WALIS are reported in italics whenever they do not refer to towns or toponyms that can be easily retrieved on topographic maps and/or geolocalization services (e.g., Google maps). Wherever possible, we kept location names in the original language, or as reported in the reviewed papers. Sites inserted in WALIS are always associated with their corresponding unique RSL ID in parenthesis. Whenever mentioned, dated samples are also listed with their unique WALIS ID, e.g. AAR ID, USeries ID, etc.

### 7.7.1 Spain (Mediterranean Coasts and Gibraltar Strait)

Along the Mediterranean coasts of Spain, Last Interglacial sea-level proxies have been preserved mostly as relic beach or subtidal deposits, containing remnants of Senegalese fauna. While some sites preserved fossil specimens of the coral *Cladocora* sp., dated to MIS 5e with U-Series (e.g. Muhs et al., 2015), many other sites rely on chronological constraints given by Amino Acid Racemization (e.g. Hearty, 1987), U-Series on mollusk shells (e.g., Hillaire-Marcel et al., 1996) and biostratigraphy (e.g., Bardají et al., 2015). Along the Mediterranean and Strait of Gibraltar coasts of Spain, the Last Interglacial sea-level indicators are concentrated in four regions: Islas Baleares (Mallorca), the southern tip of the Comunitat Valenciana (Alicante province), Murcia, and Andalucía. Zazo and Goy, 1989 also report overlapping marine levels near the Ebro Delta, in Catalonia, located slightly above sea level, dated with ESR by Brückner and Radtke (1986). As we were not able to retrieve the original papers in this area, these data points were not included in WALIS.

#### 7.7.1.1 Andalucía

The Andalucía region includes sites that are located both in the Mediterranean and on the Atlantic coast, west of the Gibraltar Strait (**Figure 66**). In this region, studies on Pleistocene shorelines date back to the late 1980s /1990s (Zazo, 1980; Zazo and Goy, 1990). Several sites were reviewed in this area by Zazo et al., 1999, and were inserted in WALIS with RSL IDs from 752 to 765 (**Figure 66**). Ages were assigned based on chronostratigraphic correlation within sites, some of which were dated using U-Series on mollusks. In general, MIS 5e deposits in this area are described as MIS 5e marine remains. As most of the geological sketches in the original paper show that they are located on a flat surface, we

inserted these data points in WALIS as marine terraces, with a broader indicative range than beach deposits.

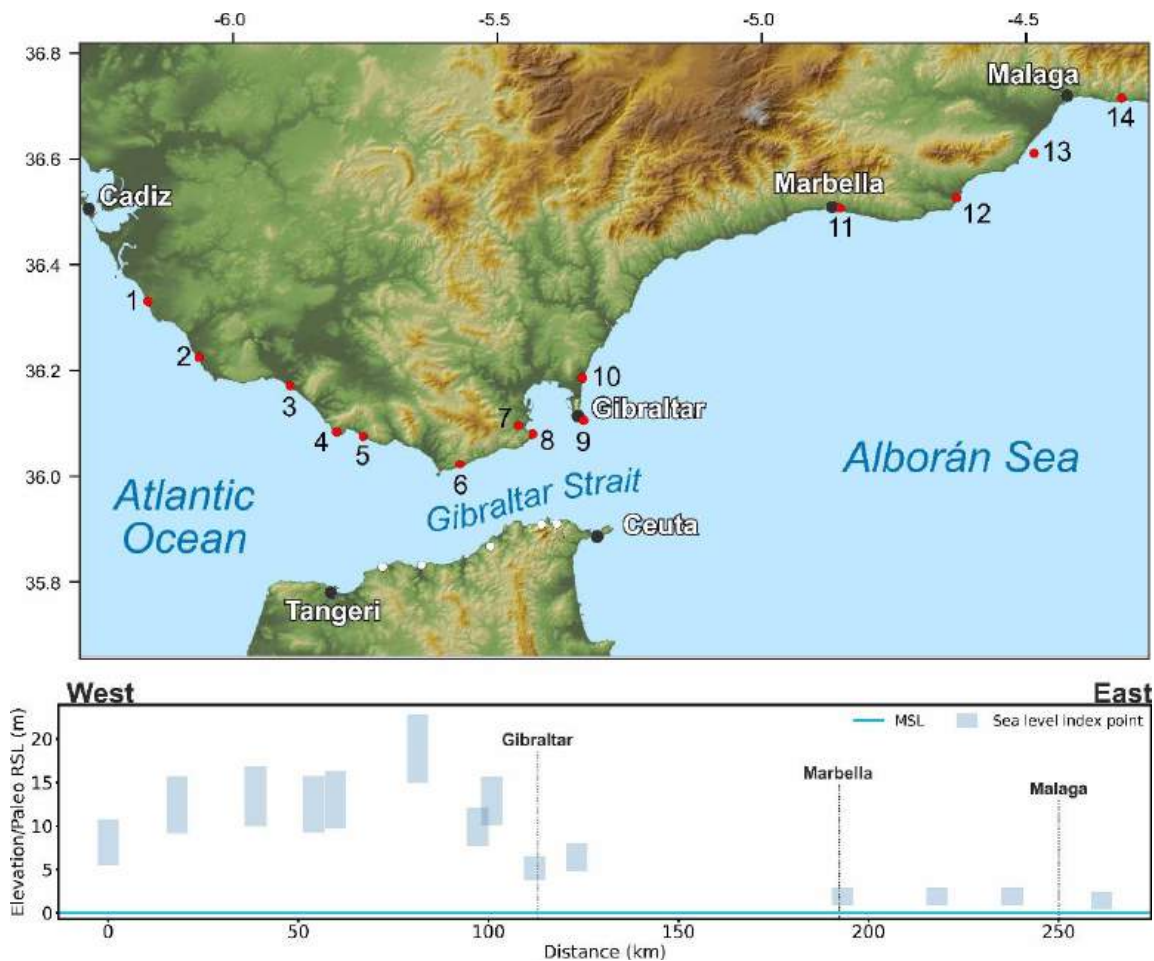


**Figure 66.** Last Interglacial sea level data for Andalucía (Spain). Upper panel: Map of sites. Red dots are sites in the region of interest, white dots are other sites within the Western Mediterranean compilation. Lower panel: Distance/Elevation graph, from West (left) to the East (right). Sites list: 1: Torre del Puerco (RSL ID 765). 2: Conil-Trafalgar (RSL ID 764). 3: Zahara (RSL ID 763). 4: Cabo Gracia (RSL ID 762). 5: Bolonia - Punta Paloma (RSL ID 761). 6: Tarifa (RSL ID 760). 7: Algeciras 1 (RSL ID 758). 8: Algeciras 2 (RSL ID 759). 9: Gibraltar (RSL ID 757). 10: La Linea (RSL ID 756). 11: Marbella (RSL ID 755). 12: Fuengirola (RSL ID 754). 13: Torremolinos (RSL ID 753). 14: El Candado (RSL ID 752).

### 7.7.1.2 Murcia

In Murcia, north of Cape Cope, several terraces attributed to different interglacials were reported by studies in the late 1980s / early 1990s (Dabrio et al., 1991; Bardají et al., 1986). The sites were later re-described by Zazo et al. (2003), who clarified that paleomagnetic data and chronostratigraphic correlations with other sites in Almeria and Alicante were used to give an age to these deposits. Within the sites in the so-called Cope Basin, the most complete was reported from a location called *Casa de Renco* (RSL ID 750), where marine conglomerates outcrop up to 5.2m a.s.l. Bardají et al. (2015) describe the lowermost sedimentological units in 11 outcrops along the Cope Basin (RSL IDs 740-750). In particular, they assign the shell-rich conglomerate of Unit D to MIS 5e, identifying different sea-level oscillations within it. The authors do not rule out a possible MIS 5a or 5c age for this unit, as its age attribution is based solely on the presence of *P. latus* and other warm-water faunas. In WALIS, we reported the 11 sites described by Bardají et al., 2015 where Unit D is reported and assigned them a general MIS 5 age.

### 7.7.1.3 Comunitat Valenciana (Alicante province)

One of the most studied Last Interglacial outcrops in continental Spain is located in the Comunitat Valenciana, within the Alicante Province, 100 km south of the city of Valencia. Here, studies on the stratigraphy of the *La Marina - El Pinet* site date back to the 1980s (Bernat et al., 1982; Hearty et al., 1987; Goy and Zazo, 1988; Goy and Zazo, 1989). More recently, Goy et al. (2006) analyzed the stratigraphy of two sections within this site (A and B, RSL IDs respectively 751 and 738), where they found evidence for an MIS 7 terrace (dated using U-Series on *Cladocora* corals). Immediately above this terrace, U-Series on mollusks (*P. latus*) yielded ages consistent with MIS 5, which were later assigned to MIS 5e by

an OSL age on oolitic sands of  $114 \pm 15$  ka (Mauz et al., 2012). It is noteworthy that the entire area shows tectonic instability, and even between the MIS 5 terrace at the two sections (separated by less than 300 meters) there is an offset of 2-3 m.

#### 7.7.1.4 Islas Baleares (Mallorca)

The island of Mallorca (**Figure 67**) has arguably preserved some of the most prominent Last Interglacial sea-level proxies for the Western Mediterranean, which have been studied since at least the late 1950s (Butzer and Cuerda, 1962; Cuerda, 1957). Stearns and Thurber, 1965 reported U-Series (obtained with alpha counting) ages on mollusk shells for 10 samples at different sites across the island. In particular, they concentrated on the *Camp de Tir* site (RSL ID 357), which is also referred to as “Es Carnatge”. This outcrop, located close to the Palma airport, is a Pleistocene beachrock deposit, composed of different units that were described in several studies (Butzer and Cuerda, 1962; Cuerda, 1957; Hearty, 1987; Zazo et al., 2003; Bardají et al., 2009). Several authors concentrated on establishing chronological constraints for the different units within the beach deposit at *Camp de Tir* (**Figure 68**), with U-Series (Hillaire-Marcel et al., 1996; Muhs et al., 2015; Zazo et al., 2003) or Amino Acid Racemization (Hearty et al., 1986; Hearty, 1987). An account of the history of investigations of the *Camp de Tir* outcrop (among others) is given in Vicens et al., 2012. Until very recently, the outcrop was divided into different units, which were assigned to “Neotyrrhenian” (ca. 2 m a.s.l., MIS 5a) and “Eutyrrhenian” (ca. 3 m a.s.l., MIS 5e) based on faunal content, U-Series on mollusks and Amino Acid Racemization. This apparent age difference has been recently ruled out by Muhs et al., 2015, who dated nine *Cladocora sp.* coral samples from the (supposed) MIS 5a unit at Camp de Tir, and obtained ages spanning the range 119-126 ka. Based on these, the authors argued that the entire *Camp de Tir* outcrop was deposited in MIS 5e. Lorscheid et al., 2017 measured the elevation of

a bioconstructed rim of vermetids close to the location where *Cladocora* corals were dated, gathering a paleo RSL elevation at *Camp de Tir* of  $2.10 \pm 0.71$  m a.s.l.

*Camp de Tir* is surely the most widely described MIS 5e outcrop in Mallorca but is not the only one. Re-assessing sites reported in previous studies, Lorscheid et al., 2017 surveyed with differential GPS other 10 sites scattered across the island. Overall, the fixed biological indicators and beach deposits at these sites show a coherent picture of paleo RSL located  $2.9 \pm 0.8$  m a.s.l. This estimate is in very good agreement with the indications of phreatic overgrowth on speleothems (Tuccimei et al., 2006, 2012). The most recent MIS 5e datum for these indicators in Mallorca is  $2.15 \pm 0.75$  m a.s.l. (Polyak et al., 2018).

In WALIS, we inserted data for 11 sites (**Figure 67**) in Mallorca as reported in Lorscheid et al., 2017, associating them with different ages as estimated at each site by previous authors. We did not include a second dataset reported by Lorscheid et al., 2017, namely shore platforms measured at higher elevations than the fossil beach deposits, due to the lack of age constraints on these features. As mentioned above, the MIS 5e in Mallorca was studied both on the open coasts and coastal caves, in the form of phreatic overgrowth on speleothems. The details of these latter indicators are reported in another WALIS compilation focussing on U-Series on cave deposits (Dumitru et al., 2020).

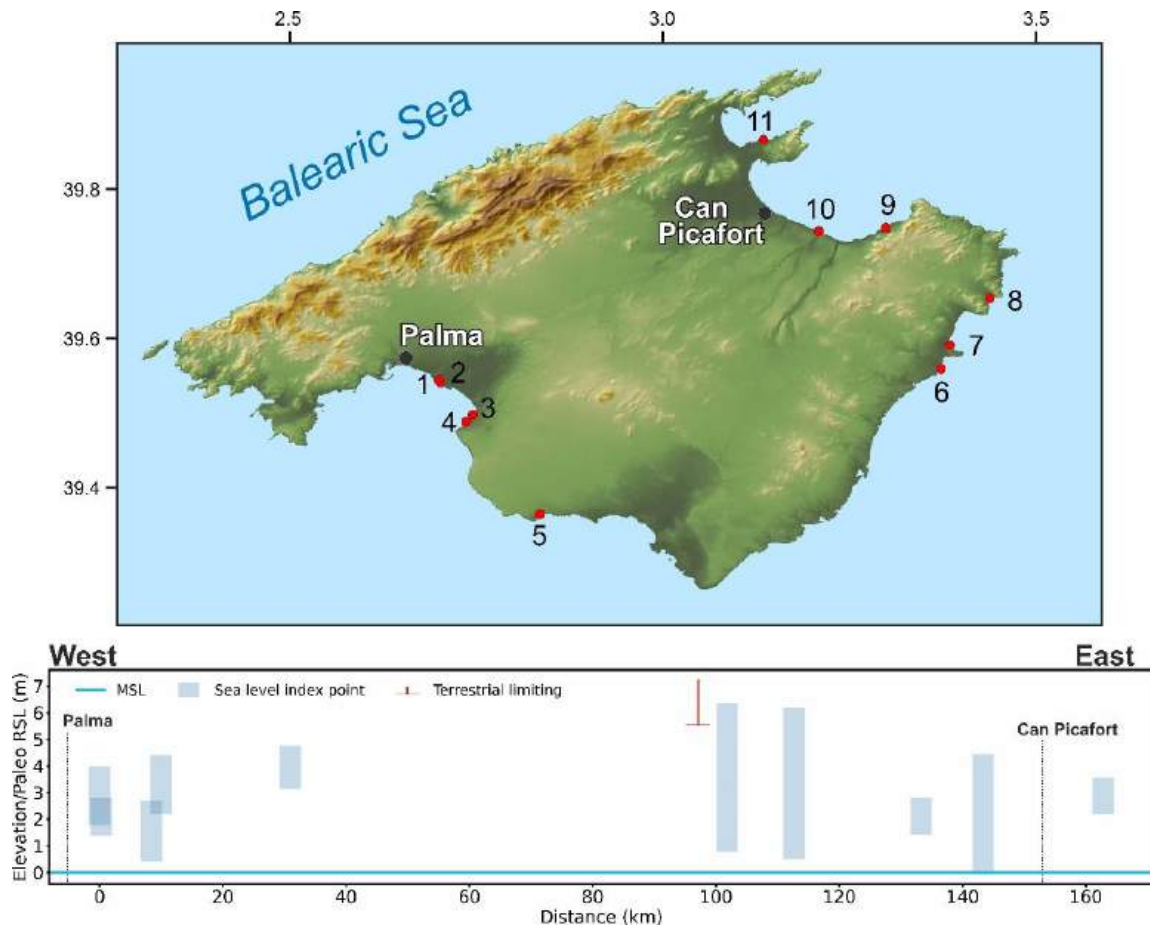


**Figure 67.** Last Interglacial sea-level data for Mallorca (Balears, Spain). Upper panel: Map of sites. Lower panel: Distance/Elevation graph, counterclockwise from West (left) to the East (right). Sites list: 1: Cala Pudent (RSL ID 779). 2: Camp de Tir Unit U4 (RSL ID 357). 3: Cova Baixa (Son Grauet) (RSL ID 780). 4: Cala Blava (RSL ID 781). 5: Cala Pi (RSL ID 782). 6: S'Illot (RSL ID 784). 7: Cala Millor (RSL ID 785). 8: Canyamel (RSL ID 786). 9: Caló des Camps (RSL ID 787). 10: Torrent de Son Real (RSL ID 788). 11: Platja de Sant Joan (RSL ID 789).



**Figure 68.** General overview of the Camp de Tir outcrop in Mallorca (RSL ID 357), Balearic Islands, Spain. The upper part of the outcrop is composed by shallow water beach sands of Last Interglacial age. Photo by A. Rovere.

### 7.7.2 Mainland France

The study of the marine Pleistocene deposits along the Mediterranean coast of France dates back to the 1950s (Masurel, 1953, Ottmann, 1954; Bonifay and Mars, 1959). The large majority of the literature is in French (Barrière, 1966; Ambert, 1999; Lumley et al., 2001; Provansal et al., 1995) while fewer studies were published in English (Dubar et al., 2008; Stearns and Thurber, 1965). In general, the overall quality of the French data is significantly lowered by the dating constraints available. A large part of the marine deposits was dated using radiocarbon techniques in search of a mid-Holocene highstand that was not present in this portion of the Mediterranean (Vacchi et al., 2016). These ages (generally >20,000 years) and the stratigraphic context of the outcrops suggest that the attribution to MIS 5 is reasonable but further analysis with updated techniques is strongly needed, because only a few studies reported ages based on AAR or U/Th dating.

#### 7.7.2.1 Languedoc-Roussillon

The Languedoc-Roussillon coast extends from the border with Spain to the Rhone Delta (**Figure 69**). Ambert (1999) compiled the most recent review of the Last Interglacial shorelines in this region. These are generally represented by beach deposits (sometimes cemented) found at different elevations, not exceeding ~8 m a.s.l. The beach deposits found near the towns of Narbonne (RSL ID 386), Leucate (RSL ID 385 and 1316), and Port la Nouvelle (RSL ID 384) are characterized by abundant faunal remains rich in *Tapes diana*, which is considered the key species for the local “Euthyrranian” stage. The single chronological constrain is provided by an ESR age on a shell collected at Port la Nouvelle (ESR ID 99) which yielded an age of  $128 \pm 15$  ka (Yokoyama et al., 1987). Our re-analysis indicates that the

maximal sea-level highstand in this portion of the French Mediterranean coast was placed at  $6.4 \pm 2.5$  m a.s.l. Ambert (1999) also reports a possible lower sea-level highstand which has been the result of a regressive phase following the maximal highstand. This was found near Leucate and is characterized by beach deposits (RSL ID 1316) which placed the RSL at  $3 \pm 2.5$  m a.s.l. This deposit was dated with both radiocarbon and U/Th techniques but both ages were not considered reliable (Ambert, 1999). The faunal assemblage is also not very peculiar, with the sole presence of *Spondylus gaederopus*.

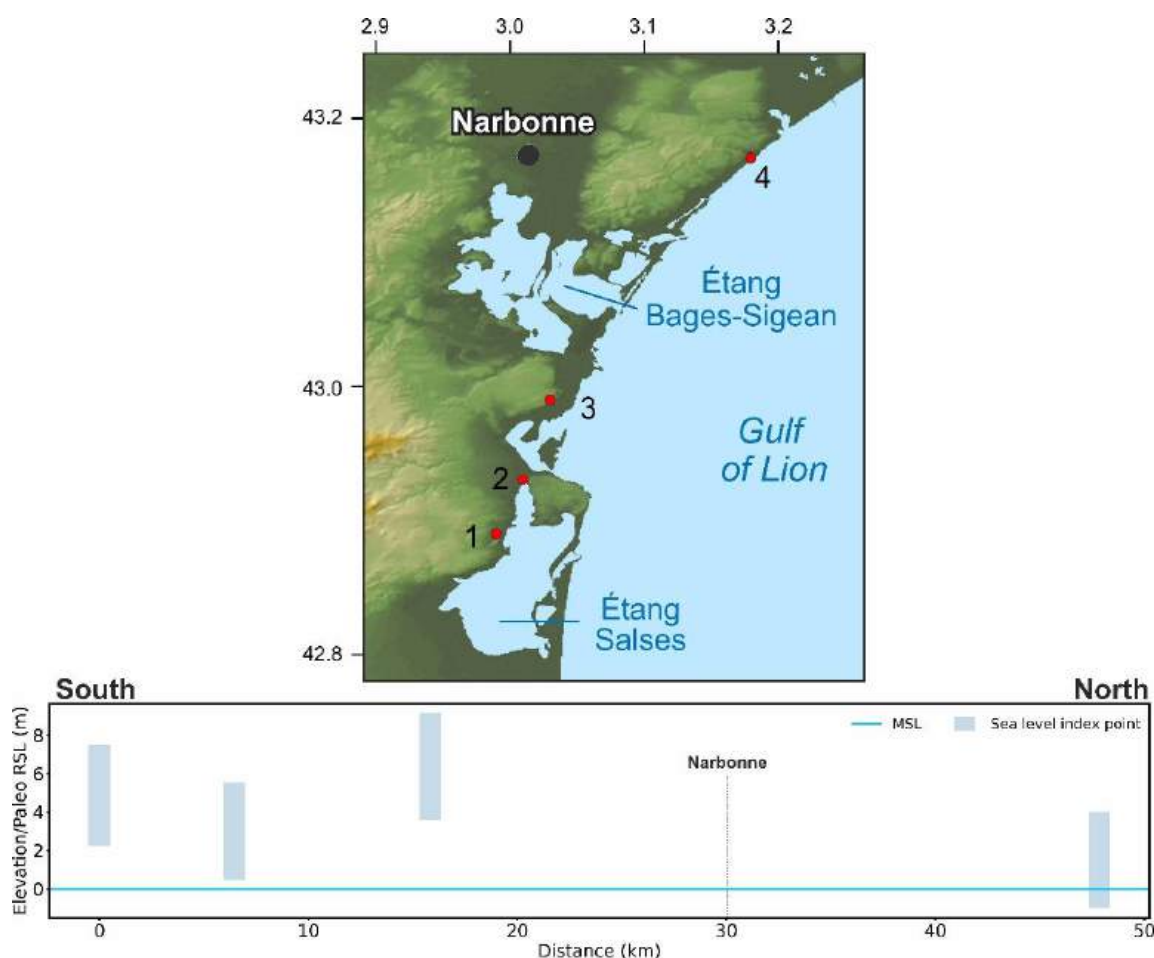


**Figure 69.** Last Interglacial sea-level data for Languedoc-Roussillon (France). Upper panel: Map of sites; Lower panel: Distance/Elevation graph, from South (left) to the North (right) . Sites list: 1: Leucate La Malpas (RSL ID 385). 2: Leucate La Franqui (RSL ID 1316). 3: Port la Nouvelle Ramandils (RSL ID 384). 4: Narbonne Saint Pierre (RSL ID 386).

### 7.7.2.2 Provence- Cote d'Azur

This portion of the Mediterranean French coast extends from the Rhone Delta to the border with Italy (**Figure 70**).

. In his review, Ambert (1999) reports a large elevation variability of the Last Interglacial shorelines which ranges from ~3 to ~22 m a.s.l. The lowest elevations of these shorelines are reported in the Marseille area. Here, the most robust indicator is represented by a lagoonal deposit sampled near the Étang de Berre (Provansal et al., 1995) which was used to reconstruct a paleo sea-level placed at  $3 \pm 1.4$  m a.s.l. (RSL ID 387). The late Pleistocene age of this deposit was provided by U/Th dating on algae (U-Series ID 795) which yielded ages comprised between 129 and 139 ka.

The majority of the data in the Provence-Cote d'Azur province were collected near the cities of Nice and Antibes (Dubar et al., 2008; Hearty et al., 1986; Gilli, 2018). Stearns and Thurber (1965) firstly attempted to date the paleo-shorelines found in this area. The U/Th dating (U-Series ID 2341) on mollusks found in beach deposits at ~20 m a.s.l. in the *Grotte de Lazaret* yielded an age of  $110 \pm 10$  ka, while other two dates performed near Monaco on beach deposits found at very different elevations (U-Series IDs 2342 at ~33.5 m a.s.l. and U-Series ID 2343, ~1.8 m a.s.l.) yielded ages between 75 and 82 ka. This variability is likely related to issues of dating mixed shell remains with U-Series (Stearns and Thurber, 1965).

More recently, Dubar et al. (2008) performed some U/Th dating (U-Series ID 1719 to 1725) on marine shells found in beach face deposits, which yielded MIS 5 ages. These deposits allowed reconstructing a paleo sea-level placed at  $14 \pm 1.1$  m a.s.l. (RSL ID 449) and at  $10.3 \pm 1.3$  m a.s.l. (RSL ID 451). The variability of the last-interglacial shoreline in this area elevation was explained by differential tectonic uplift (Dubar et al., 2008). Gilli (2018) performed a U/Th dating (U-Series

ID 1987) on a *Cladocora cespitosa* sample found in living position at Cap d'Antibes. The coral, which yielded an age of  $125 \pm 5$  ka, constrains the paleo sea-level above ca. 6 m a.s.l. during MIS 5e.

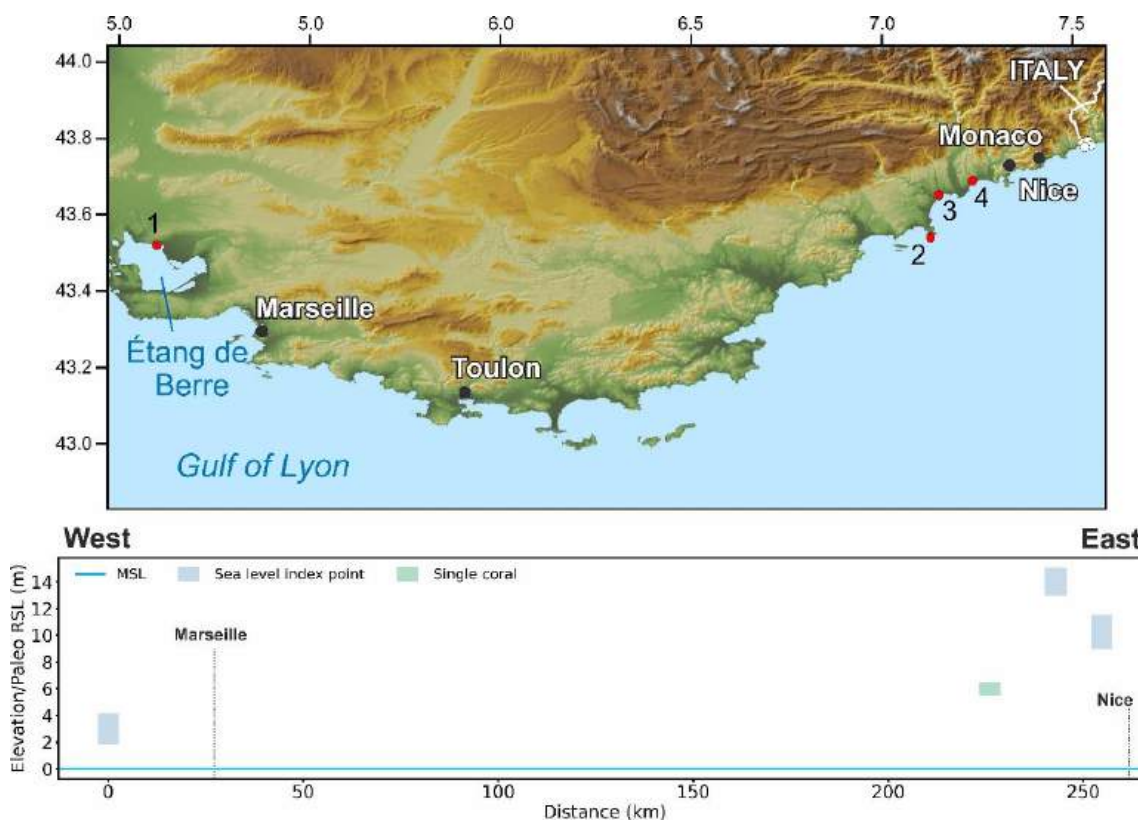


**Figure 70.** Last Interglacial sea-level data for Provence-Cote Azur (France). Upper panel: Map of sites. Lower panel: Distance/Elevation graph, from West (left) to the East (right). Sites list: 1: Étang de Berre (RSL ID 387). 2: Cap d'Antibes (USeries\_1988). 3: Nice Le Bosquet (RSL ID 449). 4: Nice Les Amandier (RSL ID 451).

### 7.7.3 Mainlan Italy

#### 7.7.3.1 Liguria

Quaternary East of the French border, Quaternary shorelines (in particular the Last Interglacial ones) are preserved at few locations along the coast of Liguria (**Figure 71**), mostly on limestone rocky coasts, and in caves. The most recent review on MIS 5e shorelines in this region was written by Federici and Pappalardo, 2006, who analyzed several studies reporting RSL indicators. A few hundred meters from the French border, several sea-level indicators are present inside caves in an area called *Balzi Rossi* (RSL IDs 233, 237, 239, 240) and, further to the East, in the *Madonna dell'Arma* cave (RSL ID 242) (Vicino, 1974; De Lumley, 1969; Isetti et al., 1962). This cluster of data was attributed to the Last Interglacial due to the presence of *P. latus* and Senegalese fauna and defines paleo RSL at an elevation of 7-12 m a.s.l. Similar deposits found in another marine cave (*Grotta Marina di Bergeggi*, RSL ID 246) give a chronologic constraint to a well-preserved upper band of *L. lithophaga* (date mussel) boreholes (**Figure 72**) at ca. 6m a.s.l. (Carobene, 2015). East of the city of Genova there is only one outcrop that was attributed to the Last Interglacial by Federici and Pappalardo, 2006, near the town of Lavagna. Here, a marine terrace at 28m a.s.l. was dated with OSL at  $139\pm 11$  ka. More recent ages confirmed that this deposit is older than MIS 5e (Marta Pappalardo, Pers. Comm. 04.02.2021). Therefore, this data point has not been included in WALIS.

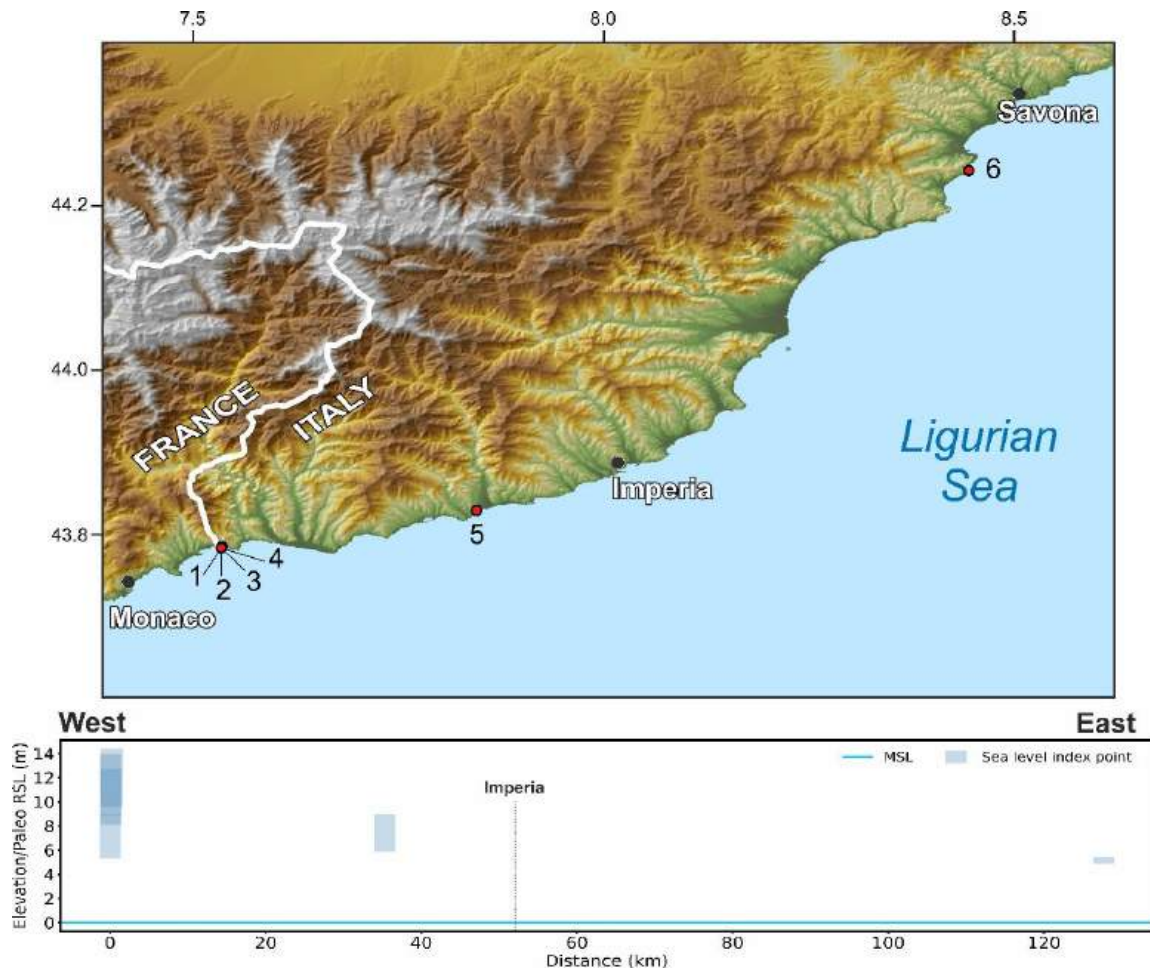


**Figure 71.** Last Interglacial sea-level data for Liguria (Italy). Upper panel: Map of sites. Lower panel: Distance/Elevation graph, from West (left) to the East (right). Sites list: 1: Ex Casino (RSL ID 240). 2: Barma Grande (RSL ID 233). 3: Bausu da Ture (RSL ID 239). 4: Grotta del Principe (RSL ID 237). 5: Madonna dell'Arma (RSL ID 242). 6: Grotta Marina di Bergeggi (RSL ID 246).



**Figure 72.** Close-up of *L. lithophaga* boreholes at ca.6m above modern sea level in the Grotta Marina di Bergeggi, Liguria, Italy (RSL ID 246). Each borehole has a diameter of approximately 2-3 cm. Photo by A. Rovere.

### 7.7.3.2 Toscana

In Toscana (Tuscany), a relatively recent review of the Last Interglacial sea-level record was compiled by Nisi et al. (2003) starting from the compilation of Bordoni and Valensise (1999), which was later summarized and implemented with new information by Ferranti et al. (2006). As a result, many of the sites in our database were already included in Ferranti et al. (2006). In WALIS, we standardize the calculation of the indicative range for many of the previously reported sites, also re-analyzing original works (**Figure 73**). We report, where available, also details on their dating. Starting from the North of Tuscany, we remark that here we do not include in our database a core in the Versilia Plain. Within this core, coastal deposits found at 60 m b.s.l. were previously attributed to MIS 5e (Antonioli et al., 1999), but more recently U/Th dating on a *Cladocora sp* coral collected from the same unit yielded an age of  $195.7 \pm 1.6$  ka (Carboni et al., 2010).

In the area of Livorno, Nisi et al. (2003) associated the Last Interglacial with the inner margin of a broadly developed marine terrace at elevations of 14 to 20 m a.s.l. referred to as Terrazzo di Livorno (Livorno Terrace). A topographic sketch of the terrace of the site named *Quercianella* (RSL ID 255, terrace elevation from Nisi et al., 2003 = 17 m a.s.l) published by Boschian et al. (2006) shows that coastal deposits on the same terrace are found several meters below the inner margin (elevation of the “fossil beach” at *Quercianella* = ca.10 m a.s.l.) and that the elevation of the inner margin of the terrace is covered by fossil dunes and soils. For this reason, unless independent constraints were available on the elevation of coastal deposits, the inner margin of the terraces reported by Nisi et al. (2003) was considered in WALIS as a terrestrial limiting. Zanchetta et al. (2004) describe several boreholes in the Livorno Terrace where coastal marine cemented sands with shells are found at 5-10 m a.s.l. Summarizing previous studies, Ciampalini et al.

(2006) clarify that these deposits are attributed to MIS 5e mostly based on Senegalese fauna.

The Livorno Terrace becomes narrower towards the south of Livorno (Boschian et al., 2006), where vertical or sub-vertical outcrops containing MIS 5e deposits were found. Mauz (1999) used OSL to date two sections, *Buca dei Corvi* (RSL IDs 325 and 326) and *Baratti* (RSL ID 327 and 328), albeit obtaining only limiting ages (*Buca dei Corvi* >10ka, *Baratti* >100ka). These sections were already described and correlated with Aminozone E (assigned to MIS 5e) with Amino Acid Racemization by Hearty et al. (1986) and Hearty and Dai Pra (1987). The *Buca dei Corvi* outcrop is reported to contain Senegalese fauna and *P. latus*.

The same authors reported similar deposits (with *P. latus* and assigned to Aminozone E) also on Pianosa Island (RSL ID 330, **Figure 74**), later also described by Antonioli et al. (2011). Here, the Aminozone E beach deposits (at 1.7 m a.s.l.) are in close relationship to remnants of *L.lithophaga* boreholes and marine erosion at higher elevations (ca. 6 to 9 m a.s.l., RSL ID 331) on the cliff. Stocchi et al. (2018) provide differential GPS measurements of these two units at Pianosa Island. These are reported in WALIS as separate entries, as it is not clear if they were formed by one or two highstands, given the impossibility to give an age constraint to the *L. lithophaga* and erosional features on the cliff. The same issue applies to a tidal notch at *Talamone* (RSL ID 335), which was recently measured by Antonioli et al. (2018) at 4.8 m a.s.l. The notch itself cannot be dated directly, but it was associated with closeby (2.7 km) deposits containing warm water fauna at *Campo Regio* (RSL ID 336, 6 m a.s.l., Hearty and Dai Pra 1987). Unfortunately, no AAR constraints are available at this site. South of the Orbetello lagoon, the Last Interglacial beach deposits were mapped by Hearty and Dai Pra (1987) at 10-13m a.s.l.

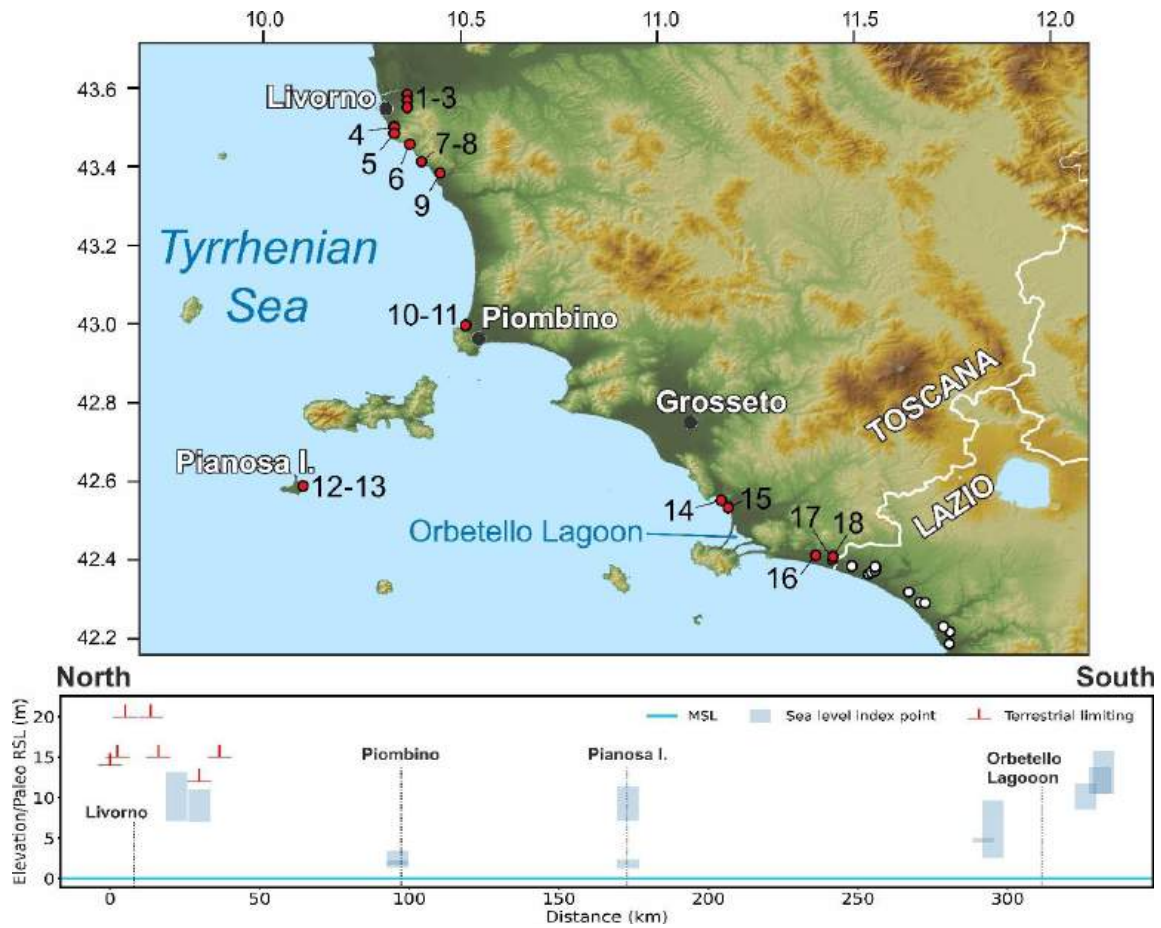


**Figure 73.** Last Interglacial sea-level data for Toscana (Italy). Upper panel: Map of sites. Red dots are sites in the region of interest, white dots are other sites within the Western Mediterranean compilation. Lower panel: Distance/Elevation graph, from North (left) to South (right). Sites list: 1: Casale Vallino (RSL ID 250). 2: Pian di Rota (RSL ID 251). 3: Bagnetti (RSL ID 252). 4: Antignano (RSL ID 253). 5: Punta Casotto (RSL ID 254). 6: Quercianella (RSL ID 255). 7: Buca dei Corvi BdC1 (RSL ID 325). 8: Buca dei Corvi BdC2 (RSL ID 326). 9: Rosignano Solvay (RSL ID 329). 10: Baratti Bar 1 (RSL ID 327). 11: Baratti Bar 2 (RSL ID 328). 12: Pianosa - Cala dei turchi Upper notch and lithophaga boreholes (RSL ID 331). 13: Pianosa - Cala dei turchi Lower beach sequence (RSL ID 330). 14: Talamone (RSL ID 335). 15: Campo Regio (RSL ID 336). 16: Selva Nera (RSL ID 332). 17: San Angelino (RSL ID 334). 18: Vado Piano (RSL ID 333).



**Figure 74.** Shelly-rich Last Interglacial deposit at Pianosa, Tuscany, Italy, at 1.7m above present sea level (RSL ID 330). Photo by A. Rovere.

### 7.7.3.3 Lazio

The border between Toscana and Lazio (Latium) administrative regions (**Figure 75**) is located in the Montalto coastal plain. Here, Hearty and Dai Pra (1987) identified and attributed to Aminozone E (corresponding to MIS 5e) several beach deposits, most of them containing Senegalese fauna. Some of these deposits were already identified at the beginning of the last century (Gignoux, 1913; Blanc, 1935; Blanc, 1936; Blanc and Segre, 1947; Blanc and Segre, 1953; Segre, 1949; Bonadonna, 1967; Bonadonna, 1967; Radtke, 1986; Ozer et al., 1987; Palieri and Sposato, 1988; Milli and Zarlenga, 1991), and were successively reviewed by Bordoni and Valensise (1999), Nisi et al. (2003) and Ferranti et al. (2006). These Last Interglacial beach deposits rise in elevation from the Tuscany-Latium border towards the town of Tarquinia, reaching 25 m a.s.l. at the *Aurelia km 103* site (RSL ID 483). Towards the city of Tarquinia, the elevation of Last Interglacial beach deposits drops again to 13-16 m a.s.l (RSL IDs 484, 479, 480), then rise in only 16 km near Civitavecchia up to 35 m a.s.l (RSL ID 494). Hearty and Dai Pra (1986) report only two beach deposits dated to MIS 5e southwards, towards the city of Rome (RSL IDs 495-496). At *Cava Rinaldi* (RSL ID 529), Marra et al. (2016, 2019) dated a fluvial-lacustrine deposit (that we consider in the database as a terrestrial limiting point) at 26 m a.s.l to MIS 5e ( $129 \pm 2$ ka) with  $^{40}\text{Ar}/^{39}\text{Ar}$  thanks to the presence of an intercalated pyroclastic-flow deposit. Fifty kilometers south of Rome, (Marra et al., 2019) dated one mollusk (*Glycymeris sp*) with ESR and one coral (*Cladocora sp.*) with U-Series from a locality called *Quadrato* (RSL ID 527), at 11 m a.s.l. The ESR sample gave an age of  $79 \pm 7$ ka, while the U-Series one yielded an age of  $198 \pm 8$ ka, which was rejected due to a probable opening of the U-Th system. Based on the ESR results and correlations of terrace levels across Lazio, Marra et al. (2019) conclude that MIS 5a peaked locally at 12 m a.s.l, MIS 5c at ca. 23 m a.s.l and MIS 5e attained much higher levels, at around 35 m a.s.l. These

conclusions are at odds with the attribution of similar deposits to Aminozone E (Hearty and Dai Pra, 1986, 1987). Also, two nearby sites (RSL IDs 497 and 498) were reported by Hearty and Dai Pra (1987) at roughly the same elevation and with similar stratigraphic characteristics of the *Quadrato* site were attributed to Aminozone E, hence to MIS 5e. Further to the South, in the Pontina plain (RSL IDs 513 to 518), Antonioli et al. (1999) reported lagoonal deposits in cores reaching several meters below present sea level, again dated to Aminozone E. Similarly, in the Fondi plain (south of the city of Latina), Antonioli et al. (1988) report MIS 5e deposits down to 6 m b.s.l (RSL ID 508). Last Interglacial sea-level indicators above present sea level (such as beach deposits and tidal notches correlated to them) were instead reported in the headlands of Circeo, Terracina, Torre Capoverde, Sperlonga, and Gaeta (Hearty and Dai Pra, 1986; Bordoni and Valensise, 1999; Ferranti et al., 2006; Antonioli et al., 2018). Within two caves, called *Grotta dei Moscerini* and *Grotta Guattari*, Marra et al. (2019, 2020) report that Schwarcz et al. (1991) dated “backbeach” deposits few meters above sea level to MIS 5a-MIS5c. Within this study, it was possible to retrieve only the paper on *Grotta Guattari* by Schwarcz et al. (1991), reporting that “*the sedimentary fill of Grotta Guattari was deposited over a short interval, commencing soon after the retreat of sea level after stage 5 and terminating at about 57,000 years B.P.*”. As it seems difficult to derive reliable sea-level information from similar indicators, we did not insert these data points into WALIS pending further studies on these sites.

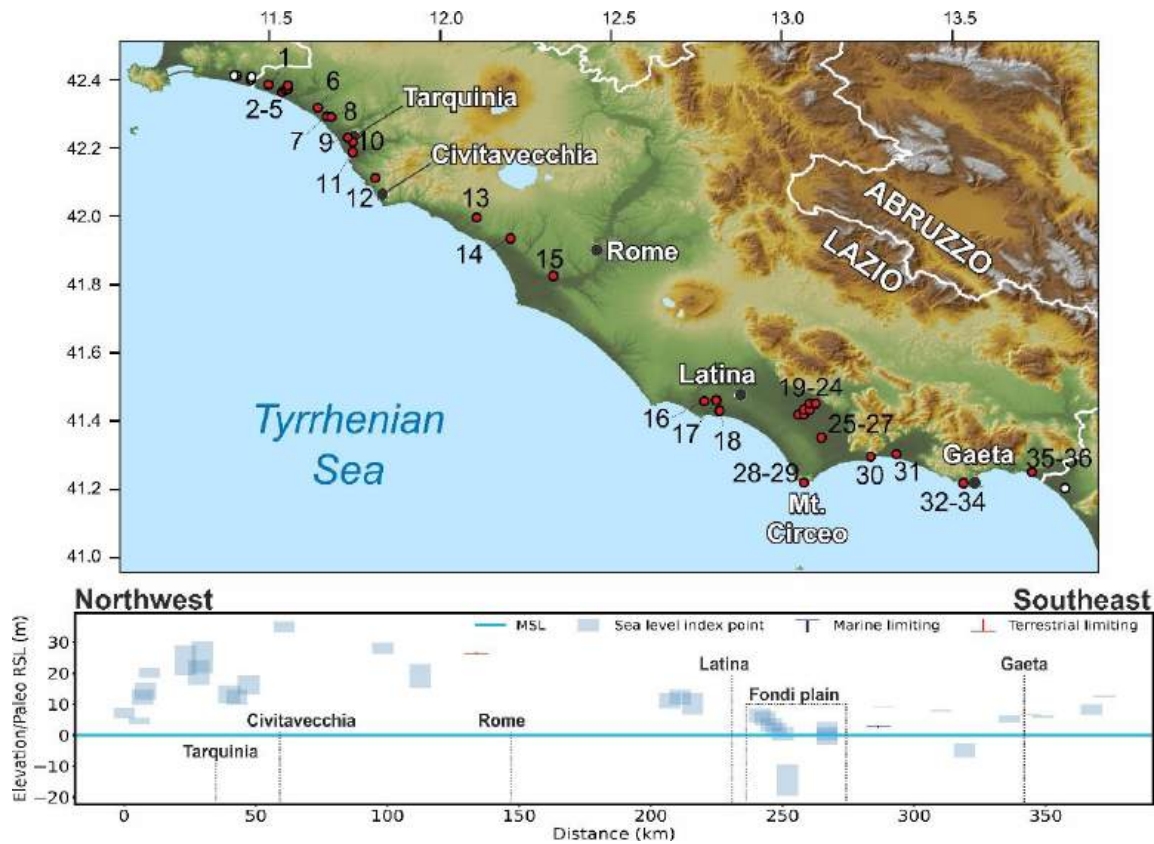


**Figure 75.** Last Interglacial sea level data for Lazio (Italy). Upper panel: Map of sites. Red dots are sites in the region of interest, white dots are other sites within the Western Mediterranean compilation. Lower panel: Distance/Elevation graph, from Northwest (left) to Southeast (right). Sites list: 1: Lasco Del Pozzo (RSL ID 354). 2: Centrale Nucleare Montalto di Castro (RSL ID 475). 3: La Ficonaccia (RSL ID 476). 4: Ponte Rotto (RSL ID 477). 5: Km 115.5 (RSL ID 478). 6: Il Mandrione, right bank of Arrone River (RSL ID 482). 7: Between Arrone and Mignone rivers (RSL ID 481). 8: Aurelia km 103 (RSL ID 483). 9: Northwest of Tarquinia railway station (RSL ID 484). 10: F. delle Serpe (RSL ID 479). 11: Casale Olivastro (RSL ID 480). 12: Monna Felice (RSL ID 494). 13: Monteroni - Cerveteri (RSL ID 495). 14: Casale di Statua (RSL ID 496). 15: Cava Rinaldi (point d) (RSL ID 529). 16: Quadrato (RSL ID 527). 17: Borgo Santa Maria, west of Latina (RSL ID 497). 18: Borgo Sabotino (RSL ID 498). 19: Pontinia I (RSL ID 513). 20: Pontinia II (RSL ID 514). 21: Pontinia III (RSL ID 515). 22: Pontinia IV (RSL ID 516). 23: Pontinia V (RSL ID 517). 24: Pontinia VI (RSL ID 518). 25: Borgo Vodice I (RSL ID 519). 26: Borgo Vodice II (RSL ID 520). 27: Borgo Vodice III (RSL ID 521). 28: Torre Rossa (RSL ID 499). 29: Circeo (Grotta delle Capre) (RSL ID 522). 30: Terracina (Pisco Montano) (RSL ID 523). 31: Fondi plain core ATP4 (RSL ID 508). 32: Torre Capoverde (RSL ID 500). 33: Sperlonga (Sant'agostino) (RSL ID 524). 34: Gaeta (Grotta del Turco) (RSL ID 525). 35: Marina di Minturno (RSL ID 501). 36: Minturno (Monte d'Argento) (RSL ID 526).

#### 7.7.3.4 Campania

South of Latium, Last Interglacial sea-level records in Campania have been reported both from subsurface (i.e., in the Garigliano and Campana coastal plains) and surface (mainly along the Cilento promontory, Sele Plain, Sorrento Peninsula, and Capri island) data (**Figure 76**). The most recent review on the Quaternary evolution of the Campania coastal plains was compiled by Santangelo et al. (2017). These authors reconstructed, with both previously published and new subsurface data, the distribution of a marine unit that was correlated to MIS 5e thanks to a U-Series age on fragments of *C. caespitosa* ( $126 \pm 11$  ka, USeries ID1964) found in the *San Marcellino core* (RSL ID 722, Romano et al., 1994, see below).

In the Garigliano Plain, at the *Masseria Transitiello* site (near the Celiole Aurunci village, RSL ID 3624), Brancaccio et al. (1990) correlated biocalcarenites (AAR ID 168) cropping at few meters above sea level with a tidal notch at 8 m a.s.l. at *Minturno-Monte D'Argento* (RSL ID 526, see the previous section). Six specimens of *Glycimeris glycimeris* from *Masseria Transitiello* have been dated with AAR giving a D/L value ( $0.40 \pm 0.02$ ) corresponding to Amminozone E, correlated to MIS 5e by Hearty and Dai Pra (1986).

In the Campania plain, MIS 5e marine deposits have been found at 50 m b.s.l. in the *San Marcellino core* (RSL ID 722) (Romano et al., 1994). Last Interglacial sea-level proxies were also found at 18 m b.s.l. in the *San Marco Evangelista* borehole (Santangelo et al., 2010), near Caserta, about 28 km far from the modern coastline (RSL ID 739). In this borehole, the Last Interglacial transgression was constrained by the integration of tephro-stratigraphic and radiometric analysis ( $^{40}\text{Ar}/^{39}\text{Ar}$ ) on volcanic layers. Towards the southern edge of the Campania Plain (near the town of Sarno), MIS 5e proxies were reported by Cinque et al. (1987) and Barra et al. (1991) at 23 m b.s.l. (top of marine unit),

constrained by U-dating on *C. caespitosa* and the warm species *Sylvestra seminis* (RSL ID 790).

In the Canello area, towards the northeast border of the Campania plain, Romano et al. (1994) assigned a marine terrace at 50 m a.s.l. to MIS 5e correlating it with the *C. caespitosa* dated at *San Marcellino* core, described above. However, a recent work (Cerrone et al., 2020 submitted, see **Section 6.1** Evolution of the Campania Plain Quaternary coastal graben (southern Apennines): constraints from raised paleoshorelines) correlates the formation of this raised marine terrace to an older MIS, constrained by new U-Series dating. This point was therefore not inserted in the database.

Last Interglacial sea-level proxies in the Sorrento Peninsula crop out mainly on the southern edge, at elevations comparable with those recorded in other tectonically stable areas of the Tyrrhenian Sea. In particular, at *Cala di Ieranto* (RSL ID 721) and *Conca dei Marini* (RSL ID 720) Brancaccio et al. (1978) dated *C. caespitosa* and mollusks to constrain the age of tidal notches at 7.5 m a.s.l. According to these authors, their sample C-2 (USeries ID 1955, on a mollusk shell) yields an age younger than the one obtained for the *C. caespitosa* as a consequence of the opening of the chemical system as confirmed by the high  $^{234}\text{U}/^{238}\text{U}$  ratio. In *Conca dei Marini*, U-Series dating and geomorphological investigations by Iannace et al. (2003) and Riccio et al. (2001) allowed recognition of three distinct Last Interglacial sea-level peaks, with a double notch at 6.5 m (RSL ID 766) and ca. 8 m a.s.l. (RSL ID 3565) and another tidal notch at 3.5 m a.s.l. (RSL ID 767). Moreover, Riccio et al. (2001) tentatively correlated to MIS 5a a tidal notch at 2 m a.s.l. at *Conca dei Marini*, and widespread visible on the southern edge of Sorrento Peninsula (RSL ID 3623). Such age estimation is supported by geomorphological correlation constrained on a date published by Brancaccio et al. (1978).

Ferranti and Antonioli (2007) measured the elevation of the Tyrrhenian tidal notch along the coasts of the Capri Island. The elevation of the notch varies

between 5.2 and 8 m a.s.l., and it has been assigned an MIS 5e age by correlation with a U-Series age on *C. caespitosa* from the bay of Ieranto, at the southern edge of Sorrento Peninsula (RSL IDs from 800 to 822, **Figure 77**) (Brancaccio et al., 1978). In the Sele coastal plain, Brancaccio et al. (1986, 1987) have recognized and dated with AAR two marine deposits bearing *Glycimeris glycimeris* specimens. Based on such dating, the *Gromola ridge* site (up to 13 m a.s.l.) has been correlated to MIS 5c (RSL ID 770), whereas the *Ponte Barizzo ridge* site, reaching an elevation of 25 m a.s.l., to MIS 5e (RSL 769).

Many records of MIS 5e were reported at elevations ranging from 7-8 up to 10-15 m a.s.l. along the coasts of the Cilento promontory. These were assigned an MIS 5 age with AAR, U-Series, and stratigraphic constraints (presence of *P. latus*). In particular, Brancaccio et al. (1990) dated marine deposits bearing *Glycimeris glycimeris* associated with the marine terraces of *Ogliastro Marina* (RSL ID 592), *Sapri* (RSL ID 791-792), and *Palinuro (Lido Ficocella)*, (RSL ID 593). The age provided from the Palinuro site is correlated to MIS 5. Also, the presence of *P. latus* fragments at elevations up to 2-3 m a.s.l. allowed Antonioli et al. (1994b) to correlate a tidal notch in the same elevation range along the Palinuro Cape (RSL ID 732) to MIS 5e.

Between *Ogliastro Marina* (Licosa Cape) and *Agropoli*, Cinque et al. (1994) recognized a flight of marine terraces and related the three lowest ones to the 3 peaks of MIS 5. This chronological attribution has been confirmed by Iannace et al. (2001) using U-Series dating on coralline algae. In this area, the marine terrace at 1.5 m a.s.l. is related to MIS 5a, the one at 5 m a.s.l. to MIS 5c, and two distinct terraces at 9 and 6.6 m a.s.l. have been assigned an MIS 5e age. A detailed morpho-stratigraphic analysis based on cross-cut relationship and Th/U age on speleothems allowed Esposito et al. (2003) to identify MIS 5c and 5a sea-level proxies in the *Cava/Riparo degli Infreschi* at 8.5 and 3.5 m a.s.l., respectively. However, recent works by Bini et al. (2020), reported no evidence for MIS 5c and MIS 5a, proposing

a different paleoenvironment reconstruction of the *Riparo degli Infreschi* outcrop (RSL IDs 3568 to 3576) based on new U-Series dating and tephra correlations. The new U-Series dates were performed on speleothems and calcite filling *L. lithophaga* boreholes; since such materials take shape above sea level, they have been included in the database as terrestrial limiting. The top of *L. lithophaga* boreholes, measured at 8.9 m a.s.l. inside the *Riparo degli Infreschi* has been related to MIS 5e (RSL ID 3568).

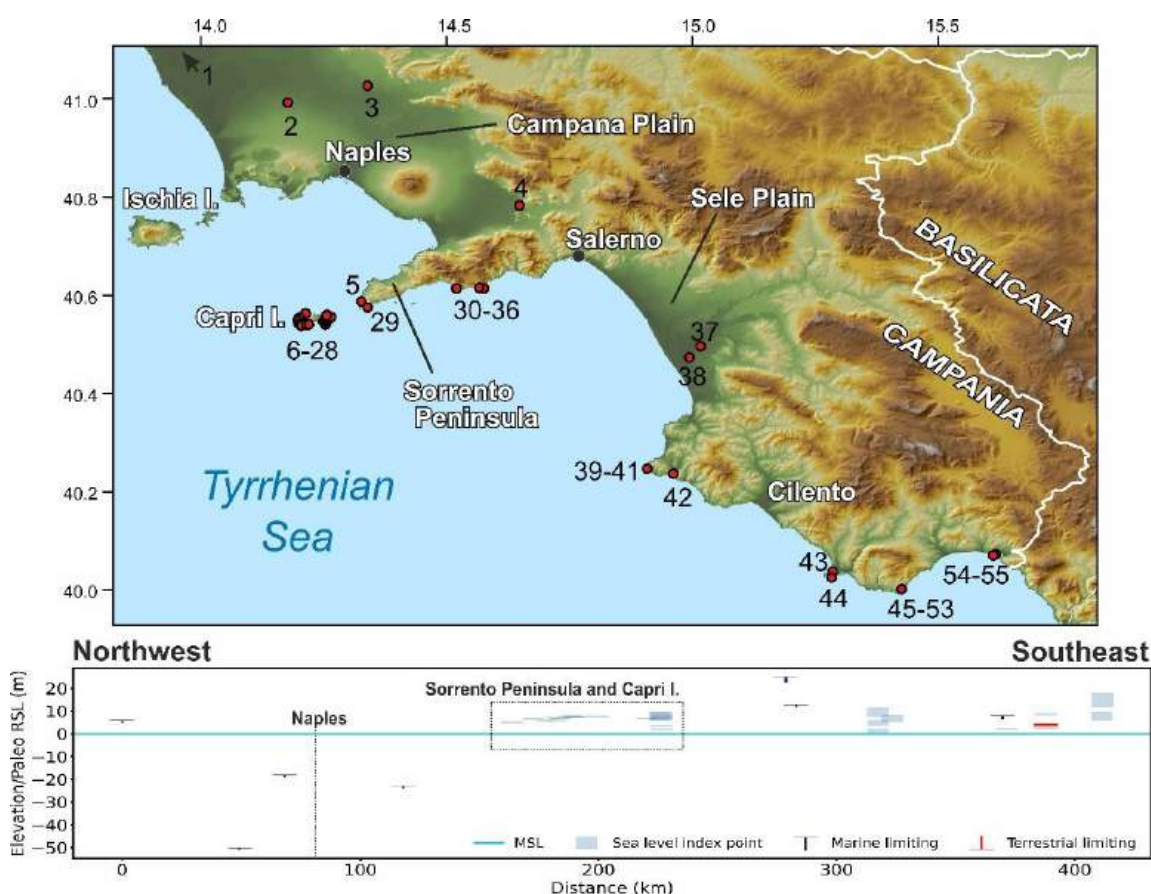


**Figure 76.** Last Interglacial sea level data for Campania (Italy). Upper panel: Map of sites. Lower panel: Distance/Elevation graph, from Northwest (left) to Southeast (right). Sites list: 1: Cellole Aurunci Masseria Transitiello (RSL ID 3624). 2: San Marcellino core (RSL ID 722). 3: San Marco Evangelista (RSL ID 739). 4: Sarno well (RSL ID 790). 5: Mitigliano (RSL ID 3581). 6: Scoglio Ricotta (I) Capri (RSL ID 821). 7: Scoglio Ricotta (II) Capri (RSL ID 822). 8: Grotta Testa del Cavallo Capri (RSL ID 800). 9: Grotta Jannarella Capri (RSL ID 801). 10: P.ta Campitiello Capri (RSL ID 802). 11: Cala del Limmo Capri (RSL ID 803). 12: Cala Articola (II) Capri (RSL ID 805). 13: Cala Articola (I) Capri (RSL ID 804). 14: Cala Articola (III) Capri (RSL ID 806). 15: Grotta Verde (I) Capri (RSL ID 807). 16: Grotta Verde (II) Capri (RSL ID 808). 17: Gr. Belvedere Capri (RSL ID 809). 18: Gr. Fontolina Capri (RSL ID 810). 19: I Faraglioni

Capri (RSL ID 811). 20: Porto di Tragara (I) Capri (RSL ID 812). 21: Porto di Tragara (II) Capri (RSL ID 813). 22: P.ta di Masullo Capri (RSL ID 814). 23: a vascio funno Capri (RSL ID 815). 24: Cala Materniana Capri (RSL ID 816). 25: Gr. Bianca (I) Capri (RSL ID 817). 26: Gr. Bianca (II) Capri (RSL ID 818). 27: P.ta della Chiavica Capri (RSL ID 819). 28: P.ta del Monaco Capri (RSL ID 820). 29: Cala di Ieranto (RSL ID 721). 30: Vettica Maggiore (RSL ID 823). 31: Grotta dello Smeraldo (RSL ID 798). 32: Conca dei Marini (III) Site I (RSL ID 767). 33: Conca dei Marini (II) Site I (RSL ID 766). 34: Conca dei Marini (I) Site I (RSL ID 720). 35: Conca dei Marini (V) (RSL ID 3623). 36: Conca dei Marini (IV) Site I (RSL ID 3565). 37: Ponte Barizzo (RSL ID 769). 38: Gromola (RSL ID 770). 39: Licosa Cape (III) (RSL ID 728). 40: Licosa Cape (II) (RSL ID 727). 41: Licosa Cape (I) (RSL ID 726). 42: Ogliastro Marina Baia Arena (RSL ID 592). 43: Palinuro Lido Ficocella (RSL ID 593). 44: Palinuro Cape (RSL ID 732). 45: The Riparo Infreschi cave (I) (RSL ID 3568). 46: The Riparo Infreschi cave (II) (RSL ID 3569). 47: The Riparo Infreschi cave (III) (RSL ID 3570). 48: The Riparo Infreschi cave (VI) (RSL ID 3573). 49: The Riparo Infreschi cave (IX) (RSL ID 3576). 50: The Riparo Infreschi cave (VIII) (RSL ID 3575). 51: The Riparo Infreschi cave (VII) (RSL ID 3574). 52: The Riparo Infreschi cave (V) (RSL ID 3572). 53: The Riparo Infreschi cave (IV) (RSL ID 3571). 54: Sapri (II) (RSL ID 792). 55: Sapri (RSL ID 791).



**Figure 77.** Tidal notch at Capri Island, a *Vascio Funno* site (RSL ID 815). Photo by A. Ascione

#### 7.7.3.5 Basilicata and Calabria, Tyrrhenian side

The Last Interglacial sea-level proxies on the Tyrrhenian seaside of Basilicata have been attributed to the marine terraces up to ca. 8-10 m a.s.l (**Figure 78**), from Fiumicello to Castrocucco (Carobene et al., 1986; Carobene and Dai Pra, 1991), and northern Calabria coast, from Castrocucco to nearby Cetraro (Torre la Testa, Carobene et al. 1986; Carobene and Dai Pra 1990). Such interpretation is based on a geomorphological correlation derived from the identification of the Middle-Late Pleistocene terraces, which have been constrained by U-Series and AAR dating on *C. caespitosa* and *Bivalvia* respectively. However, recently Cerrone et al. (2018, 2021a) have rejected such dating and have reconstructed the evolution of the area spanning from nearby Fiumicello (Basilicata) to Scalea (Calabria), providing new U-Series dating on the marine deposits (biocalcarenes bearing *C. caespitosa* corals) associated with the marine terraces corresponding to MIS 5a, 5c, and 5e, which stand up to some tens of meters.

The promontory of Capo Vaticano (RSL ID 267 to 270, 314 to 316, 3430, and 3431) has been deeply investigated in the last decades and many dating (OSL, TL, and U-Series) have been provided, but a debate on the age and spatial distribution of the marine terraces of the area is still open due to the complexity of the structural setting. Bianca et al. (2011), performed OSL dating on unconsolidated sandy layers associated with marine terraces, and correlated to MIS 5c the marine terrace at 50 m a.s.l. in Vibo Marina. The 5c terrace of Bianca et al. (2011) reaches 175 m a.s.l. at Capo Vaticano (RSL ID 269). Such correlation is strengthened by TL dating of Balescu et al. (1997). However, Pata (1947) reported *P. latus* specimens within the +50 m a.s.l. terrace in Vibo Marina (RSL ID 267), which allowed Dai Pra et al. (1991), Dumas et al. (1991), and Roberts et al. (2013) to consider such terrace of MIS 5e age. The last interpretation is supported by

Roberts et al. (2013) based on U-Series dating (USeries ID 2665 and 2666) and by the use of a synchronous correlation method.

Starting from the work of Gignoux (1913) who reported the presence of *P. latus* and Senegalese fauna in the *Bovetto* (RSL ID 306) and *Ravagnese* areas (RSL ID 304 and 305) up to ca. 130 m a.s.l., this area was investigated by Hearty et al. (1986) and Balescu et al. (1997), respectively dating the deposits with AAR and TL. Another terrace, at Altibano (RSL ID 313), was correlated by Balescu et al. (1997) to MIS 5e, while according to Dumas et al. (1988) and Dumas et al. (1987) the same terrace was formed before the Last Interglacial.

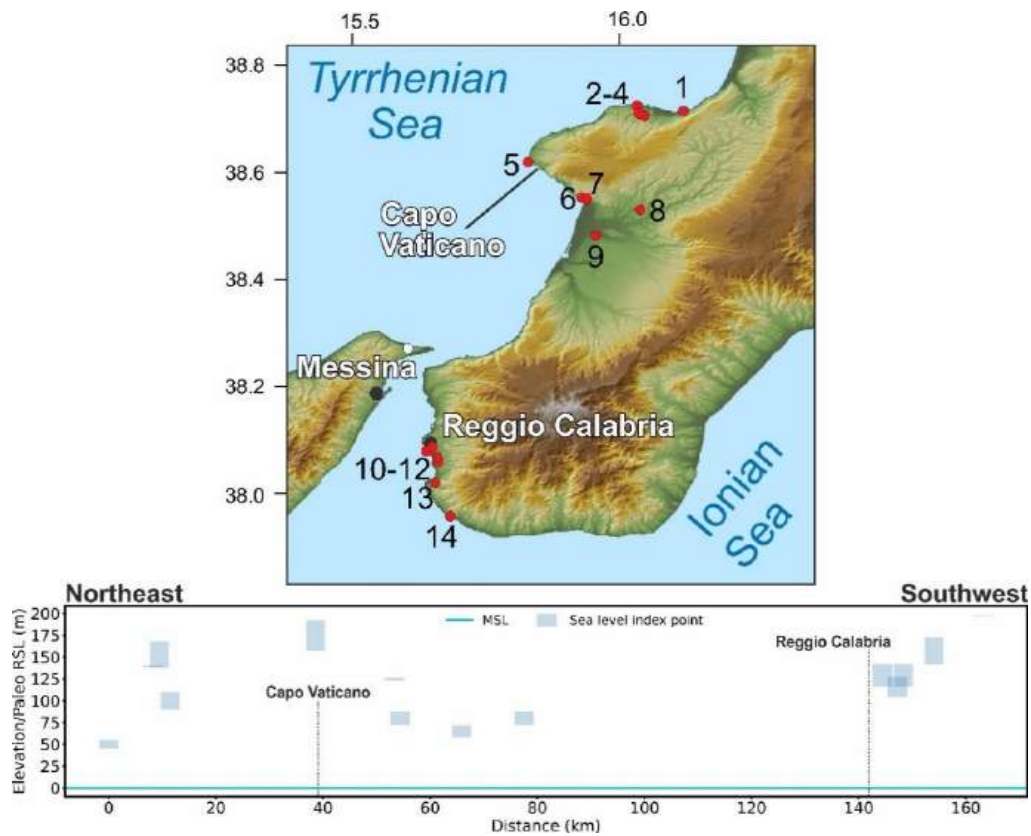


**Figure 78.** Last Interglacial sea-level data for the Tyrrhenian side of Calabria and Basilicata (Italy). Upper panel: Map of sites. Red dots are sites in the region of interest, white dots are other sites within the Western Mediterranean compilation. Lower panel: Distance/Elevation graph, from Northeast (left) to Southwest (right). Sites list: 1: Vibo Marina (RSL ID 267). 2: Paradisoni (RSL ID 315). 3: Sacco (RSL ID 316). 4: Briatico (RSL ID 268). 5: Capo Vaticano (RSL ID 269). 6: Nicotera (RSL ID 270). 7: Gioia Tauro Contrada Ianni (nearby Nicotera) (RSL ID 3431). 8: Gioia Tauro basin (RSL ID 3430). 9: Rosarno (RSL ID 314). 10: Ravagnese (RSL ID 304). 11: Trombaca (RSL ID 312). 12: Bovetto (RSL ID 306). 13: Nocella Pellaro (RSL ID 1378). 14: Altibano (RSL ID 313).

### 7.7.3.6 The Ionian coast of Basilicata and Calabria

Along the Ionian Sea coasts of Calabria and Basilicata (**Figure 79**) we identified several reports of the Last Interglacial shorelines. The Pleistocene marine terraces in Crotona and Isola di Capo Rizzuto (RSL ID 563 to 566, 1379, 3428), were first reported by Cortese (1895), and have been deeply studied by successive authors (Gignoux, 1913; Cosentino and Gliozzi, 1988; Belluomini et al., 1988; Selli, 1962; Palmentola et al., 1990; Mauz and Hassler, 2000; Ruggieri, 1948; Zecchin et al., 2009; Nalin and Massari, 2009). The MIS 5e marine terrace in this area has been traced up to ca. 80-110 m a.s.l., and was dated with AAR (Belluomini et al., 1988) and TL (Mauz and Hassler, 2000). However, based on such dating, the *Capo Colonna* Terrace (RSL ID 3634) has been correlated either to 5c or 5a. However, Nalin et al. (2012) and Palmentola et al. (1990) found *P. latus* fossils in the *Capo Colonna* Terrace. New findings of *P. latus* at the Crotona Peninsula have been reported by Bracchi et al. (2011) and Nalin et al. (2012).

In Trebisacce (RSL ID 324), at the northern border of the Sibari coastal plain, Cucci (2004) attributed an MIS 5e age (AAR IDs 97 and 98) to the marine terrace at 128 m a.s.l. The elevation of the MIS 5e marine terrace mapped by Cucci (2004) between Trebisacce and Lauropoli spans between 145 m to 115 m a.s.l. In the database, only the inner edge of the marine terrace corresponding to the Trebisacce site has been included because here a direct age constraint has been provided.

A few kilometers northeast from Trebisacce, in *Vaccarizzo* site (RSL ID 442), Santoro et al. (2009) constrained the MIS 5e marine terrace at 125 m a.s.l. by ESR dating on *Cardium sp.* (ESR ID 100).

Even if a very well developed flight of marine terraces (decreasing in elevation towards North-East) crops out along the Ionian coast of Basilicata, their age is poorly constrained.

In *Piano San Nicola* (RSL ID 416), near the town of Nova Siri, the marine terrace, which inner edge was reported at 90 m a.s.l., was correlated to MIS 5c or 5a by AAR dating (Dai Pra and Hearty 1988). An MIS 5e terrace at the same site has been identified based on geomorphological correlation. But, as no age constraints have been provided, it is not included in the database.

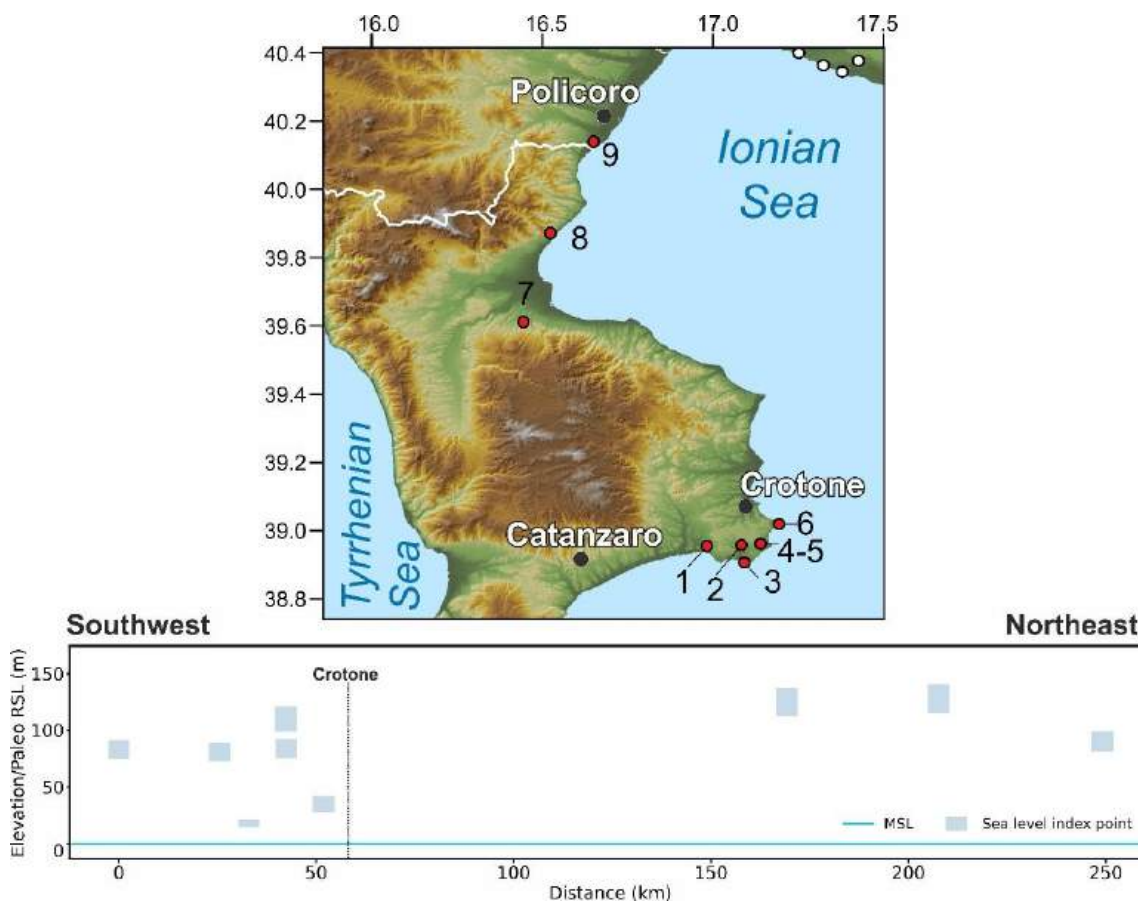


**Figure 79.** Last Interglacial sea-level data for the Ionian side of Calabria and Basilicata (Italy). Upper panel: Map of sites. Red dots are sites in the region of interest, white dots are other sites within the Western Mediterranean compilation. Lower panel: Distance/Elevation graph, from Southwest (left) to Northeast (right). Sites list: 1: San Leonardo di Cutro (RSL ID 563). 2: Manca della Mozza. (RSL ID 566). 3: Isola di Capo Rizzuto (RSL ID 565). 4: Capo Rizzuto (RSL ID 564). 5: Crotona (II) (RSL ID 3428). 6: Crotona (RSL ID 1379). 7: Capo Colonna Terrace (RSL ID 3634). 8: Vaccarizzo (RSL ID 442). 9: Trebisacce (RSL ID 324). 10: Piano San Nicola (RSL ID 416).

#### 7.7.3.7 Puglia

Along the Ionian coast of Puglia Region (**Figure 80**), near the border with Basilicata, at *Ponte del Re-Castellaneta* site (RSL ID 355) a marine terrace up to 40 m a.s.l. was correlated with MIS 5e thanks to the presence of Senegalese fauna with *P. latus* (Boenzi et al., 1985). The correlation was later confirmed by AAR dating on marine deposits bearing *Glycymeris* (Dai Pra and Hearty, 1988). Eastwards of this site, in the Taranto area and Chéradi Islands, several outcrops were studied for nearly one century (Gignoux 1913; Cotecchia et al. 1969; Hearty and Dai Pra 1992; Gigout 1960; Gigout 1962; Verri and De Angelis D'Ossat 1899; Richetti 1967; Caldara 1987). These deposits are characterized by the widespread presence of *P. latus*, Senegalese fauna and *C. caespitosa* corals (RSL ID 223 to 226, 228, 230, 355, 695 to 705, 3630 to 3632).

In particular, the section cropping out at *Il Fronte* (RSL ID 230, near the city of Taranto) has been recently analyzed in detail for stratigraphy, chronology, sedimentology, and paleoecological aspects, highlighting the possibility to use this place as a Global Stratotype Section and Point (GSSP) (Amorosi et al. 2014). The outcrop of *Il Fronte* site consists of an 8.5 m thick succession made up of 5 marine Units. Detailed facies analyses integrated with sequence stratigraphy and U-series dating allowed Amorosi et al. (2014) to reconstruct in detail sea-level fluctuations during the MIS 5e at *Il Fronte* site. In particular, the base of the succession is characterized by nearshore deposits which evolve upwards to inner-shelf and middle-outer shelf deposits. The MIS 5e coastline elevation in this area has been traced by Dai Pra and Stearns (1977) up to 35 m a.s.l. in Ponte Romano (RSL ID 3631).

South of Taranto, specimens of *P. latus* were reported in *Torre Castelluccia* (RSL ID 705), *Torre Castiglione* (RSL ID 696), and near Gallipoli. At *Torre Castelluccia*, a pocket beach at 3 m a.s.l. has been constrained to the Amminozone

C (Dai Pra and Hearty 1988), while the MIS 5e shoreline, containing *P. latus*, was located at 28 m a.s.l. in the surroundings of *Lizzano* (RSL ID 695). The MIS 5e terrace in *Torre Castiglione* (RSL ID 696) has been reported at 2.5 m a.s.l. (Dai Pra and Stearns 1977). Moreover, at *Gallipoli* site (RSL ID 3625, 3267, and 3268), *Glycymeris* specimens sampled at 8-10 m a.s.l. were constrained with AAR to MIS 5e (Dai Pra and Hearty 1988).

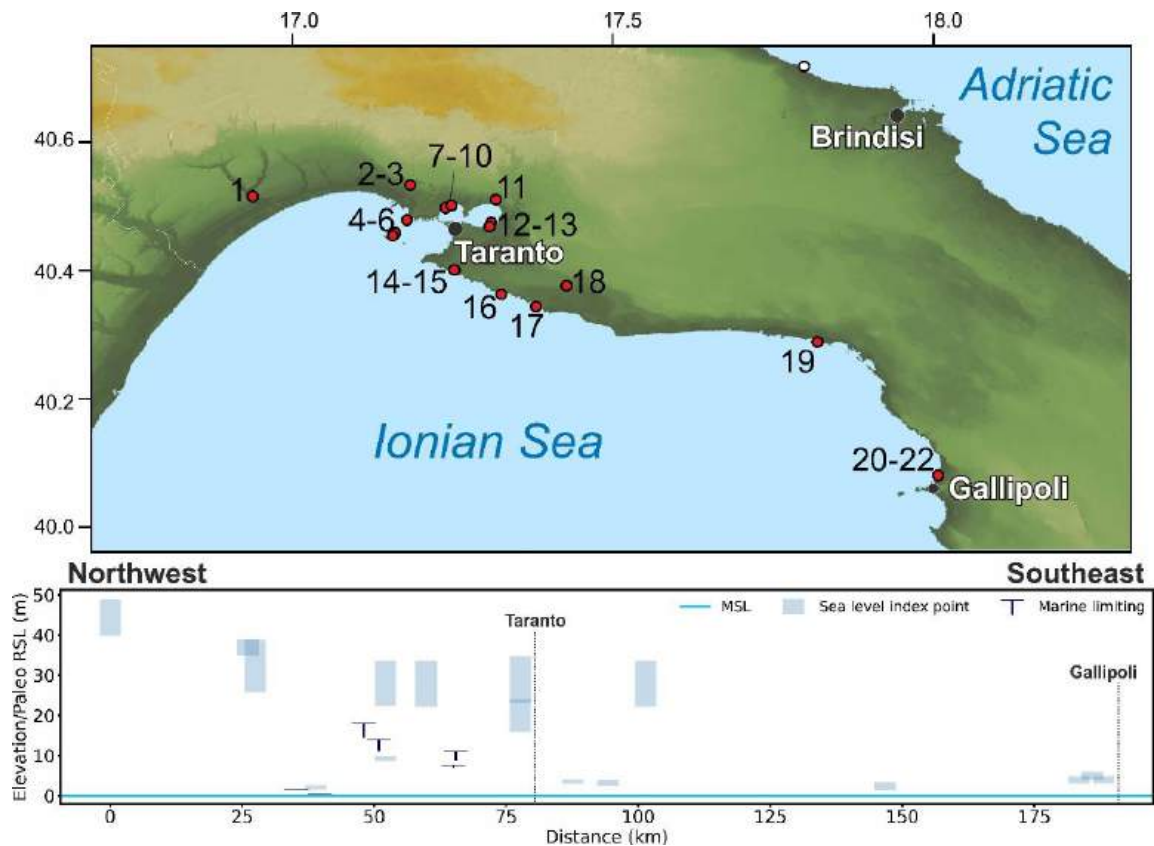


**Figure 80.** Last Interglacial sea level data for the Ionian side of Puglia (Italy). Upper panel: Map of sites. Red dots are sites in the region of interest, white dots are other sites within the Western Mediterranean compilation. Lower panel: Distance/Elevation graph, from Northwest (left) to Southeast (right). Sites list: 1: Ponte del Re (RSL ID 355). 2: Ponte Romano Taranto (RSL ID 3631). 3: Masseria S. Giovanni Taranto (RSL ID 697). 4: Punta Rondinella (RSL ID 224). 5: Punta lo Scanno (RSL ID 225). 6: Apodonia (RSL ID 228). 7: Masseria Ruggiero Taranto (RSL ID 3632). 8: Masseria Bagnara (RSL ID 704). 9: Masseria Santa Teresiola (RSL ID 223). 10: Masseria Santa Teresiola (II) (RSL ID 3630). 11: Masseria San Pietro (RSL ID 699). 12: Il Fronte (RSL ID 230). 13: Masseria Pantaleo (RSL ID 701). 14: Carelli Between Carelli and Saturo harbour (RSL ID 698). 15: Il Posto Between Il Posto and Torre Castelluccia (RSL ID 700). 16: Punta della Baracca (RSL ID 226). 17: Torre Castelluccia (RSL ID 705). 18: Lizzano (RSL ID 695). 19: Torre Castiglione (RSL ID 696). 20: Torre Sabea Gallipoli (RSL ID 3625). 21: Gallipoli (RSL ID 3627). 22: Torre San Giovanni Gallipoli (RSL ID 3628).

Towards the Adriatic Sea side of Puglia (**Figure 81**), at the bottom of *Grotta Romanelli* (RSL ID 1319), a marine deposit (elevation between 7 and 8 m a.s.l.) was correlated with MIS 5 (Blanc 1920,1928) and re-assessed by Cosentino and Gliozzi (1988). These authors, though, wrongly reported the presence of *P. latus* (Mastronuzzi et al. 2007). Based on stratigraphic correlations and U-Series dating of flowstones, Mastronuzzi et al. (2007) reported a series of sea caves along the southern Salento coasts between 0 up to 10 m a.s.l (RSL IDs 1319,1320,1323 and 1324, 3635). The sea caves were reshaped by the sea during the MIS 9.3, MIS 5e and MIS 5a. We included in the database only the speleothem (U-Series ID 2958) constraining the MIS 5a at 3 m a.s.l. in the *Grotta del Diavolo* site (RSL ID 3635) because the others dating of Mastronuzzi et al. (2007) allow defining a sea-level transgression older than MIS 5. Overall, according to the evolution modeling proposed by Mastronuzzi et al. (2007), such sea caves have been reshaped by the sea during the MIS 5e testifying to the tectonic stability of the area.

In the Apulian Tavoliere plain, the dating of *Glycymeris sp.* from *MM4* borehole (De Santis et al. 2010) allowed to include in the database three marine limiting datapoints (RSL ID 452 to 454). North of the Gargano promontory, near Ripalta at the mouth of the Fortore River floodplain, Bordoni and Valensise (1999) tentatively associated the coastal plain at 25 m a.s.l. with MIS 5e based on the dating of the Holocene plain (Mastronuzzi et al. 1989). Due to the lack of robust direct dating, this site has been inserted in the database as a limiting point (RSL ID 1317).

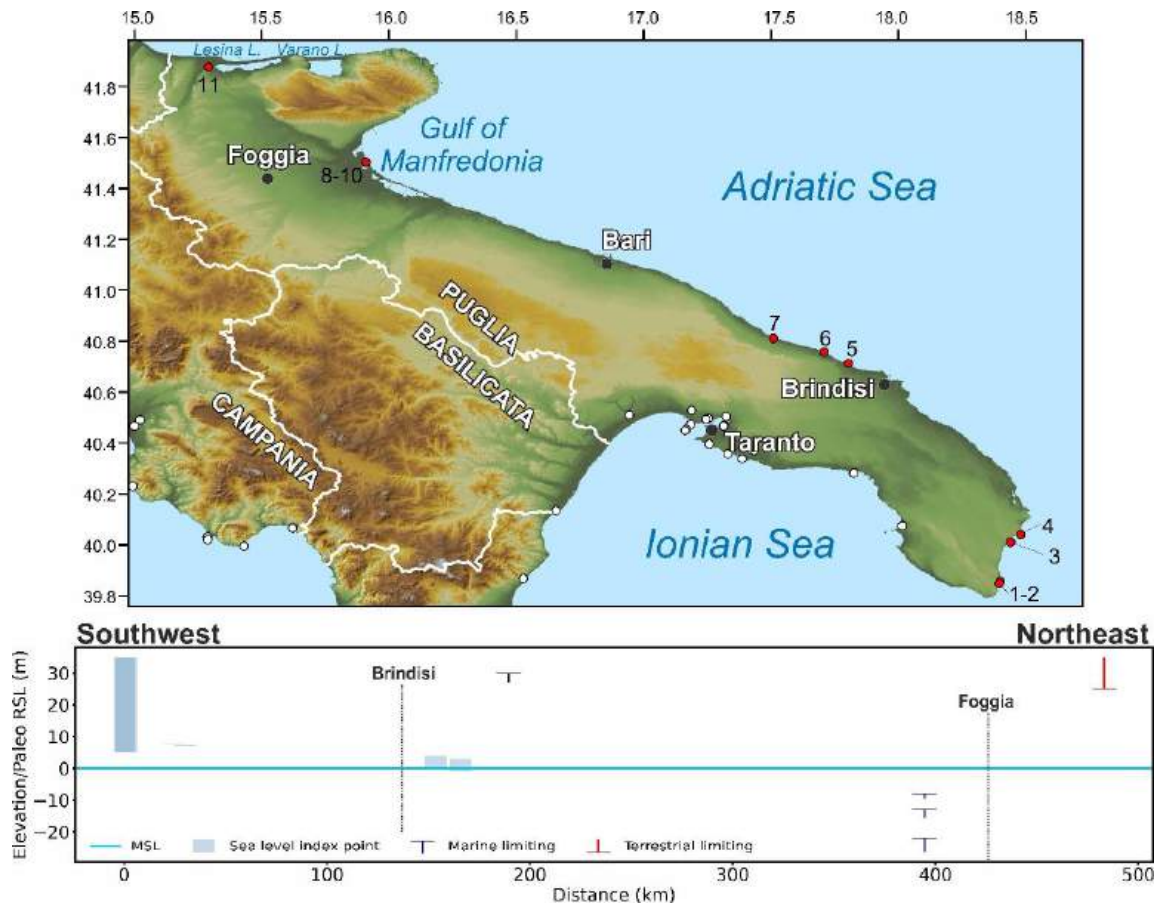


**Figure 81.** Last Interglacial sea-level data for the Adriatic side of Puglia (Italy). Upper panel: Map of sites. Red dots are sites in the region of interest, white dots are other sites within the Western Mediterranean compilation. Lower panel: Distance/Elevation graph, from Southwest (left) to Northeast (right). Sites list: 1: Marina di Novaglie Southern Site of Marina di Novaglie (RSL ID 1324). 2: Marina di Novaglie Northern Site of Marina di Novaglie (RSL ID 1323). 3: Grotta Romanelli (RSL ID 1319). 4: Grotta delle Striare (RSL ID 1320). 5: Torre Mattarelle - Torre Guaceto (RSL ID 1321). 6: Torre Santa Sabina (RSL ID 1322). 7: Villanova-Monopoli (RSL ID 1318). 8: MM4 borehole Unit 13 (RSL ID 452). 9: MM4 borehole Unit 11 (RSL ID 453). 10: MM4 borehole Unit 10 (RSL ID 454). 11: Fortore River (RSL ID 1317).

#### 7.7.3.8 Molise, Abruzzo and Marche

The coastal sector from Molise to the southern boundary of Romagna Plain (**Figure 82**) extends for about 300 km and is generally characterized by narrow sandy beaches occurring at the base of the pre-Quaternary bedrock, that is commonly very close to the Holocene coastal morphostratigraphic units and often separated from them by a cliff of 5-15 m of elevation. In some limited sectors, the rocky coast is facing the sea as near Vasto, between Fossacesia and Ortona, Numana and Ancona, Fano and Pesaro and Pesaro and Gabicce.

The previous reviews and databases of sites with deposits of Last Interglacial in the Marche region described in Ferranti et al. (2006) are derived from the work by Vannoli et al. (2004) in which some of the terraces occurring along the coast of the Marche region have been attributed to the Last Interglacial. Anyhow, the surveys carried out in the framework of the new geological map of Italy (Guerrara and Tramontana, 2011) and other recent investigations didn't find any clear evidence of coastal deposits related to the Last Interglacial. On the contrary, the terraces consist of alluvial deposits dating to the Upper Pleistocene, but they are referred to as MIS 3 and 2. In light of this new information, the sites described in Ferranti et al. (2006) as the inner margin of terraces are considered in our compilation as alluvial and not related to MIS 5e.

#### 7.7.3.9 Emilia Romagna

The alluvial plains facing the Italian side of Northern Adriatic, from Rimini to Monfalcone, are characterized by a subsiding tectonic setting, mainly related to the crustal flexuring connected to the Apennines and the compaction of Quaternary sediments (cf. Carminati et al., 2003; Ferranti et al., 2006). Thus, the deposits of MIS 5e are not cropping out in this area, but they are buried in the subsoil of the coastal plain at depths ranging from 35 to 120 m b.s.l. Anyhow, in Emilia-Romagna the Geological Survey of the region collected a vast database of underground data (i.e. logs of stratigraphic boreholes, geotechnical tests, and water wells) in which a significant number of cores sampled the coastal deposits of MIS 5e (**Figure 82**). The database has been mainly produced in the framework of the new geological map (CARG project) but has been also checked and tuned with specific stratigraphic and paleoenvironmental studies. In particular, Amorosi et al. (1999, 2004) defined the main architecture of the subsoil and characterized the depositional units for their sedimentological and palynological content.

Along the northwestern coast of Adriatic, the sediments dated to the Last Interglacial correspond to a coastal wedge consisting of a transgressive-regressive cycle, which has an average maximum thickness of 15-20 m, overlapping over the previous alluvial units, generally dating to MIS 6 (an example is reported in **Figure 83**). The marine transgression expanded on the plain and induced the progressive shifting to lagoonal, beach, and marine environments. These deposits have been later covered by the seaward progradation of deltaic systems, which can be generally related to the Po river system and the streams fed by Northern Apennines. The development of deltas probably occurred during the marine highstand of MIS 5e, around the peak of sea level. Thus, the beach facies recorded at the top of the regressive cycle are considered index points of the past RSL with uncertainty between 7 and 10 m. A more significant role is played by the lagoonal and back-

barrier deposits connected to the beach ridges, which have to be considered the most representative index point, with uncertainty between 0 and -2 m with respect to the coeval RSL. Differently, the facies of prodelta and marine platform deposited several meters below sea level and are considered only as marine limiting points. The recognition of lagoonal and back-barrier facies is based on the micropaleontological content, but also on the mollusk association consisting of *Cerastoderma glaucum*, *Loripes* sp., *Hydrobia* sp., *Bittium* sp., *Abra* sp, and *Cerithium* sp.

The marine transgression invested large areas and after the submersion, the action of waves developed an important ravinement surface that in many cases eroded almost completely the previous sediments connected to the sea-level rise (Figure 24). Thus, the beach and marine deposits of MIS 5e are often directly in contact over the older alluvial plain and separated from them by a sharp ravinement surface. It is worth noting that this sedimentary unconformity is rather easy to be recognized in the cores in northern Adriatic, representing a major tool for stratigraphic correlation, anyhow, it is not a synchronous surface, but it is time-transgressive (Massari et al., 2004; Amorosi et al., 2008 a-b).

Molluscs association is not a major chronological marker of the Last Interglacial in northern Adriatic, as the sediments are not characterized by the occurrence of Senegalese fauna with *P. latus*. Anyhow, the paleobotanical analyses carried out in few selected cores recognized the pollen associations related to warm temperate climate, characterized by broad-leaves trees which can be correlated to the general Eemian biostratigraphic unit identified also in other cores of northern Italy (Massari et al., 2004; Mullenders et al., 1996; Ravazzi et al., 2014) and, in a broader scale, in northern Europe (Peeters et al., 2019). In light of this information, in our database, the stratigraphic unit of the coastal deposits of MIS 5e has been named with the generic definition of “Adriatic Tyrrhenian (Eemian pollen unit)”. In Emilia-Romagna, reference cores for the pollen studies are the site *240-S13*, near

Russi (RSL ID 1327), *240-S8*, near Milano Marittima (RSL ID 1308), and *223-S17*, at the southern boundary of Valli di Comacchio (RSL ID 1326), and S1, south of Rimini (Amorosi et al., 1999; Campo et al., 2020).

Important geochronological constraints of these biostratigraphic units have been supported by Ferranti et al. (2006) through the ESR dates of the beach deposits forming the top of the coastal wedge and collected in cores *204-S8* (117.0 m b.s.l., RSL ID 1308), *222-S2* (112.5 m b.s.l., RSL ID 1310) and *205-S10* (85.5 m b.s.l., RSL ID 1309). They gave an age of  $129\pm 18$  ka,  $154\pm 26$  ka, and  $124\pm 20$  ka, respectively, demonstrating that the unit formed during MIS 5e. At the moment these are the only published geochronological data in NW Adriatic for the Last Interglacial, whereas some other OSL dates for younger stages of MIS 5 have been recently produced (Amorosi et al., 2016; Campo et al., 2020).

The comparison between the elevation of the markers of the Last Interglacial with the maximum elevation reached by the sea during the highstand (i.e. some meters a.s.l.), clearly indicates that the index points recognized in the subsoil of Emilia-Romagna are not useful for investigating the paleo global mean sea level. On the contrary, these data have been used by Ferranti et al. (2006) and Antonioli et al. (2009) for assessing the average rate of tectonic subsidence that occurred since the deposition of the coastal wedge of MIS 5e.

The coastal plain south of the course of the modern Po River has been significantly involved in the current tectonic deformation related to the crustal flexuring. In particular, the regional crustal subsidence increases with an SW trend; moreover, the system of thrusts and folds affecting the most external and buried part of the Apennines produced important relative uplift and downlift movements. Despite the vertical shifting suffered by the local sites, the limited chronological interval of the MIS 5e and their rather easy recognition in the subsoil allowed Amorosi et al. (2009) to reconstruct a part of the coastline and the inner limit of the lagoons extent during the Last Interglacial in the north-western Adriatic. Recently

the paleogeographic setting at the MIS 5e highstand has been strongly updated and improved for the area between Rimini and the Po Delta by Campo et al. (2020). The analysis of the database of Emilia-Romagna allows mapping the environmental facies of the coastline existing at the marine highstand. We used these data, in combination with the other available markers detected in the subsoil of Northern Italy, to depict the coastline from the Apennines to the Dinaric Alps, for a length of about 300 km (**Figure 82** and **Figure 84**).

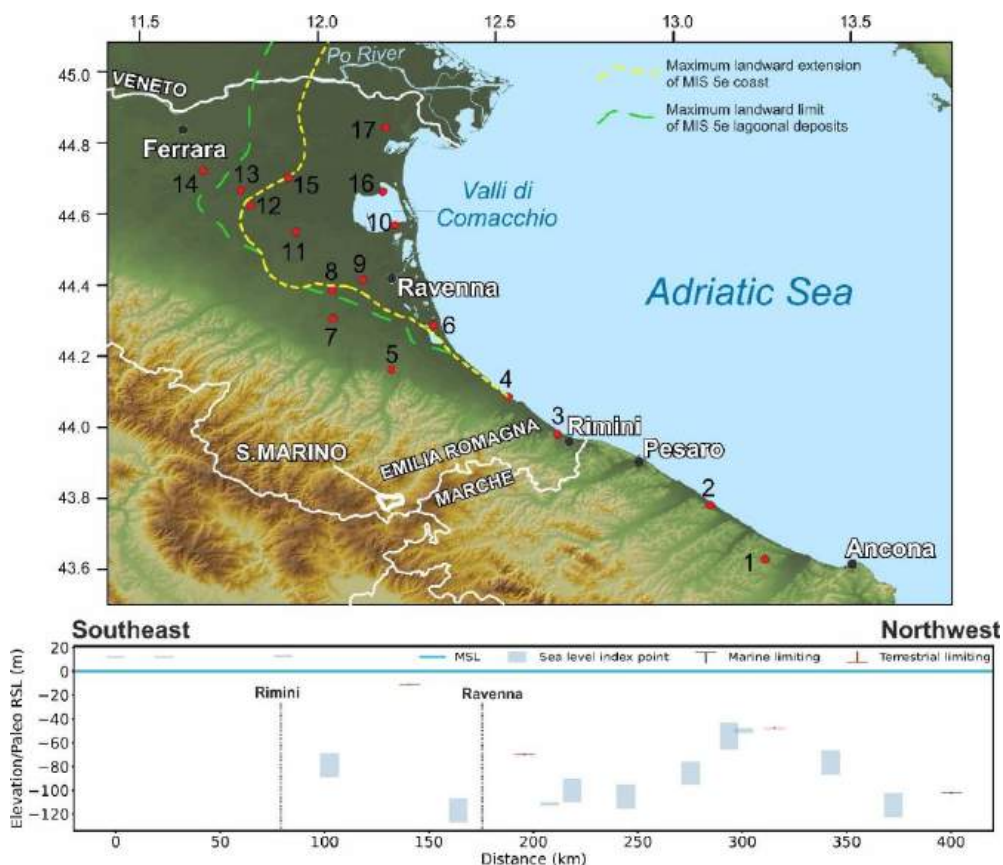


**Figure 82.** Last Interglacial sea level data for Marche and Emilia Romagna (Italy). Upper panel: Map of sites. Lower panel: Distance/Elevation graph, from Southwest (left) to Northeast (right). The lines depicting the most inner position of the coastline and of a lagoon deposits of the MIS 5e are derived from Campo et al. (2020). Sites list: 1: Metauro River (RSL ID 1333). 2: Arzilla River (RSL ID 1332). 3: Conca River (RSL ID 1331). 4: 256-S3 Viserba Core S3 (RSL ID 1330). 5: 255-S4 Cesena Core S4 (RSL ID 1329). 6: 240-S8 Milano Marittima Core S8 (RSL ID 1308). 7: 240-S2 Villafranca Core S2 (RSL ID 1328). 8: 240-S13 Russi Core S13 (RSL ID 1327). 9: 223-S12 Ravenna Core S12 (RSL ID 1325). 10: 223-S17 Mandriole Core S17 (RSL ID 1326). 11: 222-S2 Voltana Core S2 (RSL ID 1310). 12: 204-S17 Argenta Core S-17 (RSL ID 1313). 13: 204-S4 Consandolo Core S4 (RSL ID 1312). 14: 204-S15 Marrara Core S-15 (RSL ID 1315). 15: Core 204-S16 Core S-16 (RSL ID 1314). 16: 205-S10 Comacchio Core S10 (RSL ID 1309). 17: Core F187\_S1 Valle Giralda (RSL ID 1307).

#### 7.7.3.10 Veneto

In the Venetian Plain (**Figure 84**) the number of available cores for investigating the MIS 5e marine highstand is limited but, North of the modern course of the Po River, the coastal plain has not been deeply involved in significant tectonic deformations as it is part of the foreland basin of both Alps and Apennines. Thus, despite the general regional subsidence affecting this area, the sediments of Late Quaternary have not been locally deformed by thrusts and folds and this setting preserved the original geometric relationships existing between the different sectors of the coastal wedge formed during the Last Interglacial (**Figure 83**).

In the Lagoon of Venice, the deposits of MIS 5e are found underground at a depth spanning between 90 and 55 m b.s.l. and often the stratigraphic cores document a transgressive-regressive cycle. This trend can be recognized according to the landward migration of the marine facies at the base of the sequence, which overlaps on the pre-existing alluvial plain, and that was followed by the progradation of deltas and related lagoons. Near Valle Averno (core *CARG 11*, RSL ID 1304), in the southern part of the Venice Lagoon, deltaic sediments are found over the alluvial deposits between 67 and 64 m b.s.l., covered by littoral facies at 64 and 62 m b.s.l., and after by lagoon deposits at 62-60.5 m b.s.l. (Donnici and Serandrei-Barbero, 2004). According to stratigraphic correlations, the vertical succession documents the marine transgression and the successive deltaic progradation with the formation of lagoon environments (Tosi et al., 2007b). A rather similar stratigraphic setting is documented also in the northern sector of Venice Lagoon, near Portegrandi (core *CARG 12*, RSL ID 1302), where paralic deposits are found between 70 to 55 m b.s.l. According to foraminifera analyses, from 70 to 65 m b.s.l. the depositional environments pass from neritic to lagoon, whereas, from 65 to 55 m b.s.l. the sediments are mainly sandy with few fossils, probably related to the delta front (Tosi et al., 2007a). This core can be used as an

example of the rather low importance of this sequence for constraining the position of the sea level at the peak of the marine transgression of MIS 5e as the top portion could be used only as a marine limiting point at 55 m b.s.l.

In Venice, the reference stratigraphy for Pleistocene is the core *VE-1* and *VE-1bis* (RSL ID 1303), that were drilled in 1971 in the Tronchetto Island, NW of the city center (Kent et al., 2002; Massari et al., 2004 and references therein) and were analyzed for sedimentological, pollen and foraminiferal content. Core *VE-01* arrived at a depth of 950 m and, as explained in Massari et al. (2004), the tie point between the two cores is represented by a characteristic Eemian pollen assemblage correlative to MIS 5e at 74.30 m b.s.l. in the *VE-1* well and at 73.38 m b.s.l. in *VE-1bis*. The detailed investigations allowed to recognize biostratigraphic units, mainly based on pollen assemblages for Upper Pleistocene (Mullenders et al., 1996). According to Massari et al. (2004), in the core the base of the MIS 5e marine transgression is found at 78 m of depth and sediments belong to coastal facies up to to 66 m of depth and are covered by alluvial and lagoonal sediments. At 59.40-59.00 m of depth in well *VE-1bis* a poorly developed lagoonal episode is recorded and, originally it was tentatively related to MIS 5c by Massari et al. (2004) but, in the light of some new unpublished cores in the Venice mainland, it is here considered as the peak of the MIS 5e transgression.

In the eastern sector of the Veneto region, several cores have been drilled in the framework of the CARG project and allowed to follow the deposits of the MIS 5.5 from the alluvial plain to the marine facies (**Figure 83**; Pini et al., 2009; Fontana et al., 2012). In particular, a stratigraphic section has been reconstructed from the mainland, at the boundary with Friuli Venezia Giulia (core *AZX*, RSL ID 1301), to core *PRA* (RSL ID 793), to the coast (core *TdM*, RSL ID 1295, Fontana et al., 2010). In core *AZX* the MIS 5e deposits correspond to alluvial sediments characterized by warm temperate pollen from an elevation of 45.59 to 42.25 m b.s.l. (Pini et al., 2009), whereas 8 km south of this site, in core *PRA*, hyposaline internal

lagoonal deposits are found at a depth between 49.5 and 55 m (i.e. 45.5 and 51 m b.s.l.). These latter ca. 5 m rest over an alluvial plain with temperate cold pollens (Fontana et al., 2012) and have been deposited at the peak of the marine highstand when the lagoon reached its most internal position. This stratigraphic interval of lagoonal sediments represents a significant index point for relative sea-level during the peak of MIS 5e in NW Adriatic as the base of lagoon sediments rests over an over-consolidated alluvial plain referred to MIS 6 (Fontana et al., 2010).

The site of *PRA* is about 4 km upstream of the current isoline 0 m a.s.l., where brackish swamps were present up to the first part of the 20<sup>th</sup> century when reclamation has been carried out. Accordingly to this setting, also the coastline of MIS 5e reached a more landward position (**Figure 83** and **Figure 84**), as in core *TdM*, where the coastal wedge sequence containing Eemian pollen association has its base at 70.5 m b.s.l. and the facies shift from inner shelf to delta front and deltaic up to 50.4-41.7 m b.s.l. A rather similar sequence is documented also in cores *LUG* (RSL ID 1294) and *VV* (RSL ID 1293).

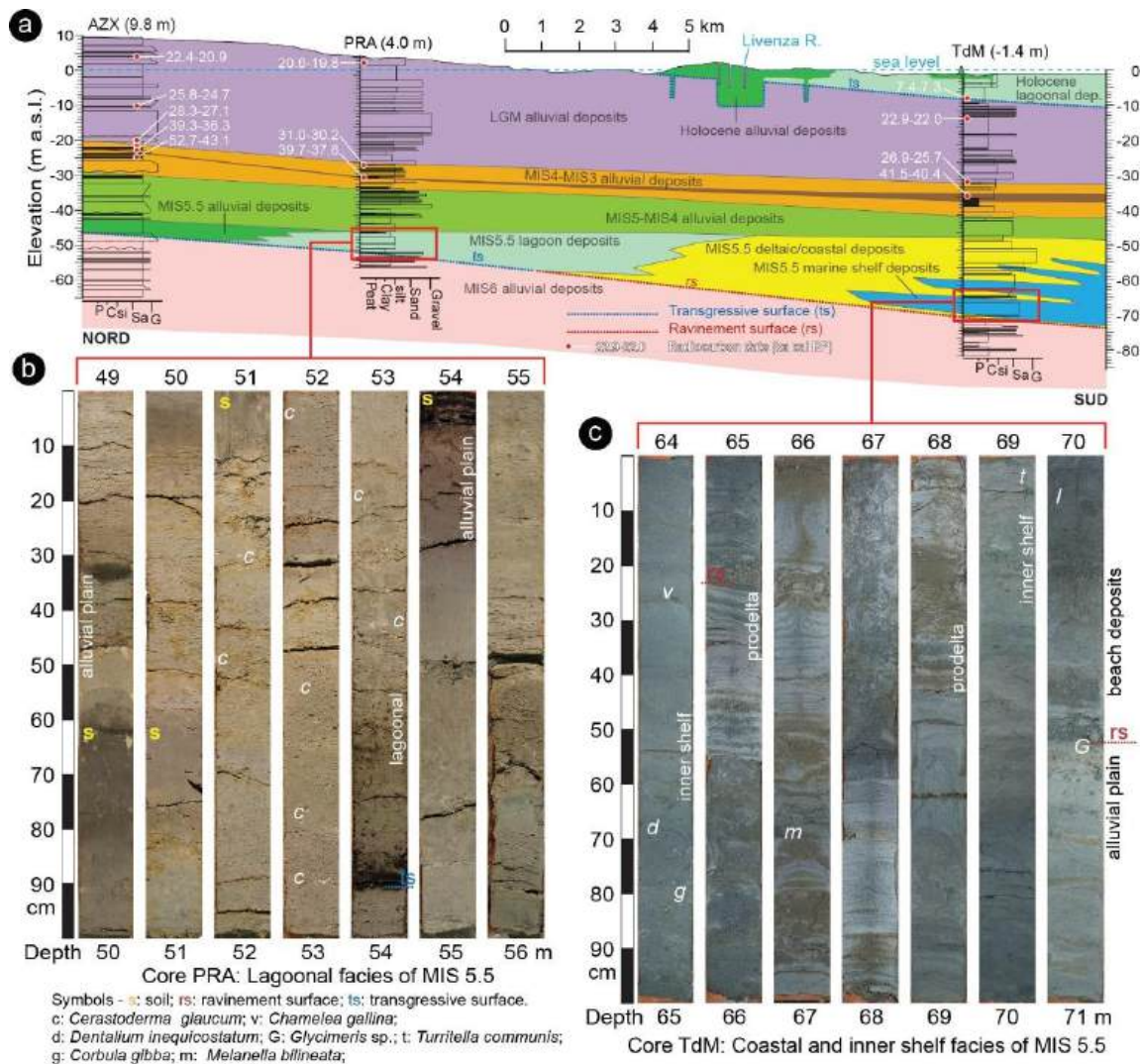


**Figure 83.** a) Stratigraphic section of the -Venetian Friulian Plain, from AZX Azzano core (RSL ID 1301) to PRA Belfiore core (RSL ID 793) to TdM Torre di Mosto core (RSL ID 1295) (modified from Fontana et al., 2010). Trace of section is indicated in **Figure 84**. b) Part of core PRA from 49 to 55 m of depth with typical sedimentary facies of lagoon environment. c) Interval of core TdM from 64 to 71 m of depth with typical facies of the basal part of the MIS 5e marine transgression.

### 7.7.3.11 Friuli Venezia Giulia

Along the coastal plain, Veneto and Friuli Venezia Giulia are not separated by a physiographic boundary (**Figure 84**), so it is not surprising that the stratigraphic setting described for the eastern sector of Veneto seems to be documented also in the easternmost region of northern Italy. Few kilometers north of the western boundary of the Grado-Marano Lagoon, Feruglio (1936) and

Lipparini (1936) described for the first time in this sector the occurrence of a paralic unit of Pleistocene age at a depth around 40-50 m. In core *PNCI* (RSL ID 1292), near Marianis of Piancada, paralic deposits are found between 57.7 b.s.l. and -35.6 m b.s.l. (Fontana et al., 2010). The top portion of this interval is characterized by the presence of coastal and lagoon mollusks and this layer has been used as a marine limiting point by Antonioli et al. (2009). Core *PNCI* was drilled in the framework of the VECTOR project (Bussetti et al., 2010), as borehole *BLGI* (RSL ID 1290), near Aquileia, which is a reference for the eastern portion of the Grado-Marano Lagoon. In this core coastal deposits are found from 55.4 to 39.1 m of depth, documenting the transgression from marine facies to lagoon deposits. This unit is interpreted as the evidence of Last Interglacial based on stratigraphic correlation. Several samples of shells from this unit in core *BLGI* have been dated with ESR, anyhow, the obtained results are characterized by large uncertainties and allow only to generically attribute the samples to MIS 5.

East of Monfalcone the coast is rocky and characterized by a karst environment, where deposits and landforms related to the Upper Pleistocene are almost completely lacking. Some evidence of Last Interglacial coastal features has been suggested in this area of the Gulf of Trieste (Albrecht and Mosetti, 1987; Antonioli et al., 2009), but in the light of this review of data, they seem not reliable. Recently, in the marine area of Miramare, the geophysical investigations highlighted the occurrence of a buried prograding wedge at a depth between 70 and 50 m b.s.l. that has been interpreted as a coastal wedge and related to MIS 5e (Romeo, 2009). It is worth noting that this sedimentary body is onlapping over the Flysch bedrock and, thus, its present elevation should have been produced by tectonics, downlifting the bedrock for at least 60 m in the last 125 ka. According to the structural framework of this region, it seems not likely to consider this unit as the product of the marine highstand of the Last Interglacial.

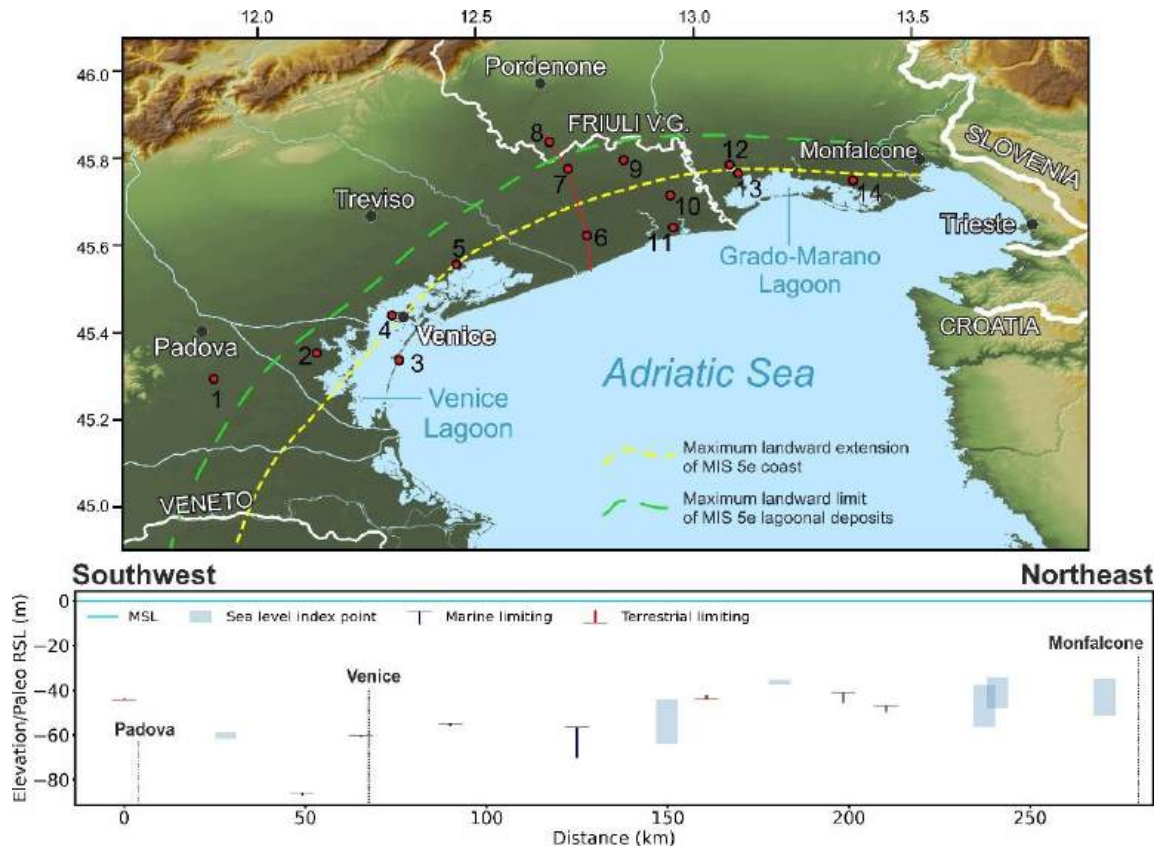


**Figure 84.** Last Interglacial sea-level data for Veneto and Friuli Venezia Giulia (Italy). Upper panel: Map of sites. Lower panel: Distance/Elevation graph, from Southwest (left) to Northeast (right). The lines depicting the most inner position of the coastline and of the lagoon deposits of the MIS 5e are modified after Antonioli et al., 2009. Sites list: 1: Ca' Borille Core (RSL ID 1306). 2: Valle Averno Core CARG 11 (RSL ID 1304). 3: Malamocco Core (RSL ID 1305). 4: VE-1 Core Venezia1 (RSL ID 1303). 5: Portegrandi Core CARG12 (RSL ID 1302). 6: TdM Torre di Mosto Core (RSL ID 1295). 7: PRA Belfiore Core (RSL ID 793). 8: AZX Azzano Core (RSL ID 1301). 9: CNC4 Concordia Sagittaria Core (RSL ID 1289). 10: LUG Lugugnana Core (RSL ID 1294). 11: VV Valle Vecchia Core (RSL ID 1293). 12: Piancada Piancada town (RSL ID 1291). 13: PNC1 Piancada Core (RSL ID 1292). 14: BLG1, Beligna Core (RSL ID 1290). The red line connecting points 6-7-8 represents the cross-section of **Figure 83**.

#### 7.7.3.12 Istria, Kvarner Gulf and Dalmatia

Along the eastern side of the Adriatic Sea, the coast presents rather homogeneous characteristics from the Gulf of Trieste, in Italy, to the northern boundary of Albania. In particular, this stretch of coast, which includes the coasts of Slovenia, Croatia, Bosnia Herzegovina, and Montenegro, is influenced by the tectonic structures of the Dinaric Alps, which have NW-SE direction and largely consist of carbonatic bedrock (Pikelj and Juračić, 2013).

At the moment, along this sector of the coast with a length of over 600 km and characterized by karst landscape, no clear evidence of RSL indicators of the MIS 5e transgression is documented. Anyhow, some indirect information can be inferred by the comparison with the index points referred to MIS 5a, which have been recently documented in the Kvarner Gulf through isotopic analyses on speleothems (cf. Dumitru et al., 2020 for a synthesis of the whole Mediterranean coast). In the submerged cave of U Vode Pit in Krk Island, Surić et al. (2009) studied two stalagmites, K-14 and K-18, collected at 14.5 m and 18.8 m b.s.l., respectively. These speleothems have been dated through U/Th and investigated for their chemical composition, leading Surić et al. (2009) to infer that they have been submerged by marine waters during highstands of MIS 5a and, thus, in case of stable conditions, sea level was higher than 14 m b.s.l. The authors suggested also the possible occurrence of a general regional tectonic uplifting in the area with long-term rates of 0.15-0.25 mm/y.

According to the reconstructions of the global sea-level curves, it is likely that the RSL at the peak of the MIS 5e was over 20 m higher than the level reached for MIS 5a. Thus, these points can be eventually interpreted as marine limiting points also for MIS 5e, but with a larger uncertainty.

This setting strongly contrasts with the situation reconstructed along the western coast of Northern Adriatic, where subsidence has been a leading process

during Quaternary. Anyhow, this asymmetric evolution of the opposite sides is not surprising, as along the Dalmatian coast the long-term geological data suggest general stability.

Another interesting site is located east of Lošinj Island, where Brunović et al. (2020) investigated the deposits recorded in the so-called Lošinj Channel, an isolation basin that during sea-level fall was separated by the rest of Adriatic because of a sill at 50 m b.s.l. In the area, the analysis of a core from a water depth of 64-62 m documented the occurrence of marine deposits and these have been tentatively dated to MS 5a based on correlation with the data produced by Surić et al. (2009). Also in this case the area is considered a stable sector because the Lateglacial and Holocene RSL index points are in agreement with the predicted sea-level curve, suggesting a limited vertical displacement.

In the northern sector of Albania, near the Bay of Drini, Marku and Gjani (2018) suggested the existence of a tidal notch at an elevation between 30 and 40 m a.s.l. referred to MIS 5e. Anyhow, as the morphological evidence supporting this interpretation is not very consistent and the age estimation is only hypothesized, this site is not considered in WALIS as a proxy for the RSL of Last Interglacial.

## 7.7.4 Corsica, Sardinia and Sicily

### 7.7.4.1 Corsica

Corse (Corsica) is the third-largest western Mediterranean Island and hosts a great number of Quaternary marine deposits (**Figure 85**) which span the whole perimeter of the Island (Conchon, 1985, 1999). Along the northern coasts of the Island (Macinaccio and St. Florent) the presence of upper limit of *Lithophaga* boreholes (RSL ID 931) and shallow coastal deposits (RSL ID 299, **Figure 86**) dominated by *Arca noe* and *Patella ferruginea* (Ottmann, 1954) seems to indicate that the maximal transgression during the last interglacial did not exceed 6.25 m a.s.l. The single chronological constrain available in this area is represented by a *Glycimeris* shell dated with AAR techniques (AAR ID 93, Hearty et al., 1986) which yielded MIS 5e age.

Along the mid to southern coasts of the Island, Conchon (1999) reports several shallow marine or lagoonal deposits that were found at elevations ranging from 1 to 3 m a.s.l. Among these, the most robust indicator is represented by some oysters found in lagoonal facies (RSL ID 321) near Figari, which allowed reconstructing a paleo-sea level at  $4 \pm 1.1$  m a.s.l. This is consistent with the elevation of some marine encrustations which constrain the paleo sea level above 3.25 m a.s.l. near Bonifacio (RSL ID 277, Nesteroff, 1984). We assumed a general MIS 5 age of this paleo sea-level stand even if a robust chronological attribution is currently not available. The shells found in all these deposits were only dated with radiocarbon techniques yielding unreliable (19 to 40 ka) ages (Delibrias et al., 1972; Nesteroff, 1984).

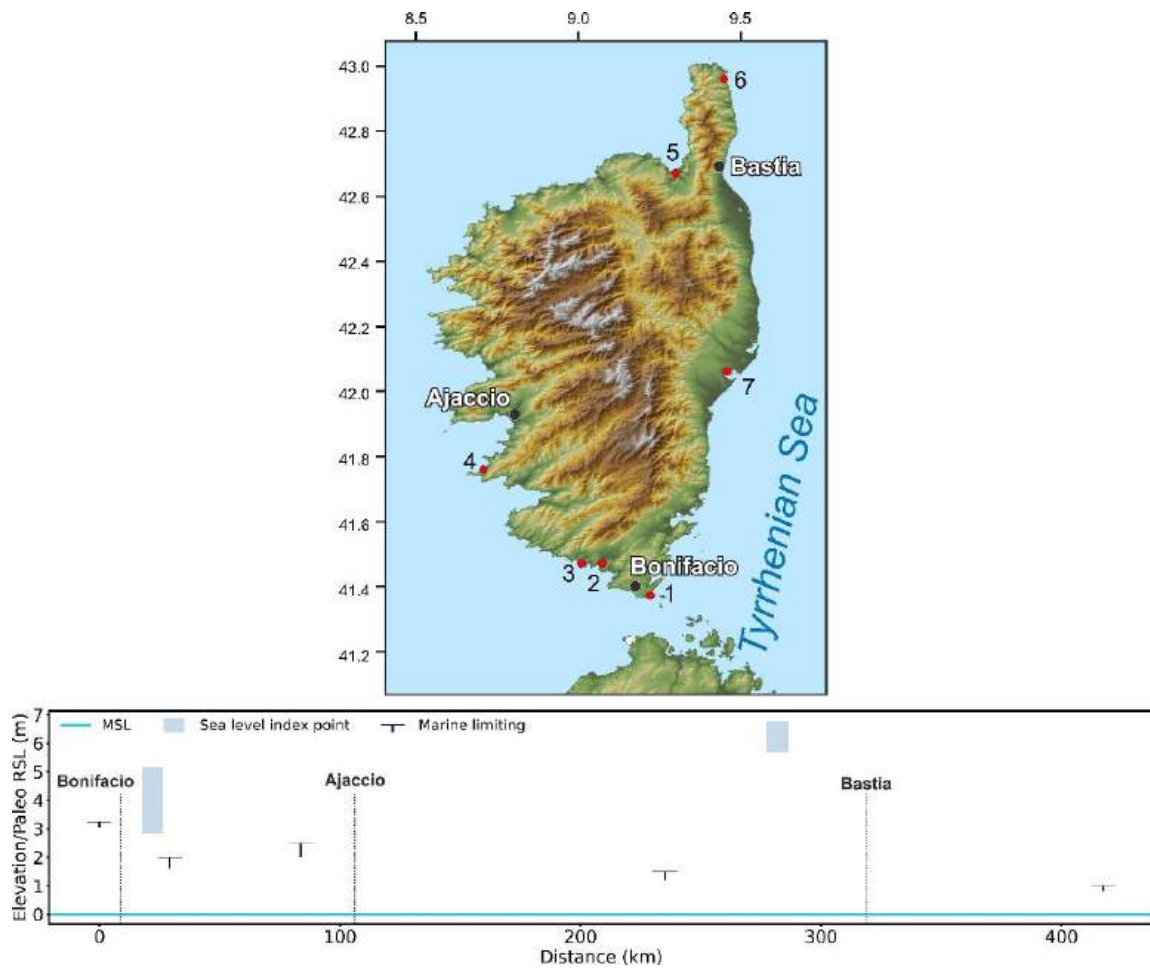


**Figure 85.** Last Interglacial sea-level data for Corsica (France). Upper panel: Map of sites. Lower panel: Distance/Elevation graph, clockwise around the island starting from the southernmost point. Sites list: 1: Piantarella (RSL ID 277). 2: Figari (RSL ID 321). 3: Arbitru (RSL ID 323). 4: Ajaccio Gulf Capo Moru (RSL ID 303). 5: St Florent (RSL ID 299). 6: Macinaggio Tamarone (RSL ID 931). 7: Urbino (RSL ID 322).



**Figure 86.** Littoral deposits in St Florent, Corsica (RSL ID 299). Photo by M. Vacchi

#### 7.7.4.2 Sardinia

Sardegna (Sardinia) represents a key Mediterranean region for the study of the Last Interglacial landforms and deposits. It is among the most tectonically stable areas of the whole Mediterranean and hosts a large abundance of late Pleistocene coastal deposits, as well as well-preserved erosional evidence of paleo sea-level highstands (Andreucci et al., 2010; Ferranti et al., 2006; Ulzega and Hearty, 1986, **Figure 87**). The most outstanding evidence of paleo sea-level stand is the presence of a fossil tidal notch that can be observed, at different elevations, both on the eastern and western coasts of the Island (Antonioli et al., 2018). Along the eastern coast, the fossil notch was observed in several sites showing variability in elevation. In *Pedralonga* (RSL ID 432) and *Capo Monte Santu* (RSL ID 435), the notch is placed at average elevations between 7.4 and 7.6 a.s.l., while it increases to 9.5 m a.s.l. in the central part of the Gulf of Orosei (RSL ID 434). In the Northern portion of the East coast, the notch was observed both in Capo Figari (RSL ID 430) and in Tavolara Island (RSL ID 431) at average elevations ranging from  $4.7\pm 0.4$  m to  $6.7\pm 0.5$  m a.s.l. In Tavolara, *Glycimeris* shells found in a marine deposit (correlated with the notch) yielded an MIS 5e age (AAR ID 92, Belluomini et al., 1986). This date is the only chronological constraint available for the whole eastern coast of Sardinia.

Along the Northern coast, Ozer et al. (1980) reported *P. latus* in beach deposits found at 2.5 m a.s.l. in Capo Testa. This level lies above a subtidal facies which was dated with AAR (AAR ID 90) yielding an age of 120 ka (Belluomini and Delitala, 1988; Kindler et al., 1997). The lack of clear intertidal deposits at this location did not allow for a precise definition of the sea-level evolution during the whole last interglacial period. The available data only indicate that the paleo sea-level was above 1.5 m a.s.l. during the MIS 5e and at or slightly below 1 m during the MIS 5c (AAR ID 91). This trend is further confirmed by an additional date

(AAR ID 94) which constrain the paleo sea level above 1.5 m a.s.l. during MIS 5e (Belluomini and Delitala, 1988).

The western coast of Sardinia hosts a large number of LIG littoral deposits which were already identified at the beginning of the last century (Issel, 1914) and widely investigated in the last 40 years (Ulzega and Hearty, 1986; Sechi et al., 2020; Carboni et al., 2014). In Capo Caccia, Alghero, and Bosa, the concomitant presence of well-preserved fossil notches (RSL IDs 382-383, Antonioli et al., 2018), beach deposits (RSL ID 388, Casini et al., 2020), and fossil bioincrustations (RSL ID 234-238, Sechi et al., 2020) robustly placed the MIS 5e shoreline between 3 and 4 m a.s.l. The quality of the chronological constrain for this area was significantly increased by a series of recent OSL dates performed near Capo Caccia (LUM ID 120; Casini et al., 2020), Alghero (LUM ID 61-64-68, Sechi et al., 2020; Andreucci et al., 2010) and in Bosa (LUM ID 75, Sechi et al., 2020).

More southwards, impressive outcrops of Upper Pleistocene littoral deposits occur in the San Giovanni del Sinis (**Figure 88**) area (Carboni et al., 2014; Andreucci et al., 2009; Lecca and Carboni, 2007). These are represented by a complete sequence which includes shoreface, foreshore, lagoonal, and dunal deposits. The age of these deposits was investigated both with OSL (Andreucci et al., 2009) and with U/Th on corals (Carboni et al., 2014; D'Orefice et al., 2012). Both techniques, (LUM ID 81 and U-Series ID 550-551 and 555 to 557) confirmed the MIS 5 ages for most of these littoral deposits, as already suggested by the presence of Senegalese fauna (Carboni and Lecca, 2008). A further AAR date (AAR ID 203) yielded MIS 5c age (Ulzega and Hearty, 1986) while a basal unit found in the northernmost sector of San Giovanni del Sinis yielded MIS 7 age (LUM ID 81, Andreucci et al., 2009). The coupled analysis of all these data indicates RSL was placed between 2 and 5 m a.s.l. during MIS 5e (RSL IDs 262, 263, 265, 266, 271). The analysis stratigraphic facies of San Giovanni del Sinis seems also to indicate that the maximal sea-level highstand is preceded by

millennial sea-level oscillations within MIS 5e, which were recorded by the different littoral facies (Carboni et al., 2014).

In the southwestern portion of the Island, the occurrence of a well-preserved tidal notch at ~2.8 to 3.5 m a.s.l. was observed from Buggerru to the Island of Sant'Antioco (RSL IDs 433,436 and 437, Antonioli et al., 2018). An MIS 5e age was attributed to this paleo-shoreline thanks to the correlation with some littoral deposits found at similar elevations. They are rich in Senegalese fauna (including *P. latus*) and were dated with AAR techniques (AAR ID 127, Ulzega and Ozer, 1980; Ulzega and Hearty, 1986).

Along the southern coast of the Island, beach deposits rich in Senegalese fauna (including *P. latus*) were found in some littoral deposits near the archeological site of Nora (Ulzega and Hearty, 1986; Kindler et al., 1997). Two AAR dates (AAR IDs 204-205) yielded MIS 5e age even if some contrasting interpretation of the age of these deposits are present in literature (Kindler et al., 1997). The facies analysis of this outcrop allowed reconstructing a paleo-shoreline placed at ~3.3 m during MIS 5e (RSL ID 1337). This elevation is in agreement with the paleo-shoreline reconstructed in the Cagliari area (RSL IDs 132, 276, 1338) whose MIS 5e age was constrained by U-Series and AAR dating (Hearty et al., 1986; Ulzega and Hearty, 1986).

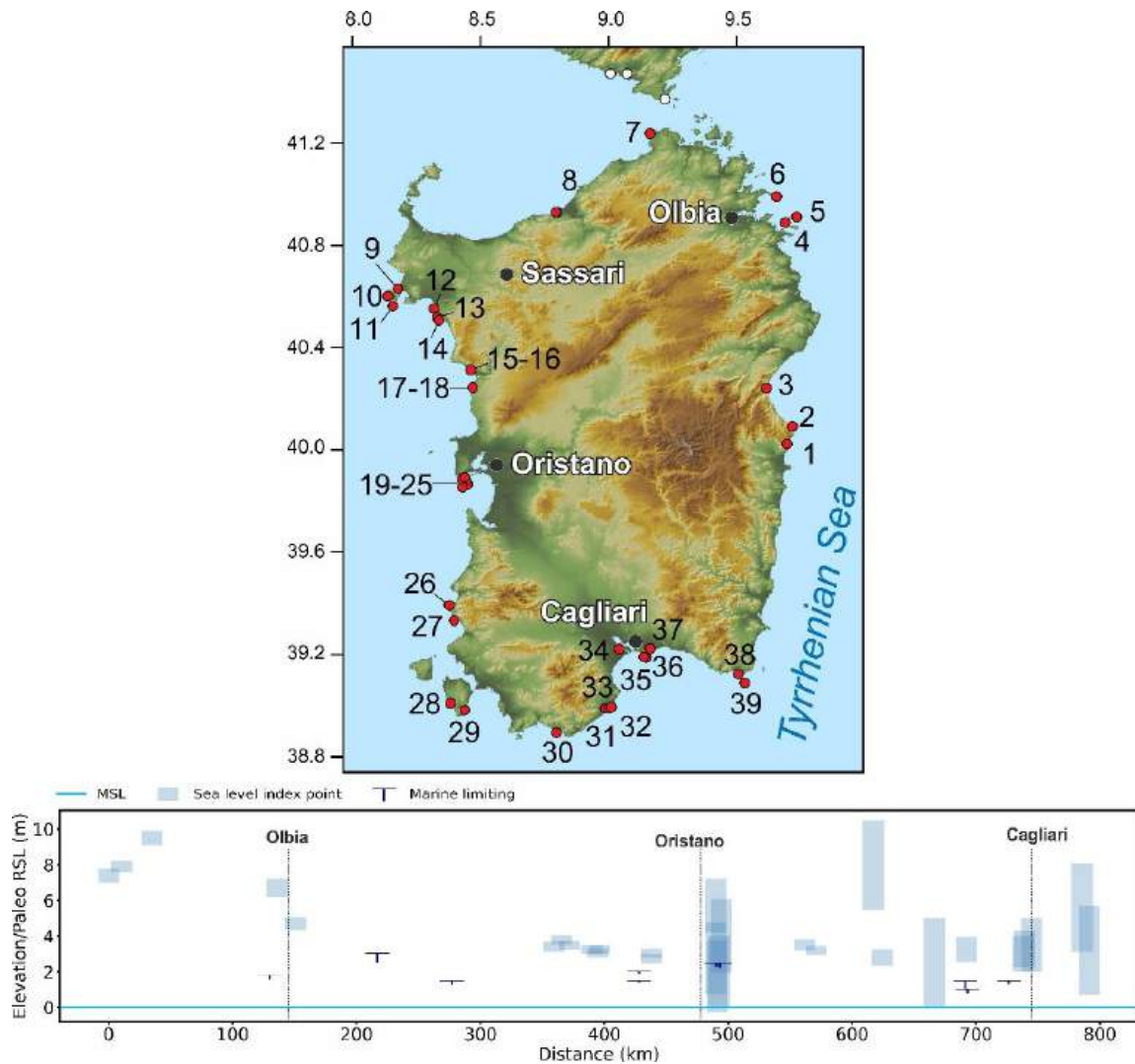


**Figure 87.** Last Interglacial sea-level data for Sardinia (Italy). Upper panel: Map of sites. Lower panel: Distance/Elevation graph, counterclockwise around the island. Sites list: 1: Pedralonga (RSL ID 432). 2: Capo Monte Santu (RSL ID 435). 3: Orosei Nord (RSL ID 434). 4: Tavolara Punta la mandria (RSL ID 292). 5: Tavolara (RSL ID 431). 6: Capo Figari (RSL ID 430). 7: Capo Testa\_santa Reparata Terrestrial limiting (RSL ID 289). 8: Capo Testa\_santa Reparata Marine limiting (RSL ID 290). 9: Badesi Mare San Pietro a Mare (RSL ID 300). 10: Cala Viola (RSL ID 388). 11: Capo Caccia 1 (RSL ID 382). 12: Capo Caccia 2 (RSL ID 383). 13: El tra (RSL ID 234). 14: Punta Padre Bellu (RSL ID 235). 15: Baurantinu (RSL ID 236). 16: Bosa (RSL ID 241). 17: Bosa (RSL ID 243). 18: Bosa (RSL ID 244). 19: San Giovanni del Sinis (RSL ID 262). 19: Porto Alabe (RSL ID 238). 20: San Giovanni del Sinis (RSL ID 271). 21: San Giovanni del Sinis (RSL ID 272). 22: San Giovanni del Sinis (RSL ID 265). 23: Faro Capo San Marco (RSL ID 266). 24: Capo San Marco (RSL ID 261). 25: San Giovanni del Sinis (RSL ID 263). 26: Buggerru (RSL ID 437). 27: Masua (RSL ID 436). 28: Sant'Antioco Cala Sapone (RSL ID 296). 29: Sant'Antioco (RSL ID 433). 30: Capo Malfatano (RSL ID 295). 31: Nora (RSL ID 1336). 32: Nora Is Fradis (RSL ID 1337). 33: Nora-Is Fradis (RSL ID 279). 34: Sa Illetta (RSL ID 278). 35: Cagliari Marina Piccola (RSL ID 1338). 36: Cagliari Cala Mosca (RSL ID 132). 37: Is Arenas (RSL ID 276). 38: Capo Carbonara Villasimius (RSL ID 293). 39: Capo Carbonara Isola dei cavoli-Cala Ponente (RSL ID 294).



**Figure 88.** Last Interglacial outcrop at San Giovanni del Sinis (RSL ID 262). In the photo, A. Rovere is pointing to the contact between subtidal (below) and intertidal (above) beds. Photo by E. Casella.

### 7.7.4.3 Sicily

Antonioli et al., 2006b reviewed the elevation of RSL indicators of the last interglacial around the coasts of Sicilia (Sicily) and the Egadi, Lampedusa, Ustica, and Eolian islands, updating former compilations, most notably the one by such as the one by Bordoni and Valensise (1999). Within the island, Antonioli et al. (2006b) distinguished four distinct tectonic sectors, that are described separately hereafter.

Sector 1 (**Figure 89**) spans between the coastal towns of Trapani and Cefalù and includes the Egadi Islands to the West. Along the Egadi island coasts, *P. latus* specimens and Senegalese fauna within fossil beaches have been found in the island of Levanzo, between 2 and 6 m a.s.l. (RSL IDs 852 to 854) by Malatesta (1957) and up to 12 m a.s.l. in Favignana (RSL ID 855) by Abate et al. (1992, 1996). Antonioli et al. (2002) measured the elevation of the tidal notches on Marettimo island at ca. 5-8 m a.s.l. (RSL ID 833 to 843). On the mainland, the areas surrounding the towns of Trapani and Marsala are characterized by marine deposits bearing *P. latus* at elevations of 2 to 5 m a.s.l. (Ruggieri and Buccheri, 1968; Ruggieri and Unti, 1988, RSL IDs 919 and 920). A similar elevation range, 2-3 m a.s.l., with the presence of sediments bearing *P. latus*, has been evaluated also between Marsala and Mazzara del Vallo area (Ruggieri et al., 1975). These deposits lie on a terrace that has the inner edge at 34 m a.s.l. (RSL ID 899).

Northwest of Trapani, Mauz et al. (1997) surveyed Last Interglacial sea-level proxies in the Gulf of Castellammare and Capo San Vito (RSL ID 827 to 845) integrating thermoluminescence dating and paleontological investigations. These authors recognized evidence of MIS 5e in the 5-18 m elevation range. Moreover, in Capo San Vito, Abate et al. (1991) signal the presence of Senegalese fauna, and Antonioli et al. (2002) dated with U-Series speleothems to constrain the age of a tidal notch. These studies have confirmed the presence of a marine terrace up to 14

m a.s.l. (RSL ID 923) and a tidal notch up to 8 m a.s.l. (RSL ID 922), both correlated to MIS 5e (Abate et al., 1996; Abate et al., 1993). Fabiani (1941), Gignoux (1913) and Antonioli et al. (2006b) reported specimens of *P. latus* between 2 and 10 m a.s.l. in Palermo (RSL IDs 896 and 832) and nearby areas (Capo Gallo, RSL ID 897), while AAR dating on *Glycimeris* allowed Hearty (1986) to reject the correlation of fossil marine deposits few tens of meters a.s.l. to MIS 5e, previously made by Ruggieri and Buccheri (1968).

Towards the easternmost point of Sector 1, Antonioli et al. (2006b) have constrained *Glycimeris*-bearing marine deposits to MIS 5a and 5c between ca. 7 to ca. 10 m a.s.l. in the area of Cefalù (RSL ID 862) with AAR. This constraint allowed to correlate to MIS 5e a tidal notch in Cefalù promontory and *La Kalura* promontory (RSL ID 863) at 29 and 30 m a.s.l. respectively. The elevation of the tidal notch decreases considerably eastward, in fact, in Capo Zafferano (RSL ID 831) it has been found at 7 m a.s.l. and constrained by AAR dating on *Arca* shells (Antonioli et al., 1994a).

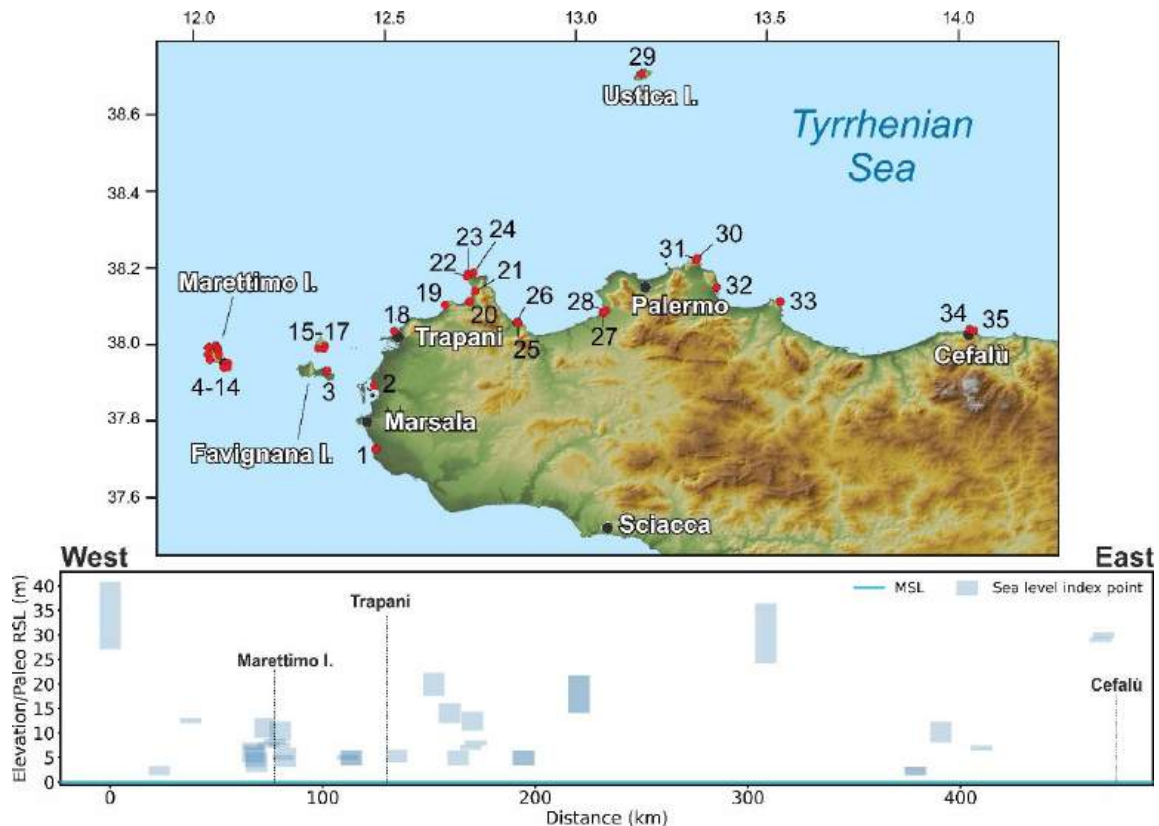


**Figure 89.** Last Interglacial sea-level data for Sicilia, sector 1 (Italy). Upper panel: Map of sites. Red dots are sites in the region of interest, white dots are other sites within the Western Mediterranean compilation. Lower panel: Distance/Elevation graph, from West (left) to East (right). Sites list: 1: Marsala-Mazzaro del Vallo Torre Scibiliana (RSL ID 899). 2: Trapani Birgi (RSL ID 919). 3: Favignana Egadi archipelago (RSL ID 855). 4: Facciazzo Marettimo Island (RSL ID 841). 5: Cala Marino Marettimo Island (RSL ID 836). 6: Cala Marino (II) Marettimo Island (RSL ID 840). 7: Cala Conca Marettimo Island (RSL ID 842). 8: Cala Nera Marettimo Island (RSL ID 843). 9: P. Pegna Marettimo Island (RSL ID 837). 10: P.ta Due Frati Marettimo Island (RSL ID 833). 11: Scalo Maestro Marettimo Island (RSL ID 834). 12: Tuono Marettimo Island (RSL ID 838). 13: Sco. Camello Marettimo Island (RSL ID 835). 14: Passo del Bue Marettimo Island (RSL ID 839). 15: Pietre Varate Levanzo Island (Egadi archipelago) (RSL ID 854). 16: Cala Dogana Levanzo Island (Egadi archipelago) (RSL ID 852). 17: Cala Fredda Levanzo Island (Egadi archipelago) (RSL ID 853). 18: Trapani- Tonnara S. Giuliano (RSL ID 920). 19: Monte Cofano Trapani (RSL ID 894). 20: Castelluzzo San Vito lo Capo (RSL ID 845). 21: Macari (RSL ID 830). 22: Cala Mancino San Vito lo Capo (RSL ID 844). 23: San Vito lo Capo W side (RSL ID 923). 24: San Vito lo Capo NE side (RSL ID 922). 25: Cala Rossa (RSL ID 828). 26: Cala Bianca (RSL ID 829). 27: Torre San Cataldo (RSL ID 827). 28: Nocella (RSL ID 826). 29: Ustica (RSL ID 916). 30: Palermo Capo Gallo (RSL ID 897). 31: Capo Gallo (RSL ID 832). 32: Palermo (RSL ID 896). 33: Capo Zafferano (RSL ID 831). 34: Cefalù (RSL ID 862). 35: Cefalù (II) La Kalura (RSL ID 863).

In southwestern Sicily (Sector 2), Antonioli et al. (2006b) reported that in the area spanning from Granitola Cape to Passero Cape no evidence of MIS 5 is present. Probably, the bedrock lithologies have played an important role in terms

of preservation of RSL indicators along the coast of Sector 2, or negative vertical movements could have downthrown MIS 5 indicators.

Sector 3 extends from the town of Pachino (to the South) to Monte Tauro (to the North). *P. latus* specimens embedded into a beach deposit have been reported by Malatesta (1985) at 15 m a.s.l. in the Pachino area (RSL ID 900). By geomorphological correlation with this terrace, beach deposits assigned to MIS 5e have been reported also in S. Lorenzo and Avola sites, at 4 and 5 m a.s.l. In Augusta (Monte Tauro), Di Grande and Scamarda (1973) and Di Grande and Neri (1988) report the presence of *P. latus* correlated with a marine terrace inner edge at 15 m a.s.l. (RSL ID 901). Meschis et al. (2020) have mapped the marine terraces along the Syracuse coast by synchronous correlation method using as age constraints U-Series dating on speleothems (Dutton et al., 2009b), which provide a terrestrial limiting point for the end of MIS 5a (*Plemmiro Cave*, RSL ID 3577). The MIS 5e terrace, according to the reconstruction of Meschis et al. (2020) spans from ca. 30 up to ca. 70 m a.s.l. This estimate, which was based on ESR dating on mammals teeth (Rhodes, 1996), is at odds with the interpretation of Bianca et al. (1999), according to which the MIS 5e marine terrace decreases from 10 m in Augusta to 75 m in Avola. In particular, the 5e terrace of Meschis et al. (2020) corresponds to the MIS 3.3 terrace of Bianca et al. (1999). However, the dating of Rhodes (1996) used by Bianca et al. (1999) has not been included in the database, as it was discarded by Antonioli et al. (2006b) as not robust.

The last sector covers the NE part of Sicily (Sector 4, **Figure 90**), and extends between the city of Catania and the town of Acquadolci, near Messina. MIS 5e sea-level proxies along the Etna coast were chronologically constrained indirectly by K-Ar dating on lava flows (Gillot et al., 1994), which was successively incised by a marine terrace (Monaco et al., 2000). The inner margin of this terrace has been reported at a maximum of 175 m a.s.l. in Aci Trezza (RSL

IDs 846 to 848) and slowly decrease in elevation towards the south, reaching a maximum of 165 m a.s.l. in Catania (RSL IDs 849 to 851).

Catalano and Guidi (2003) mapped a staircase sequence of marine terraces, including the Last Interglacial one, for the NE sector of Sicily, from the Straits of Messina to the Taormina area, but no dating or Senegalese fauna reports for these terraces are available. The first MIS 5 age constraint for the Taormina sector is an ESR dating on littoral fossils *Patella* and *Venerupis* shells, provided by Antonioli et al. (2006b) at 115 m a.s.l. (RSL ID 903), whereas Bonfiglio (1981) reports a tidal notch with serpulids in a cave at 130 m a.s.l. (RSL ID 3626).

At the northern tip of Sector 4 lies Capo Peloro, where Bonfiglio and Violanti (1983) recognized specimens of *P. latus* at 86 m. a.s.l. These were correlated to MIS 5e with AAR by Hearty et al. (1986). The marine terrace inner edge corresponding to MIS 5e has been placed at 110 m a.s.l. (RSL ID 902) by Antonioli et al. (2004) and at 125 m a.s.l. by Catalano and Guidi (2003). Since the elevation proposed by Catalano et al. (2003) is based only on a geomorphological correlation with a marine terrace at Capo Rasocolmo at 125 m a.s.l. and in the absence of more dating, such point has not been included in the database.

Hearty and Dai Pra (1986) dated *Arca* and *Glycimeris* shells related to MIS 5e deposits in the Capo Milazzo area, at ca. 90 m a.s.l. (RSL ID 921).

In the northern edge of Sector 4, Giunta et al. (2012) mapped five orders of marine terraces, two of which were dated by OSL on unconsolidated marine sands. These ages allowed correlating the terrace at 50 m a.s.l. to MIS 5e (RSL ID 924). Such correlation is supported by a synchronous correlation method (Meschis et al., 2018).

In front of the northern coast of Sector 4, also the Aeolian Islands underwent long-term uplift. The inner edge of marine terraces related to MIS 5.5 spans from 40 m a.s.l. in Filicudi (RSL ID 913-914, Lucchi et al., 2004a,b), 45 m a.s.l. on Lipari

Island (RSL IDs 909 to 911), and 115 m a.s.l. in Panarea Island (RSL IDs 917-918, Radtke, 1986).

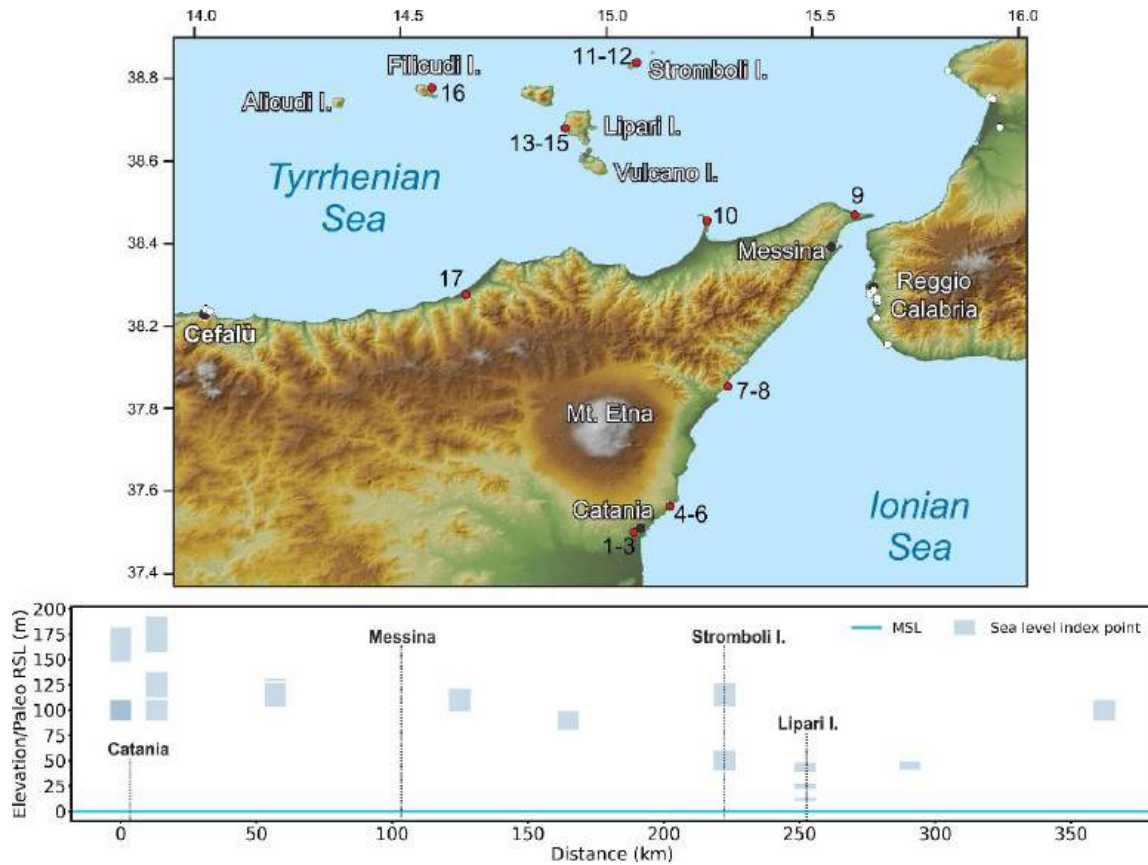


**Figure 90.** Last Interglacial sea-level data for Sicily, sector 4 (Italy). Upper panel: Map of sites. Red dots are sites in the region of interest, white dots are other sites within the Western Mediterranean compilation. Lower panel: Distance/Elevation graph, counterclockwise from Catania to Cefalù. Sites list: 1: Catania (RSL ID 849). 2: Catania (II) (RSL ID 850). 3: Catania (III) (RSL ID 851). 4: Aci Trezza (RSL ID 846). 5: Aci Trezza (II) (RSL ID 847). 6: Aci Trezza (III) (RSL ID 848). 7: Taormina (II) (RSL ID 3626). 8: Taormina (RSL ID 903). 9: Capo Peloro (RSL ID 902). 10: Milazzo (RSL ID 921). 11: Panarea (RSL ID 917). 12: Panarea (II) (RSL ID 918). 13: Lipari (I) (RSL ID 909). 14: Lipari (II) (RSL ID 910). 15: Lipari (III) (RSL ID 911). 16: Flicudi (RSL ID 914). 17: Sant'Agata di Militello (RSL ID 924).

West of the Aeolian Islands, the Last Interglacial at Ustica Island is constrained by U-Series dating on *Cladocora* and by the presence of *P. latus* at 30 m a.s.l. (RSL 916) (de Vita et al., 1998; Ruggieri and Unti, 1988; Hearty, 1986). Southwards, in front of the coasts of Tunisia, Lampedusa Island is considered stable due to the presence of a fossil beach deposit bearing *P. latus* up to 4 m a.s.l. (RSL ID 907, Buccheri et al., 1999; Segre, 1960).

### 7.7.5 Algeria

One of the earliest reports of Pleistocene deposits in Algeria (**Figure 91**) is contained in a paper written in 1911 by de Lamothe (de Lamothe, 1911). In the 1960s, this early study was further expanded upon by Stearns and Thurber (1965) and Vita-Finzi (1967), and later by Saoudi (1989). In the 1990s, studies on the tectonics of Algeria used Last Interglacial shorelines to calculate vertical tectonic rates (Meghraoui et al., 1996), an approach that has continued in more recent times (Maouche et al., 2011). The most recent study related to the Last Interglacial sea-level indicators in Algeria was done by Authemayou et al. (2016), who focused on the record in the Tipasa Province, west of Algiers. The sea-level information reviewed for Algeria was extracted from two studies: Authemayou et al. (2016) for the Tipasa area and Meghraoui et al. (1996) for the areas of Oran and Ain Techmouchent.

#### 7.7.5.1 Tipasa

In the Tipasa province, Authemayou et al. (2016) identified six sites from which cross-sections were extracted and beach deposits were sampled. To measure elevations, the authors used a combination of SPOT Digital Elevation Model (20-m vertical accuracy) and a barometric altimeter. No detailed stratigraphic description of the beach deposits is given other than their characterization as “*shelly sandstone units*”. Mollusk samples for U-Series radiometric dating were collected from what Authemayou et al. (2016) call “Terrace 1”. Three U-Series ages, identified by the original authors as Age ID n. 4, Age ID n. 21, and Age ID n. 48 are reported. Age ID n.4 was done on a sample taken from the profile *AT1* (Chenoua, RSL ID 4) and gives an age of 67 ka. Age ID n. 21 was taken from the profile *AT3* (Boun Haroun, RSL ID 6) and gives an age of 102 ka. Age ID n. 48 was taken from *AT5*

(Ain Benian, RSL ID 9) and gives an age of 130.5 ka (+4.5/-4.3). Other ages correlated to Terrace 1 come from Tipasa (*AT2* and *AT2'*, respectively RSL IDs 5 and 7) and were published by Stearns and Thurber (1965). They report U-Series ages of 140±10 ka (sample L-779a) and 125±10ka (sample L-779B); however radiometric data is not available and was not inserted in the database. The samples were taken from what the original authors called “*low-Quaternary beach deposits*”.

Maouche et al., 2011 suggested that the “Terrace 1” in the area of Tipasa is located at 175-185m a.s.l., at odds with other descriptions of this terrace. Subsequent comments and replies (Pedoja et al., 2013; Maouche et al., 2013) did not clarify this controversy, until the work of Authemayou et al. (2016) where it seems clear that the “Terrace 1” is located only up to 10 m a.s.l.

#### 7.7.5.2 Oran and Ain Techmouchent

In the Oran and Ain Techmouchent provinces, the Last Interglacial terrace is reported by Meghraoui et al. (1996) in a table within the paper, with elevations derived most likely from topographic maps (Arzew, RSL ID 11 and Cap Figalo, RSL ID 12). The only chronologic constraint that points to the Last Interglacial age is the reported presence, on these terraces, of *P. latus* which grants a tentative chronostratigraphic correlation with “Terrace 1” in the Tipasa province deposits where the same species was found.

### 7.7.6 Morocco

The Quaternary marine terraces cropping out along the Mediterranean Moroccan coasts (**Figure 91**) testify uplift during the Quaternary (El Gharbaoui, 1977). However, they have not been studied deeply as the counterpart on the Spanish coast. Pieces of evidence of the Last Interglacial from Tanger to Pointe Ciress have been related to paleo shorelines between 8 and ~20 m a.s.l (Cadet et al., 1977; El Fahssi, 1999; Poujol et al., 2014), whereas the marine Achakkar terrace at 6 m a.s.l. (Brébion et al., 1986), nearby Tanger on the Atlantic side has been U-Series constrained on mollusk shells by Stearns and Thurber, 1965 to the Last Interglacial ( $120 \pm 10$  ka).

#### 7.7.6.1 The Dhâda terrace

The *Dhâda* terrace (RSL ID 248-249) has been identified between 13 and 15 m a.s.l. and was characterized firstly by (El Abdellaoui et al., 2016). The terrace, which extends for about 1 km along the coast, is made of marine sands within shell fragments and eolian deposits. (El Abdellaoui et al., 2016) recognized two transgressive phases related to the Last Interglacial (MIS 5e) based on four U-Series dating on *Dendrophyllia ramea* (Linnaeus) corals. The age provided must be considered as a minimum age because of the high  $^{234}\text{U}/^{238}\text{U}$  activity ratio. Moreover, the Authors reject a U-Series age obtained from *Lithothamnion calcareum* algae sampled (USeries ID 2943) within the same Unit of the corals, as considered rejuvenated by secondary uranium. Such dating (USeries ID 546 to 549), allowed El Abdellaoui et al. (2016) to stratigraphically correlating the *Zhâra* (RSL ID 3598) and *Hejar-Lasfar* (RSL ID 3599) marine terraces, few kilometers eastward and westward respectively to *Dhâda* terrace, with the MIS 5e. The inner edge of the *Zhâra* and *Hejar-Lasfar* terraces is in the 13-14 m elevation range.

#### 7.7.6.2 Cape Leona

The first attempt to date the Cape Leona staircase sequence of marine terraces has been proposed by El Kadiri et al. (2010) by correlation with the U-Series dated travertines at the nearby *Beni Younech* site (RSL ID 259). Such correlation is supported by El Kadiri et al. (2010) by geochronological and topographic comparison between the Cape Leona and Moroccan Atlantic coast marine terraces (El Fahssi, 1999). However, in the same area, Abad et al. (2013) have been constrained by U-Series dating on flowstones covering marine sediments both a minimum elevation (marine limiting) and a tidal notch for the MIS 5e and 5a respectively at ca. 14 m a.s.l. (RSL ID 259) and 10 m a.s.l. (RSL ID 260). The notch at 10 m has been assigned to MIS 5a by geomorphological correlation with a beach deposit bearing calcareous algae dated ca. 84 ka (U-Series ID 554), but, according to El Abdellaoui et al. (2016), such dating is not reliable because of rejuvenation processes occurring in calcareous algae as evidenced for the *Dhâda* terrace (see the previous paragraph).

#### 7.7.6.3 Al Hoceima

The Al-Hoceima region is situated at the eastern edge of Mediterranean Morocco. At the Al-Hoceima site (RSL ID 929), Hearty (1986) dated marine deposits (AAR ID 195) bearing *Glycimeris glycimeris* and reported the occurrence of Senegalese fauna with *P. latus*. The inner-edge of the marine terrace related to MIS 5e was assessed by Poujol et al. (2014) at  $22 \pm 1$  m a.s.l. (RSL ID 3622). Such correlation is based on U-Series dating on corals (U-Series ID 2952 and 2953) and *P. Latus* (U-Series IDs 2954 and 2955) from the MIS 7 marine terrace. However, it is worth noting that the samples of Poujol et al. (2014) are affected by chemical weathering.

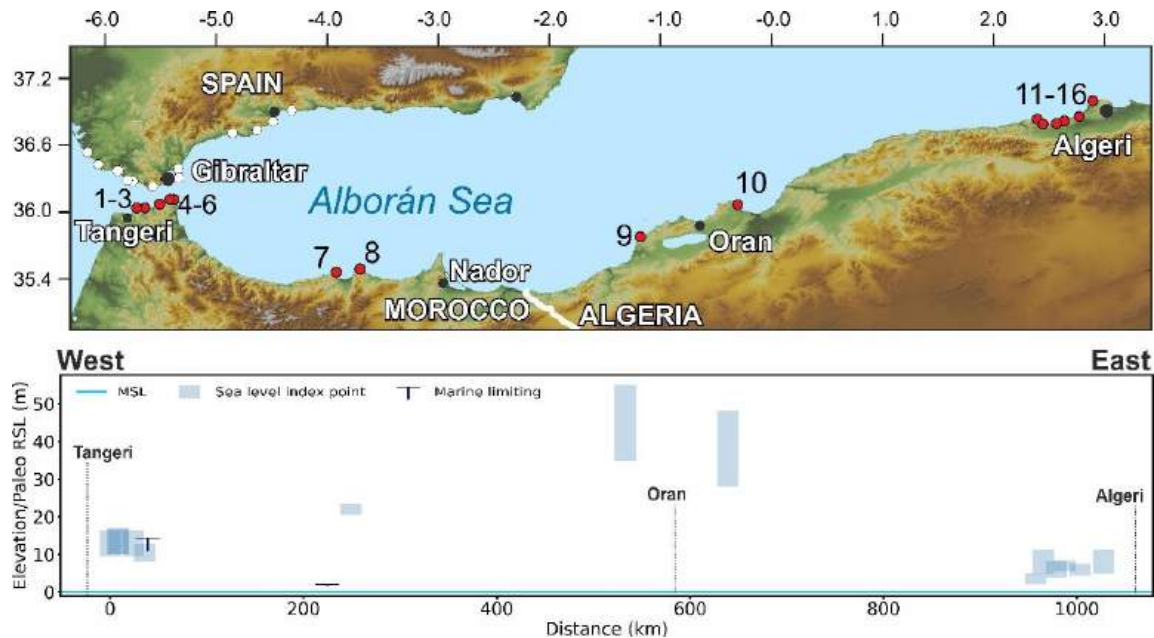


**Figure 91.** Last Interglacial sea level data for Algeria and Morocco. Upper panel: Map of sites. Red dots are sites in the region of interest, white dots are other sites within the Western Mediterranean compilation. Lower panel: Distance/Elevation graph, from West (left) to East (right). Sites list: 1: Hejar Lasfar marine terrace (RSL ID 3599). 2: Dhada marine terrace S2 (RSL ID 248). 3: Dhada marine terrace S3 (RSL ID 249). 4: Zhâra marine terrace (RSL ID 3598). 5: Cape Leona Section C (RSL ID 260). 6: Bel Younech Beach Section A (RSL ID 259). 7: Al Hoceima (RSL ID 929). 8: Rastarf Cape Al-Hoceima (RSL ID 3622). 9: Cap Figalo (RSL ID 12). 10: Arzew (RSL ID 11). 11: Chenoua Transect AT1 (RSL ID 4). 12: Tipasa Transect AT2 (RSL ID 5). 13: Tipasa Transect AT2' (RSL ID 7). 14: Bou Haroun Transect AT3 (RSL ID 6). 15: Mazafran Transect AT4 (RSL ID 8). 16: Ain Benian Transect AT5 (RSL ID 9).

## 7.8 Final remarks

MIS 5 sea-level proxies have been preserved at several sites along the coasts of the Western Mediterranean in different geological facies. In stable to slowly uplifting sites, beach deposits containing warmer-water faunal assemblages can be found a few meters above present sea level, or inside coastal caves. Along uplifted coasts, marine terraces (locally capped by coastal or marine deposits) mark the peak of the Last Interglacial transgression, which is instead found as a transgressive sequence in cores drilled in subsiding areas.

Besides MIS 5e, several locations (especially in uplifted areas) preserved remnants of MIS 5a and 5c sea-level proxies (that were also inserted in the database) and former interglacials. For example, Zazo et al. (2013) report terraces attributed to MIS 7, MIS 9, and MIS 11 along the Spanish coasts. Recent studies on cave deposits in Mallorca allowed placing important benchmarks on Early Pleistocene and Pliocene highstands (Dumitru et al., 2021; Dumitru et al., 2019). Similarly, marine overgrowth on speleothems collected from the Argentarola Cave, in Italy, allowed to establish minimum positions of sea level during the penultimate interglacial (MIS 7, Dutton et al., 2009a; Bard et al., 2002). At the moment, a standardized review of pre-MIS 5 sea-level proxies is not available. Instead, Holocene sea-level studies were compiled within a single database (Vacchi et al., 2016, 2018) following the standardized template of Khan et al. (2019). These recent reviews summarized the large tradition of studies related to Holocene sea-level proxies in this part of the Mediterranean basin (see Lambeck et al., 2004a-b for an overview).

While Western Mediterranean MIS 5 sites are often characterized by geological units with narrow indicative ranges, there has been a lack of precise measurement and datum attribution, which researchers started to address only recently (e.g., Stocchi et al., 2018; Lorscheid et al., 2017; Muhs et al., 2015;

Antonioli et al., 2018). As sea-level studies progress in the Western Mediterranean, it is imperative that the elevation of the most relevant outcrops is re-measured with accurate instrumentation (e.g., differential GNSS systems) and that elevations are referred to well-defined sea level datums.

Another issue that is common within Western Mediterranean MIS 5 proxies is the paucity of reliable absolute ages. This is in part compensated with correlations between sites supported by (bio)stratigraphic and Amino Acid Racemization correlations, but this hinders the possibility of detailing intra-interglacial dynamics, such as the presence and timing of sea-level fluctuations. While it is indeed considered possible that some Mediterranean sites recorded MIS 5e sea-level fluctuations (e.g., Hearty et al., 2007), these are often inferred from either superimposed deposits with slightly different AAR ratios or from the concurrent presence of lower deposit and upper notches (that can be only dated indirectly). In this context, future studies should be aimed at obtaining more reliable ages at sites where the MIS 5e stratigraphy points to sea-level fluctuations. This is of particular importance for the southern coasts of France and Corsica, where several interesting Last Interglacial outcrops were never corroborated by robust and state-of-the-art dating techniques. These coastal zones, mostly occurring in regions with minimal or negligible neotectonics, have the potential to provide important insights into the magnitude and the sea-level fluctuations within the MIS 5e in the western Mediterranean.

A particular situation characterizes the coastal plains of the northwestern Adriatic Sea where, because of the regional subsiding setting, deposits related to MIS 5e are found at considerable depth. Despite the limited accessibility through stratigraphic cores, they allow investigating the 3D relations existing between different sedimentary facies formed during the marine transgression. In this area, the chronostratigraphy is mainly based on pollen analyses which correlate with the Eemian paleobotanic assemblages recognized in other European regions.

Gathering more reliable ages would also help solve several scientific debates over different sites (the main ones were briefly summarized in the regional descriptions above), as well as the long-lasting debate over the presence, in the Western Mediterranean, of Senegalese fauna (and, in particular, *P. latus*) also in stages other than MIS 5e.

### 7.9 Data availability

The Western Mediterranean sea-level database is available open access and kept updated as necessary at this link: <https://doi.org/10.5281/zenodo.4497365> (Cerrone et al, 2021b). The files at this link were exported from the WALIS database interface on the 3rd of February 2021. Description of each field in the database is contained at this link: <https://doi.org/10.5281/zenodo.3961544>, which is readily accessible and searchable here: <https://walis-help.readthedocs.io/en/latest/>. More information on the World Atlas of Last Interglacial Shorelines can be found here: <https://warmcoasts.eu/world-atlas.html>. Users of our database are encouraged to cite the original data sources alongside our database and this article. The background topography for geographic images has been obtained from the Shuttle Radar Topography Mission void-filled DEM (Farr et al., 2007) unless specifically noted in the image.

### 7.10 Author contributions

All authors compiled the database and wrote the manuscript jointly. C. Cerrone curated the text for southern Italy and the southern portion of the Western Mediterranean (Algeria and Morocco). M. Vacchi curated text for France, Corsica and Sardinia. A. Fontana curated text for the Adriatic Sea. A. Rovere curated the text and data for Spain and Tyrrhenian Northern Italy.

## **8. Discussion on the new data in the regional framework and concluding remarks**

This study has provided new constraints to the elevation and age of the marine terraces located in two key areas of the Tyrrhenian margin of the Southern Apennines, i.e., the Campania Plain coastal graben and the Basilicata- northern Calabria sector. The late Quaternary tectonics of the Campania Plain is characterised by intense volcanism occurred in areas where densely populated towns and settlements are situated. The Campania Plain has been investigated by a plethora of geophysical and subsurface stratigraphy studies but direct geological observations on outcropping Quaternary units and, more importantly, paleo-sea level markers were lacking and have been provided for the first time with this study. The study bears new constraints to both the Campania Plain deformation history and vertical motions of one of its main horst block, with implications on seismic hazard of the region.

The second study area, the Basilicata - northern Calabria area, is particularly interesting for its position. In fact, it is located between two regions of the Tyrrhenian margin (namely, the Campania and southern Calabria coastal stretches), which recorded subdued vs. fast Quaternary uplift, respectively. For that area, contrasting information on late Quaternary uplift was available based on former studies (Filocamo et al., 2009, and references therein), and the new U-Series dating provided with this study represent robust constraints to its uplift history. Overall, the new data, based on detailed geomorphological, stratigraphic and geochronological analyses, allow a better understanding of late Quaternary evolution and the uplift history of the Tyrrhenian margin (**Figure 92**).

In addition, the new data fit within a standardized sea-level metadata for the Western Mediterranean coasts (Spain, France, mainland Italy, Algeria and Morocco) of the World Atlas of Last Interglacial Shorelines (WALIS).

1. The first study (Manuscript 1 and 2, **Section 6.1** *Evolution of the Campania Plain Quaternary coastal graben (southern Apennines): constraints from raised paleoshorelines* and **6.2** *Tectonic implications of raised Quaternary paleoshorelines in the NE sector of the Campania plain, southern Italy*, respectively) is focused on the northeastern sector of the Campania Plain. The study provides for the first-time field evidence of the Quaternary evolution of that area by the identification and detailed characterisation of the geomorphological, stratigraphical and structural features of a raised marine terrace flight. In addition, the new data contribute to constrain both the structural framework, which governed the formation of the Campania Plain graben, and the geomorphological evolution of the main horst blocks, located at the northern boundary of the sub-basin where active volcanoes are located. The main focus of the study were the study of marine terraces outcropping along the southern mountain front, c.15 km length, of Mt. Fellino ridge, which is bounded by a c. E-W oriented extensional fault zone, namely Polvica fault. The study allowed the reconstruction of (i) the shoreline development in response to erosional/depositional processes governed by relative sea level change, in the framework of coeval extensional tectonics, and (ii) a chronological framework for the outcropping paleoshorelines. In particular, the outcropping paleoshoreline remnants are assigned to two displaced marine terraces, namely T2 and T1. These terraces occur at elevations variable along the Mt. Fellino ridge, and are framed in the + 50 – 80 m range for T1 and the + 75 – 200 m range for T2. The faults offsetting the T2 marine deposits (namely, E-W striking normal faults and NNW striking transfer faults) are interpreted as part of a single, segmented extensional fault system controlled by roughly N-S to NNW-SSE horizontal extension. The identified extensional system, being consistent with the regional structure imaged by seismic data, represents the

first field evidence of the tectonics controlling the formation of the Campania Plain coastal graben. The elevation of T2 is higher in the middle of the ridge and it decreases in a specular way laterally, suggesting an uplift variation along the strike of the Polvica fault. The synchronous correlation method, constrained by U-series dating on a calcite vein, which postdates marine sands of the T2, allowed modelling of paleoshorelines T1 and T2 uplifted in the footwall of the Polvica Fault and their correlation with MIS 7 and 9, respectively. In addition, along-strike variation of uplift rate of Polvica Fault have been assessed between c. 0.2 to 0.6 mm/y due to the geometry of the fault and the estimated uplift rate has been associated to footwall uplift. Besides the difficulties to isolate the regional component due to lack available information, its contribution to the uplift of the paleoshorelines in Polvica area has been excluded considering the few evidences of the nearby horst blocks (0.2 mm/y for the Sorrento Peninsula and 0.12 mm/y for the Cilento). Moreover, by integration of subsurface and surface data, a mean throw rate of 0.4 mm/y was calculated for the Polvica Fault during the Middle Pleistocene to Present. By this study, an in-depth investigation on the paleoseismicity of the NE edge of Campania Plain is suggested. The results presented in this work, providing new direct evidence that effectively complements the large amount of existing subsurface datasets, allow for a significant step forward in the understanding of the tectonic and sedimentary processes governing the Quaternary development of the Tyrrhenian back-arc basin margin.

2. The second study (Manuscript 3, **Section 6.3** *Sea level fluctuations along the raised Tyrrhenian margin of northern Calabria-Basilicata (southern Italy): New U-series dating of late Quaternary paleoshorelines*) has been devoted to the analysis of marine terraces along the c. 25 km coastal sector of Basilicata - Calabria, where a flight of Quaternary marine terraces between 0 and 160 m crops out, reaching 240 m to the south of the investigated area. Detailed geomorphological-stratigraphical analyses on remnants of paleoshorelines located within 60 m a.s.l. have shown that the rocky coast of the investigated coastal stretch has been affected by multiple relative sea level fluctuations, during which reworking of older shorelines has occurred. U-series dating of coral *Cladocora caespitosa* and calcite concretions, either predating or postdating individual paleoshorelines, has allowed the construction of a chronological framework for the identified relative sea-level markers, and their correlation with MIS 7, distinct peaks of MIS 5 and MIS 6e. In addition, a Relative Sea Level curve for the study area has been reconstructed for the late Quaternary. A mean uplift rate since the Last Interglacial has been evaluated in the range of c. 0.24 mm/y, one order of magnitude larger than former estimates. The obtained uplift rate value has been used to infer the elevations of MIS 5a, 5c and 6e peaks, which are higher than those reported in most of the sea-level curves worldwide, and in particular + 1.5/2 m, - 8 m and c. -34 m above and below the modern mean sea level, respectively. However, the MIS 5a paleo-elevation of the sea level obtained is consistent with evidence from stable areas of the western Mediterranean (e.g., Baleari island, Bardaji et al., 2009). Worth noting, in this study is reported for the first time the occurrence of the MIS 6e paleoshoreline in the Mediterranean. Our results demonstrate that a mere sequential correlation may be misleading in the interpretation of flights of marine terraces, and indicates that multiple age controls are crucial to

unravelling the complex interaction between uplift and sea level fluctuations in uplifted coastal areas. On the large scale, these results pose new constraints to be considered in evaluations of ice sheet volumes during those substages. In fact, it appears that sea level curves derived from oxygen isotope records tend to overestimate the continental ice sheets mass and maybe also underestimating the drop of global ocean temperature during MIS 6 and following MIS 5e.

Even if the study of the higher paleoshorelines in the Basilicata-northern Calabria area is beyond the aim of this work, the new findings allow to discuss former geomorphological and tectonic interpretations, according to which the marine terraces in the 160 to 240 m a.s.l. elevation range are related to the Early Pleistocene, while the 15 to 100 m a.s.l. to the Middle Pleistocene and those at ca. 8m to the Late Pleistocene (Filocamo et al., 2009). Such interpretations were based on the chronological framework by Carobene et al., (1986), which rested on U-series dating that have been rejected with this dissertation. Assuming a constant uplift rate of  $\sim 0.24$  mm/y calculated for the study area based on our new reconstruction, the paleoshorelines standing at 150-160 m could be tentatively related to the Middle-Pleistocene (MIS 13-15).

The northern Calabria uplift is considered as the response to a regional, deep-seated phenomenon and, in particular, the response in the southern Apennines to the rebound of the detached Apulian slab, which has followed shortening in the mountain belt (e.g., Cinque et al., 1993; Ascione et al., 2012). For other areas of the eastern Tyrrhenian margin, i.e. for areas in southern Calabria (e.g., Dumas et al., 1987, 1982; Ferranti et al., 2006 and reference therein) fault-related components of uplift have been invoked to justify high uplift rates. Net evidence of a fault-related contribution to uplift has been also recognised, with this study, in the Mt. Fellino area the raise of which is mainly the response to uplift of the

footwall block of the Polvica Fault. If the Basilicata – northern Calabria sector is considered, no net evidence of a fault-related contribution to uplift has been identified. Specifically, the spatial distribution of the identified paleoshorelines does not show any net evidence of along-coast displacement in the entire investigated coastal stretch, which extends for about 25 km in length. Moreover, the rather constant vertical position of each of the paleoshorelines (particularly, the MIS5 paleoshorelines, which crop out in the entire coastal stretch) is suggestive of a large-scale phenomenon governing uplift, rather than of uplift governed by a fault in the offshore, where however some moderate magnitude earthquake is recorded (e.g., CPTI15, Rovida et al., 2019, 2020). However, in order to rule out the occurrence of active faults in the offshore, further investigations should be carried out by means of, e.g., the integration of the onshore information based on this study with information from the offshore (based on, e.g., the analysis of offshore seismic profiles) and with new onshore information from the coastal stretch to the south of the one investigated with this study, e.g., the Diamante-Cetraro sector, where the presence of material such as corals or speleothems suitable for U-series dating is reported in Literature. By integrating the results of this study with available data from other studied sectors (**Figure 92c**), during the Middle Pleistocene, the Tyrrhenian side of Southern Apennines is characterised by an alternation of subsiding areas (e.g., the coastal plains of Garigliano, Campania, Sele and the offshore of the northern Calabria area) with the Sorrento Peninsula and Cilento (Mt. Bulgheria) areas subject to uplift. Such behaviour changes since the Last Interglacial, when most of the Campania margin becomes substantially stable. In contrast, the Campania Plain is still subject to subsidence (**Figure 92d**), and the Basilicata-northern Calabria still experience moderate uplift (ca. 0.24 mm/y). Former studies point to the Sele Plain coastal graben recording slightly uplift. Such uplift appears quite “anomalous” if the substantial stability of adjacent headlands (Sorrento peninsula and Cilento) is considered. In order to gain information on this

issue, during my doctorate I prepared for U-series analysis some samples of *C. caespitosa* from a core drilled in the southern part of the Sele Plain. Unfortunately, due to COVID-19 sanitary emergency this part of the work could not be developed. Although not exhaustive to unravel the late Quaternary behaviour of the entire northern Campania to northern Calabria coastal stretch, the results of this study provide new data and constraints useful to the reconstruction of both sea level curves for the Mediterranean area and the Quaternary evolution of the Tyrrhenian margin on a regional scale. Regarding this last point, it is worth noting that the estimated uplift rates are consistent with those estimated for passive margins worldwide (e.g., Pedoja et al., 2014).

3. Complementing the new results, the third study (Manuscript 4, **Section 7. Last Interglacial sea-level proxies in the Western Mediterranean**) carried out in the framework of “The World Atlas of Last Interglacial Shorelines” (WALIS), synthesises existing knowledge on MIS 5 paleoshorelines on the regional scale. In fact, a database with raw data concerning the Relative Sea level point for the Western Mediterranean area has been compiled. The database follows a standard used to uniform the information derived from previous works on sea level indicators both about the chronological age constraints and their geological meaning. Many previous studies presented already in Literature have been reviewed for the Western Mediterranean, an area that is in the far field from the influence of the glaciers. That means the Western Mediterranean could be suitable to provide very good sea level proxies in order to estimate accurately the eustatic sea level during the last 125 ka time span and to better constrain the GIA-models. This kind of database could be very useful to determine areas where to carry out in-depth analyses of MIS 5 sea level markers.

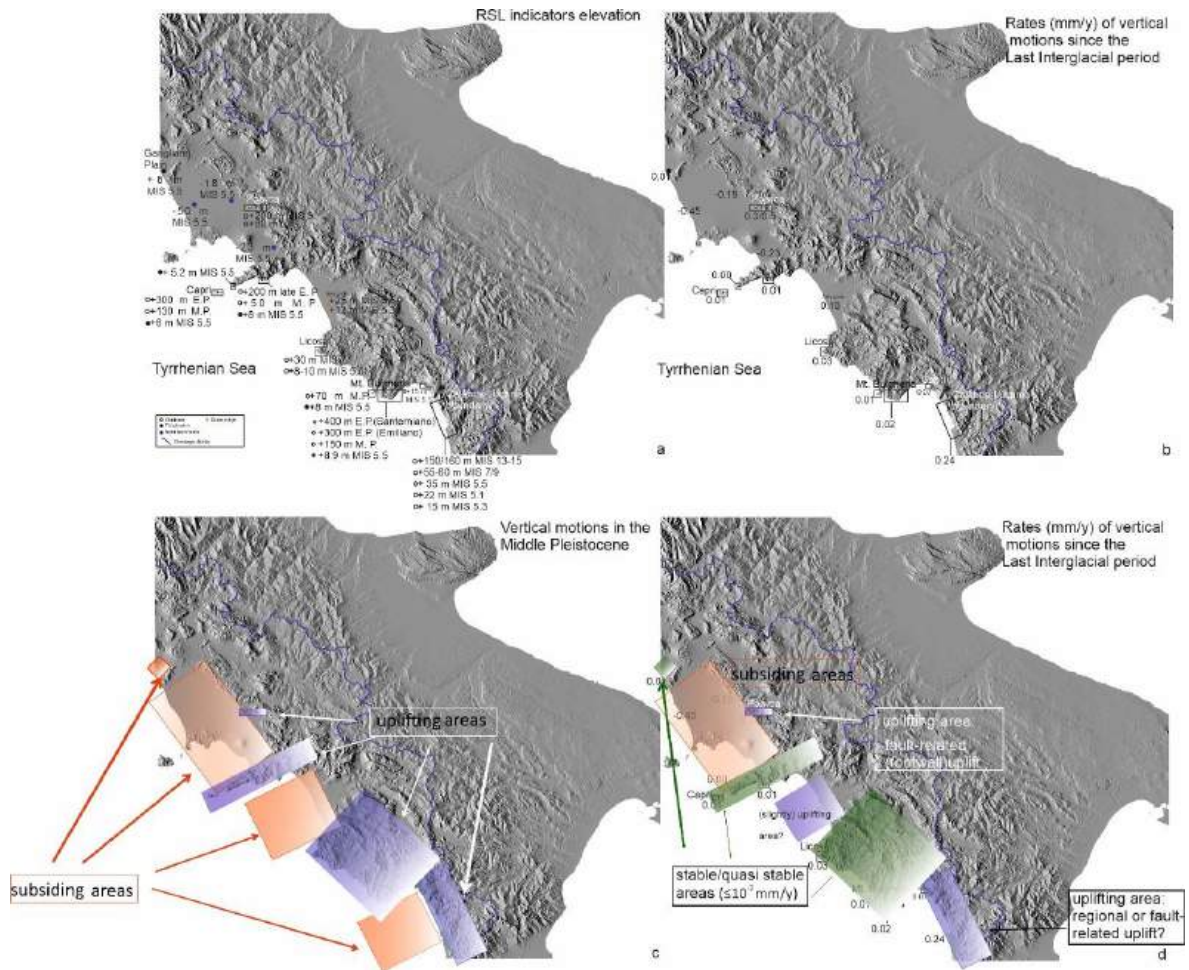


**Figure 92.** a) Southern Apennines hillshade map (resolution 90 m) with elevation of Quaternary paleoshorelines along the Tyrrhenian coast. The blue line indicates the drainage divide; b) Uplift rate calculated for the Last Interglacial span time for the Tyrrhenian coasts from Campania to northern Calabria; c) vertical motion map during the Middle Pleistocene; d) rates (mm/y) of vertical motion since the Last Interglacial time.

## References

- Abad, M., Rodríguez-Vidal, J., Aboumaria, K., Zaghloul, M.N., Cáceres, L.M., Ruiz, F., Martínez-Aguirre, A., Izquierdo, T., Chamorro, S., 2013. Evidence of MIS 5 sea-level highstands in Gebel Mousa coast (Strait of Gibraltar, North of Africa). *Geomorphology* 182, 133–146. <https://doi.org/10.1016/j.geomorph.2012.11.004>
- Abate, B., Di Maggio, C., Incandela, A., Renda, P., 1991. Nuovi dati sulla geologia della penisola di Capo San Vito (Sicilia NW). *Mem. Soc. Geol. Ital.* 47, 15–25.
- Abate, B., Ferrini, G., Incandela, A., Renda, P., 1992. Ritrovamento di depositi a *Strombus bubonius* nell'isola di Favignana. *Riv. Mineraria Sicil.* 162, 37–46.
- Abate, B., Di Maggio, C., Incandela, A., Renda, P., 1993. Carta geologica dei Monti di Capo San Vito, scala 1:25.000. *Dip. di Geol. e Geod. dell'Università di Palermo*.
- Abate, B., Buccheri, G., Renda, P., Incandela, A., 1996. Le Sezioni Tirreniane delle località “La Conca e Punta Libeccio” (Isola di Marettimo-Arcipelago delle Egadi, Sicilia N-O). *Indagini stratigrafica e paleoecologica. Boll. Soc. Geol. Ital.* 115, 145–158.
- Adhemar, J.A., 1842. *Révolutions de la mer, déluges périodiques*. Carilian-Goeury V., R.G., Paris 184.
- Aitken, M.J., 1985. *Thermoluminescence dating*. London, Academic Press 280.
- Amato, A., 2000. Estimating Pleistocene tectonic uplift rates in the South-Eastern Apennines (Italy) from erosional landsurfaces and marine terraces. Slaymaker, O. (Ed.), *Geomorphol. Hum. Act. Glob. Environ. Chang.* Wiley, New York 67–87.
- Albrecht, P. and Mosetti, F., 1987. Karst evolution and sea level. *Memorie Società Geologica Italiana*, 40, 383–387.
- Ambert, P., 1999. Les formations littorales pléistocènes du Languedoc [Pleistocene shorelines of Languedoc]. *Quaternaire* 10, 83–93. <https://doi.org/10.3406/quate.1999.1633>
- Amorosi, Colalongo, Pasini and Preti, 1999. Sedimentary response to Late Quaternary sea-level changes in the Romagna coastal plain (northern Italy), *Sedimentology*, 46(1), 99–121, doi:10.1046/j.1365-3091.1999.00205.x.
- Amorosi, A., Colalongo, M.L., Fiorini, F., Fusco, F., Pasini, G., Vaiani, S.C., Sarti, G., 2004. Palaeogeographic and palaeoclimatic evolution of the Po Plain from 150-ky core records. *Glob. Planet. Change* 40, 55–78. [https://doi.org/10.1016/S0921-8181\(03\)00098-5](https://doi.org/10.1016/S0921-8181(03)00098-5)
- Amorosi A. Fontana A., A.F.P.S.B.A., 2008a. Post-LGM sedimentation and Holocene shoreline evolution in the NW Adriatic coastal are. *Geo Acta* 7.
- Amorosi, A., Pavesi, M., Lucchi, M.R., Sarti, G., Piccin, A., 2008b. Climatic

- signature of cyclic fluvial architecture from the Quaternary of the central Po Plain Italy. *Sediment. Geol.* 209, 58–68. <https://doi.org/10.1016/j.sedgeo.2008.06.010>
- Amorosi, A., Pacifico, A., Rossi, V., Ruberti, D., 2012. Late Quaternary incision and deposition in an active volcanic setting: The Volturno valley fill, southern Italy. *Sediment. Geol.* 282, 307–320. <https://doi.org/10.1016/j.sedgeo.2012.10.003>
- Amorosi, A., Antonioli, F., Bertini, A., Marabini, S., Mastronuzzi, G., Montagna, P., Negri, A., Rossi, V., Scarponi, D., Taviani, M., Angeletti, L., Piva, A., Vai, G.B., 2014. The Middle-Upper Pleistocene Fronte Section (Taranto, Italy): An exceptionally preserved marine record of the Last Interglacial. *Glob. Planet. Change* 119, 23–38. <https://doi.org/10.1016/j.gloplacha.2014.04.007>
- Amorosi, A., Maselli, V., Trincardi, F., 2016. Onshore to offshore anatomy of a late Quaternary source-to-sink system (Po Plain Adriatic Sea Italy). *Earth-Science Rev.* 153, 212–237. <https://doi.org/10.1016/j.earscirev.2015.10.010>
- Anderson, Densmore, Ellis, 1999. The generation and degradation of marine terraces. *Basin Res.* 11, 7–19. <https://doi.org/10.1046/j.1365-2117.1999.00085.x>
- Andreucci, S., Pascucci, V., Murray, A.S., Clemmensen, L.B., 2009. Late Pleistocene coastal evolution of San Giovanni di Sinis, west Sardinia (Western Mediterranean). *Sediment. Geol.* 216, 104–116.
- Andreucci, S., Clemmensen, L.B., Murray, A.S., Pascucci, V., 2010. Middle to late Pleistocene coastal deposits of Alghero northwest Sardinia (Italy):~Chronology and evolution. *Quat. Int.* 222, 3–16. <https://doi.org/10.1016/j.quaint.2009.07.025>
- Anthony, E.J., 2008. Shore processes and their Palaeoenvironmental applications. *Elvesier*.
- Antonioli, F., Dai Pra, G., Hearty, P.J., 1988. I sedimenti quaternari nella fascia costiera della Piana di Fondi (Lazio meridionale). *Boll. della Soc. Geol. Ital.* 107, 491–501.
- Antonioli, F., Belluomini, G., Ferranti, L., Improta, S., Reitano, G., 1994a. Il sito preistorico dell'arco naturale di Capo Zafferano (Sicilia). Aspetti geomorfologici e relazione con le variazioni del livello marino olocenico. *Quat.* 7 (1), 109–118.
- Antonioli, F., Cinque, A., Ferranti, L., Romano, P., 1994b. Emerged and submerged quaternary marine terraces of Palinuro Cape (southern Italy). *Mem. Descr. Cart. Geol. d'Italia LII*, 237–260.
- Antonioli, F., Leoni, G., 1998. Siti archeologici sommersi e loro utilizzazione quali indicatori per lo studio delle variazioni recenti del livello del mare. *Quat.* 11 (1), 53–66.
- Antonioli, F., Girotti, O., Improta, S., Nisi, M.F., Puglisi, C., Verrubbi, V., 1999a.

- Nuovi dati sulla trasgressione marina olocenica nella pianura versiliese, in: Proceedings of the Meeting 'Le Pianure', Ferrara. pp. 214–218.
- Antonioli, F., Silenzi, S., Vittori, E., Villani, C., 1999b. Sea level changes and tectonic mobility: Precise measurements in three coastlines of Italy considered stable during the last 125 ky. *Phys. Chem. Earth Part A Solid Earth Geod.* 24, 337–342. [https://doi.org/10.1016/s1464-1895\(99\)00038-1](https://doi.org/10.1016/s1464-1895(99)00038-1)
- Antonioli, F., Cremona, G., Immordino, F., Puglisi, C., Romagnoli, C., Silenzi, S., Valpreda, E., Verrubbi, V., 2002. New data on the Holocene sea-level rise in NW Sicily (Central Mediterranean Sea). *Glob. Planet. Change* 34, 121–140. [https://doi.org/10.1016/S0921-8181\(02\)00109-1](https://doi.org/10.1016/S0921-8181(02)00109-1)
- Antonioli, F., Lambeck, K., Kershaw, S., Rust, D., Sylos Labini, S., Segre, A., Verrubbi, Belluomini, G., Dai Pra, G., Ferranti, L., Improta, S., Vesica, P., 2004. Evidence for non-uniform uplift rates in southern Italy (Calabria and eastern Sicily: Taormina, St. Alessio, Ganzirri, Scilla, Ioppolo, Capo Rizzuto) on glacialcycle timescales. *Quat. Nov.* VIII, 187–192.
- Antonioli, F., Ferranti, L., Kershaw, S., 2006a. A glacial isostatic adjustment origin for double MIS 5.5 and Holocene marine notches in the coastline of Italy. *Quat. Int.* 145–146, 19–29. <https://doi.org/https://doi.org/10.1016/j.quaint.2005.07.004>
- Antonioli, F., Kershaw, S., Renda, P., Rust, D., Belluomini, G., Cerasoli, M., Radtke, U., Silenzi, S., 2006b. Elevation of the last interglacial highstand in Sicily (Italy): A benchmark of coastal tectonics. *Quat. Int.* 145–146, 3–18. <https://doi.org/10.1016/j.quaint.2005.07.002>
- Antonioli, F., Ferranti, L., Lambeck, K., Kershaw, S., Verrubbi, V., Dai Pra, G., 2006c. Late Pleistocene to Holocene record of changing uplift rates in southern Calabria and northeastern Sicily (southern Italy, Central Mediterranean Sea). *Tectonophysics* 422, 23–40. <https://doi.org/10.1016/j.tecto.2006.05.003>
- Antonioli, F., Ferranti, L., Fontana, A., Amorosi, A., Bondesan, A., Braitenberg, C., Dutton, A., Fontolan, G., Furlani, S., Lambeck, K., Mastronuzzi, G., Monaco, C., Spada, G., Stocchi, P., 2009. Holocene relative sea-level changes and vertical movements along the Italian and Istrian coastlines. *Quat. Int.* 206, 102–133. <https://doi.org/10.1016/j.quaint.2008.11.008>
- Antonioli, F., D'Orefice, M., Ducci, S., Firmati, M., Foresi, L.M., Graciotti, R., Pantaloni, M., Perazzi, P., Principe, C., 2011. Palaeogeographic reconstruction of northern Tyrrhenian coast using archaeological and geomorphological markers at Pianosa island (Italy). *Quat. Int.* 232, 31–44. <https://doi.org/10.1016/j.quaint.2010.03.017>
- Antonioli, F., Lo Presti, V., Rovere, A., Ferranti, L., Anzidei, M., Furlani, S., Mastronuzzi, G., Orru, P.E., Scicchitano, G., Sannino, G., Spampinato, C.R., Pagliarulo, R., Deiana, G., de Sabata, E., Sansò, P., Vacchi, M., Vecchio, A.,

2015. Tidal notches in Mediterranean Sea : a comprehensive analysis. *Quat. Sci. Rev.* 119, 66–84. <https://doi.org/10.1016/j.quascirev.2015.03.016>
- Antonioli, F., Ferranti, L., Stocchi, P., Deiana, G., Presti, V. Lo, Furlani, S., Marino, C., Orru, P., Scicchitano, G., Trainito, E., others, 2018. Morphometry and elevation of the last interglacial tidal notches in tectonically stable coasts of the Mediterranean Sea. *Earth-Science Rev.* 185, 600–623.
- Argnani, A., Bortoluzzi, G., Bozzani, A., Canepa, A., Ligi, M., Palumbo, V., Serracca, P., Tricardi, F., 1989. Sedimentary dynamics on the Eastern Tyrrhenian margin, Italy. *PS/87 Cruise report. G. di Geol.* 51/1, 165–178.
- Armijo, R., Meyer, B., King, G.C.P., Rigo, A., Papanastassiou, D., 1996. Summary for Policymakers, in: *Intergovernmental Panel on Climate Change (Ed.), Climate Change 2013 - The Physical Science Basis*. Cambridge University Press, Cambridge, pp. 1–30. <https://doi.org/10.1017/CBO9781107415324.004>
- Ascione, A., Cinque, A., 1997. Fault scarps in the southern Apennines: Origin, age and tectonic significance (in Italian). *Quat.* 10, 285–292.
- Ascione, A., Romano, P., 1999. Vertical movements on the eastern margin of the Tyrrhenian extensional basin. New data from Mt. Bulgheria (Southern Apennines, Italy). *Tectonophysics* 315, 337–356. [https://doi.org/10.1016/S0040-1951\(99\)00279-6](https://doi.org/10.1016/S0040-1951(99)00279-6)
- Ascione, A., Ciarcia, S., Di Donato, V., Mazzoli, S., Vitale, S., 2012. The Pliocene-Quaternary wedge-top basins of southern Italy: an expression of propagating lateral slab tear beneath the Apennines. *Basin Res.* 24, 456–474. <https://doi.org/10.1111/j.1365-2117.2011.00534.x>
- Ascione, A., Mazzoli, S., Petrosino, P., Valente, E., 2013. A decoupled kinematic model for active normal faults: Insights from the 1980,  $m_s = 6.9$  Irpinia earthquake, southern Italy. *Bull. Geol. Soc. Am.* 125, 1239–1259. <https://doi.org/10.1130/B30814.1>
- Auriemma, R., Solinas, E., 2009. Archaeological remains as sea level change markers: A review. *Quat. Int.* 206, 134–146. <https://doi.org/10.1016/j.quaint.2008.11.012>
- Authemayou, C., Pedoja, K., Heddar, A., Molliex, S., Boudiaf, A., Ghaleb, B., Lanoe, B.V.V., Delcaillau, B., Djellit, H., Yelles, K., Nexer, M., 2016. Coastal uplift west of Algiers (Algeria): pre- and post-Messinian sequences of marine terraces and rias and their associated drainage pattern. *Int. J. Earth Sci.* 106, 19–41. <https://doi.org/10.1007/s00531-016-1292-5>
- Bada, J.L., Belluomini, G., Bonfiglio, L., Branca, M., Burgio, E., Delitalia, L., 1991. Isoleucine epimerization ages of Quaternary mammals from Sicily. *Quat.* 4 (1a), 46–54.
- Baggioni, M., Suc, J.P., & Vernet, J.L., 1981. Le Plio-Pleistocene de Camerota (Italie Meridionale): geomorphologie e paleoflores. *Geobios* 14 (2), 229–237.

- Baker, R.G.V., Haworth, R.J., 1999. Evidence for the nature of late Holocene sea level fall on the New South Wales coast from fixed biological indicators: was the fall smooth or fluctuating. Kesby, J.A., Stanely, J.M., McLean, R.F., Olive, L.J. (eds). *Geodiversity readings Aust. Geogr. close 20th century*, Spec. publications 6. Inst. Aust. Geogr. Canberra, 351–360.
- Balescu, S., Lamothe, M., Lh, R., 1997. Thermoluminescence dating tests of Pleistocene sediments from uplifted marine shorelines along the southwest coastline of the Calabrian Peninsula ( southern Italy ) :::'• ROSARNO ~ n Sicily /. *Palaeogeogr. Palaeoclimatol. Palaeoecol.* 130, 25–41.
- Barattolo, F., Cinque, A., D'Alessandro, E., Guida, M., Romano, P., & Ermolli, E.R., 1992. Geomorfologia ed evoluzione tettonica quaternaria dell' Isola di Capri. Estratto da *Stud. Geol. Camerti*, Vol. Spec. 1, 221–229.
- Barberi, F., Innocenti, F., Lirer, L., Munno, R., Pescatore, T., & Santacrose, R., 1978. The Campania Ignimbrite: a major prehistoric eruption in the neapolitan area (Italy). *Bullettin Volcanol.* 41,1, 1–22.
- Bard, E., Hamelin, B., Fairbanks, R.G., 1990. U-Th ages obtained by mass spectrometry in corals from Barbados: sea level during the past 130.000 years. *Nature* 346, 456–458.
- Bard, E., Antonioli, F., Silenzi, S., 2002. Sea-level during the penultimate interglacial period based on a submerged stalagmite from Argentarola Cave (Italy). *Earth Planet. Sci. Lett.* 196, 135–146.
- Bardají, T., Civis, J., Dabrio, C.J., Goy, J.L., Somoza, L., 1986. Geomorfología y estratigrafía de las secuencias marinas y continentales cuaternarias de la Cuenca de Cope, Murcia, España, in: *Estudios Sobre Geomorfología Del Sur de España*. pp. 11–16.
- Bardají, T., Goy, J.L., Zazo, C., Hillaire-Marcel, C., Dabrio, C.J., Cabero, A., Ghaleb, B., Silva, P.G., Lario, J., 2009a. Sea level and climate changes during OIS 5e in the Western Mediterranean. *Geomorphology* 104, 22–37. <https://doi.org/10.1016/j.geomorph.2008.05.027>
- Bardají, T., Goy, J.L., Zazo, C., Hillaire-Marcel, C., Dabrio, C.J., Cabero, A., Ghaleb, B., Silva, P.G., Lario, J., 2009b. Reply to the comments by Mauz, B. and Antonioli, F. on “Sea Level and Climate Changes during OIS 5e in the Western Mediterranean.” *Geomorphology* 110, 231–235. <https://doi.org/https://doi.org/10.1016/j.geomorph.2009.05.007>
- Bardají, T., Cabero, A., Lario, J., Zazo, C., Silva, P.G., Goy, J.L., Dabrio, C.J., 2015. Coseismic vs. climatic factors in the record of relative sea level changes: an example from the Last Interglacials in SE Spain. *Quat. Sci. Rev.* 113, 60–77. <https://doi.org/https://doi.org/10.1016/j.quascirev.2014.10.005>
- Barra, D., Cinque, A., Gewalt, M., & Hurtgen, C., 1991. L'ospite caldo *Sylvestra seminis* (Bonaduce, Masoli & Pugliese, 1976) (Crustacea, Ostracoda): un possibile marker dell'Ultimo Interglaciale dell'area Mediterranea. *Quat.* 4 (2),

327–332.

- Barra, D., Romano, P., Santo, A., Campajola, L., Roca, V., Tuniz, C., 1996. The Versilian trasgression in the Volturno river plain (Campania, Southern Italy): Palaeoenvironmental history and chronological data. *Quat.* 9, 445–458.
- Barrière, J., 1966. Le rivage tyrrhénén de létang de Bages et de Sigean (Aude). *Bull. l'Association française pour létude du Quat.* 3, 251–283. <https://doi.org/10.3406/quate.1966.1046>
- Bartole, R., Savelli, D., Tramontana, M., Wezel, F.C., 1984. Structural and sedimentary features in the Tyrrhenian margin off Campania, Southern Italy. *Mar. Geol.* 55, 163–180. [https://doi.org/10.1016/0025-3227\(84\)90067-7](https://doi.org/10.1016/0025-3227(84)90067-7)
- Bartrum, J.A., 1916. High-water rock platforms: a phase of shoreline erosion. *Trans. Proc. New Zeal. Inst.* 16, 132–134.
- Bartrum, J.A., 1926. “Abnormal” shore platforms. *J. Geol.* 34, 793–806.
- Bellucci, F., 1994. New stratigraphic knowledges on volcanic deposits in the underground od southern Camapanian Plain. *Boll. Soc. Geol. Ital.* 113, 395–420.
- Bellucci, F., 1998. New stratigraphic knowledges on avas and pyroclastic deposits in the underground of Somma-Vesuvio area. *Boll. Soc. Geol. Ital.* 117, 385–405.
- Belluomini, G., Branca, M., Delitala, L., Pecorini, G., Spano, C., 1986. Isoleucine epimerization dating of Quaternary marine deposits in Sardinia, Italy in Dating Mediterranean shorelines. *Zeitschrift für Geomorphol. Suppl.* 109–117.
- Belluomini, G., Delitala, L., 1988a. Amino acid racemization dating of Quaternary deposits of Central and Southern Italy. *Org. Geochem.* 13, 735–740.
- Belluomini, G., Gliozzi, E., Ruggieri, G., Branca, M., Delitalia, L., 1988b. First dates on the terraces of the Crotona Peninsula (Calabria, Southern Italy). *Boll. Soc. Geol. Ital.* 107, 249–254.
- Belluomini, G., Caldara, M., Casini, C., Cerasoli, M., Manfra, L., Mastronuzzi, G., Palmentola, G., Sanso, P., Tuccimei, P., Vesica, P.L., 2002. The age of Late Pleistocene shorelines and tectonic activity of Taranto area , Southern Italy. *Quat. Sci. Rev.* 21, 525–547. [https://doi.org/S0277-3791\(01\)00097-X](https://doi.org/S0277-3791(01)00097-X)
- Bender, M., Fairbank, R.G., Taylor, F.W., Matthews, R.K., Goddard, J.G., Broecker, W.S., 1979. Uranium series dating of the Pleistocene reef tracts of Barbados, West Indies. *Geol. Soc. Amer. Bull.* 90, 577.
- Benjamin, J., Rovere, A., Fontana, A., Furlani, S., Vacchi, M., Inglis, R.H., Galili, E., Antonioli, F., Sivan, D., Miko, S., Mourtzas, N., Felja, I., Meredith-Williams, M., Goodman-Tchernov, B., Kolaiti, E., Anzidei, M., Gehrels, R., 2017. Late Quaternary sea-level changes and early human societies in the central and eastern Mediterranean Basin: An interdisciplinary review. *Quat. Int.* 449, 29–57. <https://doi.org/10.1016/j.quaint.2017.06.025>
- Benvenuti, M., Martini, I.P., 2002. Analysys of terrestrial hyperconcentrated flows

- and their deposits. Bak, V., Martini, I.P., Garzon, G., (eds), Flood Megafloods Process. Depos. (Ed. by). I.A.S., Spec. Publ. Vol. 32, O, 167–193.
- Berger, A.L., 1981. The Astronomical Theory of Paleoclimates, in: Berger, A. (Ed.), Climatic Variations and Variability: Facts and Theories: NATO Advanced Study Institute First Course of the International School of Climatology, Ettore Majorana Center for Scientific Culture, Erice, Italy, March 9--21, 1980. Springer Netherlands, Dordrecht, pp. 501–525. [https://doi.org/10.1007/978-94-009-8514-8\\_29](https://doi.org/10.1007/978-94-009-8514-8_29)
- Bernart, M., Paskoff, R., & Sanlaville, P., 1985. Datation de terrasses marines de la côte est de la Tunisie: Méthode lo-U appliquée aux mollusques fossiles, un exemple de contamin. Blair, T.C. Sedimentol. debris-flow-dominated Warm Spring Canyon Alluv. fan, Death Val. California. Sedimentol. 46, 941–965.
- Bernat, M., JC, E., JC, B., others, 1982. Nouvelles datations Io-U sur des Strombes du dernier Interglaciaire en Méditerranée (La Marina, Espagne) et implications géologiques. Comptes rendus des seances l'academie Sci. Paris II–295.
- Bianca, M., Monaco, C., Tortorici, L., Cernobori, L., 1999. Quaternary normal faulting in southeastern Sicily (Italy): A seismic source for the 1693 large earthquake. Geophys. J. Int. 139, 370–394. <https://doi.org/10.1046/j.1365-246X.1999.00942.x>
- Bianca, M., Catalano, S., De Guidi, G., Gueli, A.M., Monaco, C., Ristuccia, G.M., Stella, G., Tortorici, G., Tortorici, L., Troja, S.O., 2011. Luminescence chronology of Pleistocene marine terraces of Capo Vaticano peninsula (Calabria, Southern Italy). Quat. Int. 232, 114–121. <https://doi.org/10.1016/j.quaint.2010.07.013>
- Bini, M., Zanchetta, G., Drysdale, R.N., Giaccio, B., Stocchi, P., Vacchi, M., Hellstrom, J.C., Couchoud, I., Monaco, L., Ratti, A., Martini, F., Sarti, L., 2020. An end to the Last Interglacial highstand before 120 ka: Relative sea-level evidence from Infreschi Cave (Southern Italy). Quat. Sci. Rev. 250, 106658. <https://doi.org/10.1016/j.quascirev.2020.106658>
- Bintanja, R., van de Wal, R.S.W., Oerlemans, J., 2002. Modelled atmospheric temperatures and global sea levels over the past million years. Nature 437, 125–128.
- Bird, E.C.F., Dent, O.F., 1966. Shore platforms on the South Coast of New South Wales. Austral Geogr. 10, 97–111.
- Bird, E.C., 1976. Coasts (2d ed.), in: Canberra, Australian National University Press. p. 282.
- Bish, D.L., & Post, J., 1993. Quantitative mineralogical analysis using the Rietveld full pattern fitting method. Am. Mineral. 78, 932–940.
- Blair, T.C., McPherson, J.G., 1994. Alluvial fans and their natural distinction from rivers based on morphology, hydraulic processes, sedimentary processes, and facies. J. Sediment. Res. A64, 451–490.

- Blair, T.C., McPherson, J.G., 1998. Recent debris-flow processes and resultant form and facies of the Dolomite alluvial fan, Owens Valley, California. *J. Sediment. Res.* 68, 800–818.
- Blair, T.C., 1999. Sedimentology of the debris-flow-dominated Warm Spring Canyon alluvial fan, Death Valley, California. *Sedimentology* 46, 941–965.
- Blanc, G.A., 1920. Grotta Romanelli I. Stratigrafia dei depositi e natura e origine di essi. *Arch. per l'Antropologia e l'Etnologia* 50, 1–39.
- Blanc, G.A., 1928. Grotta Romanelli II. Dati ecologici e paleontologici. *Arch. per l'Archeologia e l'Etnologia* 58, 1–50.
- Blanc, A.C., 1935. Stratigrafia del Canale Mussolini nell'Agro Pontino. N/A.
- Blanc, A.C., 1936. Una spiaggia pleistocenica a Strombus bu bonius presso Palidoro (Roma). *Ist. Ital. di Antropologia*.
- Blanc, A.C., Segre, A.G., 1947. Nuovi giacimenti tirreniani e paleolitici sulla costiera tra Sperlonga e Gaeta. *Hist. Nat.* 2, 1–2.
- Blanc, A.C., Segre, A.G., 1953. Excursion au Mont Circé, in: 4th Conf Int Assoc Quatern Res. Rome-Pisa. pp. 87–106.
- Blancon, P., Eisenhauer, A., Fietzke, J., Liebetrau, V., 2009. Rapid sea-level rise and reed back-stepping at the close of the last interglacial highstand. *Nature* 458, 881–884.
- Bloom, A.L., W.S., B., Chappell, J.M.A., Matthews, R.K., Mesolella, K.J., 1974. Quaternary sea level fluctuations on a tectonic coast: new  $^{230}\text{Th}/^{234}\text{U}$  dates from the Huon Peninsula, New Guinea. *Quat. Res.* 4, 185–205.
- Blott, S., Pye, K., 2001. A grain size distribution and statistics package for the analysis of unconsolidated sediments. *Earth Surf. Process. Landforms* 26, 1237–1248. <https://doi.org/10.1002/esp.261>
- Boenzi, F., Caldara, M., Pennetta, L., 1985. (The Tyrrhenian transgression in the Castellana envions, Taranto, Italy). *Geol. Appl. e Idrogeol.* 20, 163–175.
- Bonadonna, F.P., 1967a. Studi sul pleistocene del Lazio; IV, La linea di costa tirreniana di Ponte Galeria (Roma). *Quaternaria* 9, 285–299.
- Bonadonna, F.P., 1967b. Studi sul Pleistocene del Lazio. III. Linee di costa lungo il litorale di Tarquinia (Lazio settentrionale). *Geol. Rom.* 6, 131–135.
- Bonaduce, G., Ruggieri, G., Russo, A., 1987. The ostracode genus *Mutulus* and some so-called *Mutulus* from the Mediterranean Miocene-Pleistocene. *Boll. Soc. Paleontol. Ital.* 26 (3), 251–268.
- Bonfiglio, L., 1981. Terrazzi marini e depositi continentali quaternari di Taormina (Sicilia). *Quaternaria*.
- Bonfiglio, L., Violanti, L., 1983. Prima segnalazione di Tirreniano ed evoluzione Pleistocenica del Capo Peloro (Sicilia Nord-Orientale). *Geogr. Fis. Din. Quat.* 6, 3–15.
- Bonifay, E., Mars, P., 1959. Le Tyrrhenien dans le cadre de la chronologie quaternaire mediterraneenne. *Bull. la Société Géologique Fr.* S7-I, 62–78.

- <https://doi.org/10.2113/gssgfbull.s7-i.1.62>
- Bordoni, P., Valensise, G., 1999. Deformation of the 125 ka marine terrace in Italy: tectonic implications. *Geol. Soc. London, Spec. Publ.* 146, 71–110. <https://doi.org/10.1144/gsl.sp.1999.146.01.05>
- Borelli, A., Ciampo, G., De Falco, M., Guida, M., 1988. La morfogenesi del M. Bulgheria (Campania) durante il Pleistocene inferiore e medio. *Mem. Soc. Geol. Ital.* 41, 667–672.
- Boschian, G., Bossio, A., Dall'Antonia, B., Mazzanti, R., 2006. Il Quaternario della Toscana Costiera.
- Bouillin, J.P., 1984. Nouvelle interprétation de la liaison Apennin-Maghrébides en Calabre; conséquences sur la paléogéographie téthyssienne entre Gibraltar et les Alpes. *Rev. Géologie Dyn. Géographie Physique* 25 (5), 321–338.
- Bracchi, V.A., Nalin, R., Basso, D., 2011. Persistrombus latus-bearing deposits south of Isola di Capo Rizzuto, Calabria (Southern Italy). *Quat. - Ital. J. Quat. Sci.* 24, 23–25.
- Brain, M.J., 2016. Past, Present and Future Perspectives of Sediment Compaction as a Driver of Relative Sea Level and Coastal Change. *Curr. Clim. Chang. Reports* 2, 75–85. <https://doi.org/10.1007/s40641-016-0038-6>
- Brancaccio, L., Capaldi, G., Cinque, A., Pece, R., Sgrosso, I., 1978. Th/U dating of corals from a Tyrrhenian beach in Sorrentine Peninsula (southern Italy). *Quaternaria* 20, 175–183.
- Brancaccio, L., Cinque, A., & Sgrosso, I., 1979. L'analisi morfologica dei versanti come strumento per la ricostruzione di eventi neotettonici. *Mem. della Soc. Geol. Ital.* 19, 621–626.
- Brancaccio, L., Cinque, A., Scarpa, R., & Sgrosso, I., 1981. Evoluzione neotettonica e sismicità in Penisola Sorrentina e in Baronia. *Rend. della Soc. Geol. Ital.* 4, 145–149.
- Brancaccio, L., Cinque, A., Belluomini, G., Branca, M., Delitalia, L., 1986. Isoleucine epimerization dating and tectonic significance of Upper Pleistocene sea-level features of the Sele Plain (Southern Italy). *Zeitschrift für Geomorphol.* 62, 159–166.
- Brancaccio, L., Cinque, A., D'Angelo, G., Russo, F., Santangelo, N., & Sgrosso, I., 1987. Evoluzione tettonica e geomorfologica della Piana del Sele (Campania, Appennino meridionale). *Geogr. Fis. e Din. Quat.* 10, 47–55.
- Brancaccio, L., Cinque, A., Russo, F., Belluomini, G., Branca, M., Delitalia, L., 1990. Segnalazione e datazione di depositi marini tirreniani sulla costa campana. *Boll. della Soc. Geol. Ital.* 109, 259–265.
- Brancaccio, L., Cinque, A., Romano, P., Roskopf, C., Russo, F., Santangelo, N., Santo, A., 1991. Geomorphology and neotectonic evolution of a sector of the Tyrrhenian flank of the Southern Apennines (Region of Naples, Italy). *Zeitschrift für Geomorphol. N.F.* 82, 47–58.

- Brancaccio, L., Fiume, G., Grimaldi, M., Rapolla, A., & Romano, P., 1994. Gravimetric analysis in the low Solofrana river valley (Salerno) and considerations on its Quaternary evolution. *Quat.* 117,2, 131–138.
- Brancaccio, L., Cinque, A., Romano, P., Roskopf, C., Russo, F., Santangelo, N., 1995. L'evoluzione delle pianure costiere della Campania: Geomorfologia e Neotettonica. *Mem. Soc. Geogr. Ital.* LIII, 313–337.
- Bravi, S., Civile, D., Martino, C., & Putignano, M.L., 2006. La struttura da interferenza nei carbonati mesozoici della dorsale di Monte Fellino (Appennino Campano). *Boll. della Soc. Geol. Ital.* 125, 105–116.
- Brébion, P., Raynal, J.P., Texier, J., Alouan, M., 1986. Nouvelles données sur le Quaternaire atlantique à Casablanca et Achakar. *Comptes Rendus l'Académie des Sci. Série II* 302 (14), 901–904.
- Brideau, M., A., Roberts, N., J., 2015. Mass Movement in Bedrock. Shroder, J.F., Davies, T., (eds), *Landslide Hazards, Risks, Disasters* 43–90. <https://doi.org/http://dx.doi.org/10.1016/B978-0-12-396452-6.00003-3>.
- Brocchini, D., Principe, C., Castradori, D., Laurenzi, M.A., Gorla, L., 2001. Quaternary evolution of the southern sector of the Campanian Plain and early Somma-Vesuvius activity: Insights from the Trecase 1 well. *Mineral. Petrol.* 73, 67–91. <https://doi.org/10.1007/s007100170011>
- Brückner, H., 1986. Stratigraphy, evolution and age of quaternary marine terraces in Marocco and Spain. *Zeitschrift für Geomorphol. Suppl.* 62, 83–101.
- Brückner, H., Radtke, U., 1986. Paleoclimatic implications derived from profiles along the Spanish Mediterranean coast, in: *Symposium on Climatic Fluctuations during the Quaternary in the Western Mediterranean Regions.* pp. 467–486.
- Bruno, P.P.G., Cippitelli, G., Rapolla, A., 1998. Seismic study of the Mesozoic carbonate basement around Mt. Somma–Vesuvius, Italy. *J. Volcanol. Geotherm. Res.* 84, 311–322. [https://doi.org/10.1016/S0377-0273\(98\)00023-7](https://doi.org/10.1016/S0377-0273(98)00023-7)
- Bruno, P.P., Di Fiore, V., Ventura, G., 2000. Seismic study of the '41st Parallel' Fault System offshore the Campanian–Latial continental margin, Italy. *Tectonophysics* 324, 37–55. [https://doi.org/10.1016/S0040-1951\(00\)00114-1](https://doi.org/10.1016/S0040-1951(00)00114-1)
- Brunović, D., Miko, S., Hasan, O., Papatheodorou, G., Ilijanić, N., Misericchi, S., Correggiari, A., Geraga, M., 2020. Late Pleistocene and Holocene paleoenvironmental reconstruction of a drowned karst isolation basin (Lošinj Channel {NE} Adriatic Sea). *Palaeogeogr. Palaeoclimatol. Palaeoecol.* 544, 109587. <https://doi.org/10.1016/j.palaeo.2020.109587>
- Bryan, K., 1996. The steric component of sea level rise associated with enhanced greenhouse warming; a model study. *Clim. Dyn.* 12, 545–555.
- Buccheri, G., Renda, P., Morreale, C., Sorrentino, G., 1999. Il Tirreniano dell'isola di Lampedusa (Arcipelago Pelagiano, Agrigento, Italia). Le successioni di cala

- MAluk e Cala Uccello. *Boll. Soc. Geol. Ital.* 118, 361–373.
- Busetti, M., Baradello, L., Caburlotto, A., Gordini, E., Zanolla, C., Accettella, D., Antonioli, F., Paganini, P., 2010. Indagini geofisiche per lo studio dell'evoluzione Tardo-Pleistocenica ed Olocenica della Laguna di Grado e Marano (Adriatico Settentrionale). Workshop finale Project VECTOR (Vulnerability of the Italian coastal area and marine Ecosystems to Climatic changes and Their role in the Mediterranean carbon cycles), Roma, 18-19 ottobre 2010.
- Butler, R.W.H., Mazzoli, S., Corrado, S., De Donatis, M., Di Bucci, D., Gambini, R., Naso, G., Nicolai, C., Scrocca, D., Shiner, P., Zucconi, V., 2004. Applying thick-skinned tectonic models to the Apennine thrust belt of Italy: limitations and implications. *AAPG Mem.* 82, 647–667.
- Butzer, K.W., Cuerda, J., 1962. Coastal stratigraphy of southern Mallorca and its implications for the Pleistocene chronology of the Mediterranean Sea. *J. Geol.* 70, 398–416.
- Cadet, J.-P., Fourniguet, J., Gigout, M., Guillemin, M., Pierre, G., 1977. Les resultats de l'analyse structurale et de la neotectonique des littoraux; La neotectonique des littoraux. *Bull. la Société Géologique Fr.* S7-XIX, 600–605. <https://doi.org/10.2113/gssgfbull.S7-XIX.3.600>
- Caiazza, C., Ascione, A., Cinque, A., 2006. Late Tertiary-Quaternary tectonics of the Southern Apennines (Italy): New evidences from the Tyrrhenian slope. *Tectonophysics* 421, 23–51. <https://doi.org/10.1016/j.tecto.2006.04.011>
- Caldara, M., 1987. La sezione tirreniana di Ponte del Re (Castellaneta Marina, Taranto): analisi paleoecologica. *Atti della Soc. Toscana Sci. Nat. Mem. A* XCIII 129–163.
- Campo, B., Bruno, L., Amorosi, A., 2020. Basin-scale stratigraphic correlation of late Pleistocene-Holocene (MIS 5e-MIS1) strata across the rapidly subsiding Po Basin (northern Italy). *Quat. Sci. Rev.* 237, 106300. <https://doi.org/10.1016/j.quascirev.2020.106300>
- Caputo, R., 2007. Sea-level curves : Perplexities of an end-user in morphotectonic applications. *Glob. Planet. Change* 57, 417–423. <https://doi.org/10.1016/j.gloplacha.2007.03.003>
- Carboni, S., Lecca, L., 2008. L'archivio stratigrafico del Tirreniano della Sardegna.
- Carboni, M.G., Bergamin, L., Di Bella, L., Esu, D., Cerone, E.P., Antonioli, F., Verrubbi, V., 2010. Palaeoenvironmental reconstruction of late Quaternary foraminifera and molluscs from the ENEA borehole (Versilian plain, Tuscany, Italy). *Quat. Res.* 74, 265–276.
- Carboni, S., Lecca, L., Hillaire-Marcel, C., Ghaleb, B., 2014. MIS 5e at San Giovanni di Sinis (Sardinia Italy): Stratigraphy, U/Th dating and "eustatic" inferences. *Quat. Int.* 328–329, 21–30. <https://doi.org/10.1016/j.quaint.2013.12.052>

- Carobene, L., 1972. Osservazioni sui solchi di battente attuali ed antichi nel golfo di Orosei in Sardegna. *Mem. della Soc. Geol. Ital.* 19, 641–649.
- Carobene, L., 1980. Terrazzi marini, eustatismo e neotettonica. *Geogr. Fis. e Din. Quat.* 3, 35–41.
- Carobene, L., Dai Pra, G., Gewalt, M., 1986. Niveaux marins du Pléistocène moyen-supérieur de la côte tyrrhénienne de la Calabre (Italie méridionale) Datations  $^{230}\text{Th}/^{234}\text{U}$  et tectonique récente. *Zeitschrift für Geomorphol. Supp.-Bd.*, 141–158.
- Carobene, L., Dai Pra, G., 1990. Genesis, Chronology and Tectonics of the Quaternary marine terraces of the Tyrrhenian coast of northern Calabria (Italy). Their correlation with climatic variations. *Quat.* 3, 75–94.
- Carobene, L., Dai Pra, G., 1991. Middle and Upper Pleistocene sea level highstands along the Tyrrhenian coast of Basilicata (Southern Italy). *Quat.* 4, 173–202.
- Carobene, L., 2015. Marine Notches and Sea-Cave Bioerosional Grooves in Microtidal Areas: Examples from the Tyrrhenian and Ligurian Coasts- Italy. *J. Coast. Res.* 313, 536–556. <https://doi.org/10.2112/jcoastres-d-14-00068.1>
- Carminati, E., Doglioni, C., Scrocca, D., 2003. Apennines subduction-related subsidence of Venice (Italy). *Geophys. Res. Lett.* 30. <https://doi.org/10.1029/2003gl017001>
- Casciello, E., Cesarano, M., & Pappone G., 2006. Extensional detachment faulting on the tyrrhenian margin of the Southern Apennines contractional belt (Italy). *J. Geol. Soc. London* 163,4, 617–629.
- Casero, P., Roure, F., Endignoux, L., Moretti, I., Muller, C., Sage, L., Vially, R., 1988. Neogene Geodynamic Evolution of the southern Apennines. *Mem. Soc. Geol. It.* 41, 109–120.
- Casini, L., Andreucci, S., Sechi, D., Huang, C.-Y., Shen, C.-C., Pascucci, V., 2020. Luminescence dating of Late Pleistocene faults as evidence of uplift and active tectonics in Sardinia, W Mediterranean. *Terra Nova*.
- Catalano, S., Cinque, A., 1995. L'evoluzione neotettonica dei Peloritani settentrionali (Sicilia nord-orientale): il contributo di una analisi geomorfologica preliminare. *Stud. Geol. Camerti Volume Spe.*
- Catalano, S., Guidi, G. De, 2003. Late Quaternary uplift of northeastern Sicily : relation with the active normal faulting deformation. *J. Geodyn.* 36, 445–467. [https://doi.org/10.1016/S0264-3707\(02\)00035-2](https://doi.org/10.1016/S0264-3707(02)00035-2)
- Catalano, S., De Guidi, G., Monaco, C., Tortorici, G., Tortorici, L., 2003. Long-term behaviour of the late Quaternary normal faults in the Straits of Messina area (Calabria arc): structural and morphological constraints. *Quat. Int.* 101/102, 81–91.
- Cella, F., Fedi, M., Florio, G., Grimaldi, M., Rapolla, A., 2007. Shallow structure of the Somma-Vesuvius volcano from 3D inversion of gravity data. *J. Volcanol. Geotherm. Res.* 161, 303–317.

- <https://doi.org/10.1016/j.jvolgeores.2006.12.013>
- Cerrone, C., Ascione, A., Balassone, G., Mormone, A., Robustelli, G., Soligo, M., Tuccimei, P., 2018. INQUA Focus Group Earthquake Geology and Seismic Hazards INQUA Focus Group Earthquake Geology and Seismic Hazards. *Act. Tectonics Archeoseismology* 25–27.
- Cerrone, C., Di Donato, V., Mazzoli, S., Robustelli, G., Soligo, M., Tuccimei, P., Ascione, A., 2020. Evolution of the Campania Plain Quaternary coastal graben (southern Apennines): constraints from raised paleoshorelines. *Geomorphology* submitted.
- Cerrone, C., Ascione, A., Robustelli, G., Balassone, G., Soligo, M., Tuccimei, P., 2021a. Late Quaternary sea-level fluctuations along the raised Tyrrhenian margin of northern Calabria-Basilicata (southern Italy): New U-series dating of paleoshorelines. Submitted to *Quat. Sci. Rev.*
- Cerrone, C., Vacchi, M., Fontana, A., Rovere, A., 2021b. Last Interglacial sea-level index points in the Western Mediterranean, doi:10.5281/zenodo.4497365
- Channell, J.E.T., D’Argenio, B., Horvát, F., 1979. Adria, the African promontory, in *Mesozoic Mediterranean paleogeography*. *Earth Sci. Rev.* 15 (3), 213–292.
- Chappell, J., Shackleton, N.J., 1986. Oxygen isotopes and sea level. *Nature* 324, 137–140.
- Chappell, J., Omura, A., Esat, T., McCulloch, M., Pandolfi, J., Ota, Y., Pillans, B., 1996. Reconciliation of late Quaternary sea levels derived from coral terraces at Huton Peninsula with deep sea oxygen isotope records. *Earth Planet Sci. Lett.* 141, 227–236.
- Chapman, N., Berryman, K., Villamor, P., Epstein, W., Cluff, L., Kawamura, H., 2014. Active Faults and Nuclear Power Plants. *Eos, Trans. Am. Geophys. Union* 95, 33–34. <https://doi.org/10.1002/2014EO040001>
- Choubert, G., Faure-Muret, A., Hilali, E., Houzay, J.P., de Lamotte, D.F., 1984. Carte géologique du Rif au 1/50.000, feuille Boudinar. *Notes Mém. Serv. Géol. Marocc.* 299.
- Ciampalini, A., Ciulli, L., Sarti, G., Zanchetta, G., 2006. Nuovi dati geologici del sottosuolo del “Terrazzo di Livorno.” *Atti della Soc. Toscana di Sci. Nat. Mem.* 111, 75–82.
- Ciampo, G., 1976. Ostracodi pleistocenici di Cala Bianca (Marina di Camerota, Salerno). *Boll. Soc. Paleontol. Ital.* 15, 3–23.
- Cinque, A., Alinaghi, H.H., Laureti, L., Russo, F., 1987. Preliminary observations on the geomorphological evolution of the Sarno Plain, Campania, southern Apennines. *Geogr. Fis. e Din. Quat.* 10, 161–174.
- Cinque, A., Romano, P., 1990. Segnalazione di nuove evidenze di antiche linee di riva in Penisola Sorrentina (Campania). *Geogr. Fis. e Din. Quat.* 13, 23–36.
- Cinque, A., 1991. La trasgressione versiliana nella piana del Sarno (Campania). *Geogr. Fis. e Din. Quat.* 14, 63–71.

- Cinque, A., Patacca, E., Scandone, P., & Tozzi, M., 1993. Quaternary kinematic evolution of the Southern Apennines. Relationships between surface geological features and deep lithospheric structures. *Ann. di Geofis.* 36, 249–259.
- Cinque A., Romano P., Roskopf C., Santangelo N., Santo A., 1994. Morfologie costiere e depositi quaternari tra Agropoli e Ogliastro Marina (Cilento - Italia Meridionale). *Il Quaternario – It. J. Quat. Sci.* 7(1), 3-16.
- Cinque, A., De Pippo, T., Romano, P., 1995. Coastal slope terracing and relative sea-level changes: Deductions based on computer simulations. *Earth Surf. Process. Landforms* 20, 87–103. <https://doi.org/10.1002/esp.3290200108>
- Cinque, A., Ascione, A., & Caiazzo, C., 2000. Spatial and temporal distribution of Quaternary faultings in the Southern Apennines. Galadini F., Meletti C. Rebez A. *Le Ric. del GNDT nel campo della pericolosità sismica.* CNR- Grup. Naz. per la Dif. dai Terremoti, Roma (In Ital. with English Abstr).
- Cinque, A., & Irollo, G., 2004. Il “Vulcano di Pompei”: nuovi dati geomorfologici e stratigrafici. *Quat. - Ital. J. Quat. Sci.* 17 (1), 101–116.
- Conchon, O., 1985. Le Quaternaire littoral de Corse : nouvelles données. *Bull. l'Association française pour l'étude du Quat.* 22, 13–20. <https://doi.org/10.3406/quate.1985.1522>
- Conchon, O., 1999. Le littoral de Corse (France) au Quaternaire [Corsica coast (France Western Mediterranean) during the Quaternary]. *Quaternaire* 10, 95–105. <https://doi.org/10.3406/quate.1999.1634>
- Cortese, E., 1895. Descrizione geologica della Calabria. *Mem. Desc. Cart. Geol. Ital.* 9, 1–310.
- Cosentino, D., Gliozzi, E., 1988. Considerazioni sulle velocità di sollevamento di depositi eutirreniani dell'Italia meridionale e della Sicilia. *Mem. della Soc. Geol. Ital.* 41, 653–665.
- Cotecchia, V., Dai Pra, G., Magri, G., 1969. Oscillazioni tirreniane e oloceniche del livello del mare nel Golfo di Taranto, corredate da datazioni con il metodo del radiocarbonio. *Geol. Appl. e Idrogeol.* 4, 93–148.
- Creveling, J.R., Mitrovica, J.X., Hay, C.C., Austermann, J., Kopp, R.E., 2015. Revisiting tectonic corrections applied to Pleistocene sea-level highstands. *Quat. Sci. Rev.* 111, 72–80. <https://doi.org/https://doi.org/10.1016/j.quascirev.2015.01.003>
- Croll, J., 1875. *Climate and Time, in their Geological Realtions: A Theory of Secular Changes of the Earth's Climate.* D. Applet. Co., New York 577.
- Cucci, L., 2004. Raised marine terraces in the Northern Calabrian Arc (Southern Italy): A ~ 600 kyr-long geological record of regional uplift. *Ann. Geophys.* 47, 1391–1406. <https://doi.org/10.4401/ag-3350>
- Cuerda, J., 1957. Fauna marina del Tirreniense de la Bahía de Palma (Mallorca). *Bolletì la Soc. d'Història Nat. les Balear.* 3, 3–75.

- Cutler, K.B., Edwards, R.L., Taylor, F.W., Cheng, H., Adkins, J., Gallup, C.D., Cutler, P.M., Burr, G.S., Bloom, A.L., 2003. Rapid sea-level fall and deep-ocean temperature change since the last interglacial period. *Earth Planet. Sci. Lett.* 206, 253–271. [https://doi.org/10.1016/S0012-821X\(02\)01107-X](https://doi.org/10.1016/S0012-821X(02)01107-X)
- D’Elia, G., Di Girolamo, P., & Guida, M., 1987. Geological and petrological characteres of some quaternary calckaline tufites of Cilento (southern Italy). *Boll. Soc. Geol. Ital.* 106, 699–716.
- D’Orefice, M., Graciotti, R., Lo Mastro, S., Muraro, C., Pantaloni, M., Soligo, M., Tuccimei, P., 2012. U/Th dating of a *Cladocora coespitosa* from Capo San Marco marine Quaternary deposits (Sardinia, Italy). *Alp. Mediterr. Quat.* 25, 3.
- Dabrio, C.J., Zazo Cardaña, C., Goy Goy, J.L., Santisteban Bové, C., Bardajì Azcárate, T., Somoza Losada, L., 1991. Neogene and Quaternary fan-delta deposits in southeastern Spain. *Field Guide. Cuad. Geol. ibérica* 327–400.
- Dai Pra, G., Stearns, C.E., 1977. Sul Tirreniano di Taranto. Datazioni su coralli con il metodo del Th230/U234. *Geol. Rom.* 16, 231–242.
- Dai Pra, G., Hearty, P.J., 1988. I livelli marini pleistocenici del Golfo di Taranto. Sintesi Geocronostratigrafica e tettonica. *Mem. Soc. Geol. Ital.* 41, 637–644.
- Dai Pra, G., Miyauchi, T., Anselmi, B., Galletti, M., Paganin, G., 1991. Età dei depositi a *Strombus bubonius* di Vibo Valentia MARina (Italia Meridionale). *Quat.* 6 (1), 139–144.
- Dalca, A. V., Ferrier, K.L., Mitrovica, J.X., Perron, J.T., Milne, G.A., Creveling, J.R., 2013. On postglacial sea level—III. Incorporating sediment redistribution. *Geophys. J. Int.* 194, 45–60. <https://doi.org/10.1093/gji/ggt089>
- Damiani, A.V., 1970. Terrazzi marini e sollevamenti differenziali fra i Bacini del Lao e del Corvino (Calabria settentrionale). *Ital. J. Geosci.* 89, 145–158.
- Darwing, C., 1846. Geological observations on South America: Being the third part of the Geology of the Voyage of the Beagle. Smith, Elder and Compani.
- de Lamothe, R., 1911. Les anciennes lignes de rivage du Sahel d’Alger et d’une partie de la côte Algérienne. Société géologique de France.
- De Lumley, H., 1969. Le Paléolithique inférieur et moyen du Midi méditerranéen dans son cadre géologique. Tome I. Ligurie--Provence. Persée-Portail des revues scientifiques en SHS.
- De Santis, V., Caldara, M., Torres, T. De, Ortiz, J.E., 2010. Stratigraphic units of the Apulian Tavoliere plain ( Southern Italy ): Chronology , correlation with marine isotope stages and implications regarding vertical movements. *Sediment. Geol.* 228, 255–270. <https://doi.org/10.1016/j.sedgeo.2010.05.001>
- de Vita, S., Laurenzi, M.A., Orsi, G., Voltaggio, M., 1998. Application of Ar Ar and U. *Quat. Int.* 47/48, 117–127.
- Delibrias, G., Guillier, M.T., Labeyrie, J., 1972. Gif natural radiocarbon measurements VII. *Radiocarbon* 14, 280–320.

- Destro, N., 1995. Release fault: A variety of cross fault in linked extensional fault systems, in the Sergipe-Alagoas Basin, NE Brazil. *J. Struct. Geol.* 17. [https://doi.org/10.1016/0191-8141\(94\)00088-H](https://doi.org/10.1016/0191-8141(94)00088-H)
- Dewey, J.F., Helman, M.L., Turco, E., Hutton, D.H.W., Knott, S.D., 1989. Kinematics of the western Mediterranean. *Geol. Soc. London Spec. Publ.* 265–283. <https://doi.org/10.1144/GSL.SP.1989.045.01.15>
- Di Grande, A., Scamarda, G., 1973. Segnalazione di livelli a Strombus B. nei dintorni di Augusta. *Boll. delle Seudte dell'Accademia Gioenia di Sci. Nat. di Catania XI*, 157–172.
- Di Grande, A., Neri, M., 1988. Tirreniano a Strombus bubonius a M. Tauro (Augusta-Siracusa). *Rend. Soc. Geol. Ital.* 11, 57–58.
- Dogliani, C., Moretti, I., Roure, F., 1991. Basal lithospheric detachment, eastward mantle flow and mediterranean geodynamics: A discussion. *J. Geodyn.* 13, 47–65. [https://doi.org/https://doi.org/10.1016/0264-3707\(91\)90029-E](https://doi.org/https://doi.org/10.1016/0264-3707(91)90029-E)
- Donnici S., S.-B.R., 2004. Paleogeografia e cronologia dei sedimenti tardopleistoceni ed olocenici presenti nel sottosuolo di Valle Averte (Laguna di Venezia, bacino centrale). *Lav. Soc. Veneziana Sci. Nat.* 29.
- Dorale, J., Onac, B.P., Fornos, J.J., Gines, J., Gines, A., Tuccimei, P., Peate, D.W., 2010. Sea-level highstand 81,000 years ago in Mallorca. *Science* 327, 860–863. <https://doi.org/10.1126/science.1181725>
- Downs, R.T., & Hall-Wallace, M., 2003. The American Mineralogist crystal structure database. *Am. Min.* 88, 247–250.
- Dubar, M., Innocent, C., Sivan, O., 2008. Radiometric dating (U/Th) of the lower marine terrace (MIS 5.5) west of Nice (French Riviera): Morphological and neotectonic quantitative implications. *Comptes Rendus Geosci.* 340, 723–731. <https://doi.org/10.1016/j.crte.2008.07.012>
- Dumas, B., Guérémi, P., Lhénaff, R. and, Raffy, J., 1982. Le soulèvement quaternaire de la Calabre méridionale. *Rev. Géologie Dyn. Géographie Phys.* 23, 27–40.
- Dumas, B., Gueremy, P., Lhenaff, R., Raffy, J., 1987. Rates of uplift as shown by raised Quaternary shorelines in Southern Calabria (Italy). *Zeitschrift fur Geomorphol. N.F. Suppl.* 63, 119–132.
- Dumas, B., Gueremy, P., Hearty, P.J., Lhenaff, R., Raffy, J., 1988. Morphometric analysis and amino acid geochronology of uplifted shorelines in a tectonic region near Reggio Calabria, South Italy. *Palaeogeogr. Palaeoclimatol. Palaeoecol.* 68, 273–289. [https://doi.org/10.1016/0031-0182\(88\)90045-4](https://doi.org/10.1016/0031-0182(88)90045-4)
- Dumas, B., Guérémy, P., Haong, C.T., Lhénaff, R., Raffy, J., 1991. Gisement et rivages tyrrhéniens de Vibo Marina (Italie du Sud): datation  $^{230}\text{Th}/^{234}\text{U}$ , soulèvement différentiel de la Calabre méridionale. *Comptes Rendus Acad. des Sci. Paris* 312, 785–791.
- Dumas, B., Raffy, J., 2004. Late Pleistocene tectonic activity deduced from uplifted

- marine terraces in Calabria, facing the Strait of Messina. *Quat. Nov.* 8, 79–99.
- Dumas, B., Guérémy, P., Raffy, J., 2005. Evidence for sea-level oscillations by the “characteristic thickness” of marine deposits from raised terraces of Southern Calabria (Italy). *Quat. Sci. Rev.* 24, 2120–2136. <https://doi.org/10.1016/j.quascirev.2004.12.011>
- Dumitru, O.-A., Polyak, V.J., Asmerom, Y., Onac, B.P., 2020. A global standardized database of Last Interglacial (sensu lato, ~130 to 75 ka) sea level records from U-series dated cave deposits. <https://doi.org/10.5281/zenodo.4313861>
- Dumitru, O.A., Austermann, J., Polyak, V.J., Fornós, J.J., Asmerom, Y., Ginés, J., Ginés, A., Onac, B.P., 2021. Sea-level stands from the Western Mediterranean over the past 6.5 million years. *Sci. Rep.* 11, 1–10.
- Dumitru, O.A., Austermann, J., Polyak, V.J., Fornós, J.J., Asmerom, Y., Ginés, J., Ginés, A., Onac, B.P., 2019. Constraints on global mean sea level during Pliocene warmth. *Nature* 574, 233–236.
- Dutton, A., Bard, E., Antonioli, F., Esat, T.M., Lambeck, K., McCulloch, M.T. 2009a. Phasing and amplitude of sea-level and climate change during the penultimate interglacial. *Nature Geosci.* 2(5), 355–359. DOI:10.1038/NGEO470
- Dutton, A., Scicchitano, G., Monaco, C., Desmarchelier, J.M., Antonioli, F., Lambeck, K., Esat, T.M., Fifield, L.K., McCulloch, M.T., Mortimer, G., 2009b. Uplift rates defined by U-series and <sup>14</sup>C ages of serpulid-encrusted speleothems from submerged caves near Siracusa, Sicily (Italy). *Quat. Geochronol.* 4, 2–10. <https://doi.org/10.1016/j.quageo.2008.06.003>
- Dutton, A., Lambeck, K., 2012. Ice Volume and Sea Level During the Last Interglacial. *Science.* 337, 216–219. <https://doi.org/10.1126/science.1205749>
- Eagleson, P.S., Dean, R.G., 1966. Small amplitude wave theory. *Estuary coastline hydrodynamics McGraw-Hill, New York* 744.
- Edwards, M.A., Grasemann, B., 2009. Mediterranean snapshots of accelerated slab retreat: subduction instability in stalled continental collision. *Geol. Soc. London, Spec. publication* 311, 155–192.
- El Abdellaoui, J.E., Petit, F., Ghaleb, B., Ozer, A., 2016. Sea-level fluctuation during MIS 5e and geomorphological context on the southern coast of the Strait of Gibraltar (Morocco). *Geomorphol. Reli. Process. Environ.* 22, 287–301. <https://doi.org/10.4000/geomorphologie.11467>
- El Fahssi, A., 1999. Tectonique Alpine, Néotectonique et étude des formations marines quaternaire de la rive sud de Détroit de Gibraltar entre Tanger et Sebta (Rif-Maroc). Thèse Dr. troisième cycle, Univ. Mohammed V, Rabat, MAroc, 253.
- El Gharbaoui, A., 1977. Note préliminaire sur l'évolution géomorphologique de la péninsule de Tanger. *Bull. la Société Géologique Fr.* S7-XIX, 615–622.

- <https://doi.org/10.2113/gssgfbull.S7-XIX.3.615>
- El Kadiri, K., de Galdeano, C.S., Pedrera, A., Chalouan, A., Galindo-Zaldívar, J., Julià, R., Akil, M., Hlila, R., Ahmamou, M., 2010. Eustatic and tectonic controls on Quaternary Ras Leona marine terraces (Strait of Gibraltar, northern Morocco). *Quat. Res.* 74, 277–288. <https://doi.org/10.1016/j.yqres.2010.06.008>
- Elter, P., Giglia, G., Tongiorgi, M., & Trevisan, L., 1975. Tensional and compressional areas in the recent (Tortonian to Present) evolution of North Apennines. *Boll. di Geofis. Teor. Appl.* 17, 3–18.
- Emiliani, C., 1955. Pleistocene temperatures. *J. Geol.* 63, 585–599.
- Emiliani, C., 1966. Palaeotemperature analysis of Caribbean cores P 6304-8 and P 6304-9 and a generalised temperature curve for the last 425,000 years. *J. Geol.* 74, 109–126.
- England, P., Molnar, P., 1990. Surface uplift, uplift of rocks, and exhumation of rocks. *Geology* 18, 1173–1177. [https://doi.org/10.1130/0091-7613\(1990\)018<1173:SUUORA>2.3.CO;2](https://doi.org/10.1130/0091-7613(1990)018<1173:SUUORA>2.3.CO;2)
- Ericson, J., Vorosmarty, C., Dingman, S., Ward, L., Meybeck, M., 2006. Effective sea-level rise and deltas: Causes of change and human dimension implications. *Glob. Planet. Change* 50, 63–82. <https://doi.org/10.1016/j.gloplacha.2005.07.004>
- Esposito, C., Filocamo, F., Marciano, R., Romano, P., Santangelo, N., Scarciglia, F., & Tuccimei, P., 2003. Late Quaternary shorelines in southern Cilento (Mt. Bulgheria): morphostratigraphy and chronology. *Quat.* 16 (1), 3–14.
- Evelpidou, N., Kampolis, I., Pirazzoli, P.A., Vassilopoulos, A., 2012a. Global sea-level rise and the disappearance of tidal notches. *Glob. Planet. Change* 92–93, 248–256. <https://doi.org/10.1016/j.gloplacha.2012.05.013>
- Evelpidou, N., Pirazzoli, P., Vassilopoulos, A., Spada, G., Ruggieri, G., Tomasin, A., 2012b. Late holocene sea level reconstructions based on observations of roman fish tanks, Tyrrhenian coast of Italy. *Geoarchaeology* 27, 259–277. <https://doi.org/10.1002/gea.21387>
- Evelpidou, N., Pirazzoli, P.A., 2015. Environmental Management and Governance, Chapter 12, in C.W. Finkl and C. Makowski (eds.), *Environmental Management and Governance: Advances in Coastal and Marine Resources*, Coastal Research Library 8, Coastal Research Library. Springer International Publishing, Cham. <https://doi.org/10.1007/978-3-319-06305-8>
- Fabiani, R., 1941. Tracce di Tirreniano a Strombus bubonius entro la città di Palermo. *Boll. Soc. Sci. Nat. ed Econ.* XIX, 1–7.
- Faccenna, C., Becker, T.W., Lucente, F.P., Jolivet, L., & Rossetti, F., 2001. History of subduction and back-arc extension in the Central Mediterranean. *Geophys. J. Res.* 145, 809–820.
- Faccenna, C., Piromallo, C., Crespo-Blanc, A., Jolivet, L., Rossetti, F., 2004.

- Lateral slab deformation and the origin of the western Mediterranean arcs. *Tectonics* 23. <https://doi.org/10.1029/2002TC001488>
- Fairbridge, R.W., 1952. Marine erosion. *Proc. Seventh Pacific Sci. Congr.* 3. Pacific Assoc. 347–359.
- Fairbridge, R.W., 1961. Eustatic changes of sea level. *Phys. Chem. earth* 4, 99–185.
- Fairbridge, R.W., 1968. *The Encyclopedia of Geomorphology*. Rheinold, New York 1295.
- Fairbanks, R.G., Matthews, R., 1978. The marine oxygen isotope record in Pleistocene coral, Barbados, West Indies. *Quat. Res.* 10, 181–196.
- Farr, T.G., Rosen, P.A., Caro, E., Crippen, R., Duren, R., Hensley, S., Kobrick, M., Paller, M., Rodriguez, E., Roth, L. and Seal, D., 2007. The shuttle radar topography mission. *Reviews of geophysics*, 45(2).
- Faure Walker, J.P., Roberts, G.P., Cowie, P.A., Papanikolaou, I., Michetti, A.M., Sammonds, P., Wilkinson, M., McCaffrey, K.J.W., Phillips, R.J., 2012. Relationship between topography, rates of extension and mantle dynamics in the actively-extending Italian Apennines. *Earth Planet. Sci. Lett.* 325–326, 76–84. <https://doi.org/10.1016/j.epsl.2012.01.028>
- Federici, P.R., Pappalardo, M., 2006. Evidence of Marine Isotope Stage 5.5 highstand in Liguria (Italy) and its tectonic significance. *Quat. Int.* 145–146, 68–77. <https://doi.org/10.1016/j.quaint.2005.07.003>
- Ferranti, L., Antonioli, F., Mauz, B., Amorosi, A., Dai Pra, G., Mastronuzzi, G., Monaco, C., Orrù, P., Pappalardo, M., Radtke, U., Renda, P., Romano, P., Sansò, P., Verrubbi, V., 2006. Markers of the last interglacial sea-level high stand along the coast of Italy: Tectonic implications. *Quat. Int.* 145–146, 30–54. <https://doi.org/10.1016/j.quaint.2005.07.009>
- Ferranti, L., Monaco, C., Antonioli, F., Maschio, L., Kershaw, S., Verrubbi, V., 2007. The contribution of regional uplift and coseismic slip to the vertical crustal motion in the Messina Straits, southern Italy: Evidence from raised Late Holocene shorelines. *J. Geophys. Res.* 112, B06401. <https://doi.org/10.1029/2006JB004473>
- Ferranti, L., Antonioli, F., 2007. Misure del solco Tirreniano (MIS 5.5) nell'isola di Capri: valutazione di attività tettonica durante il Pleistocene superiore. *Il Quaternario – It. J. Quat. Sci.* 20(2), 125-136.
- Ferranti, L., Monaco, C., Morelli, D., Antonioli, F., Maschio, L., 2008. Holocene activity of the Scilla Fault, Southern Calabria: Insights from coastal morphological and structural investigations. *Tectonophysics* 453, 74–93. <https://doi.org/10.1016/j.tecto.2007.05.006>
- Feruglio, E., 1936. Sedimenti marini nel sottosuolo della bassa friulana, *Bollettino Società Geologica Italiana*, 55.
- Filocamo, F., 2006. Evoluzione Quaternaria del margine Tirrenico dell'Appennino

- Meridionale tra il Golfo di Sapri e la Foce del Fiume Lao: studio stratigrafico e geomorfologico. Phd thesis 1–340.
- Filocamo, F., 2007. Evoluzione quaternaria del margine tirrenico dell'Appennino meridionale tra il Golfo di Sapri e la foce del fiume Lao: studio stratigrafico e geomorfologico. PhD Thesis, Federico II University, Napoli, Italy, 340 pp. Available at <http://www.fedoa.unina.it>.
- Filocamo, F., Romano, P., Di Donato, V., Esposito, P., Mattei, M., Porreca, M., Robustelli, G., Russo Ermolli, E., 2009. Geomorphology and tectonics of uplifted coasts: New chronostratigraphical constraints for the Quaternary evolution of Tyrrhenian North Calabria (southern Italy). *Geomorphology* 105, 334–354. <https://doi.org/10.1016/j.geomorph.2008.10.011>
- Flemming, N.C., 1965. Form and relation to present sea level of Pleistocene marine erosion features. *Jour. Geol.* 73, no. 5, 799–811.
- Flemming, N.C., 1969. Archeological evidence for eustatic change of sea level and earth movements in the western Mediterranean during the last 2000 years. *Geol. Soc. Am. Special pa.*
- Flemming, N.C., 1979. Archeological indicators of sea level. *Les Indic. niveaux Mar. Paris Ocean. Fasc. hors-sèr.*, 149-65 Special pa.
- Flemming, N.C., Pirazzoli, P.A., 1981. Archéologie des côtes de la Crète. *Hist. Archéol., les Dossiers* 50, 66–81.
- Flemming, N.C., Webb, C.O., 1986. Regional patterns of coastal tectonics and eustatic change of sea level in the Mediterranean during the last 10,000 years derived from archaeological data. *Zeitschrift für Geomorphol.* December, Suppl-Bd62 1–29.
- Florio, G., Fedi, M., Cella, F., Rapolla, A., 1999. The Campanian Plain and Phlegrean Fields: structural setting from potential field data. *J. Volcanol. Geotherm. Res.* 91, 361–379. [https://doi.org/10.1016/S0377-0273\(99\)00044-X](https://doi.org/10.1016/S0377-0273(99)00044-X)
- Fontana, A., Mozzi, P., Bondesan, A., 2010. Late pleistocene evolution of the Venetian\Friulian Plain. *Rendiconti Lincei* 21, 181–196. <https://doi.org/10.1007/s12210-010-0093-1>
- Fontana A., Bondesan A., Meneghel M., Toffoletto F., Vitturi A. and Bassan V. (eds), 2012. Note illustrative della Carta Geologica d'Italia alla scala 1:50.000 - Foglio 107 Portogruaro. Regione Veneto, Infocartografica, 216 pp.
- Gallen, S.F., Wegmann, K.W., Bohnenstiehl, D.R., Pazzaglia, F.J., Brandon, M.T., Fassoulas, C., 2014. Active simultaneous uplift and margin-normal extension in a forearc high, Crete, Greece. *Earth Planet. Sci. Lett.* 398, 11–24. <https://doi.org/10.1016/j.epsl.2014.04.038>
- Galli, P., Galadini, F., Pantosti, D., 2008. Twenty years of paleoseismology in Italy. *Earth-Science Rev.* 88, 89–117. <https://doi.org/10.1016/j.earscirev.2008.01.001>

- Gary, M., McAfee, R.J., Wolf, C.L., 1972. Glossary of Geology. Jr., eds. Washington, D.C. \_ Am. Geol. Inst. 805.
- Gaki-Papanastassiou, K., Karymbalis, E., Papanastassiou, D., Maroukian, H., 2009. Quaternary marine terraces as indicators of neotectonic activity of the Ierapetra normal fault SE Crete (Greece). *Geomorphology* 104, 38–46.
- Ghisetti, F., 1992. Fault parameters in the Messina Strait (southern Italy) and relations with the seismogenic source. *Tectonophysics* 210, 117–133. [https://doi.org/https://doi.org/10.1016/0040-1951\(92\)90131-O](https://doi.org/https://doi.org/10.1016/0040-1951(92)90131-O)
- Giaccio, B., Isaia, R., Fedele, F.G., Di Canzio, E., Hoffecker, J., Ronchitelli, A., Sinityn, A.A., Anikovich, M., Lisitsyn, S.N., Popov, V. V., 2008. The Campanian Ignimbrite and Codola tephra layers: Two temporal/stratigraphic markers for the Early Upper Palaeolithic in southern Italy and eastern Europe. *J. Volcanol. Geotherm. Res.* 177, 208–226. <https://doi.org/10.1016/j.jvolgeores.2007.10.007>
- Giaccio, B., Hajdas, I., Isaia, R., Deino, A., Nomade, S., 2017. High-precision  $^{14}\text{C}$  and  $^{40}\text{Ar}/^{39}\text{Ar}$  dating of the Campanian Ignimbrite (Y-5) reconciles the time-scales of climatic-cultural processes at 40 ka. *Sci. Rep.* 7, 45940. <https://doi.org/10.1038/srep45940>
- Gignoux, M., 1913. Les formations marines pliocenes et quaternaires de l'Italie du Sud et de la Sicilie. *Ann. Univ. Lyon* 35, 1–693.
- Gigout, M., 1960. Sur le quaternaire marin de Tarente (Italie). *Comptes Rendus Hebd. l'Académie des Sèances* 250, 1094–1096.
- Gigout, M., 1962. Sur le Tyrrhénien de la Méditerranée occidental. *Quaternaria* 6.
- Gilbert, G., 1890. Lake Bonneville. *U.S. Geol. Surv. Monogr. No.* 1 438.
- Gill, E.D., 1972. The relationship of present shore platforms to past sea levels. *Boreas* 1, 1–25.
- Gilli, E., 2018. Karstodyssée 2016, Analyse des marqueurs eustatiques, tectoniques et tsunamiques dans les karsts littoraux méditerranéens, in: Rapport de Mission. Paris 8 University.
- Gillot, P.-Y., Kiefer, G., & Romano, R., 1994. The evolution of Mount Etna in the light of potassium-argon dating. *Ann. di Geofis.* 36, 267–282.
- Ginés, J., Ginés, A., Fornós, J.J., Tuccimei, P., Onac, B.P., Gràcia, F., 2012. Phreatic Overgrowths on Speleothems ( POS ) from Mallorca , Spain : Updating forty years of research. In Ginés, A., Ginés, J., Gómez-Pujol, L., Onac, B.P. & Fornós, J.J. (eds) 2012. Mallorca: A Mediterranean benchmark for Quaternary Studies. *Mom. Soc. Nat. Balears*, 18: 111-146. ISBN 978-84-7632-995-5.
- Giraudi, C., Frezzotti, M., 1997. Late Pleistocene glacial events in the Central Apennines, Italy. *Quat. Res.* 48, 280–290.
- Giunta, G., Gueli, A.M., Monaco, C., Orioli, S., Ristuccia, G.M., Stella, G., Troja, S.O., 2012. Middle-Late Pleistocene marine terraces and fault activity in the

- Sant'Agata di Militello coastal area (north-eastern Sicily). *J. Geodyn.* 55, 32–40. <https://doi.org/10.1016/j.jog.2011.11.005>
- Gornitz, V., 2005. Eustasy. *Encycl. Coast. Sci.* Springer 439–442.
- Goy, J.L., Zazo, C., 1988. Sequences of quaternary marine levels in Elche Basin (eastern Betic Cordillera, Spain). *Palaeogeogr. Palaeoclimatol. Palaeoecol.* 68, 301–310.
- Goy, J. L. and Zazo, C., 1989. The role of neotectonics in the morphologic distribution of the Quaternary marine and continental deposits of the Elche Basin, southeast Spain, *Tectonophysics*, 163(3-4), 219–225.
- Goy, J.L., Hillaire-Marcel, C., Zazo, C., Ghaleb, B., Dabrio, C.J., González, Á., Bardajì, T., Civis, J., Preda, M., Yébenes, A., Forte, A.M., 2006. Further evidence for a relatively high sea level during the penultimate interglacial: open-system U-series ages from La Marina (Alicante East Spain). *Geodin. Acta* 19, 409–426. <https://doi.org/10.3166/ga.19.409-426>
- Gueguen, E., Doglioni, C., Fernandez, M., 1997. Lithospheric boudinage in the Western Mediterranean back-arc basin. *Terra Nov.* 9, 2–5.
- Gueguen, E., Doglioni, C., Fernandez, M., 1998. On the post-25 Ma geodynamic evolution of the western Mediterranean. *Tectonophysics* 298, 259–269.
- Guerrera, F. and Tramontana, M. (Eds.) 2011. Note illustrative della Carta Geologica d'Italia alla scala 1:250.000, Foglio 241 Senigallia. Regione Marche, ISPRA, 116 pp.
- Gutscher, M.A., Kopp, H., Krastel, S., Bohrmann, G., Garlan, T., Zaragosi, S., Klauke, I., Wintersteller, P., Loubrieu, B., Le Faou, Y., San Pedro, L., Dominguez, S., Rovere, M., Mercier de Lepinay, B., Ranero, C., Sallares, V., 2017. Active tectonics of the Calabrian subduction revealed by new multi-beam bathymetric data and high-resolution seismic profiles in the Ionian Sea (Central Mediterranean). *Earth Planet. Sci. Lett.* 461, 61–72. <https://doi.org/10.1016/j.epsl.2016.12.020>
- Harzhauser, M., Kronenberg, G., 2008. A note on *Strombus coronatus* Defrance, 1827 and *Strombus coronatus* Roding, 1798 (Mollusca : Gastropoda). *The Veliger* 50, 120–128.
- Head, M.J., Gibbard, P., Salvador, A., 2008. The Quaternary: Its character and definition. *Episodes* 31, 234–238. <https://doi.org/10.18814/epiugs/2008/v31i2/009>
- Hearty, P.J., Bonfiglio, L., Donata, V., & Barney, J.S., 1986a. Age of Late Quaternary marine deposits of southern Italy determined by aminostratigraphy, faunal correlation and uranium-series dating. *Riv. Ital. di Paleontol. Stratigr.* 92, 149–164.
- Hearty, P., J., 1986b. An inventory of last Interglacial (sensu lato) age deposits from the Mediterranean basin: a study of isoleucine epimerization and U-series dating. *Zeitschrift fur Geomorphol. Suppl.* 62, 51–69.

- Hearty, P.J., Miller, G.H., Stearns, C.E., Szabo, B.J., 1986c. Aminostratigraphy of Quaternary shorelines in the Mediterranean basin. *Geol. Soc. Am. Bull.* 97, 850–858.
- Hearty, P.J., Dai Pra, G., 1986d. Aminostratigraphy of Quaternary marine deposits in the Lazio region of central Italy. *Zeitschrift für Geomorphol.* 62, 131–140.
- Hearty, P.J., 1987a. New data on the Pleistocene of Mallorca. *Quat. Sci. Rev.* 6, 245–257.
- Hearty, P.J., Dai Pra, G., 1987b. Ricostruzione paleogeografica degli ambienti litoranei quaternari della Toscana e del Lazio settentrionale con l'impiego dell'aminostratigrafia. *Boll. Serv. Geol. d'Italia* 106, 189–224.
- Hearty, P.J., Hollin, J.T., Dumas, B., 1987. Geochronology of Pleistocene littoral deposits on the Alicante and Almeria coasts of Spain. *Trab. sobre Neogeno-Quaternario* 10.
- Hearty, P., Dai Pra, G., 1992. The age and stratigraphy of middle Pleistocene and younger deposits along the Gulf of Taranto (southeast Italy). *J. Coast. Res.* 8, 882–905.
- Hearty, P.J., 2002. Revision of the late Pleistocene stratigraphy of Bermuda. *Sediment. Geol.* 153, 1–21. [https://doi.org/10.1016/S0037-0738\(02\)00261-0](https://doi.org/10.1016/S0037-0738(02)00261-0)
- Hearty, P.J., Hollin, J.T., Neumann, A.C., O'Leary, M.J., McCulloch, M., 2007. Global sea-level fluctuations during the Last Interglaciation ( MIS 5e ). *Quat. Sci. Rev.* 26, 2090–2112. <https://doi.org/10.1016/j.quascirev.2007.06.019>
- Hibbert, F.D., Rohling, E.J., Dutton, A., Williams, F.H., Chutcharavan, P.M., Zhao, C., Tamisiea, M.E., 2016. Coral indicators of past sea-level change: A global repository of U-series dated benchmarks. *Quat. Sci. Rev.* 145, 1–56.
- Hillaire-Marcel, C., Gariépy, C., Ghaleb, B., Goy, J.-L., Zazo, C., Barcelo, J.C., 1996. U-series measurements in tyrrhenian deposits from mallorca. Further evidence for two last-interglacial high sea levels in the Balearic Islands. *Quat. Sci. Rev.* 15, 53–62. [https://doi.org/10.1016/0277-3791\(95\)00079-8](https://doi.org/10.1016/0277-3791(95)00079-8)
- Hills, E.S., 1972. Shore platforms and wave ramps. *Geol. Mag.* 109, 81–88.
- Hodell, D.A., Charles, C.D., Curtis, J.H., Mortyn, P.G., Ninnemann, U.S., Venz, K.A., 2003. Data report oxygen isotope stratigraphy of ODP LEG 177 sites 1088, 1089, 1090, 1093 and 10941. *Proc. Ocean Drill. Progr. Sci. Results* 177, 1–26.
- Hodgkin, E.P., 1964. Rate of erosion of intertidal limestone. *Zeitschrift für Geomorphol.* 8, 385–392.
- Houghton, S.L., Roberts, G.P., Papanikolaou, I.D., McArthur, J.M., 2003. New 234U- 230Th coral dates from the western Gulf of Corinth: Implications for extensional tectonics. *Geophys. Res. Lett.* 30, 2013. <https://doi.org/10.1029/2003GL018112>
- Hungr, O., Leroueil, S., Picarelli, L., 2014. The Varnes classification of landslides types, an update. *Landslides* 11, 167–194.

- Hutton, F.W., 1885. Sketch of the geology of New York. *Q. J. Geol. Soc* 41, 191–220.
- Iannace, A., Romano, P., Santangelo, N., Santo, A., Tuccimei, P., 2001. The OIS 5c along Licosa cape promontory (Campania region, southern Italy): morphostratigraphy and U/Th dating. *Zeitschrift für Geomorphol. N.F.* 45(3), 307–319.
- Iannace, A., Romano, P., & Tuccimei, P., 2003. U/Th dating and geochemistry of carbonate concretions associated with upper Pleistocene fossil shorelines of the Sorrento Peninsula (Conca dei Marini, southern Italy). *Quat. - Ital. J. Quat. Sci.* 6 (1Bis), 49–54.
- Iannace, A., Bonardi, G., D’Errico, M., Mazzoli, S., Perrone, V., Vitale, S., 2005. Structural setting and tectonic evolution of the Apennine Units of northern Calabria. *Comptes Rendus - Geosci.* 337, 1541–1550. <https://doi.org/10.1016/j.crte.2005.09.003>
- Iannace, A., Vitale, S., D’Errico, M., Mazzoli, S., Di Staso, A., Macaione, E., Messina, A., Reddy, S.M., Somma, R., Zamparelli, V., Zattin, M. & Bonardi, G., 2007. The carbonate tectonic units of northern Calabria (Italy): a record of Apulian palaeomargin evolution and Miocene convergence, continental crust subduction, and exhumation of HP-LT rocks. *J. Geol. Soc. London* 164, 1165–1186.
- Letti, A., & Sgrosso, I., 1963. Formazioni marine plio-pleistoceniche nei dintorni di Cicciano (Nola). *Boll. Soc. Naturisti Napoli* 62, 109–111.
- Iezzi, F., Mildon, Z., Walker, J.F., Roberts, G., Goodall, H., Wilkinson, M., Robertson, J., 2018. Coseismic Throw Variation Across Along-Strike Bends on Active Normal Faults: Implications for Displacement Versus Length Scaling of Earthquake Ruptures. *J. Geophys. Res. Solid Earth* 123, 9817–9841. <https://doi.org/10.1029/2018JB016732>
- Ijima, T., Takahashi, T., Nakamura, K., 1956. Wave characteristics in the surf zone observed by stereophotography. *Proc. 3rd Japanese Conf. Coast. Eng.* 99–116.
- Imbrie, J., Hays, J.D., Martinson, D.G., McIntyre, A., Mix, A.C., Morley, J.J., Pisias, N.G., Prell, W.L., Shackleton, N.J., 1984. The orbital theory of Pleistocene climate: support from a revised chronology of the main  $\delta^{18}O$  record. Berger, A.L., al. (Ed.), *Milankovitch Clim. Part I*. Reidel Publ. Company, Dordr. 269–305.
- Imbrie, J., Mix, A.C., Martinson, D.G., 1993. Milankovitch theory viewed from Devil Hole. *Nature* 363, 531–533.
- INGV, 2018. DISS Working Group (2018). Database of Individual Seismogenic Sources (DISS), Version 3.2.1: A compilation of potential sources for earthquakes larger than M 5.5 in Italy and surrounding areas. <http://diss.rm.ingv.it/diss/>. <https://doi.org/DOI:10.6092/INGV.IT-DISS3.2.1>.
- IPCC, Stocker, T.F., Qin, D., Plattner, G.-K., Tignor, M., Allen, S.K., Boschung,

- J., Nauels, A., Xia, Y., Bex, V., Midgley, P.M., 2013. Climate Change. The Physical Science Basis. Working Group, I Contribution to Fifth Assessment Report of the Intergovernmental Panel on Climate Change-Abstract for Decision-Makers
- Ippolito, F., Ortolani, F., Russo, M., 1973. Struttura marginale tirrenica dell'Appennino Campano: Reinterpretazione di dati di antiche ricerche di idrocarburi. *Mem. della Soc. Geol. Ital.* 12, 227–250.
- Isetti, G., de Lumley, H., Miskovsky, J.C., 1962. Il giacimento musteriano della grotta della Madonna dell'Arma presso Bussana (Sanremo). *Riv. di Stud. liguri* 5–116.
- ISPRA, 2014a. Foglio 448 Ercolano della Carta Geologica d'Italia alla scala 1:50.000. ISPRA, Roma, [https://www.ispraambiente.gov.it/Media/carg/448\\_ERCOLANO/Foglio.html](https://www.ispraambiente.gov.it/Media/carg/448_ERCOLANO/Foglio.html), last accessed July 2020.
- ISPRA, 2014b. Note illustrative della Carta Geologica d'Italia alla scala 1:50.000-Foglio 448 Ercolano. ISPRA, Roma, [https://www.ispraambiente.gov.it/Media/carg/note\\_illustrative/448\\_Ercolano.pdf](https://www.ispraambiente.gov.it/Media/carg/note_illustrative/448_Ercolano.pdf), last accessed July 2020.
- Issel, A., 1908. Liguria preistorica. a cura della Società ligure di Storia Patria.
- Issel, A., 1914. Lembi fossiliferi quaternarie recenti nella Sardegna meridionale. *Accad. Naz. dei Lincei, Ser. 5*, 759–770.
- Issfl, A., 1914. Lembi fossiliferi quaternari o recenti osservati nella Sardegna meridionale dai prof. D. Lovisato.
- Ivanovich, M., Vita-Finzi, C., Hennig, G.J., 1983. Uranium-series dating of molluscs from uplifted Holocene beaches in the Persian Gulf. *Nature* 302, 408–410. <https://doi.org/10.1038/302408a0>
- Jara-Muñoz, J., Melnick, D., Padoja, K., and Strecker, M.R., 2019. TerraceM-2: A Matlab R Interface for Mapping and Modeling Marine and Lacustrine Terraces. *Front. Earth Sci.* 7:255, 1–18. <https://doi.org/10.3389/feart.2019.00255>
- Johnson, D.W., 1919. Shore processes and shoreline development. New York John Wiley Sons 584.
- Johnson, D.W., 1931. Supposed two metre eustatic bench of the pacific shore. *Int. Geog. Cong.* 13, 158–163.
- Johnson, A.M., 1984. Debris flow. Brunnsden, D., Prior, D. B. (eds), *Slope Instab.* John Wiley Sons, Chichester 257–361.
- Jouzel, J., Hoffmann, G., Parrenin, F., Waelbroeck, C., 2002. Atmospheric oxygen 18 and sea.level chages. *Quat. Sci. Rev.* 21, 307–314.
- Kastens, K.A., Mascle, J., Auroux, C., Bonatti, E., Broglia, C., Channell, J., Curzi, P., Emeis, K.C., Glacon, G., Hasegawa, S., Hieke, W., Mascle, G., McCoy, F., Mckenzie, J., Mendelson, J., Muller, C., Réhault, J.P., Robertson, A., Sartori,

- R., Sprovieri, R., Torii, M., 1988. ODP Leg 107 in the Tyrrhenian Sea : Insights into passive margin and back-arc basin evolution. *GSA Bull.* 100, 1140–1156.
- Kattsov, V.M., Källén, E., Cattle, H.P., Christensen, J., Drange, H., Hanssen-Bauer, I., Jóhannesen, T., Karol, I., Räisänen, J., Svensson, G., 2005. Future Climate Change: Modeling and Scenarios for Arctic.
- Kaufman, A., Broecker, W., 1965. Comparison of Th230 and C14 ages for carbonate materials from lakes Lahontan and Bonneville. *J. Geophys. Res.* 70, 4039–4054. <https://doi.org/10.1029/JZ070i016p04039>
- Kaufman, A., Broecker, Wallace, S., Ku, T., L., Thurber, D., L., 1971. The status of U-series methods of mollusk dating. *Geochemica Cosmochem. Acta* 35, 1155–1183.
- Kaufman, A., Ghaleb, B., Wehmiller, J.F., Hillaire-Marcel, C., 1996. Uranium concentration and isotope ratio profiles within *Mercenaria* shells: Geochronological implications. *Geochim. Cosmochim. Acta* 60, 3735–3746. [https://doi.org/https://doi.org/10.1016/0016-7037\(96\)00190-1](https://doi.org/https://doi.org/10.1016/0016-7037(96)00190-1)
- Kázmér, M., Taboroši, D., 2012. Bioerosion on the small scale-examples from the tropical and subtropical littoral. *Hantkeniana* 7, 37–94.
- Kelletat, D., 1988. Zonality of modern coastal processes and sea-level indicators. *Palaeogeogr. Palaeoclimatol. Palaeoecol.* 68, 219–230.
- Kelletat, D.H., 2005. Notches. Schwartz, M.L. (Ed.), *Encycl. Coast. Sci.* Springer, Dordr. 728–729.
- Kemp, A.C., 2015. Paleo constraints on future sea-level rise. *Curr Clim Chang. Rep* 1, 205–215.
- Kennedy, D.M., 2015. Where is the seaward edge? A review and definition of shore platform morphology. *Quat. Sci. Rev.* 147, 99–108.
- Kent, D. V, Rio, D., Massari, F., Kukla, G., Lanci, L., 2002. Emergence of Venice during the Pleistocene. *Quat. Sci. Rev.* 21, 1719–1727. [https://doi.org/10.1016/s0277-3791\(01\)00153-6](https://doi.org/10.1016/s0277-3791(01)00153-6)
- Khan, N.S., Horton, B.P., Engelhart, S., Rovere, A., Vacchi, M., Ashe, E.L., Törnqvist, T.E., Dutton, A., Hijma, M.P., Shennan, I., 2019. Inception of a global atlas of sea levels since the Last Glacial Maximum. *Quat. Sci. Rev.* 220, 359–371. <https://doi.org/10.1016/j.quascirev.2019.07.016>
- Kindler, P., Davaud, E., Strasser, A., 1997. Tyrrhenian coastal deposits from Sardinia (Italy): a petrographic record of high sea levels and shifting climate belts during the last interglacial (isotopic substage 5e). *Palaeogeogr. Palaeoclimatol. Palaeoecol.* 133, 1–25.
- Kirk, R.M., 1977. Rates and forms of erosion on intertidal platforms at Kaikoura Peninsula, South Island, New Zealand. *New Zeal. J. Geol. Geophys.* 20, 571–613.
- Kopp, R.E., Simons, F.J., Mitrovica, J.X., Maloof, A.C., Oppenheimer, M., 2009.

- Probabilistic assessment of sea level during the last interglacial stage. *Nature* 462, 863–867. <https://doi.org/10.1038/nature08686>
- Kopp, R.E., Hay, C.C., Little, C.M., Mitrovica, J.X., 2015. Geographic Variability of Sea-Level Change. *Curr. Clim. Chang. Reports* 1, 192–204. <https://doi.org/10.1007/s40641-015-0015-5>
- Kowalewsky, D.B., 1984. Wave-built terrace, in: *Beaches and Coastal Geology*. Springer US, New York, NY, p. 855. [https://doi.org/10.1007/0-387-30843-1\\_485](https://doi.org/10.1007/0-387-30843-1_485)
- Kronenberg, G., Lee, H.G., 2006. Genera of american strombid gastropods (Gastropoda: Strombidae) and remarks on their phylogeny. *The Veliger* 49, 256–264.
- Labeyrie, L.D., Duplessy, J.C., Blanc, P.L., 1987. Variations in mode of formation and temperature of ocean deep waters over the past 125,000 years. *Nature* 327, 477–481.
- Laborel, J., 1986. Vermetids. van Plassche O Sea-level Res. a Man. Collect. Eval. data. *Geo Books, Norwich* 281–310.
- Laborel, J., Morhange, C., Lafont, R., Le Campion, J., Laborel-Deguen, F., & Sartoretto, S., 1994. Biological evidence of sea-level rise during the last 4500 years on the rocky coasts of continental southwestern France and Corsica. *Mar. Geol.* 120, 203–223.
- Laborel, J., Laborel-Deguen, F., 1996. Biological indicators of Holocene sea-level and climatic variations on rocky coasts of tropical and subtropical regions. *Quat. Int.* 31, 53–60.
- Laborel, J., Laborel-Deguen, F., 2005. Sea-level indicators, biologic. *Schwartz ML Encycl. Coast. Sci.* Springer, Dordr. 833–834.
- Lajoie, K., 1986. Coastal tectonics. *Act. tectonics* 95–124.
- Lambeck, K., Chappell, J., 2001. Sea Level Change Through the Last Glacial Cycle. *Science.* 292, 679–686. <https://doi.org/10.1126/science.1059549>
- Lambeck, Kurt, Antonioli, F., Purcell, A., Silenzi, S., 2004a. Sea-level change along the Italian coast for the past 10,000yr. *Quat. Sci. Rev.* 23, 1567–1598. <https://doi.org/10.1016/j.quascirev.2004.02.009>
- Lambeck, K., Antonioli, F., Purcell, T., Stirling, C.H., 2004b. MIS 5.5 Sea Level in the Mediterranean and Inferences on the Global Ice Volumes during Late MIS 6 and MIS 5.5.
- Lambeck, K., Purcell, A., 2005. Sea-level change in the Mediterranean Sea since the LGM: Model predictions for tectonically stable areas. *Quat. Sci. Rev.* 24, 1969–1988. <https://doi.org/10.1016/j.quascirev.2004.06.025>
- Lambeck, K., Anzidei, M., Antonioli, F., Benini, A., Verrubbi, V., 2018. Tyrrhenian sea level at 2000 BP: evidence from Roman age fish tanks and their geological calibration. *Rend. Lincei* 29, 69–80. <https://doi.org/10.1007/s12210-018-0715-6>

- Larson, A. C., & Von Dreele, R.B., 2004. General Structure Analysis System (GSAS), Los Alamos National Laboratory Report LAUR 86-748 (2004).
- Lawrence Edwards, R., Chen, J.H., Wasserburg, G.J., 1987.  $^{238}\text{U}/^{234}\text{U}$ / $^{230}\text{Th}/^{232}\text{Th}$  systematics and the precise measurement of time over the past 500,000 years. *Earth Planet. Sci. Lett.* 81, 175–192. [https://doi.org/10.1016/0012-821X\(87\)90154-3](https://doi.org/10.1016/0012-821X(87)90154-3)
- Lea, D.W., Martin, P.A., Pak, D.K., Spero, H.J., 2002. Reconstructing a 350 ky history of sea level using planktonic Mg/Ca and oxygen isotope records from a Cocos Ridge core. *Quat. Sci. Rev.* 21, 283–293.
- Lecca, L., Carboni, S., 2007. The Tyrrhenian section of San Giovanni di Sinis (Sardinia): stratigraphic record of an irregular single high stand. *Riv. Ital. di Paleontol. e Stratigr.* 113, 509.
- Lipparini, T., 1936. I fossili dei sedimenti marini nel sottosuolo della bassa pianura friulana. *Boll. Soc. Geol. Ital.* 55.
- Lisiecki, L.E., Raymo, M.E., 2005. A Pliocene-Pleistocene stack of 57 globally distributed benthic  $\delta^{18}\text{O}$  records. *Paleoceanography* 20, 1–17. <https://doi.org/10.1029/2004PA001071>
- Locati, M., Camassi, R., Rovida, A., Ercolani, E., Bernardini, F., Castelli, V., Caracciolo, C.H., Tertulliani, A., Rossi, A., Azzaro, R., D’Amico, S., Amico, S.D., Conte, S., Rocchetti, E., 2016. DBMI15, the 2015 version of the Italian Macroseismic Database.
- Lorscheid, T., Stocchi, P., Casella, E., Gómez-Pujol, L., Vacchi, M., Mann, T., Rovere, A., 2017. Paleo sea-level changes and relative sea-level indicators: Precise measurements indicative meaning and glacial isostatic adjustment perspectives from Mallorca (Western Mediterranean). *Palaeogeogr. Palaeoclimatol. Palaeoecol.* 473, 94–107. <https://doi.org/10.1016/j.palaeo.2017.02.028>
- Lorscheid, T., Rovere, A., 2019. The indicative meaning calculator – quantification of paleo sea-level relationships by using global wave and tide datasets. *Open Geospatial Data, Softw. Stand.* 4. <https://doi.org/10.1186/s40965-019-0069-8>
- Lucchi, F., Tranne, C.A., Calanchi, N., Pirazzoli, P., Romagnoli, C., Radtke, U., Reyss, J., Rossi, P.L., 2004a. Stratigraphic constraints to date Late-Quaternary ancient shorelines and to evaluate vertical movements at Lipati (Aeolian Islands). *Quat. Int.* 115/116, 105–115.
- Lucchi, F., Tranne, C.A., Calanchi, N., Rossi, P.L., 2004b. Late Quaternary fossil shorelines in the Aeolian Islands (Southern Tyrrhenian Sea): evaluation of long-term vertical displacements. *Quat. Nov.* VIII, 49–62.
- Ludwig, K.R., 2003. User’s Manual for Isoplot 3.00: A Geochronological Toolkit for Microsoft Excel, Special publication / Berkeley Geochronology Center. Kenneth R. Ludwig.
- Lumley, H. De, Khatib, S., Echassoux, A., Todisco, D., 2001. Les lignes de rivage

- quaternaire en relation avec les sites paléolithiques des Alpes-Maritimes et de la Ligurie occidentale. *Rev. d'Archéométrie* 25, 125–134. <https://doi.org/10.3406/arsci.2001.1008>
- Lunt, D.J., Abe-Ouchi, A., Bakker, P., Berger, A., Braconnot, P., Charbit, S., Fischer, N., Herold, N., Jungclauss, J.H., Khon, V.C., Krebs-Kanzow, U., Langebroek, P.M., Lohmann, G., Nisancioglu, K.H., Otto-Bliesner, B.L., Park, W., Pfeiffer, M., Phipps, S.J., Prange, M., Rachmayani, R., Renssen, H., Rosenbloom, N., Schneider, B., Stone, E.J., Takahashi, K., Wei, W., Yin, Q., Zhang, Z.S., 2013. A multi-model assessment of last interglacial temperatures. *Clim. Past* 9, 699–717. <https://doi.org/10.5194/cp-9-699-2013>
- Lyell, C., 1837. Principles of geology: being an inquiry how far the former changes of the earth's surface are referable to causes now in operation. J. Kay, Jun Brother.
- Malatesta, A., 1957. Terreni faune ed industrie quaternarie dell'arcipelago delle Egadi. *Quaternaria* IV, 165–257.
- Malatesta, A., 1985. Geologia e paleobiologia dell'era glaciale. *La Nuova Ital. Sci.* 282.
- Malinverno, A., Ryan, W.B.F., 1986. Extension in the Tyrrhenian Sea and shortening in the Apennines as result of arc migration driven by sinking of the lithosphere. *Tectonics* 5, 227–245. <https://doi.org/10.1029/TC005i002p00227>
- Maouche, S., Meghraoui, M., Morhange, C., Belabbes, S., Bouhadad, Y., Haddoum, H., 2013. Reply to the comment of Pedoja et al. by Maouche, S., Meghraoui, M., Morhange, C., Belabbes, S., Bouhadad, Y. and Haddoum, H. on the published paper: Maouche, S., Meghraoui, M., Morhange, C., Belabbes, S., Bouhadad, Y. and Haddoum, H., 2011, Active coastal thrusting and folding, and uplift rate of the Sahel anticline and Zemmouri earthquake area (Tell Atlas, Algeria), *Tectonophysics*, 509 (2011) 69--80. *Tectonophysics* 245–247.
- Maouche, S., Meghraoui, M., Morhange, C., Belabbes, S., Bouhadad, Y., Haddoum, H., 2011. Active coastal thrusting and folding, and uplift rate of the Sahel Anticline and Zemmouri earthquake area (Tell Atlas, Algeria). *Tectonophysics* 509, 69–80.
- Mariani, M., Prato, R., 1988. I bacini neogenici costieri del margine tirrenico: Approccio sismico-stratigrafico. *Mem. della Soc. Geol. Ital.* 41, 519–531.
- Marku, S. and Gjani, E.: The evolution of Holocene Transgression in Drini Bay. Northwestern Albania. *Journal International 1655 Environmental Application and Science*, 13(1), 33-40, 2018.
- Marra, F., Florindo, F., Anzidei, M., Sepe, V., 2016. Paleo-surfaces of glacio-eustatically forced aggradational successions in the coastal area of Rome: Assessing interplay between tectonics and sea-level during the last ten interglacials. *Quat. Sci. Rev.* 148, 85–100.

- <https://doi.org/10.1016/j.quascirev.2016.07.003>
- Marra, F., Bahain, J.-J., Jicha, B.R., Nomade, S., Palladino, D.M., Pereira, A., Tolomei, C., Voinchet, P., Anzidei, M., Aureli, D., Ceruleo, P., Falguères, C., Florindo, F., Gatta, M., Ghaleb, B., Rosa, M. La, Peretto, C., Petronio, C., Rocca, R., Rolfo, M.F., Salari, L., Smedile, A., Tombret, O., 2019. Reconstruction of the {MIS} 5.5 5.3 and 5.1 coastal terraces in Latium (central Italy): A re-evaluation of the sea-level history in the Mediterranean Sea during the last interglacial. *Quat. Int.* 525, 54–77. <https://doi.org/10.1016/j.quaint.2019.09.001>
- Marra, F., Rolfo, M.F., Gaeta, M., Florindo, F., 2020. Anomalous Last Interglacial Tyrrhenian sea levels and Neanderthal settling at Guattari and Moscerini caves (central Italy). *Sci. Rep.* 10. <https://doi.org/10.1038/s41598-020-68604-z>
- Massari, F., Rio, D., Barbero, R.S., Asioli, A., Capraro, L., Fornaciari, E., Vergerio, P.P., 2004. The environment of Venice area in the past two million years. *Palaeogeogr. Palaeoclimatol. Palaeoecol.* 202, 273–308. [https://doi.org/10.1016/s0031-0182\(03\)00640-0](https://doi.org/10.1016/s0031-0182(03)00640-0)
- Mastronuzzi, G., Palmentola, G., and Richetti, G., 1989. Aspetti della evoluzione olocenica della costa pugliese. *Mem. della Soc. Geol. Ital.* 42, 287–300.
- Mastronuzzi, G., Quinif, Y., Sansò, P., Selleri, G., 2007. Middle-Late Pleistocene polycyclic evolution of a stable coastal area (southern Apulia, Italy). *Geomorphology* 86, 393–408. <https://doi.org/10.1016/j.geomorph.2006.09.014>
- Masurel, Y., 1953. Observations sur la structure et la morphologie des Iles d'Hyères. *Ann. Geogr.* 62, 241–258. <https://doi.org/10.3406/geo.1953.13610>
- Mauz, B., Buccheri, G., Zöller, L., Greco, A., 1997. Middle to upper Pleistocene morphostructural evolution of the NW-coast of Sicily: Thermoluminescence dating and palaeontological-stratigraphical evaluations of littoral deposits. *Palaeogeogr. Palaeoclimatol. Palaeoecol.* 128, 269–285. [https://doi.org/10.1016/S0031-0182\(96\)00033-8](https://doi.org/10.1016/S0031-0182(96)00033-8)
- Mauz, B., 1999. Late Pleistocene records of littoral processes at the Tyrrhenian Coast (Central Italy): depositional environments and luminescence chronology. *Quat. Sci. Rev.* 18, 1173–1184. [https://doi.org/10.1016/s0277-3791\(98\)00071-7](https://doi.org/10.1016/s0277-3791(98)00071-7)
- Mauz, B., Hassler, U., 2000. Luminescence chronology of Late Pleistocene raised beaches in southern Italy : new data of relative sea-level changes. *Mar. Geol.* 170, 187–203.
- Mauz, B., Antonioli, F., 2009. Comment on "Sea level and climate changes during OIS 5e in the Western Mediterranean" by T. Bardajì J.L. Goy J.L., C. Zazo, C. Hillaire-Marcel, C.J. Dabrio, A. Cabero, B. Ghaleb, P.G. Silva, J. Lario, *Geomorphology* 110, 227–230. <https://doi.org/10.1016/j.geomorph.2009.05.001>

- Mauz, B., Fanelli, F., Elmejdoub, N., Barbieri, R., 2012. Coastal response to climate change: Mediterranean shorelines during the Last Interglacial (MIS5). *Quat. Sci. Rev.* 54, 89–98. <https://doi.org/10.1016/j.quascirev.2012.02.021>
- Mauz, B., Vacchi, M., Green, A., Hoffmann, G. and Cooper, A., 2015. Beachrock: a tool for reconstructing relative sea level in the 1690 far-field, *Marine Geology*, 362, 1–16.
- Mauz, B., 2020. Database of last interglacial sea-level proxies in the eastern Mediterranean. <https://doi.org/10.5281/zenodo.4454553>
- Mazzoli, S., Helman, M., 1994. Neogene patterns of relative plate motion for Africa-Europe: some implications for recent central Mediterranean tectonics. *Geol. Rundschau* 83, 464–468. <https://doi.org/10.1007/BF00210558>
- Meghraoui, M., Morel, J.L., Andrieux, J., Dahmani, M., 1996. Pliocene and Quaternary tectonics of the Tell-Rif mountains and Alboran sea, a complex zone of continent-continent convergence. *Bull. la Société Géologique Fr.* 167, 141–157.
- Meschis, M., Roberts, G.P., Robertson, J., & Briant, R.M., 2018. The Relationships Between Regional Quaternary Uplift, Deformation Across Active Normal Faults, and Historical Seismicity in the Upper Plate of Subduction Zones: The Capo D’Orlando Fault, NE Sicily. *Tectonics* 37, 1231–1255. <https://doi.org/10.1029/2017TC004705>
- Meschis, M., Scicchitano, G., Roberts, G.P., Robertson, J., Barreca, G., Monaco, C., Spampinato, C., Sahy, D., Antonioli, F., Mildon, Z.K., Scardino, G., 2020. Regional Deformation and Offshore Crustal Local Faulting as Combined Processes to Explain Uplift Through Time Constrained by Investigating Differentially Uplifted Late Quaternary Paleoshorelines: The Foreland Hyblean Plateau, SE Sicily. *Tectonics* 39. <https://doi.org/10.1029/2020tc006187>
- Milankovitch, M., 1941. Kanon der Erdbestrahlung und seine Anwendung auf das Eiszeitenproblem. *R. Serbian Acad. Spec. Publ.* 133, 633.
- Milano, G., Ventura, G., Di Giovambattista, R., 2002. Seismic evidence of longitudinal extension in the Southern Apennines chain (Italy): The 1997–1998 Sannio-Matese seismic sequence. *Geophys. Res. Lett.* 29, 64–65. <https://doi.org/10.1029/2002GL015188>
- Milano, G., Petrazzuoli, S., Ventura, G., 2004. Effects of hydrothermal circulation on the strain field of the Campanian Plain (southern Italy). *Terra Nov.* 16, 205–209. <https://doi.org/10.1111/j.1365-3121.2004.00556.x>
- Mildon, Z.K., Roberts, G.P., Faure Walker, J.P., Iezzi, F., 2017. Coulomb stress transfer and fault interaction over millennia on non-planar active normal faults: The Mw 6.5–5.0 seismic sequence of 2016–2017, central Italy. *Geophys. J. Int.* 210, 1206–1218. <https://doi.org/10.1093/gji/ggx213>
- Milia, A., Torrente, M.M., 1999. Tectonics and stratigraphic architecture of a peri-

- Tyrrhenian half-graben (Bay of Naples, Italy). *Tectonophysics* 315, 301–318. [https://doi.org/10.1016/S0040-1951\(99\)00280-2](https://doi.org/10.1016/S0040-1951(99)00280-2)
- Milia, A., Torrente, M.M., Massa, B., Iannace, P., 2013. Progressive changes in rifting directions in the Campania margin (Italy): New constrains for the Tyrrhenian Sea opening. *Glob. Planet. Change* 109, 3–17. <https://doi.org/10.1016/j.gloplacha.2013.07.003>
- Milia, A., Torrente, M.M., 2015. Tectono-stratigraphic signature of a rapid multistage subsiding rift basin in the Tyrrhenian-Apennine hinge zone (Italy): A possible interaction of upper plate with subducting slab. *J. Geodyn.* 86, 42–60. <https://doi.org/10.1016/j.jog.2015.02.005>
- Milli, S., Zarlenga, F., 1991. Analisi di facies dei depositi tirreniani (Duna Rossa) affioranti nell'area di Castel Porziano- Pomezia (Roma). *Quat.* 4, 233–248.
- Milne, G.A., Mitrovica, J.X., 1998. Postglacial sea-level change on a rotating Earth. *Geophys. J. Int.* 133, 1–19. <https://doi.org/10.1046/j.1365-246X.1998.1331455.x>
- Mitrovica, J.X., Davis, J.L., Shapiro, I.I., 1994. A spectral formalism for computing three-dimensional deformations due to surface loads: 1. Theory. *J. Geophys. Res. Solid Earth* 99, 7057–7073. <https://doi.org/10.1029/93JB03128>
- Miyauchi, T., Dai Pra, G., Sylos Labini, S., 1994. Geochronology of Pleistocene marine terraces and regional tectonics in the Tyrrhenian coast of South Calabria, Italy. *Quat.* 7, 17–34.
- Monaco, C., Tortorici, L., 2000. Active faulting in the Calabrian arc and eastern Sicily. *J. Geodyn.* 29, 407–424.
- Monaco, C., Catalano, S., De Guidi, G., Gresta, S., Langer, H., Tortorici, L., 2000. The Geological map of the urban area of Catania (Eastern Sicily): morphotectonic and seismotectonic implication. *Mem. Soc. Geol. Ital.* 55, 425–438.
- Monaco, C., Barreca, G., Di Stefano, A., 2017. Quaternary marine terraces and fault activity in the northern mainland sectors of the Messina Strait (southern Italy). *Ital. J. Geosci.* 136, 337–346. <https://doi.org/10.3301/IJG.2016.10>
- Morhange, C., Marriner, N., 2015. Archeological and biological relative sea-level indicators. *Handb. Sea-Level Res.* First Ed. Ed. by Ian Shennan, Antony J. Long, Benjamin P. Horton. © 2015 John Wiley Sons, Ltd. Publ. 2015 by John Wiley Sons, Ltd. Chapter 9, 146–156.
- Mörner, N., 1982. Sea level curves, in: *Beaches and Coastal Geology. Encyclopedia of Earth Sciences.* Springer, Boston, MA. [https://doi.org/10.1007/0-387-30843-1\\_399](https://doi.org/10.1007/0-387-30843-1_399)
- Mörner, N.-A., 1996. Rapid changes in coastal sea level. *J. Coast. Res.* 12 (4), 797–800.

- Moussat, E., Rehault, J.P., Fabbri, A., 1986. Rifting et évolution tectono-sédimentaire du Bassin Tyrrhénien au cours du Neogene et du Quaternaire. *Giorn. di Geol* 3, 48, 1/2, 41–62.
- Muhs, D.R., Kennedy, G.L., Rockwell, T.K., 1994. Uranium-series ages of marine terraces corals from the Pacific Coast of North America and Implications for Last-Interglacial sea level history. *Quat. Res.* 42, 72–87.
- Muhs, D.R., Simmons, K.R., Meco, J., Porat, N., 2015. Uranium-series ages of fossil corals from Mallorca Spain: The “Neotyrrhenian” high stand of the Mediterranean Sea revisited. *Palaeogeogr. Palaeoclimatol. Palaeoecol.* 438, 408–424. <https://doi.org/10.1016/j.palaeo.2015.06.043>
- Mullenders, W., Favero, V., Coremans, M., Dirickx, M., 1996. Analysis of pollen surveys from Venice [Analyses polliniques de sondages a Venise (VE-I, VE-I BIS, VE-II)]. *Aardkd. Meded.* 7, 87–117.
- Nalin, R., & Massari, F., 2009. Facies and stratigraphic anatomy of a temperate carbonate sequence (Capo Colonna Terrace, late Pleistocene, southern Italy). *J. Sed. Res.* 79, 210–225.
- Nalin, R., Bracchi, V.A., Basso, D., Francesco, & M., 2012. Persistrombus latus (Gmelin) in the upper Pleistocene deposits of the marine terraces of the Crotona peninsula (southern Italy). *Ital. J. Geosci.* 131 (1), 95–101. <https://doi.org/https://doi.org/10.3301/IJG.2011.25>
- Nesteroff, W., 1984. Étude de quelques grès de plage du sud de la Corse: datations <sup>14</sup>C et implications néotectoniques pour le bloc corso-sarde. *MOM Éditions* 8, 99–111.
- Neumann, A.C., 1968. Biological erosion of limestone coasts. Fairbridge, R. W. (Ed.), *Encycl. Geomorphol.* Rheinold, New York 75–81.
- Neumann, A., C., Hearty, P.J., 1996. Rapid sea-level changes at the close of the last interglacial (stage 5e) recorded in Bahamian Island geology. *Geology* 24, 775–778.
- Nisi, M.F., Antonioli, F., Pra, G.D., Leoni, G., Silenzi, S., 2003. Coastal deformation between the Versilia and the Garigliano plains (Italy) since the last interglacial stage. *J. Quat. Sci.* 18, 709–721. <https://doi.org/10.1002/jqs.803>
- Ortolani, F., & Aprile, F., 1978. Nuovi dati sulla struttura profonda della Piana Campana a sud est del fiume Volturno. *Boll. Soc. Geol. Ital.* 97, 561–608.
- Otvos, E.G., 2000. Beach ridges—definitions and significance. *Geomorphology* 32, 83–108.
- Ottmann, F., 1954. Le Quaternaire marin du cap Corse [with discussion]. *Bull. la Société Géologique Fr.* S6-IV, 565–570. <https://doi.org/10.2113/gssgfbull.s6-iv.7-9.565>
- Ozer, A., Paskoff, R., Sanlaville, P., Ulzega, A., 1980. Essai de corrélation du

- Pléistocène supérieur de la Sardaigne et de la Tunisie. *Comptes Rendus Hebd. des Séances l'Académie des Sci. Série D, Sci. Nat.* 291, 801–804.
- Ozer, A., 1986. Les niveaux marins au Pléistocène supérieur en Méditerranée occidentale. *Evol. dei litorali. Atti del convegno Organ. dal Cent. Ric. Energ. della Trisaia-ENEA, Policoro* 241–261.
- Ozer, A., Demoulin, A., Dai Pra, G., 1987. Les indices morphologiques temoins de la stabilité tectonique de la bordure littorale du Lazio meridional (Italie). *Zeitschrift für Geomorphol. Suppl.* 63, 103–117.
- Palieri, L., Sposato, A., 1988. Segnalazione di fauna a *Strombus bubonius* nell'area compresa tra Tarquinia e Montalto di Castro. *Quat.* 1, 161–166.
- Palmentola, G., Carobene, L., Mastronuzzi, G., & Sansò, P., 1990. I terrazzi marini pleistocenici della penisola di Crotona (Calabria). *Geogr. Fis. e Din. Quat.* 13, 75–80.
- Pasini, G., Colalongo, M.L., 1994. Proposal for the erection of the Santernian/Emilian boundary stratotype (Lower Pleistocene) and a new data on the Pliocene/Pleistocene boundary stratotype. *Boll. Soc. Paleontol. Ital.* 33 (1), 101–120.
- Pata, O., 1947. Su di un nuovo giacimento a *Strombus bubonius* Lmk. presso Vibo Valentia. *Atti della Soc. Toscana di Sci. Nat.* 54, 156–166.
- Patacca, E., Sartori, R., Scandone, P., 1990. Tyrrhenian basin and Apenninic Arcs: kinematic relations since Late Tortonian times. *Mem. Soc. Geol. It* 45, 425–451. [https://doi.org/10.1007/978-94-011-2016-6\\_7](https://doi.org/10.1007/978-94-011-2016-6_7)
- Patacca, E., Scandone, P., 2001. Late thrust propagation and sedimentary response in the thrust-belt—foredeep system of the Southern Apennines (Pliocene-Pleistocene). *Anat. an Orogen Apennines Adjac. Mediterr. Basins* 401–440. [https://doi.org/10.1007/978-94-015-9829-3\\_23](https://doi.org/10.1007/978-94-015-9829-3_23)
- Patacca, E., Scandone, P., 2007. Geology of the Southern Apennines. *Boll. della Soc. Geol. Ital. Vol. Spec.* 7, 75–119.
- Pedoja, K., Husson, L., Regard, V., Cobbold, P.R., Ostanciaux, E., Johnson, M.E., Kershaw, S., Saillard, M., Martinod, J., Furgerot, L., Weill, P., Delcaillau, B., 2011. Relative sea-level fall since the last interglacial stage: Are coasts uplifting worldwide? *Earth-Science Rev.* 108, 1–15. <https://doi.org/https://doi.org/10.1016/j.earscirev.2011.05.002>
- Pedoja, K., Djellit, H., Authemayou, C., Deverchere, J., Strzeczynski, P., Heddar, A., Nexer, M., Boudiaf, A., 2013. Comment on Active coastal thrusting and folding, and uplift rate of the Sahel Anticline and Zemmouri earthquake area (Tell Atlas, Algeria), by S. Maouche, M. Meghraoui, C. Morhange, S. Belabbes, Y. Bouhadad, H. Haddoum. [*Tectonophysics*, 2011, 509, 69–80. *Tectonophysics* 601, 236–244. <https://doi.org/10.1016/j.tecto.2012.08.043>
- Pedoja, K., Husson, L., Johnson, M.E., Melnick, D., Witt, C., Pochat, S., Nexer, M., Delcaillau, B., Pinagina, T., Poprawski, Y., Authemayou, C., Elliot, M.,

- Regard, V., Garestier, F., 2014. Coastal staircase sequences reflecting sea-level oscillations and tectonic uplift during the Quaternary and Neogene. *Earth-Science Rev.* 132, 13–38. <https://doi.org/https://doi.org/10.1016/j.earscirev.2014.01.007>
- Peeters, J., Cohen, K.M., Thrana, C., Busschers, F.S., Martinius, A.W., Stouthamer, E., Middelkoop, H., 2019. Preservation of Last Interglacial and Holocene transgressive systems tracts in the Netherlands and its applicability as a North Sea Basin reservoir analogue. *Earth-Science Rev.* 188, 482–497. <https://doi.org/10.1016/j.earscirev.2018.10.010>
- Phillips, B.A.M., 1970. Effective levels of marine planation on raised and present rock platforms. *Rév. Géog. Montr.* 24, 227–240.
- Pierson, T.C., 1980. Erosion and deposition by debris flows at Mt. Thomas, North Canterbury, New Zealand. *Earth Surf. Process.* 5, 227–247.
- Pikelj, K., Juračić, M., 2013. Eastern Adriatic Coast (EAC): Geomorphology and Coastal Vulnerability of a Karstic Coast. *J. Coast. Res.* 289, 944–957. <https://doi.org/10.2112/jcoastres-d-12-00136.1>
- Pini, R., Ravazzi, C., Donegana, M., 2009. Pollen stratigraphy, vegetation and climate history of the last 215 ka in the Azzano Decimo core (plain of Friuli, north-eastern Italy). *Quat. Sci. Rev.* 28, 1268–1290. <https://doi.org/10.1016/j.quascirev.2008.12.017>
- Pirazzoli, P.A., 1976. Sea-level variation in the Northwest Mediterranean during Roman times. *Science.* 194, 519–21.
- Pirazzoli, P.A., 1979. Les viviers à poissons romains en Méditerranée. *Les Indic. niveaux Mar. Paris Ocean. Fasc. hors.-sér.*, 5, 191–201.
- Pirazzoli, P.A., 1986. Marine notches. Van Plassche, O. (Ed.), *Sea-level Res. a Man. Collect. Eval. data.* Geo Books, Norwich, 361–400.
- Pirazzoli, P.A., 1987. Sea-level change in the Mediterranean. *Sea Lev. Chang. by Tooley Shennan.*
- Pirazzoli, P.A., Radtke, U., Hantoro, W.S., Jounnic, C., Hoang, C.T., Causse, C., Borell Best, M., 1993. A one million-year-long sequence of marine terraces on Sumba Island, Indonesia. *Mar. Geol.* 109, 221–236.
- Pirazzoli, P.A., 1996. Sea-level changes. The last 20.000 years. John Wiley Sons, Chichester 210.
- Pirazzoli, P.A., 2005. Marine Terraces. *Encyclopedia of Coastal Science.* Springer 632–633.
- Pirazzoli, P.A., 2007. Sea level studies; geomorphological indicators. *Elias SA Encycl. Quat. Sci.* Elsevier, Oxford 2974–2983.
- Pisias, N.G., Mix, A.C., Zahn, R., 1990. Nonlinear response in the global climate system: evidence from benthic oxygen isotopic record in core RC13-110. *Paleoceanography* 147–160.
- Polyak, V.J., Onac, B.P., Fornós, J.J., Hay, C., Asmerom, Y., Dorale, J.A., Ginés,

- J., Tuccimei, P., Ginés, A., 2018. A highly resolved record of relative sea level in the western Mediterranean Sea during the last interglacial period. *Nat. Geosci.* 11, 860–864.
- Poujol, A., Ritz, J.F., Tahayt, A., Vernant, P., Condomines, M., Blard, P.H., Billant, J., Vacher, L., Tibari, B., Hni, L., Idrissi, A.K., 2014. Active tectonics of the Northern Rif (Morocco) from geomorphic and geochronological data. *J. Geodyn.* 77, 70–88. <https://doi.org/10.1016/j.jog.2014.01.004>
- Provansal, M., Quinif, Y., Verrecchia, E., Arnaud, P.M., 1995. Identification d'un littoral tyrrhénien en bordure de l'Etang de Berre (Bouches-du-Rhône, France méridionale). *Comptes rendus l'Académie des Sci. Série 2. Sci. la terre des planètes* 320, 867–872.
- Radtke, U., 1986. Value and risk of radiometric dating of shorelines-geomorphological and geochronological investigations in central Italy, Eolian Islands and Ustica (Sicily). *Zeitschrift für Geomorphol. Suppl-Bd* 62, 167–181.
- Rasmussen, H., 2000. Nearshore and alluvial facies in the Sant Llorenç del Munt depositional system: recognition and development. *Sediment. Geol.* 138, 71–98. [https://doi.org/https://doi.org/10.1016/S0037-0738\(00\)00144-5](https://doi.org/https://doi.org/10.1016/S0037-0738(00)00144-5)
- Ravazzi, C., Pini, R., Badino, F., De Amicis, M., Londeix, L., Reimer, P.J., 2014. The latest LGM culmination of the Garda Glacier (Italian Alps) and the onset of glacial termination. Age of glacial collapse and vegetation chronosequence. *Quat. Sci. Rev.* 105, 26–47. <https://doi.org/10.1016/j.quascirev.2014.09.014>
- Rehault, J.P., Moussat, E., Fabbri, A., 1987. Structural evolution of the Tyrrhenian back-arc basin. *Mar. Geol.* 74, 123–150.
- Rhodes, E.J., 1996. ESR dating of tooth enamel. Basile, B., Chilardi, S. (Eds.), *Siracusa, le Ossa dei Giganti, lo scavo Archeol. di Contrada Fusco. Lomb. Palermo* 39–44.
- Riccio, A., Ruggieri, G., & Romano, P., 1999. Upper Pleistocene sea level history: new data from geomorphology, stratigraphy and sedimentology on fossil shorelines in Sorrento Peninsula (southern Italy). *FIST, GeoItalia riassunti*, 226–227.
- Riccio, A., Riggio, F., Romano, P., 2001. Sea level fluctuations during Oxygen Isotope Stage 5: New data from fossil shorelines in the Sorrento Peninsula (Southern Italy). *Zeitschrift für Geomorphol.* 45, 121–138.
- Richetti, G., 1967. Osservazioni preliminari sulla geologia e morfologia dei depositi quaternari dei dintorni del Mar Piccolo (Taranto). *Atti dell'Accademia Gioenia di Sci. Nat. Catania* 6 (XVIII), 123–130.
- Roberts, G.P., Houghton, S.L., Underwood, C., Papanikolaou, I., Cowie, P.A., van Calsteren, P., Wigley, T., Cooper, F.J., McArthur, J.M., 2009. Localization of Quaternary slip rates in an active rift in 10 5 years: An example from central

- Greece constrained by 234 U- 230 Th coral dates from uplifted paleoshorelines. *J. Geophys. Res.* 114, B10406. <https://doi.org/10.1029/2008JB005818>
- Roberts, G.P., Meschis, M., Houghton, S., Underwood, C., Briant, R.M., 2013. The implications of revised Quaternary palaeoshoreline chronologies for the rates of active extension and uplift in the upper plate of subduction zones. *Quat. Sci. Rev.* 78, 169–187. <https://doi.org/10.1016/j.quascirev.2013.08.006>
- Robertson, J., Meschis, M., Roberts, G.P., Ganas, A., Gheorghiu, D.M., 2019. Temporally Constant Quaternary Uplift Rates and Their Relationship With Extensional Upper-Plate Faults in South Crete (Greece), Constrained With 36Cl Cosmogenic Exposure Dating. *Tectonics* 38, 1189–1222. <https://doi.org/10.1029/2018TC005410>
- Robustelli, G., 2019. Geomorphic constraints on uplift history in the Aspromonte Massif, southern Italy. *Geomorphology* 327, 319–337. <https://doi.org/https://doi.org/10.1016/j.geomorph.2018.11.011>
- Rohling, E.J., Fenton, M., Jorissen, F.J., Bertrand, P., Ganseen, G., Caulets, J., 1998. Magnitudes of sea-level lowstands of the past 500.000 years. *Nature* 394, 162–165.
- Rohling, E.J., Foster, G.L., Grant, K.M., Marino, G., Roberts, A.P., Tamisiea, M.E., Williams, F., 2014. Sea-level and deep-sea-temperature variability over the past 5.3 million years. *Nature* 508, 477–82. <https://doi.org/10.1038/nature13230>
- Rolandi, G., Bellucci, F., Heizler, M.T., Belkin, H.E., De Vivo, B., 2003. Tectonic controls on the genesis of ignimbrites from the Campanian Volcanic Zone, southern Italy. *Mineral. Petrol.* 79, 3–31. <https://doi.org/10.1007/s00710-003-0014-4>
- Romano, P., 1992. La distribuzione dei depositi marini pleistocenici lungo le coste della Campania. Stato delle conoscenze e prospettive di ricerca. *Stud. Geol. Camerti special nu*, 265–269.
- Romano, P., Santo, A., Voltaggio, M., 1994a. L'evoluzione geomorfologica della piana del fiume Volturno (Campania) durante il tardo Quaternario (Pleistocene medio-superiore-Olocene). *Quat. - Ital. J. Quat. Sci.*
- Romano, P., Santo, A., Voltaggio, M., 1994b. L'evoluzione geomorfologica della piana del fiume Volturno (Campania) durante il tardo Quaternario (Pleistocene medio-superiore-Olocene). *Quat. - Ital. J. Quat. Sci.*
- Romeo, R., 2009. Studio geofisico integrato ad alta risoluzione dei depositi marini e della struttura del substrato della riviera di Miramare (Golfo di Trieste). PhD Thesis University of Trieste.
- Rosi, M., & Sbrana, A., 1987. Phlegrean Fields. *Quad. "La Ric. Sci. CNR Roma* 114,9, 1–175.

- Rovere, A., Antonioli, F., Bianchi, C.N., 2015. Fixed biological indicators, in: Handbook of Sea-Level Research. John Wiley & Sons, Ltd, pp. 268–280. <https://doi.org/https://doi.org/10.1002/9781118452547.ch18>
- Rovere, A., Raymo, M.E., Vacchi, M., Lorscheid, T., Stocchi, P., Gómez-pujol, L., Harris, D.L., Casella, E., Leary, M.J.O., Hearty, P.J., 2016a. Earth-Science Reviews The analysis of Last Interglacial ( MIS 5e ) relative sea-level indicators : Reconstructing sea-level in a warmer world. *Earth Sci. Rev.* 159, 404–427. <https://doi.org/10.1016/j.earscirev.2016.06.006>
- Rovere, A., Stocchi, Paolo, Vacchi, M., 2016b. Eustatic and Relative Sea Level Changes. *Curr. Clim. Chang. Reports* 221–231. <https://doi.org/10.1007/s40641-016-0045-7>
- Rovere, A., Ryan, D., Murray-Wallace, C., Simms, A., Vacchi, M., Dutton, A., Gowan, E., 2020. Descriptions of database fields for the World Atlas of Last Interglacial Shorelines (WALIS) (Version 1,0). Zenodo. <https://doi.org/http://doi.org/10.5281/zenodo.3961544>
- Rovida, A., Locati, M., Camassi, R., Lolli, B., Gasperini, P. (eds., 2016. *Catalogo Parametrico dei Terremoti Italiani (CPTI15)*. Ist. Naz. di Geofis. e Vulcanol.
- Rovida, A., Locati, M., Camassi, R., Lolli, B., Gasperini, P., 2019. *Catalogo Parametrico dei Terremoti Italiani (CPTI)*, versione 2.0. Istituto Nazionale di Geofisica e Vulcanologia. <https://doi.org/https://doi.org/10.13127/CPTI/CPTI15.2>
- Rovida, A., Locati, M., Camassi, R., Lolli, B., Gasperini, P., 2020. The Italian earthquake catalogue CPTI15. *Bull. Earthq. Eng.* 18, 2953–2984. <https://doi.org/https://doi.org/10.1007/s10518-020-00818-y>
- Royden, L., Patacca, E., Scandone, P., 1987. Segmentation and configuration of subducted lithosphere in Italy: An important control on thrust-belt and foredeep-basin evolution. *Geology* 15, 714–718.
- Royden, L.H., 1993. The tectonic expression slab pull at continental convergent boundaries. *Tectonics* 12, 303–325.
- Ruberti, D., Vigliotti, M., 2017. Land use and landscape pattern changes driven by land reclamation in a coastal area: the case of Volturno delta plain, Campania Region, southern Italy. *Environ. Earth Sci.* 76, 694. <https://doi.org/10.1007/s12665-017-7022-x>
- Ruddiman, W.F., Raymo, M.E., Martinson, D.G., Clement, B.M., Backman, J., 1989. Pleistocene evolution: northern hemisphere ice sheets and North Atlantic Ocean. *Paleoceanography* 4 (4), 353–412.
- Ruggieri, G., 1948. Il terrazzo marino presiciliano della Penisola di Crotona. *Giorn. Geol. Ser. 3* 20, 39–62.
- Ruggieri, G., Buccheri, G., 1968. Una malacofauna Tirreniana dell'isola di Ustica (Sicilia). *Geol. Rom.* VII, 27–58.
- Ruggieri, G., Unti, A., Unti, M., Moroni, M.A., 1975. La Calcarenite di Marsala

- (Pleistocene Inferiore) e i terreni contermini. *Boll. Soc. Geol. Ital.* 93, 723–733.
- Ruggieri, G., Unti, A., 1988. Una malacofauna del Tirreniano di Birgi Nuovo (Trapani). *Nat. Sicil.* XII, 19–32.
- Santangelo, Nicoletta, Ciampo, G., Di Donato, V., Esposito, P., Petrosino, P., Romano, P., Ermolli, E.R., Santo, A., Toscano, F., Villa, I., 2010. Late quaternary buried lagoons in the northern campania plain (southern Italy): Evolution of a coastal system under the influence of volcano-tectonics and eustatism. *Ital. J. Geosci.* 129, 156–175. <https://doi.org/10.3301/IJG.2009.12>
- Santangelo, N., Romano, P., Ascione, A., Russo Ermolli, E., 2017. Quaternary evolution of the Southern Apennines coastal plains: a review. *Geol. Carpathica* 68, 43–56. <https://doi.org/10.1515/geoca-2017-0004>
- Santoro, E., Mazzella, M.E., Ferranti, L., Randisi, A., Napolitano, E., Rittner, S., Radtke, U., 2009. Raised coastal terraces along the Ionian Sea coast of northern Calabria, Italy, suggest space and time variability of tectonic uplift rates. *Quat. Int.* 206, 78–101. <https://doi.org/10.1016/j.quaint.2008.10.003>
- Santoro, E., Ferranti, L., Burrato, P., Mazzella, M.E., Monaco, C., 2013. Deformed Pleistocene marine terraces along the Ionian Sea margin of southern Italy: Unveiling blind fault-related folds contribution to coastal uplift. *Tectonics* 32, 737–762. <https://doi.org/10.1002/tect.20036>
- Saoudi, N., 1989. Pliocène et Pléistocène inférieur et moyen du Sahel d'Alger. ENAL, Alger.
- Sartori, R., 1990. The Main Results of ODP Leg 107 in the Frame of Neogene To Recent Geology of Peri-Tyrrhenian Areas. *Proc. Ocean Drill. Program, Sci. Results*, Vol. 107 107, 715–730.
- Savelli, C., Schreider, A.A., 1991. The opening processes in the deep Tyrrhenian basins of Marsili and Vavilov, as deduced from magnetic and chronological evidence of their igneous crust. *Tectonophysics* 190, 119–131. [https://doi.org/https://doi.org/10.1016/0040-1951\(91\)90358-Y](https://doi.org/https://doi.org/10.1016/0040-1951(91)90358-Y)
- Scandone, P., 1979. Origin of the Tyrrhenian Sea and Calabrian Arc. *Ital. J. Geosci.* 98, 27–34.
- Scandone, R., Bellucci, F., Lirer, L., Rolandi, G., 1991. The structure of the Campanian Plain and the activity of the Neapolitan volcanoes (Italy). *J. Volcanol. Geotherm. Res.* 48, 1–31. [https://doi.org/10.1016/0377-0273\(91\)90030-4](https://doi.org/10.1016/0377-0273(91)90030-4)
- Scarciglia, F., Terribile, F., Colombo, C., Cinque, A., 2003. Late Quaternary climatic changes in Northern Cilento (Southern Italy): an integrated geomorphological and paleopedological study. *Quat. Int.* 106–107, 141–158. [https://doi.org/10.1016/S1040-6182\(02\)00169-6](https://doi.org/10.1016/S1040-6182(02)00169-6)

- Scarciglia, F., Pulice, I., 2006. Soil chronosequences on Quaternary marine terraces along the northwestern coast of Calabria (Southern Italy). *Quat. Int.* 156–157, 133–155.
- Schettino, A., Turco, E., 2011. Tectonic history of the western Tethys since the Late Triassic. *Geol. Soc. Am. Bulletin* 123, 89–105.
- Schrag, D., Hampt, G., Murray, D., 1996. Pore fluid constraints on the temperature and oxygen isotope composition of the glacial ocean. *Science* (80-). 272, 1930–1932.
- Schwarcz, H.P., Bietti, A., Buhay, W.M., Stiner, M.C., Grun, R., Segre, A., 1991a. On the reexamination of Grotta Guattari: uranium-series and electron-spin-resonance dates.
- Schwarcz, H.P., Buhay, W., Grün, R., Stiner, M., Kuhn, S., Miller, G.H., 1991b. Absolute dating of sites in coastal Lazio. *Quat. Nov.* 1, 51–67.
- Sechi, D., Andreucci, S., Stevens, T., Pascucci, V., 2020. Age and significance of late Pleistocene *Lithophyllum byssoides* intertidal algal ridge, NW Sardinia, Italy. *Sediment. Geol.* 400, 105618.
- Segre, A.G., 1949. Tracce di morfologia subaerea sul fondo marino litoraneo del Lazio meridionale. *Hist. Nat.* 3, 1–3.
- Segre, A., 1960. Geologia. Zavattari, E. (Ed.), *Biogeogr. delle isole Pelagie*. *Rend. Accad. Naz. Lincei XL*, 115–162.
- Selli, R., 1962. Le Quaternarie marin du versant Adriatique-Jonien de la Péninsule italienne. *Quaternaria* 6, 391–413.
- Selvaggi, G., Chiarabba, C., 1995. Seismicity and P-wave velocity image of the Southern Tyrrhenian subduction zone. *Geophys. J. Int.* 121, 818–826. <https://doi.org/10.1111/j.1365-246X.1995.tb06441.x>
- Sgarella, F., Moncharmont Zei, M., 1993. Benthic Foraminifera of the Gulf of Naples (Italy): systematics and autoecology. *Boll. Soc. Paleontol. Ital.* 32, 145–264.
- Sgrosso, I., & Ciampo, G., 1966. Sulla presenza di terreni calabriesi nei dintorni di Camerota. *Boll. Soc. Naturisti Napoli* 75, 561–587.
- Shackleton, N.J., Opdyke, N.D., 1973. Oxygen isotope and paleomagnetic stratigraphy of equatorial Pacific core V28-238: oxygen isotope temperature and ice volume on a  $10^5$  years and  $10^6$  years scale. *Quat. Res.* 3, 39–55.
- Shackleton, N.J., 1987. Oxygen isotopes, ice volumes and sea level. *Quat. Sci. Rev.* 6, 183–190.
- Shackleton, N.J., 2000. The 100,000 year ice age cycle identified and found to lag temperature, carbon dioxide and orbital eccentricity. *Science.* 289, 1897–1902.
- Shackleton, N.J., Chapman, M., Sánchez-Goni, M.F., Pailler, D., Lancelot, Y., 2002. The classic marine isotope substage 5e. *Quat. Res.* 58, 14–16. <https://doi.org/10.1006/qres.2001.2312>

- Shackleton, N.J., Sánchez-Goñi, M.F., Pailler, D., Lancelot, Y., 2003. Marine isotope substage 5e and the Eemian interglacial. *Glob. Planet. Change* 36, 151–155. [https://doi.org/10.1016/S0921-8181\(02\)00181-9](https://doi.org/10.1016/S0921-8181(02)00181-9)
- Shennan, I., 2015. Handbook of sea-level research. *Handb. sea-level Res.* Chichester Wiley 3–15. <https://doi.org/https://doi.org/10.1002/9781118452547.ch2>.
- Shultz, A.W., 1984. Subaerial debris flow deposition in the Upper Paleozoic Cutler Formation, western Colorado. *J. Sediment. Petrol.* 54, 759–772.
- Siddall, M., Rohling, E.J., Almogi-Labin, A., Hemleben, C., Meischner, D., Schmelzer, I., Smeed, D. a, 2003. Sea-level fluctuations during the last glacial cycle. *Nature* 423, 853–858. <https://doi.org/10.1038/nature01690>
- Siddall, M., Chappell, J., Potter, E.K., 2006. Eustatic sea level during past interglacials. *Dev. Quat. Sci.* 7, 75–92. [https://doi.org/10.1016/S1571-0866\(07\)80032-7](https://doi.org/10.1016/S1571-0866(07)80032-7)
- Sivan, D., Sisma-Ventura, G., Greenbaum, N., Bialik, O.M., Williams, F.H., Tamisiea, M.E., Rohling, E.J., Frumkin, A., Avnaim-Katav, S., Shtienberg, G., Stein, M., 2016. Eastern Mediterranean sea levels through the last interglacial from a coastal-marine sequence in northern Israel. *Quat. Sci. Rev.* 145, 204–225. <https://doi.org/https://doi.org/10.1016/j.quascirev.2016.06.001>
- Sivan, D., Galili, E., 2020. The last interglacial sea-level record of the Israeli coastline - WALIS database of sea-level indicators. <https://doi.org/10.5281/zenodo.4274178>
- Smith, G.A., Lowe, D.R., 1991. Lahars: volcanohydrologic events and deposition in the debris flow hyperconcentrated flow continuum. *Fish. R. V.*, Smith G.A. (eds), *Sediment. Volcan. settings*, Soc. Sediment. Geol. Special Pu, 59–70.
- Sohn, Y.K., Rhee, C.W., Kim, B.C., 1999. Debris Flow and Hyperconcentrated Flood-Flow Deposits in an Alluvial Fan, Northwestern Part of the Cretaceous Yongdong Basin, Central Korea. *J. Geol.* 107, 111–132.
- Spratt, R.M., Lisiecki, L.E., 2016. A Late Pleistocene sea level stack. *Clim. Past* 12, 1079–1092. <https://doi.org/10.5194/cp-12-1079-2016>
- Stanley, D., & Wezel, F.C., 1985. Geological evolution of the Mediterranean Basin. Springer, Berlin 589.
- Stearns, C.E., Thurber, D.L., 1965. Th230/U234 dates of late Pleistocene marine fossils from the Mediterranean and Moroccan littorals. *Prog. Oceanogr.* 4, 293–305.
- Stirling, C.H.L., Esat, T.M., Lambeck, K., Mcculloch, M.T., 1998. Timing and duration of the Last Interglacial: evidence for a restricted interval of widespread coral reef growth. *Earth Planet. Sci. Lett.* 160, 745–762.
- Stocchi, P., Spada, G., 2007. Glacio and hydro-isostasy in the Mediterranean Sea: Clark's zones and role of remote ice sheets. *Ann. Geophys.* 50, 741–761. <https://doi.org/10.4401/ag-3054>

- Stocchi, P., Vacchi, M., Lorscheid, T., de Boer, B., Simms, A.R., van de Wal, R.S.W., Vermeersen, B.L.A., Pappalardo, M., Rovere, A., 2018. MIS 5e relative sea-level changes in the Mediterranean Sea: Contribution of isostatic disequilibrium. *Quat. Sci. Rev.* 185, 122–134. <https://doi.org/10.1016/j.quascirev.2018.01.004>
- Suess, E., 1906. *The face of the earth*. Oxford Clarendon Press.
- Sunamura, T., 1972. A study on the formation of continental shelves. *Geogr. Rev. Japan* 45, 813–823.
- Sunamura, T., 1975. A laboratory study of wave-cut platform formation. *J. Geol.* 83, 389–397.
- Sunamura, T., 1977. A relationship between wave-induced cliff erosion and erosive force of waves. *J. Geol.* 85, 613–618.
- Sunamura, T., 1978a. Mechanism of shore platform formation on the southeastern coast of the Izu Peninsula, Japan. *J. Geol.* 86, 211–222.
- Sunamura, T., 1978b. A mathematical model of submarine platform development. *Math. Geol.* 10, 53–58.
- Sunamura, T., 1983. Processes of sea cliff and platform erosion. Komar, P. D., ed., *CRC Handb. Coast. Process. Eros.* Boca Raton, Florida, CRC Press. 233–265.
- Sunamura, T., 1991. The elevation of shore platform: a laboratory approach to the unsolved problem. *J. Geol.* 99, 761–766.
- Sunamura, T., 1992. *Geomorphology of rocky coast*. John Wiley Son Ltd.
- Surić, M., Richards, D.A., Hoffmann, D.L., Tibljaš, D., Juračić, M., 2009. Sea-level change during {MIS} 5a based on submerged speleothems from the eastern Adriatic Sea (Croatia). *Mar. Geol.* 262, 62–67. <https://doi.org/10.1016/j.margeo.2009.03.005>
- Taboroši, D., Kázmér, M., 2013. Erosional and depositional textures and structures in coastal karst landscapes. Lace, M.J., Mylroie, J. (eds). *Coast. karst landforms*. *Coast. Res. Libr.* 5. Springer, Berlin.
- Takahashi, T., 1974. Geomorphological study of shore platforms- analytical and genetical. *Sci. Rept Tohoku Univ.*, 7th Ser. 24, 115–163.
- Tarquini, S., Tarquini, S., Isola, I., Favalli, M., Mazzarini, F., Bisson, M., Pareschi, M.T., Boschi, E., 2007. TINITALY/01: a new Triangular Irregular Network of Italy. *Ann. Geophys.* 50, 407–425. <https://doi.org/10.4401/ag-4424>
- Tarquini, S., Vinci, S., Favalli, M., Doumaz, F., Fornaciai, A., Nannipieri, L., 2012. Release of a 10-m-resolution DEM for the Italian territory: Comparison with global-coverage DEMs and anaglyph-mode exploration via the web. *Comput. Geosci.* 38, 168–170. <https://doi.org/10.1016/j.cageo.2011.04.018>
- Toby, B.H., 2001. EXPGUI, a graphical user interface for GSAS. *J. Appl. Crystallogr.* 34, 210–213.
- Tortorici, G., Bianca, M., de Guidi, G., Monaco, C., Tortorici, L., 2003. Fault activity and marine terracing in the Capo Vaticano area (southern Calabria)

- during the Middle-Late Quaternary. *Quat. Int.* 101–102, 269–278.  
[https://doi.org/10.1016/S1040-6182\(02\)00107-6](https://doi.org/10.1016/S1040-6182(02)00107-6)
- Torres, T., Ortiz, J.E., Arribas, I., 2013. Variations in racemization/epimerization ratios and amino acid content of *Glycymeris* shells in raised marine deposits in the Mediterranean. *Quat. Geochronol.* 16, 35–49.  
<https://doi.org/10.1016/j.quageo.2012.11.002>
- Tosi, L., Rizzetto, F., Bonardi, M., Donnici, S., Serandrei Barbero, R., Toffoletto, F. (Eds.),  
 2007°. Note illustrative della 1830 Carta Geologica alla scala 1:50.000, foglio 128 Venezia. APAT - Regione Veneto, 164 pp.
- Tosi, L., Rizzetto, F., Bonardi, M., Donnici, S., Serandrei Barbero, R., Toffoletto, F. (Eds.),  
 2007b. Note illustrative della Carta Geologica alla scala 1:50.000, foglio 129 Chioggia–Malamocco. APAT - Regione Veneto, 164 pp.
- Trenhaile, A.S., 1978. The shore platforms of Gaspé, Québec. *Ann. Assoc. Am. Geog.* 68, 95–114.
- Trenhaile, A.S., 1987. The geomorphology of rock coasts. Oxford, Oxford Univ. Press 384.
- Tuccimei, P., Ginés, J., Delitala, M.C., Ginés, A., Gràcia, F., Fornós, J.J., Taddeucci, A., 2006. Last interglacial sea level changes in Mallorca island (Western Mediterranean). High precision U-series data from phreatic overgrowths on speleothems. *Zeitschrift für Geomorphol.* 1–21.
- Tuccimei, P., Onac, B.P., Dorale, J.A., Ginés, J., Fornós, J.J., Ginés, A., Spada, G., Ruggieri, G., Mucedda, M., 2012. Decoding last interglacial sea-level variations in the western Mediterranean using speleothem encrustations from coastal caves in Mallorca and Sardinia: A field data--model comparison. *Quat. Int.* 262, 56–64.
- Tucker, G.E., McCoy, S.W., Whittaker, A.C., Roberts, G.P., Lancaster, S.T., Phillips, R., 2011. Geomorphic significance of postglacial bedrock scarps on normal-fault footwalls. *J. Geophys. Res. Earth Surf.* 116, 1–14.  
<https://doi.org/10.1029/2010JF001861>
- Turco, E., Macchiavelli, C., Mazzoli, S., Schettino, A., Pierantoni, P.P., 2012. Kinematic evolution of Alpine Corsica in the framework of Mediterranean mountain belts. *Tectonophysics.*  
<https://doi.org/10.1016/J.TECTO.2012.05.010>
- Turney, C.S.M., Jones, R.T., 2010. Does the Agulhas Current amplify global temperatures during super-interglacials? *J. Quat. Sci.* 25, 839–843.  
<https://doi.org/https://doi.org/10.1002/jqs.1423>
- Ulzega, A., Ozer, A., 1980. Comptes-rendus de l'excursion. Table ronde sur le Tyrrhénien la Sardaigne. *INQUA* 3–112.
- Ulzega, A., Hearty, P.J., 1986. Geomorphology, stratigraphy and geochronology

- of Late Quaternary marine deposits in Sardinia. *Z. Geomorphol. NF, Suppl. Bd 62*, 119–129.
- Vacchi, M., Marriner, N., Morhange, C., Spada, G., Fontana, A., Rovere, A., 2016. Multiproxy assessment of Holocene relative sea-level changes in the western Mediterranean: Sea-level variability and improvements in the definition of the isostatic signal. *Earth-Science Rev.* 155, 172–197.
- Vacchi, M., Ghilardi, M., Spada, G., Currás, A., Robresco, S., 2017. New insights into the sea-level evolution in Corsica (NW Mediterranean) since the late Neolithic. *J. Archaeol. Sci. Reports* 12, 782–793. <https://doi.org/10.1016/j.jasrep.2016.07.006>
- Vacchi, M., Ghilardi, M., Melis, R.T., Spada, G., Giaime, M., Marriner, N., Lorscheid, T., Morhange, C., Burjachs, F., Rovere, A., 2018. New relative sea-level insights into the isostatic history of the Western Mediterranean. *Quat. Sci. Rev.* 201, 396–408.
- Valente, E., Ascione, A., Santangelo, N., Santo, A., 2019a. Late Quaternary geomorphological evolution and evidence of post-campania ignimbrite (40ka) fault activity in the inner sector of the Sarno Plain (southern Apennines, Italy). *Alp. Mediterr. Quat.* 32, 185–197. <https://doi.org/https://doi.org/10.26382/AMQ.2019.13>
- Valente, E., Buscher, J.T., Jourdan, F., Petrosino, P., Reddy, S.M., Tavani, S., Corradetti, A., & Ascione, A., 2019b. Constraining mountain front tectonic activity in extensional setting from geomorphology and Quaternary stratigraphy: A case study from the Matese ridge, southern Apennines. *Quat. Sci. Rev.* 219, 47–67.
- Van De Plassche, O., 1986. Introduction. van Plassche O., Ed. *Sea-level Res. a Man. Collect. Eval. data. Dordr. Springer Netherlands* 1–23. [https://doi.org/https://doi.org/10.1007/978-94-009-4215-8\\_1](https://doi.org/https://doi.org/10.1007/978-94-009-4215-8_1).
- Vannoli, P., Basili, R., Valensise, G., 2004. New geomorphic evidence for anticlinal growth driven by blind-thrust faulting along the northern Marche coastal belt (central Italy). *J. Seismol.* 8, 297–312. <https://doi.org/10.1023/b:jose.0000038456.00574.e3>
- Verri, A., De Angelis D'Ossat, G., 1899. Cenni sulla geologia di Taranto. *Boll. della Soc. Geol. Ital.* XVIII, 179–210.
- Vesica, P.L., Tuccimei, P., Turi, B., Fornós, J.J., Ginés, A., Ginés, J., 2000. Late Pleistocene Paleoclimates and sea-level change in the Mediterranean as inferred from stable isotope and U-series studies of overgrowths on speleothems, Mallorca, Spain. *Quat. Sci. Rev.* 19, 865–879. [https://doi.org/https://doi.org/10.1016/S0277-3791\(99\)00026-8](https://doi.org/https://doi.org/10.1016/S0277-3791(99)00026-8)
- Vicens, D., Gràcia, F., Ginés, A., 2012. Quaternary beach deposits in Mallorca: paleontological and geomorphological data. *Ginés, A.; Ginés, J.; Gomez-Pujol, L* 55–84.

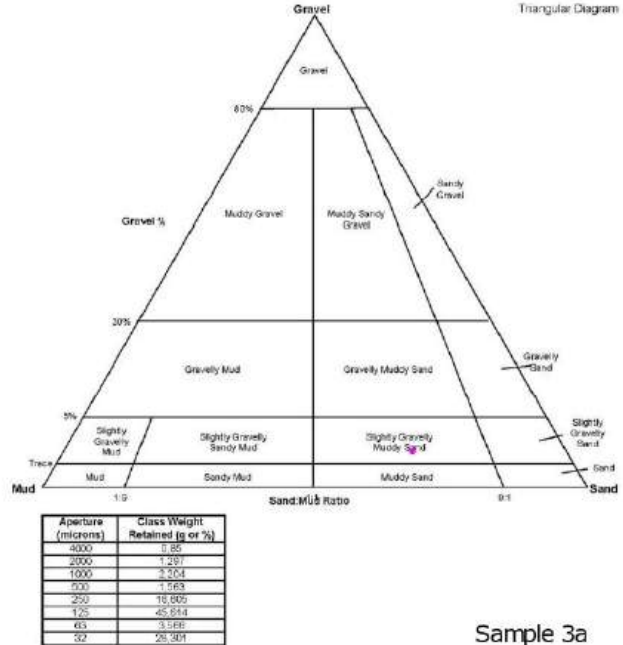
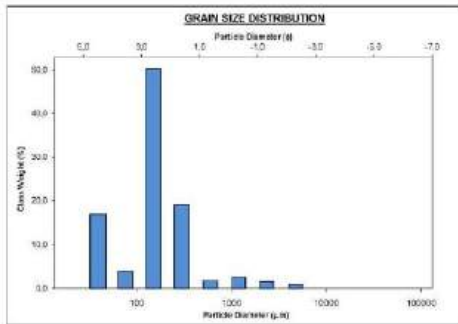
- Vicino, G., 1974. La spiaggia tirreniana dei Balzi Rossi nei recenti scavi nella zona dell'ex-Casinó. *Atti XVI Riun. Sci. Ist. Ital. di Preist. e Protostoria* 75–84.
- ViDEPI, 2009. Project Free data on oil exploration in Italy. © 2009-2010 Ministero dello Sviluppo Economico UNMIG, Società Geologica Italiana, Assomineraria. <http://unmig.sviluppoeconomico.gov.it/videpi/>. Acc. 20 November 2015.
- Vita-Finzi, C., 1967. Late Quaternary alluvial chronology of northern Algeria. *Man* 2, 205–215.
- Vitale, S., Ciarcia, S., 2013. Tectono-stratigraphic and kinematic evolution of the southern Apennines/Calabria–Peloritani Terrane system (Italy). *Tectonophysics* 583, 164–182. <https://doi.org/https://doi.org/10.1016/j.tecto.2012.11.004>
- Waelbroeck, C., Labeyrie, L., Michel, E., Duplessy, J.C., McManus, J.F., Lambeck, K., Balbon, E., Labracherie, M., 2002. Sea-level and deep water temperature changes derived from benthic foraminifera isotopic records. *Quat. Sci. Rev.* 21, 295–305. [https://doi.org/10.1016/S0277-3791\(01\)00101-9](https://doi.org/10.1016/S0277-3791(01)00101-9)
- Wehmiller, J.F., Simmons, K.R., Cheng, H., Edwards, R.L., Martin-mcnaughton, J., York, L.L., Krantz, D.E., Shen, C., 2004. Uranium-series coral ages from the US Atlantic Coastal Plain – the “ 80 ka problem ” revisited. *Quat. Int.* 120, 3–14. <https://doi.org/10.1016/j.quaint.2004.01.002>
- Wells, D.L., Coppersmith, K.J., 1994. New Empirical Relationships among Magnitude, Rupture Length, Rupture Width, Rupture Area, and Surface Displacement. *Bull. Seismol. Soc. Am.* 84, 974–1002. <https://doi.org/10.1029/93JB01566>
- Wentworth, C.K., 1938. Marine bench-forming processes: water-level weathering. *J. Geomorph.* 1, 6–32.
- Westaway, R., 1993. Quaternary uplift of southern Italy. *J. Geophys. Res.* 98, 21741–21772. <https://doi.org/https://doi.org/10.1029/93JB01566>
- Woodroffe, C.D., McGregor, H.V., Lambeck, K., Smithers, S.G., Fink, D., 2012. Mid-Pacific microatolls record sea-level stability over the past 5000 yr. *Geology* 40, 951–954.
- Yokoyama, Y., Nguyen, H., Shen, G., Quaegebeur, J.P., Koumba, N., 1987. Datation par les méthodes des familles de l'uranium et la résonance de spin électronique (ESR) du remplissage de la grotte des Ramandils à Port-la-Nouvelle (Aude, France). *Cypsel Rev. prehistòria i protohistòria* 151–154.
- Yokoyama, Y., Lambeck, K., De Deckker, P.P.J., Fifield, L.K., 2000. Timing of the last glacial maximum from observed sea-level minima. *Nature* 406, 713–716.
- Zanchetta, G., Bonadonna, F.P., Marcolini, F., Ciampalini, A., Fallick, A.E., Leone, G., Michelucci, L., 2004. Intra-Tyrrhenian cooling event deduced by non-marine mollusc assemblage at Villa S. Giorgio (Livorno, Italy).
- Zazo, C., 1980. El Cuaternario marino-continental y el límite Plio-Pleistoceno en

- el litoral de Cádiz. Universidad Complutense de Madrid.
- Zazo, C., Goy, J.L., 1989. Sea-Level Changes in the Iberian Peninsula During the Last 200,000 Years, in: Scott, D.B., Pirazzoli, P.A., Honig, C.A. (Eds.), Late Quaternary Sea-Level Correlation and Applications: Walter S. Newman Memorial Volume. Springer Netherlands, Dordrecht, pp. 27–39. [https://doi.org/10.1007/978-94-009-0873-4\\_2](https://doi.org/10.1007/978-94-009-0873-4_2)
- Zazo, C., Goy, J.L., 1990. Hoja Vejer de la Frontera (no 1073= 1076). Plioceno Super. y Cuaternario. Mapa Geológico España 1, 2o.
- Zazo, C., Silva, P.G., Goy, J.L., Hillaire-Marcel, C., Ghaleb, B., Lario, J., Bardají, T., González, A., 1999. Coastal uplift in continental collision plate boundaries: data from the Last Interglacial marine terraces of the Gibraltar Strait area (south Spain). *Tectonophysics* 301, 95–109. [https://doi.org/10.1016/s0040-1951\(98\)00217-0](https://doi.org/10.1016/s0040-1951(98)00217-0)
- Zazo, C., Goy, J.L., Hillaire-Marcel, C., Gillot, P.-Y., Soler, V., González, J.-Á., Dabrio, C.J., Ghaleb, B., 2002. Raised marine sequences of Lanzarote and Fuerteventura revisited- a reappraisal of relative sea-level changes and vertical movements in the eastern Canary Islands during the Quaternary. *Quat. Sci. Rev.* 21, 2019–2046.
- Zazo, C., Goy, J.L., Dabrio, C.J., Bardají, T., Hillaire-Marcel, C., Ghaleb, B., González-Delgado, J.-Á., Soler, V., 2003. Pleistocene raised marine terraces of the Spanish Mediterranean and Atlantic coasts: records of coastal uplift sea-level highstands and climate changes. *Mar. Geol.* 194, 103–133. [https://doi.org/10.1016/s0025-3227\(02\)00701-6](https://doi.org/10.1016/s0025-3227(02)00701-6)
- Zazo, C., Goy, J., Dabrio, C., Soler, V., Hillaire-Marcel, C., Ghaleb, B., González-Delgado, J.A., Bardají, T., Cabero, A., 2007. Quaternary marine terraces on Sal Island (Cape Verde archipelago). *Quat. Sci. Rev.* 26, 876–893.
- Zecchin, M., Nalin, R., Roda, C., 2004. Raised Pleistocene marine terraces of the Crotona peninsula (Calabria, southern Italy): facies analysis and organization of their deposits. *Sediment. Geol.* 172, 165–185.
- Zecchin, M., Civile, D., Caffau, M., & Roda, C., 2009. Facies and cycle architecture of a Pleistocene marine terrace (Crotona, southern Italy): A sedimentary response to late Quaternary, high-frequency glacio-eustatic changes. *Sed. Geol.* 216, 138–157.
- Zomeni, Z., 2021. Last interglacial (MIS 5e) sea-level proxies in Cyprus, Eastern Mediterranean. <https://doi.org/10.5281/zenodo.4438721>

# Appendixes

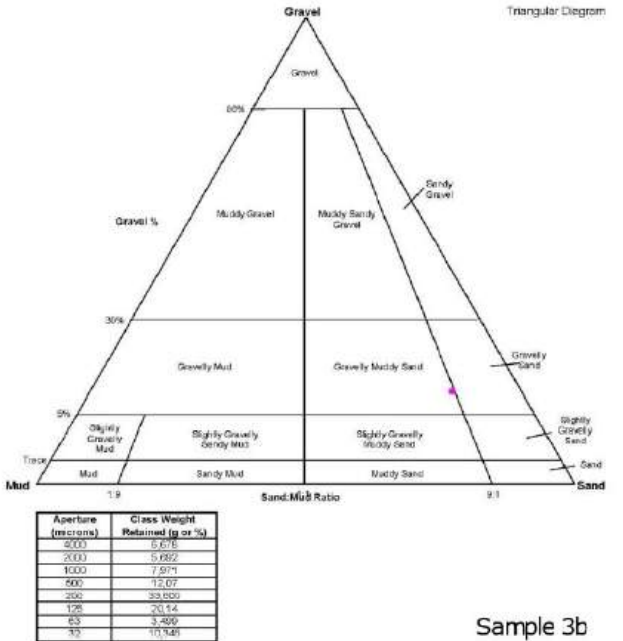
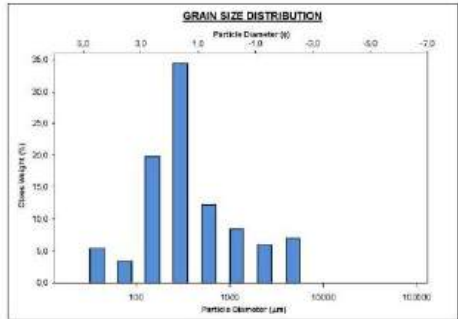
## Supplementary materials from Section 6.1

SAMPLE STATISTICS						
SAMPLE IDENTITY: <b>Sample 3a</b>			TEXTURAL GROUP: <b>Slightly Gravelly Muddy Sand</b>			
SAMPLE TYPE: <b>Thinned, Poorly Sorted</b>			SEDIMENT NAME: <b>Slightly Very Fine Gravelly Very Coarse Silty Fine Sand</b>			
M		S		GRAIN SIZE DISTRIBUTION		
MODE 1	102.5	3,737	GRAVEL	2.1%	COARSE SAND	1.8%
MODE 2	302.5	1,747	SAND	69.9%	MEDIUM SAND	16.6%
MODE 3	47.52	4,427	MUD	28.0%	FINE SAND	16.7%
$D_w$	40.95	1,619			V FINE SAND	3.9%
MEDIAN or $D_{50}$	144.5	3,751	V COARSE GRAVEL	0.0%	V COARSE SILT	25.0%
$D_w$	325.7	4,620	COARSE GRAVEL	0.0%	COARSE SILT	0.0%
$(D_{75} / D_{25})$	8.010	2,859	MEDIUM GRAVEL	0.0%	MEDIUM SILT	0.0%
$(D_{75} - D_{25})$	395.7	3,032	FINE GRAVEL	0.0%	FINE SILT	0.0%
$(D_{75} / D_{10})$	5.031	1,639	V FINE GRAVEL	1.2%	V FINE SILT	0.0%
$(D_{75} - D_{10})$	115.3	1,630	V COARSE SAND	2.2%	CLAY	0.0%
METHOD OF MOMENTS			FOLK & WARD METHOD			
Attributes:	Geometric	Logarithmic	Geometric	Logarithmic	Description	
MENUS (M)	243.0	735.1	3,910	124.5	Very Fine Sand	
SORTING (S)	52.61	2,428	1,383	2,915	Poorly Sorted	
SKEWNESS (Sk)	0.285	0.946	-0.945	-0.111	Fine Skewed	
KURTOSIS (K)	52.31	4.937	4.947	1.047	Mezokurtic	



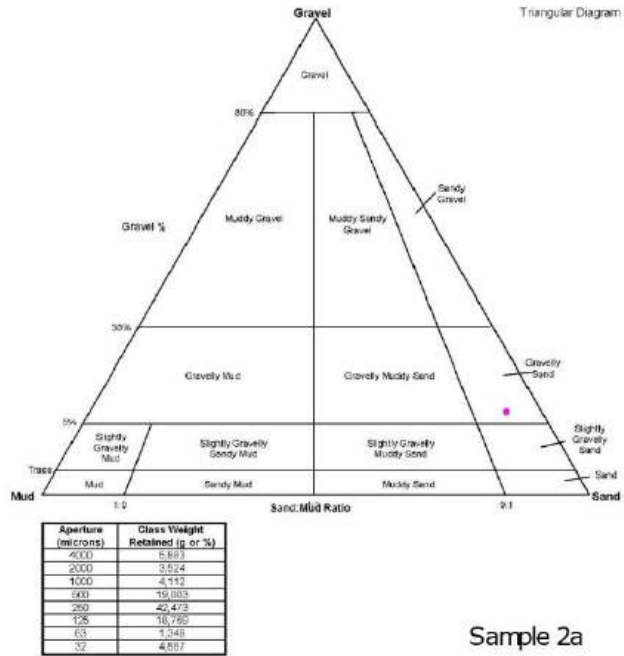
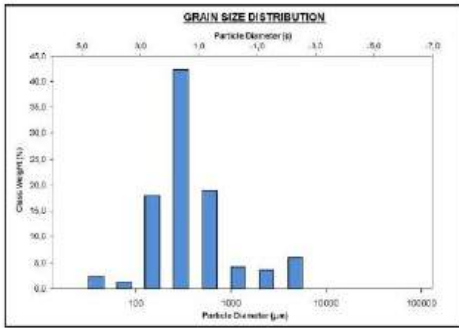
Sample 3a

SAMPLE STATISTICS						
SAMPLE IDENTITY: <b>Sample 3b</b>			TEXTURAL GROUP: <b>Gravelly Muddy Sand</b>			
SAMPLE TYPE: <b>Polymodal, Poorly Sorted</b>			SEDIMENT NAME: <b>Fine Gravelly Very Coarse Silty Medium Sand</b>			
M		S		GRAIN SIZE DISTRIBUTION		
MODE 1	307.5	1,747	GRAVEL	0.3%	COARSE SAND	13.1%
MODE 2	162.5	2,281	SAND	77.4%	MEDIUM SAND	23.0%
MODE 3	90.0	0,747	MUD	0.2%	FINE SAND	20.1%
$D_w$	61.99	-1,222			V FINE SAND	3.6%
MEDIAN or $D_{50}$	295.5	1,759	V COARSE GRAVEL	0.0%	V COARSE SILT	10.2%
$D_w$	330.5	0,021	COARSE GRAVEL	0.0%	COARSE SILT	0.0%
$(D_{75} / D_{25})$	37.35	-3,345	MEDIUM GRAVEL	0.0%	MEDIUM SILT	0.0%
$(D_{75} - D_{25})$	2238.2	5,223	FINE GRAVEL	0.0%	FINE SILT	0.0%
$(D_{75} / D_{10})$	4,054	3,929	V FINE GRAVEL	5.7%	V FINE SILT	0.0%
$(D_{75} - D_{10})$	467.1	2,084	V COARSE SAND	0.0%	CLAY	0.0%
METHOD OF MOMENTS			FOLK & WARD METHOD			
Attributes:	Geometric	Logarithmic	Geometric	Logarithmic	Description	
MENUS (M)	736.3	353.3	1,962	353.6	Medium Sand	
SORTING (S)	1214.4	3,380	1,787	3,493	Poorly Sorted	
SKEWNESS (Sk)	2.919	0.444	-0.444	0.217	Coarse Skewed	
KURTOSIS (K)	8.365	2,937	2,937	1,343	Leptokurtic	



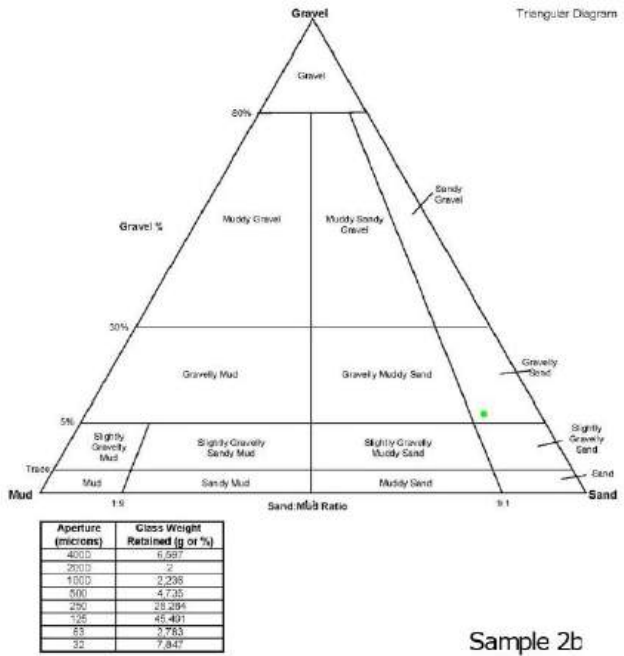
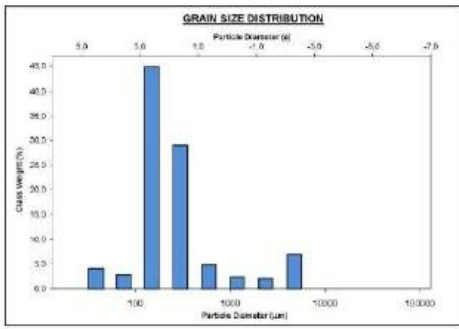
Sample 3b

SAMPLE STATISTICS					
SAMPLE IDENTITY: <b>Sample 2a</b>			TEXTURAL GROUP: <b>Gravelly Sand</b>		
SAMPLE TYPE: Threshold, Poorly Sorted			SEDIMENT NAME: Fine Gravelly Medium Sand		
	mm	$\phi$	GRAIN SIZE DISTRIBUTION		
MODE 1	302.5	1.747	GRAVEL: 9.4%	COARSE SAND: 19.0%	
MODE 2	825.0	0.747	SAND: 85.6%	MEDIUM SAND: 43.3%	
MODE 3	152.5	2.747	MUD: 4.9%	FINE SAND: 18.8%	
$D_{10}$	134.5	2.435		V FINE SAND: 1.4%	
MEDIAN or $D_{50}$	307.5	1.700	V COARSE GRAVEL: 0.0%	V COARSE SILT: 0.8%	
$D_{60}$	433.7	2.895	COARSE GRAVEL: 0.0%	COARSE SILT: 0.0%	
$(D_{60} - D_{10})$	9.97	-0.968	MEDIUM GRAVEL: 0.0%	MEDIUM SILT: 0.0%	
$(D_{30} - D_{10})$	1199.2	3.310	FINE GRAVEL: 5.0%	FINE SILT: 0.0%	
$(D_{30} - D_{60})$	3.192	3.084	V FINE GRAVEL: 0.5%	V FINE SILT: 0.0%	
$(D_{10} - D_{60})$	354.5	1.674	V COARSE SAND: 4.1%	CLAY: 0.0%	
METHOD OF MOMENTS			FOLK & WARD METHOD		
	Arithmetic	Geometric	Logarithmic	Geometric	Logarithmic
MEAN (M)	461.7	395.2	1.481	315.8	1.693
SKWNESS (S)	1119.0	2.765	1.481	2.706	1.493
KURTOSIS (K)	2.090	5.701	-0.701	0.155	-0.155
				1.478	1.473
					Description
					Medium Sand
					Finely Sorted
					Coarse Skewed
					Leptokurtic



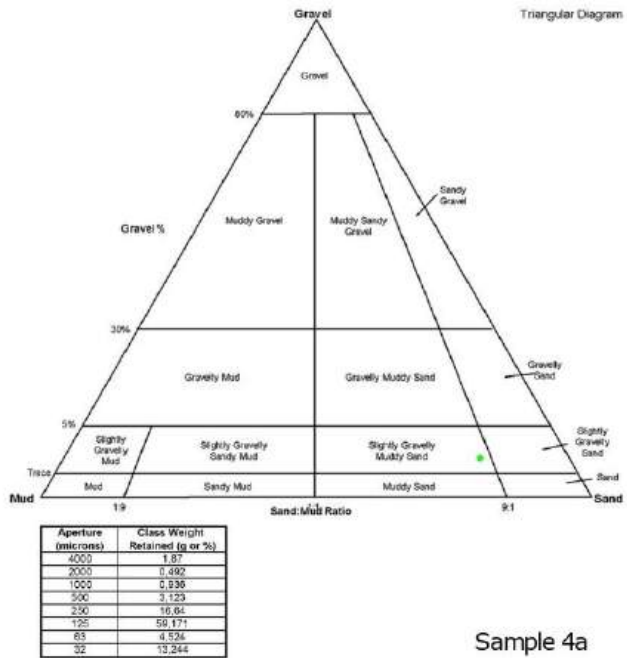
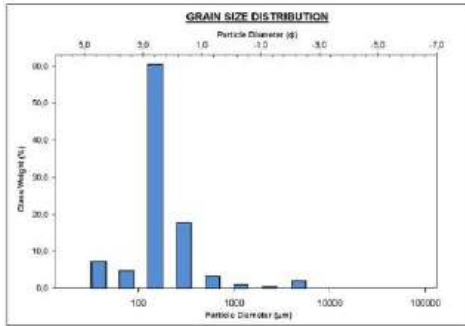
Sample 2a

SAMPLE STATISTICS					
SAMPLE IDENTITY: <b>Sample 2b</b>			TEXTURAL GROUP: <b>Gravelly Sand</b>		
SAMPLE TYPE: Threshold, Poorly Sorted			SEDIMENT NAME: Fine Gravelly Fine Sand		
	mm	$\phi$	GRAIN SIZE DISTRIBUTION		
MODE 1	152.5	2.737	GRAVEL: 5.6%	COARSE SAND: 4.7%	
MODE 2	302.5	1.747	SAND: 93.0%	MEDIUM SAND: 28.3%	
MODE 3	490.0	-0.948	MUD: 7.8%	FINE SAND: 41.3%	
$D_{10}$	92.0	-1.181		V FINE SAND: 2.0%	
MEDIAN or $D_{50}$	171.4	3.545	V COARSE GRAVEL: 0.0%	V COARSE SILT: 7.8%	
$D_{60}$	134.0	3.051	COARSE GRAVEL: 0.0%	COARSE SILT: 0.0%	
$(D_{60} - D_{10})$	13.68	-0.708	MEDIUM GRAVEL: 0.0%	MEDIUM SILT: 0.0%	
$(D_{30} - D_{10})$	1091.0	3.772	FINE GRAVEL: 0.0%	FINE SILT: 0.0%	
$(D_{30} - D_{60})$	2.282	1.704	V FINE GRAVEL: 0.0%	V FINE SILT: 0.0%	
$(D_{10} - D_{60})$	178.5	1.171	V COARSE SAND: 2.2%	CLAY: 0.0%	
METHOD OF MOMENTS			FOLK & WARD METHOD		
	Arithmetic	Geometric	Logarithmic	Geometric	Logarithmic
MEAN (M)	561.1	241.1	2.652	193.1	2.328
SKWNESS (S)	1170.8	3.836	1.893	2.508	-1.338
KURTOSIS (K)	0.024	1.319	-1.315	0.448	-0.448
				2.291	2.291
					Description
					Fine Sand
					Poorly Sorted
					Very Coarse Skewed
					Very Leptokurtic



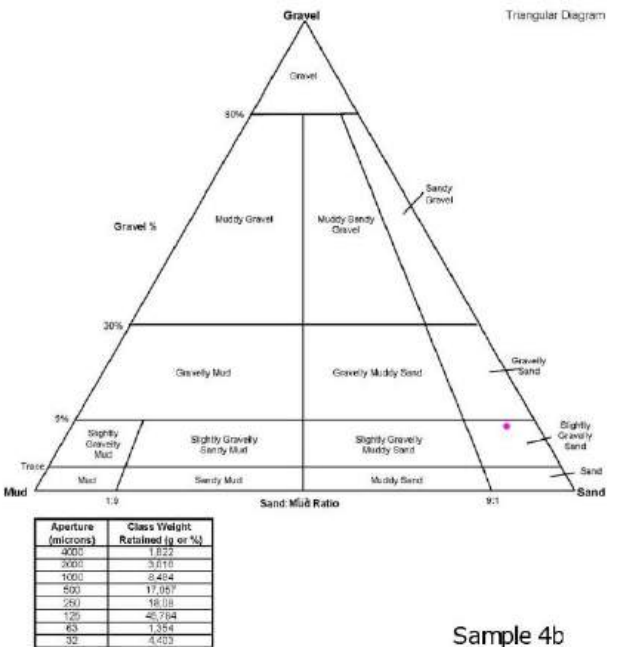
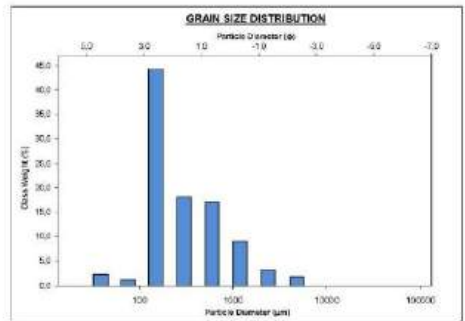
Sample 2b

SAMPLE STATISTICS																																																			
SAMPLE IDENTITY: <b>Sample 4a</b>		TEXTURAL GROUP: <b>Slightly Gravelly Muddy Sand</b>																																																	
SAMPLE TYPE: <b>Bimodal, Poorly Sorted</b>		SEDIMENT NAME: <b>Slightly Fine Gravelly Very Coarse Silty Fine Sand</b>																																																	
<table border="1"> <thead> <tr> <th>MODE</th> <th>μ</th> <th>σ</th> </tr> </thead> <tbody> <tr> <td>MODE 1</td> <td>152.5</td> <td>2.737</td> </tr> <tr> <td>MODE 2</td> <td>302.5</td> <td>1.747</td> </tr> <tr> <td>MODE 3</td> <td>53.57</td> <td>1.603</td> </tr> </tbody> </table>		MODE	μ	σ	MODE 1	152.5	2.737	MODE 2	302.5	1.747	MODE 3	53.57	1.603	<table border="1"> <thead> <tr> <th colspan="2">GRAIN SIZE DISTRIBUTION</th> </tr> </thead> <tbody> <tr> <td>GRAVEL</td> <td>2.4%</td> </tr> <tr> <td>COARSE SAND</td> <td>3.1%</td> </tr> <tr> <td>MEDIUM SAND</td> <td>16.6%</td> </tr> <tr> <td>FINE SAND</td> <td>30.2%</td> </tr> <tr> <td>V FINE SAND</td> <td>4.7%</td> </tr> <tr> <td>V COARSE GRAVEL</td> <td>0.0%</td> </tr> <tr> <td>V COARSE SILT</td> <td>13.1%</td> </tr> <tr> <td>COARSE GRAVEL</td> <td>0.0%</td> </tr> <tr> <td>COARSE SILT</td> <td>0.0%</td> </tr> <tr> <td>MEDIUM GRAVEL</td> <td>0.0%</td> </tr> <tr> <td>MEDIUM SILT</td> <td>0.0%</td> </tr> <tr> <td>FINE GRAVEL</td> <td>1.9%</td> </tr> <tr> <td>FINE SILT</td> <td>0.0%</td> </tr> <tr> <td>V FINE GRAVEL</td> <td>0.6%</td> </tr> <tr> <td>V FINE SILT</td> <td>0.0%</td> </tr> <tr> <td>V COARSE SAND</td> <td>0.9%</td> </tr> <tr> <td>CLAY</td> <td>0.0%</td> </tr> </tbody> </table>		GRAIN SIZE DISTRIBUTION		GRAVEL	2.4%	COARSE SAND	3.1%	MEDIUM SAND	16.6%	FINE SAND	30.2%	V FINE SAND	4.7%	V COARSE GRAVEL	0.0%	V COARSE SILT	13.1%	COARSE GRAVEL	0.0%	COARSE SILT	0.0%	MEDIUM GRAVEL	0.0%	MEDIUM SILT	0.0%	FINE GRAVEL	1.9%	FINE SILT	0.0%	V FINE GRAVEL	0.6%	V FINE SILT	0.0%	V COARSE SAND	0.9%	CLAY	0.0%
MODE	μ	σ																																																	
MODE 1	152.5	2.737																																																	
MODE 2	302.5	1.747																																																	
MODE 3	53.57	1.603																																																	
GRAIN SIZE DISTRIBUTION																																																			
GRAVEL	2.4%																																																		
COARSE SAND	3.1%																																																		
MEDIUM SAND	16.6%																																																		
FINE SAND	30.2%																																																		
V FINE SAND	4.7%																																																		
V COARSE GRAVEL	0.0%																																																		
V COARSE SILT	13.1%																																																		
COARSE GRAVEL	0.0%																																																		
COARSE SILT	0.0%																																																		
MEDIUM GRAVEL	0.0%																																																		
MEDIUM SILT	0.0%																																																		
FINE GRAVEL	1.9%																																																		
FINE SILT	0.0%																																																		
V FINE GRAVEL	0.6%																																																		
V FINE SILT	0.0%																																																		
V COARSE SAND	0.9%																																																		
CLAY	0.0%																																																		
<table border="1"> <thead> <tr> <th colspan="2">METHOD OF MOMENTS</th> <th colspan="2">FOLK &amp; WARD METHOD</th> <th rowspan="2">Description</th> </tr> <tr> <th>Arithmetic</th> <th>Geometric</th> <th>Geometric</th> <th>Logarithmic</th> </tr> <tr> <th>μ</th> <th>σ</th> <th>μ</th> <th>σ</th> </tr> </thead> <tbody> <tr> <td>MEAN (μ)</td> <td>282.0</td> <td>185.0</td> <td>2.045</td> <td>181.3</td> <td>2.732</td> <td>Fine Sand</td> </tr> <tr> <td>SORTING (σ)</td> <td>858.9</td> <td>2.237</td> <td>1.161</td> <td>2.074</td> <td>1.050</td> <td>Poorly Sorted</td> </tr> <tr> <td>SKEWNESS (sk)</td> <td>8,240</td> <td>1.378</td> <td>-1.375</td> <td>-0.001</td> <td>0.001</td> <td>Symmetrical</td> </tr> <tr> <td>KURTOSIS (k)</td> <td>41.91</td> <td>7.579</td> <td>7.579</td> <td>3.523</td> <td>3.523</td> <td>Extremely Leptokurtic</td> </tr> </tbody> </table>		METHOD OF MOMENTS		FOLK & WARD METHOD		Description	Arithmetic	Geometric	Geometric	Logarithmic	μ	σ	μ	σ	MEAN (μ)	282.0	185.0	2.045	181.3	2.732	Fine Sand	SORTING (σ)	858.9	2.237	1.161	2.074	1.050	Poorly Sorted	SKEWNESS (sk)	8,240	1.378	-1.375	-0.001	0.001	Symmetrical	KURTOSIS (k)	41.91	7.579	7.579	3.523	3.523	Extremely Leptokurtic									
METHOD OF MOMENTS		FOLK & WARD METHOD		Description																																															
Arithmetic	Geometric	Geometric	Logarithmic																																																
μ	σ	μ	σ																																																
MEAN (μ)	282.0	185.0	2.045	181.3	2.732	Fine Sand																																													
SORTING (σ)	858.9	2.237	1.161	2.074	1.050	Poorly Sorted																																													
SKEWNESS (sk)	8,240	1.378	-1.375	-0.001	0.001	Symmetrical																																													
KURTOSIS (k)	41.91	7.579	7.579	3.523	3.523	Extremely Leptokurtic																																													



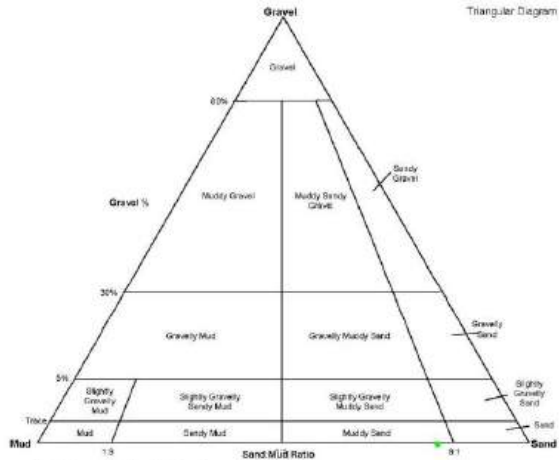
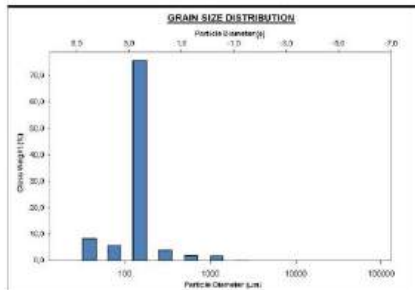
Sample 4a

SAMPLE STATISTICS																																																			
SAMPLE IDENTITY: <b>Sample 4b</b>		TEXTURAL GROUP: <b>Slightly Gravelly Sand</b>																																																	
SAMPLE TYPE: <b>Unimodal, Poorly Sorted</b>		SEDIMENT NAME: <b>Slightly Very Fine Gravelly Fine Sand</b>																																																	
<table border="1"> <thead> <tr> <th>MODE</th> <th>μ</th> <th>σ</th> </tr> </thead> <tbody> <tr> <td>MODE 1</td> <td>152.5</td> <td>2.737</td> </tr> <tr> <td>MODE 2</td> <td>302.5</td> <td>1.747</td> </tr> <tr> <td>MODE 3</td> <td>505.0</td> <td>0.747</td> </tr> </tbody> </table>		MODE	μ	σ	MODE 1	152.5	2.737	MODE 2	302.5	1.747	MODE 3	505.0	0.747	<table border="1"> <thead> <tr> <th colspan="2">GRAIN SIZE DISTRIBUTION</th> </tr> </thead> <tbody> <tr> <td>GRAVEL</td> <td>5.6%</td> </tr> <tr> <td>COARSE SAND</td> <td>17.1%</td> </tr> <tr> <td>MEDIUM SAND</td> <td>10.1%</td> </tr> <tr> <td>FINE SAND</td> <td>45.8%</td> </tr> <tr> <td>V FINE SAND</td> <td>1.4%</td> </tr> <tr> <td>V COARSE GRAVEL</td> <td>0.0%</td> </tr> <tr> <td>V COARSE SILT</td> <td>4.9%</td> </tr> <tr> <td>COARSE GRAVEL</td> <td>0.0%</td> </tr> <tr> <td>COARSE SILT</td> <td>0.0%</td> </tr> <tr> <td>MEDIUM GRAVEL</td> <td>0.0%</td> </tr> <tr> <td>MEDIUM SILT</td> <td>0.0%</td> </tr> <tr> <td>FINE GRAVEL</td> <td>1.9%</td> </tr> <tr> <td>FINE SILT</td> <td>0.0%</td> </tr> <tr> <td>V FINE GRAVEL</td> <td>3.7%</td> </tr> <tr> <td>V FINE SILT</td> <td>0.0%</td> </tr> <tr> <td>V COARSE SAND</td> <td>0.0%</td> </tr> <tr> <td>CLAY</td> <td>0.0%</td> </tr> </tbody> </table>		GRAIN SIZE DISTRIBUTION		GRAVEL	5.6%	COARSE SAND	17.1%	MEDIUM SAND	10.1%	FINE SAND	45.8%	V FINE SAND	1.4%	V COARSE GRAVEL	0.0%	V COARSE SILT	4.9%	COARSE GRAVEL	0.0%	COARSE SILT	0.0%	MEDIUM GRAVEL	0.0%	MEDIUM SILT	0.0%	FINE GRAVEL	1.9%	FINE SILT	0.0%	V FINE GRAVEL	3.7%	V FINE SILT	0.0%	V COARSE SAND	0.0%	CLAY	0.0%
MODE	μ	σ																																																	
MODE 1	152.5	2.737																																																	
MODE 2	302.5	1.747																																																	
MODE 3	505.0	0.747																																																	
GRAIN SIZE DISTRIBUTION																																																			
GRAVEL	5.6%																																																		
COARSE SAND	17.1%																																																		
MEDIUM SAND	10.1%																																																		
FINE SAND	45.8%																																																		
V FINE SAND	1.4%																																																		
V COARSE GRAVEL	0.0%																																																		
V COARSE SILT	4.9%																																																		
COARSE GRAVEL	0.0%																																																		
COARSE SILT	0.0%																																																		
MEDIUM GRAVEL	0.0%																																																		
MEDIUM SILT	0.0%																																																		
FINE GRAVEL	1.9%																																																		
FINE SILT	0.0%																																																		
V FINE GRAVEL	3.7%																																																		
V FINE SILT	0.0%																																																		
V COARSE SAND	0.0%																																																		
CLAY	0.0%																																																		
<table border="1"> <thead> <tr> <th colspan="2">METHOD OF MOMENTS</th> <th colspan="2">FOLK &amp; WARD METHOD</th> <th rowspan="2">Description</th> </tr> <tr> <th>Arithmetic</th> <th>Geometric</th> <th>Geometric</th> <th>Logarithmic</th> </tr> <tr> <th>μ</th> <th>σ</th> <th>μ</th> <th>σ</th> </tr> </thead> <tbody> <tr> <td>MEAN (μ)</td> <td>455.5</td> <td>278.3</td> <td>1.846</td> <td>253.1</td> <td>1.582</td> <td>Medium Sand</td> </tr> <tr> <td>SORTING (σ)</td> <td>750.3</td> <td>2.591</td> <td>1.374</td> <td>2.300</td> <td>1.215</td> <td>Poorly Sorted</td> </tr> <tr> <td>SKEWNESS (sk)</td> <td>3.058</td> <td>3.735</td> <td>-0.736</td> <td>0.551</td> <td>-0.501</td> <td>Very Coarse Skewed</td> </tr> <tr> <td>KURTOSIS (k)</td> <td>21.15</td> <td>3.446</td> <td>3.446</td> <td>0.696</td> <td>0.696</td> <td>Leptokurtic</td> </tr> </tbody> </table>		METHOD OF MOMENTS		FOLK & WARD METHOD		Description	Arithmetic	Geometric	Geometric	Logarithmic	μ	σ	μ	σ	MEAN (μ)	455.5	278.3	1.846	253.1	1.582	Medium Sand	SORTING (σ)	750.3	2.591	1.374	2.300	1.215	Poorly Sorted	SKEWNESS (sk)	3.058	3.735	-0.736	0.551	-0.501	Very Coarse Skewed	KURTOSIS (k)	21.15	3.446	3.446	0.696	0.696	Leptokurtic									
METHOD OF MOMENTS		FOLK & WARD METHOD		Description																																															
Arithmetic	Geometric	Geometric	Logarithmic																																																
μ	σ	μ	σ																																																
MEAN (μ)	455.5	278.3	1.846	253.1	1.582	Medium Sand																																													
SORTING (σ)	750.3	2.591	1.374	2.300	1.215	Poorly Sorted																																													
SKEWNESS (sk)	3.058	3.735	-0.736	0.551	-0.501	Very Coarse Skewed																																													
KURTOSIS (k)	21.15	3.446	3.446	0.696	0.696	Leptokurtic																																													



Sample 4b

SAMPLE STATISTICS																																																																										
SAMPLE IDENTITY: <b>Sample 5a</b>		TEXTURAL GROUP: <b>Slightly Clayey Muddy Sand</b>																																																																								
SAMPLE TYPE: <b>Unconsolidated, Noncohesive, Sorted</b>		SEGMENT NAME: <b>Slightly Very Fine Gravelly Very Coarse Silty Fine Sand</b>																																																																								
<table border="1"> <thead> <tr> <th>MODE 1</th> <th>MODE 2</th> <th>MODE 3</th> </tr> </thead> <tbody> <tr> <td>162.8</td> <td>2.787</td> <td></td> </tr> <tr> <td>D<sub>10</sub></td> <td>16.42</td> <td>2.497</td> </tr> <tr> <td>MEDIAN or D<sub>50</sub></td> <td>148.0</td> <td>2.789</td> </tr> <tr> <td>D<sub>60</sub></td> <td>177.1</td> <td>4.013</td> </tr> <tr> <td>C<sub>u</sub> (D<sub>60</sub> / D<sub>10</sub>)</td> <td>10.79</td> <td>1.728</td> </tr> <tr> <td>C<sub>u</sub> (D<sub>50</sub> / D<sub>10</sub>)</td> <td>106.7</td> <td>1.613</td> </tr> <tr> <td>(D<sub>60</sub> - D<sub>10</sub>)</td> <td>1.584</td> <td>1.138</td> </tr> <tr> <td>(D<sub>60</sub> - D<sub>50</sub>)</td> <td>96.32</td> <td>0.261</td> </tr> </tbody> </table>		MODE 1	MODE 2	MODE 3	162.8	2.787		D <sub>10</sub>	16.42	2.497	MEDIAN or D <sub>50</sub>	148.0	2.789	D <sub>60</sub>	177.1	4.013	C <sub>u</sub> (D <sub>60</sub> / D <sub>10</sub> )	10.79	1.728	C <sub>u</sub> (D <sub>50</sub> / D <sub>10</sub> )	106.7	1.613	(D <sub>60</sub> - D <sub>10</sub> )	1.584	1.138	(D <sub>60</sub> - D <sub>50</sub> )	96.32	0.261	<table border="1"> <thead> <tr> <th colspan="4">GRAIN SIZE DISTRIBUTION</th> </tr> </thead> <tbody> <tr> <td>GRAVEL</td> <td>10.7%</td> <td>COARSE SAND</td> <td>1.0%</td> </tr> <tr> <td>SAND</td> <td>85.2%</td> <td>MEDIUM SAND</td> <td>0.0%</td> </tr> <tr> <td>M.D.</td> <td>14.7%</td> <td>FINE SAND</td> <td>77.3%</td> </tr> <tr> <td></td> <td></td> <td>V. FINE SAND</td> <td>0.0%</td> </tr> <tr> <td>V. COARSE GRAVEL</td> <td>0.0%</td> <td>V. COARSE SILT</td> <td>14.7%</td> </tr> <tr> <td>COARSE GRAVEL</td> <td>0.0%</td> <td>COARSE SILT</td> <td>0.0%</td> </tr> <tr> <td>MEDIUM GRAVEL</td> <td>0.0%</td> <td>MEDIUM SILT</td> <td>0.0%</td> </tr> <tr> <td>FINE GRAVEL</td> <td>0.0%</td> <td>FINE SILT</td> <td>0.0%</td> </tr> <tr> <td>V. FINE GRAVEL</td> <td>0.0%</td> <td>V. FINE SILT</td> <td>0.0%</td> </tr> <tr> <td>V. COARSE SAND</td> <td>1.0%</td> <td>CLAY</td> <td>0.0%</td> </tr> </tbody> </table>		GRAIN SIZE DISTRIBUTION				GRAVEL	10.7%	COARSE SAND	1.0%	SAND	85.2%	MEDIUM SAND	0.0%	M.D.	14.7%	FINE SAND	77.3%			V. FINE SAND	0.0%	V. COARSE GRAVEL	0.0%	V. COARSE SILT	14.7%	COARSE GRAVEL	0.0%	COARSE SILT	0.0%	MEDIUM GRAVEL	0.0%	MEDIUM SILT	0.0%	FINE GRAVEL	0.0%	FINE SILT	0.0%	V. FINE GRAVEL	0.0%	V. FINE SILT	0.0%	V. COARSE SAND	1.0%	CLAY	0.0%
MODE 1	MODE 2	MODE 3																																																																								
162.8	2.787																																																																									
D <sub>10</sub>	16.42	2.497																																																																								
MEDIAN or D <sub>50</sub>	148.0	2.789																																																																								
D <sub>60</sub>	177.1	4.013																																																																								
C <sub>u</sub> (D <sub>60</sub> / D <sub>10</sub> )	10.79	1.728																																																																								
C <sub>u</sub> (D <sub>50</sub> / D <sub>10</sub> )	106.7	1.613																																																																								
(D <sub>60</sub> - D <sub>10</sub> )	1.584	1.138																																																																								
(D <sub>60</sub> - D <sub>50</sub> )	96.32	0.261																																																																								
GRAIN SIZE DISTRIBUTION																																																																										
GRAVEL	10.7%	COARSE SAND	1.0%																																																																							
SAND	85.2%	MEDIUM SAND	0.0%																																																																							
M.D.	14.7%	FINE SAND	77.3%																																																																							
		V. FINE SAND	0.0%																																																																							
V. COARSE GRAVEL	0.0%	V. COARSE SILT	14.7%																																																																							
COARSE GRAVEL	0.0%	COARSE SILT	0.0%																																																																							
MEDIUM GRAVEL	0.0%	MEDIUM SILT	0.0%																																																																							
FINE GRAVEL	0.0%	FINE SILT	0.0%																																																																							
V. FINE GRAVEL	0.0%	V. FINE SILT	0.0%																																																																							
V. COARSE SAND	1.0%	CLAY	0.0%																																																																							
<table border="1"> <thead> <tr> <th colspan="6">METHOD OF MOMENTS</th> </tr> <tr> <th>Arithmetic</th> <th>Geometric</th> <th>Logarithmic</th> <th>Geometric</th> <th>Logarithmic</th> <th>Descriptor</th> </tr> </thead> <tbody> <tr> <td>MEAN (μ)</td> <td>161.9</td> <td>150.7</td> <td>2.036</td> <td>119.1</td> <td>Very Mud Sand</td> </tr> <tr> <td>SKEWNESS (γ)</td> <td>100.5</td> <td>1.768</td> <td>0.638</td> <td>1.728</td> <td>Moderately Sorted</td> </tr> <tr> <td>KURTOSIS (κ)</td> <td>46.48</td> <td>5.935</td> <td>5.648</td> <td>3.273</td> <td>Extremely Leptokurtic</td> </tr> </tbody> </table>		METHOD OF MOMENTS						Arithmetic	Geometric	Logarithmic	Geometric	Logarithmic	Descriptor	MEAN (μ)	161.9	150.7	2.036	119.1	Very Mud Sand	SKEWNESS (γ)	100.5	1.768	0.638	1.728	Moderately Sorted	KURTOSIS (κ)	46.48	5.935	5.648	3.273	Extremely Leptokurtic																																											
METHOD OF MOMENTS																																																																										
Arithmetic	Geometric	Logarithmic	Geometric	Logarithmic	Descriptor																																																																					
MEAN (μ)	161.9	150.7	2.036	119.1	Very Mud Sand																																																																					
SKEWNESS (γ)	100.5	1.768	0.638	1.728	Moderately Sorted																																																																					
KURTOSIS (κ)	46.48	5.935	5.648	3.273	Extremely Leptokurtic																																																																					



Aperture (microns)	Class Weight Retained (g or %)
475	0
250	0.007
150	0.004
75	1.838
37.5	1.833
19	2.888
9.5	3.44
4.75	14.588

Sample 5a

### Supplementary materials from Section 6.3

**Supplementary Table T1:** Agreement indices of the refinements according to Larson and Von Dreele (1997).

SAMPLE ID	Rwp (%)	Rp (%)	$\chi^2$
TFZ2W	4.83	2.11	1.22
SLC	5.26	2.08	1.06
FMCO7	6.57	4.19	2.52
GRP2	4.68	2.10	2.02
TFZ2	3.03	1.56	2.08
MMRR11w	4.76	2.12	3.22
GRP1	6.80	4.33	5.48
FMCO8w	2.20	1.42	2.10
FMCO8s	2.53	1.32	2.65
MMR11s	7.02	4.56	3.58
MMR10w	8.81	4.21	4.02
MMR10s	2.67	1.88	2.08
TFZ1	2.22	1.47	2.78
PDR	4.89	2.13	2.22
OLG3	2.95	1.77	2.05
TRR1	4.88	2.57	1.68

Note: Rwp, weighted agreement factor; Rp, profile agreement factor;  $\chi^2$ : goodness-of-fit indicator.

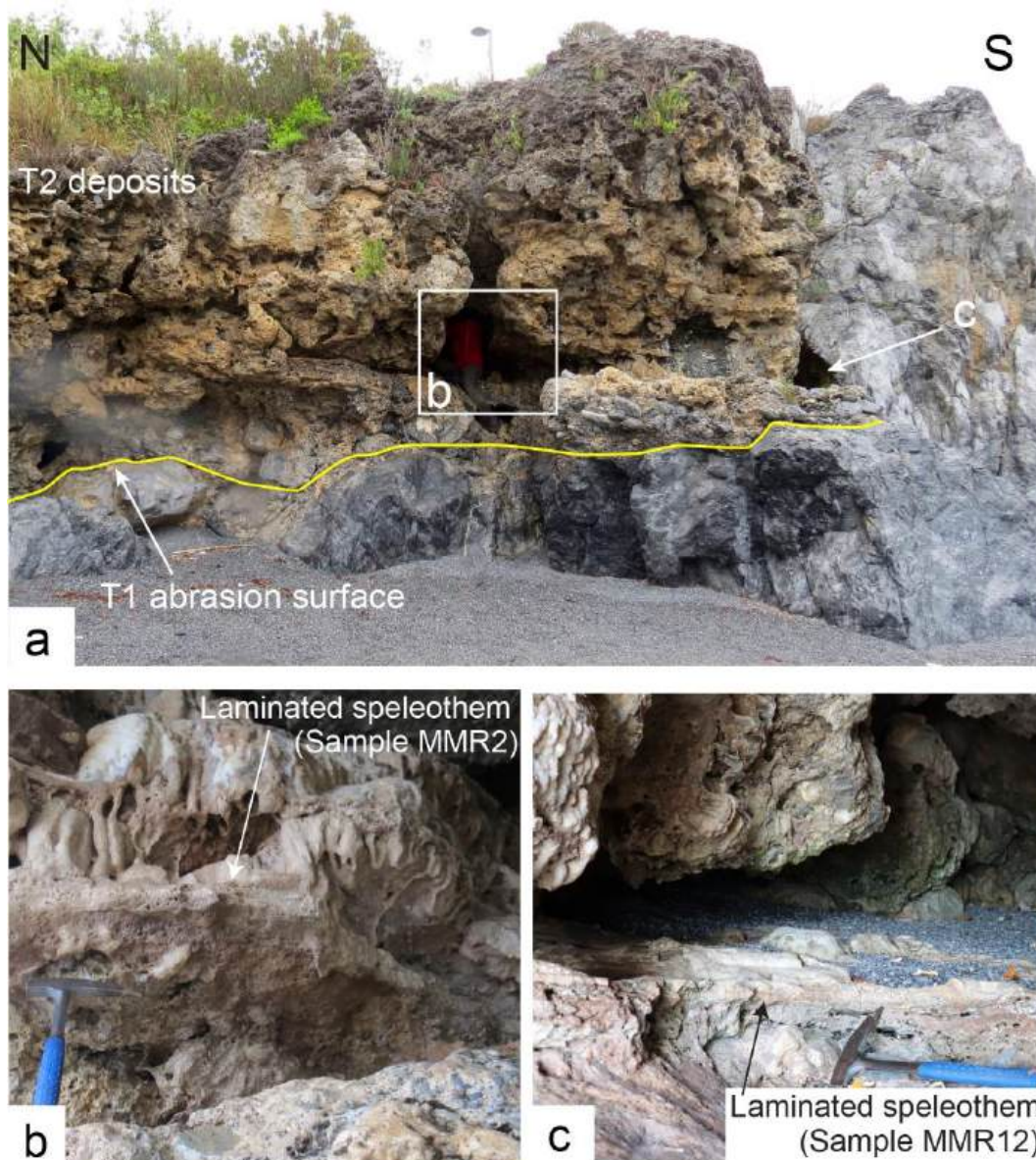
**Supplementary Table T2** Calcite standards used for stable isotopes analysis

External Std Dev	$d^{13}C$	$d^{18}O$	<b>n</b>
ISO-A	0,06	0,14	41
ACROS	0,07	0,10	19

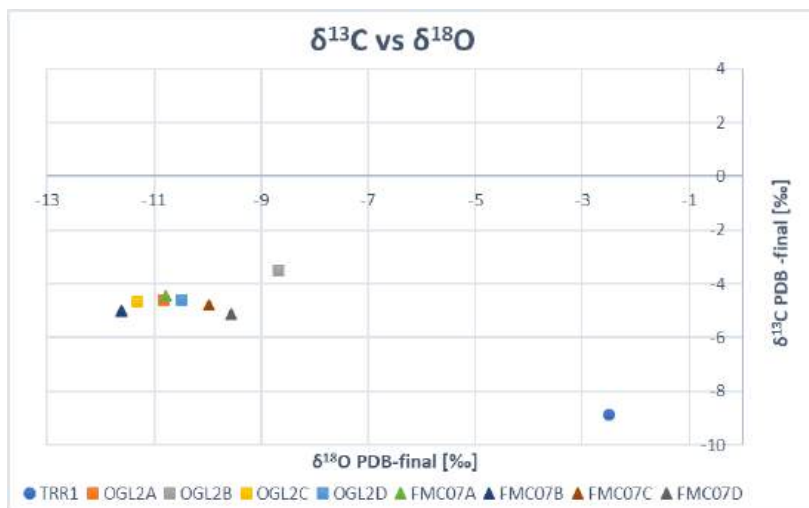
**Supplementary Table T3**  $\delta^{13}\text{C}$  and  $\delta^{18}\text{O}$  isotope stable analysis results

<b>Sample ID</b>	<b>Time Code</b>	<b>Running No.</b>	<b><math>\text{d}^{13}\text{C}^{\text{PDB}}</math> - final [‰]</b>	<b><math>\pm \sigma</math></b>	<b><math>\text{d}^{18}\text{O}^{\text{PDB}}</math>-final [‰]</b>	<b><math>\pm \sigma</math></b>
TRR1	2019/05/14 04:48:41	GB 72308	-2,49	0,03	-8,88	0,01
OGL2A	2019/05/14 05:00:26	GB 72309	-10,82	0,02	-4,60	0,07
OGL2B	2019/05/14 05:12:12	GB 72310	-8,67	0,03	-3,50	0,04
OGL2C	2019/05/14 05:23:57	GB 72311	-11,31	0,03	-4,66	0,07
OGL2D	2019/05/14 05:35:44	GB 72312	-10,49	0,04	-4,60	0,05
FMC07A	2019/05/14 05:47:29	GB 72313	-10,79	0,04	-4,46	0,04
FMC07B	2019/05/14 05:59:15	GB 72314	-11,61	0,02	-5,01	0,06
FMC07C	2019/05/14 06:11:01	GB 72315	-9,98	0,03	-4,79	0,05
FMC07D	2019/05/14 06:22:48	GB 72316	-9,57	0,02	-5,13	0,05

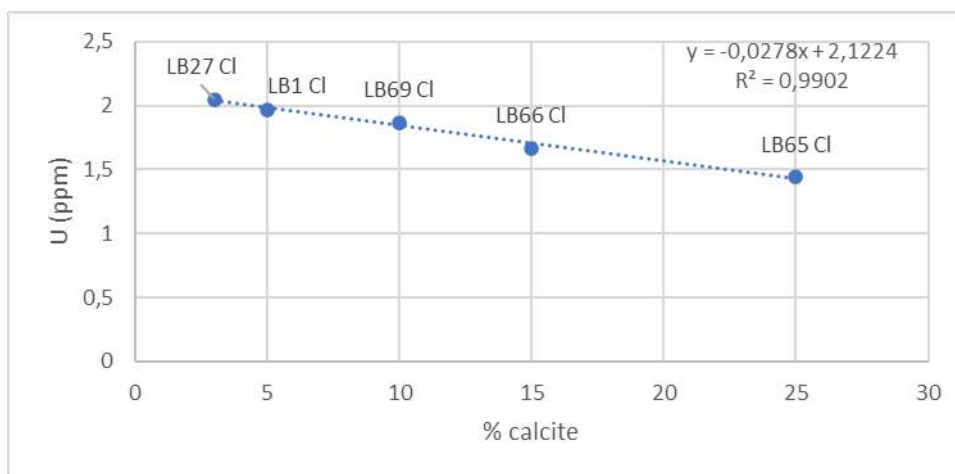
**Supplementary Figure S1** Locations and detailed views of the laminated speleothems sampled in the Marina di Maratea site. a: View of the abandoned sea cliff in the northern side of the Marina di Maratea bay, with two caves formed in the T2 deposits (b) and carbonate rocks (c, in the background). b and c: detailed views of the caves shown in diagram a; the cave fills consist of continental breccia and speleothems. The arrows in diagrams b and c indicate the laminated speleothems sampled for U-series dating (samples MMR2 and MMR12, respectively).



**Supplementary Figure S2.** Stable isotope diagram of calcite concretions sampled at the Fiumicello (FMC07), Ogliastro (OGL2) and Torre Dino (TRR1) sites. Due to the laminated nature of the speleothems of the Ogliastro and Fiumicello sites, samples OGL2 and FMC07 have been divided and subsampled in four parts (A-D series).



**Supplementary Figure S3.** Uranium abundances versus calcite contents of corals dated by  $^{230}\text{Th}/^{234}\text{U}$  in Carobene et al. (1986). Labels next to datapoints are the samples name.



**Supplementary Figure S4** Uranium abundances versus elevation of corals-bearing shoreline deposits (Carobene et al., 1986). Labels next to datapoints are the samples name.

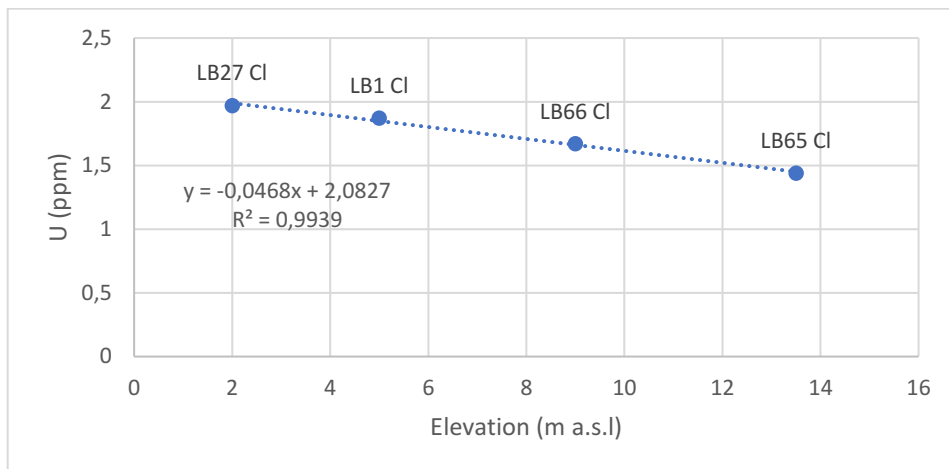


**Table 6.3.2** Uranium contents (mg/g), activity ratios, and  $^{230}\text{Th}/^{234}\text{U}$  ages of the analysed corals and calcite concretions ( $1\sigma$ ). The analysed coral are *Cladocora Caespitosa* specimens with a calcite content  $< 3\%$

Sample ID	Locality	Lat	Long	Sample type	$^{238}\text{U}$		$^{234}\text{U}/^{238}\text{U}$	$^{230}\text{Th}/^{23}\text{U}_{\text{meas}}$		$^{230}\text{Th}/^{232}\text{Th}$	$^{230}\text{Th}/^{234}\text{U}$		Age (ka)	$^{234}\text{U}/^{238}\text{U}_{\text{init}}$	$1\sigma$			
					[mg/g]	$1\sigma$		$1\sigma$	$1\sigma$		calc	$1\sigma$						
GRP2	Grotta del Prete	39.859910°	15.791797°	coral	2.468	± 0.062	1.150	± 0.025	0.544	± 0.016	131.844	± 12.509			83.8	± 3.6	1.190	± 0.032
SLC	Scalea	39.819173°	15.783385°	coral	2.066	± 0.041	1.254	± 0.024	0.608	± 0.016	146.208	± 14.051			98.0	± 4.0	1.335	± 0.032
FMC01	Fiumicello	39.998549°	15.698754°	coral	1.806	± 0.045	1.095	± 0.021	0.785	± 0.040	124.200	± 13.136	-	-	161	± 18	1.150	± 0.033
TFZ2W	Torre Fiuzzi	39.871695°	15.786390°	coral	2.287	± 0.046	1.052	± 0.018	0.673	± 0.021	87.949	± 12.641	-	-	120	± 7	1.073	± 0.025
PDA2	Punta Iudia	39.954596°	15.735311°	speleothem	1.038	± 0.034	1.193	± 0.013	0.476	± 0.022	8.096	± 0.301	-	-	64	± 6	1.231	± 0.016
OGL2	Ogliastro	39.999880°	15.690515°	speleothem	0.215	± 0.005	1.009	± 0.019	0.510	± 0.015	109.354	± 14.221	-	-	78	± 3	1.011	± 0.024
MMR12	Marina di Maratea	39.958416°	15.734494°	speleothem	0.485	± 0.016	1.058	± 0.021	0.525	± 0.019	3.324	± 0.059	0.461	± 0.029	67	± 6	1.070	± 0.025
FMC07	Fiumicello	39.998538°	15.698920°	speleothem	0.598	± 0.012	1.046	± 0.011	0.532	± 0.020	60.019	± 7.583	0.528	± 0.071	81	± 5	1.082	± 0.014
MDN01	Grotta della Madonna	39.896664°	15.784890°	speleothem	1.067	± 0.047	0.979	± 0.018	0.814	± 0.031	1.955	± 0.061	0.749	± 0.058	152	33 / -26	0.968	± 0.028
SLC05	Scalea	39.819138°	15.783407°	speleothem	0.539	± 0.017	1.075	± 0.018	0.634	± 0.028	6.283	± 0.245	0.602	± 0.046	99	± 12	1.099	± 0.024
PNT3	Pantano	39.897712°	15.784326°	speleothem	1.333	± 0.037	1.009	± 0.011	0.395	± 0.015	113.780	± 12.502			54.8	± 2.7	1.011	± 0.013
CSC8	Castrocucco	39.932927°	15.746692°	speleothem	0.345	± 0.006	1.018	± 0.013	0.765	± 0.022	12.745	± 0.507	0.753	± 0.026	151.0	± 11	1.028	± 0.020
MMR2	Marina di Maratea	39.958403°	15.734543°	speleothem	0.385	± 0.012	1.079	± 0.023	0.584	± 0.022	13.800	± 0.609	0.568	± 0.041	90.0	± 10	1.102	± 0.030
TRR1	Torre Dino	39.836211°	15.769875°	speleothem	10.363	± 0.452	0.980	± 0.007	0.513	± 0.034	2.288.467	± 321.587			78.8	± 7.7	0.975	± 0.008

# Geomorphological Map of Basilicata-northern Calabria coastal stretch

